MODELING AND STATE OF CHARGE ESTIMATION OF ELECTRIC VEHICLE BATTERIES

Ryan Ahmed

McMaster University, Ryan.ahmed@mcmaster.ca

MODELING AND STATE OF CHARGE ESTIMATION OF ELECTRIC VEHICLE BATTERIES

MODELING AND STATE OF CHARGE ESTIMATION OF ELECTRIC VEHICLE BATTERIES

By
RYAN AHMED, M.A.SC, P.ENG., SCPM
Stanford Certified Project Manager

A Thesis
Submitted to the School of Graduate Studies
in Partial Fulfilment of the Requirements
for the Degree of Doctor of Philosophy
in Mechanical Engineering

McMaster University

Permission to Use

In presenting this thesis in partial fulfillment of the requirements for a Postgraduate degree from McMaster University, I agree that the Libraries of this University may make it freely available for inspection. I further agree that the permission for copying this thesis in any manner, in whole or in part for scholarly purposes, may be granted by the professors who supervised my thesis work or, in their absence, by the Head of the Department or the Faculty Dean in which my thesis work was conducted. It is understood that any copying or publication or use of this thesis or parts thereof for financial gain shall not be allowed without my written permission. It is also understood that due recognition shall be given to me and McMaster University in any scholarly use which may be made of any material in my thesis. Requests for permission to copy or to make other use of material in this thesis, in whole or part, should be addressed to:

Head of the Department of Mechanical Engineering

McMaster University

Faculty of Engineering

1280 Main Street West

Hamilton, Ontario L8S 4L6

Canada

Doctor of Philosophy (2014) McMaster University
(Mechanical Engineering) Hamilton, Ontario

TITLE: Modeling and State of Charge Estimation of Electric Vehicle Batteries

AUTHOR: Ryan Ahmed, M.A.Sc, P.Eng., SCPM (McMaster University)
SUPERVISOR: Dr. Saeid R. Habibi and Dr. Jimi Tjong
NUMBER OF PAGES: xvii, 288

This work is dedicated to my parents Laila T. and Mohamed A. Ali

All I have and will achieve are only possible due to your love and sacrifices

Abstract

Electric vehicles have received substantial attention in the past few years since they provide a more sustainable, efficient, and greener transportation alternative in comparison to conventional fossil-fuel powered vehicles. Lithium-Ion batteries represent the most important component in the electric vehicle powertrain and thus require accurate monitoring and control. Many challenges are still facing the mass market production of electric vehicles; these challenges include battery cost, range anxiety, safety, and reliability. These challenges can be significantly mitigated by incorporating an efficient battery management system. The battery management system is responsible for estimating, in real-time, the battery state of charge, state of health, and remaining useful life in addition to communicating with other vehicle components and subsystems. In order for the battery management system to effectively perform these tasks, a high-fidelity battery model along with an accurate, robust estimation strategy must work collaboratively at various power demands, temperatures, and states of life. Lithium ion batteries are considered in this research. For these batteries, electrochemical models represent an attractive approach since they are capable of modeling lithium diffusion processes and track changes in lithium concentrations and potentials inside the electrodes and the electrolyte. Therefore, electrochemical models provide a connection to the physical reactions that occur in the battery thus favoured in state of charge and state of health estimation in comparison to other modeling techniques.

The research presented in this thesis focuses on advancing the development and implementation of battery models, state of charge, and state of health estimation strategies. Most electrochemical battery models have been verified using simulation data and have rarely been experimentally applied. This is because most electrochemical battery model parameters are considered proprietary information to their manufacturers. In addition, most battery models have not accounted for battery aging and degradation over the lifetime of the vehicle using real-world driving cycles. Therefore, the first major contribution of this research is the formulation of a new battery state of charge parameterization strategy. Using this strategy, a full-set of parameters for a reduced-order electrochemical model can be estimated using real-world driving cycles while accurately calculating the state of charge. The developed electrochemical model-based state of charge parameterization strategy depends on a number of spherical shells (model states) in conjunction with the final value theorem. The final value theorem is applied in order to calculate the initial values of lithium concentrations at various shells of the electrode. Then, this value is used in setting up constraints for the optimizer in order to achieve accurate state of charge estimation. Developed battery models at various battery states of life can be utilized in a real-time battery management system. Based on the developed models, estimation of the battery critical surface charge using a relatively new estimation strategy known as the Smooth Variable Structure Filter has been effectively applied. The technique has been extended to estimate the state of charge for aged batteries in addition to healthy ones.

In addition, the thesis introduces a new battery aging model based on electrochemistry. The model is capable of capturing battery degradation by varying the effective electrode volume, open circuit potential-state of charge relationship, diffusion coefficients, and solid-electrolyte interface resistance. Extensive experiments for a range of aging scenarios have been carried out over a period of 12 months to emulate the entire life of the battery. The applications of the proposed parameterization method combined with experimental aging results significantly improve the reduced-order electrochemical model to adapt to various battery states of life. Furthermore, online and offline battery model parameters identification and state of charge estimation at various states of life has been implemented. A technique for tracking changes in the battery OCV-R-RC model parameters as battery ages in addition to estimation of the battery SOC using the relatively new Smooth Variable Structure Filter is presented. The strategy has been validated at both healthy and aged battery states of life using driving scenarios of an average North-American driver. Furthermore, online estimation of the battery model parameters using square-root recursive least square (SR-RLS) with forgetting factor methodology is conducted. Based on the estimated model parameters, estimation of the battery state of charge using regressed-voltage-based estimation strategy at various states of life is applied.

The developed models provide a mechanism for combining the standalone estimation strategy that provide terminal voltage, state of charge, and state of health estimates based on one model to incorporate these different aspects at various battery states of life. Accordingly, a new model-based estimation strategy known as the interacting multiple model (IMM) method has been applied by utilizing multiple models at various states of life. The method is able to improve the state of charge estimation accuracy and stability, when compared with the most commonly used strategy. This research results in a number of novel contributions, and significantly advances the development of robust strategies that can be effectively applied in real-time onboard of a battery management system.

Keywords: Lithium-Ion Batteries, genetic Algorithm optimization, electrochemical battery model, parameter identification, state of charge estimation, Battery management systems (BMS), interacting multiple models (IMM), state of charge (SOC), state of health (SOH), filtration, estimation.

Acknowledgements

The author would like to express his gratitude to his academic supervisor, Dr. S.R. Habibi, for his supervision, advice, and guidance from the very early stage of this research until the writing phase of this thesis.

I convey special acknowledgement and gratitude to my industrial supervisor and technical leader at Ford Powertrain Engineering Research and Development Center (PERDC), Dr. Jimi Tjong for his invaluable insights, technical expertise, and support during this research.

Financial support provided by Ford Motor Company, the School of Graduate Studies, the Department of Mechanical Engineering, and the Ontario Government's Graduate Scholarship Program is acknowledged.

I genuinely thank my fellow researchers at Ford PERDC for their endless support; Dr. Mohammed El-Sayed, Dr. Doug Chang, and Dr. Haran Arasaratnam. I also thank my fellow colleagues at MathWorks Inc.; Dr. Javier Gazzari, Mr. Robyn Jackey, Mr. Aubrey da Cunha, and Mr. Kevin Rzemien. I gratefully thank my colleagues at McMaster University; Dr. Andrew Gadsden and Dr. Dhafar Al-Ani for their help.

I would also like to express my gratitude to my family, my mother Laila, my father Mohamed Ali, and my siblings, Heba and Maged for their endless encouragement and support throughout my entire academic career.

Co-Authorship

This thesis has been prepared in accordance with the regulations for a sandwich thesis format or as a compilation of research papers stipulated by the faculty of graduate studies at McMaster University. This thesis consists of the following papers:

Paper I

Ryan Ahmed, Mohammed El Sayed, Jimi Tjong, and Saeid Habibi, "***Literature Review of Battery Models, State of Charge, and State of Health Estimation Strategies***".

Literature review has been conducted by Ryan Ahmed. Paper I was written by Ryan Ahmed. Dr. Mohamed El Sayed assisted with data collection and, Dr. Jimi Tjong, and Dr. Saeid Habibi supervised the research work; reviewed and revised the journal paper.

Paper II

Ryan Ahmed, Mohammed El Sayed, Jimi Tjong, and Saeid Habibi, "***Reduced-Order Electrochemical Model Parameters Identification and SOC Estimation for Healthy and Aged Li-Ion Batteries. Part I: Parameterization Model Development for Healthy Batteries***", IEEE Journal of Emerging and Selected Topics in Power Electronics, special issue on Electrification and Transportation, 2014, Pages: 659 - 677 (Volume: 2, Issue: 3).

Design of experiment, experimental data collection, parameterization model development, and data analysis have been conducted by Ryan Ahmed. Paper II was written by Ryan Ahmed. Dr. Mohamed El Sayed assisted with data collection and provided technical guidance and assistance. Dr. Jimi Tjong, and Dr. Saeid Habibi supervised the research work; reviewed and revised the journal paper.

Paper III

Ryan Ahmed, Mohammed El Sayed, Jimi Tjong, and Saeid Habibi, "***Reduced-Order Electrochemical Model Parameters Identification and SOC Estimation for Healthy and***

Aged Li-Ion Batteries. Part II: Aged Battery Model and State of Charge Estimation", IEEE Journal of Emerging and Selected Topics in Power Electronics, special issue on Electrification and Transportation, 2014, Pages: 678 - 690 (Volume: 2, Issue: 3).

Design of experiment, experimental data collection, aging model development, and data analysis have been conducted by Ryan Ahmed. Paper III was written by Ryan Ahmed. Dr. Mohamed El Sayed assisted with data collection and provided technical guidance and assistance. Dr. Jimi Tjong, and Dr. Saeid Habibi supervised the research work, reviewed and revised the journal paper.

Paper IV

Ryan Ahmed, Ienkaran Arasaratnam, Mohamed El-Sayed, Jimi Tjong, and Saeid Habibi, "***Online and Offline Parameters Identification and SOC Estimation for Healthy and Aged Electric Vehicle Batteries Based on Equivalent Circuit Models***".

Design of experiment, experimental data collection, aging model development, and data analysis have been conducted by Ryan Ahmed. Paper IV was written by Ryan Ahmed.

Dr. Ienkaran and Dr. Mohamed El-Sayed assisted with data collection, troubleshooting, analysis, and provided technical guidance and assistance. Dr. Jimi Tjong, and Dr. Saeid Habibi supervised the research work, reviewed and revised the journal paper.

Paper V

Ryan Ahmed, Andrew Gadsden, Mohamed El-Sayed, Jimi Tjong, Saied Habibi, "***Aged Battery State of Charge Estimation based on Interacting Multiple Models***".

Battery aging model development, and data analysis have been conducted by Ryan Ahmed. Paper V was written by Ryan Ahmed. The interacting multiple model strategy has been implemented by Dr. Andrew Gadsden. Dr. Mohammed El Sayed assisted with data generation and, Dr. Jimi Tjong and Dr. Saeid Habibi supervised the research work, reviewed and revised the journal paper.

Table of Contents

List of figures

List of Tables

Chapter 1: Introduction

This chapter provides an introduction to the research conducted; including the problem statement, research contributions and novelty, and organization of the thesis.

1.1 Problem Statement

Recently, the automotive industry is experiencing a major technology shift from conventional, fossil-fuel propelled vehicles to electrified hybrids (HEVs), plug-in hybrids (PHEVs), and battery electric vehicles (BEVs). As vehicles become more electrified, this brings technical challenges that must be addressed in order to accelerate the wide adoption of this emerging technology. Batteries represent a core component for the electric vehicle powertrain and therefore require accurate real-time supervisory control and monitoring. The battery management system (BMS) is responsible for accurate monitoring of critical parameters such as the battery pack state of charge (SOC), state of health (SOH), and remaining useful life (RUL). Furthermore, the BMS communicates with other critical onboard controllers and subsystems, maintains cell balancing, performs thermal management, and ensures safety.

As an example to demonstrate the necessity of having a robust SOC and SOH estimation technique on board of an electric vehicle, consider the following: "*As per October, 2012, there are 112 documented cases of customers complaining of capacity loss in their electric vehicles*", [1]. In addition, around 11.8% of the total number of Nissan Leaf vehicles sold in Arizona have exhibited a loss in capacity gauge bars (Note: first capacity bar represents 15% capacity loss and 6.25 in the subsequent bars), [1].

For the SOH, BEVs and HEVs have been on the market for quite a short period of time thus possible malfunctions in batteries are of great concern. Therefore, adaptive control of batteries is necessary to account for aging and degradation in performance that might affect vehicle range of operation and charging efficiency, [2]. Furthermore, safety is of great concern, since EVs are relatively new to the automotive market (E.g. Ford focus and Nissan Leaf have been on the market for only 3 years) as such new vehicles typically need some time for the assessment of their performance in real-world operations (until odometer reaches 150,000 miles), [3]. Any severe fires due to battery overcharge or short circuits would result in loss of market share and, to customers moving away from acquisition of electric vehicles. Accordingly, health monitoring and estimating the remaining useful life for battery systems is extremely important.

Since electric and hybrid vehicles have been recently introduced to the market, it will require some time to assess their performance in real-world driving conditions. In particular, batteries might suffer from irreversible degradation due to cycling and that in turn adversely affects the SOC estimation accuracy which is of great concern to drivers. Accordingly, the battery management system (BMS) has to be adaptive to at least partly compensate for aging and degradation in performance that might affect the vehicle range of operation and charging efficiency.

In order for the BMS to accurately estimate the battery SOC, SOH, and RUL, the BMS needs an accurate, high-fidelity battery mathematical model along with a robust estimation strategy to work collaboratively at various states, power demands, and temperatures. This is a tremendously challenging task since battery packs run under dynamic charging and discharging currents based on the driving pattern (acceleration and regenerative braking) of the driver.

As demonstrated in the literature, and reinforced in this thesis, most battery models that currently exist in the literature do not account for aging and degradation. Models have been developed based on single battery state of life at a fresh (healthy) state. As battery ages, most battery models suffer from divergence problems in terminal voltage calculation which in turn affects the state of charge estimation accuracy. It is therefore the goal of this research to further advance and develop battery aging models based on electrochemistry and equivalent circuit based models and track changes that occur in the battery parameters as battery degrades.

Regarding electrochemical battery models, a large majority of electrochemical-based models presented in the literature are based on computer simulations and have not been parameterized using experimental data. In addition, the full-set of the reduced-order electrochemical model parameters have not been identified using real-world driving cycles while calculating the state of charge. Furthermore, no state of charge parameterization model has been developed to adjust the spherical volume-based state of charge calculation accordingly. Therefore, this thesis overcomes this gap in the literature and provides a generic technique for parameter identification using evolutionary algorithms. The technique has been used to estimate the full-set of the reduced-order electrochemical model parameters based on a 3.3V, 2.3Ah Lithium Iron Phosphate (LiFePO4) battery at various states of life. Furthermore, the thesis includes a new electrochemical model-based SOC parameterization strategy based on the number of spherical shells (model states) and on the final value theorem. The final value theorem is applied in order to calculate the initial values of lithium concentrations at various shells of the electrode. Then, this value has been used in setting up a constraint for the optimizer in order to achieve accurate SOC estimation. Developed battery models at various battery states of life can be utilized in a real-time battery management system.

1.2 Research Contributions and Novelty

The overview of the research conducted in this thesis is as shown below in Figure 1.1. The first main contribution of this research project is the development of a new state of charge parameterization strategy based on the number of electrode shell concentrations and the final value theorem. This creates new opportunities to fit current and voltage experimental data and identify the reduced-order electrochemical model parameters while evaluating the state of charge based on the electrode concentration spherical average. Extensive testing using real-world driving cycles such as the Urban Dynamometer driving Schedule (UDDS) have been conducted on fresh lithium-Iron Phosphate cells at controlled temperatures. Identification of the full-set of the electrochemical model parameters have been carried out. The model has been validated using an aggressive driving cycle such as the US06 driving cycle.

In addition, the parameterized electrochemical model creates new opportunities and possibilities for developing aging models by varying the effective electrode volume. An extensive array of accelerated aging tests have been carried out at elevated temperature over a period of 12 months. This period was used to age the cell from 100% capacity to their end-of-life specified by most automotive manufacturers at 80%. The proposed electrochemical model has been validated and expanded upon to enable tracking parametric changes that would reflect battery aging. These parameters include the open circuit voltage-state of charge relationship, the solid particle diffusion coefficient, the solid-electrolyte-interface resistance, and the stoichiometry ratio values. The model has been validated using different driving cycles that have not been previously used during the optimization phase. The methodology can be applied to any battery chemistry with different specifications.

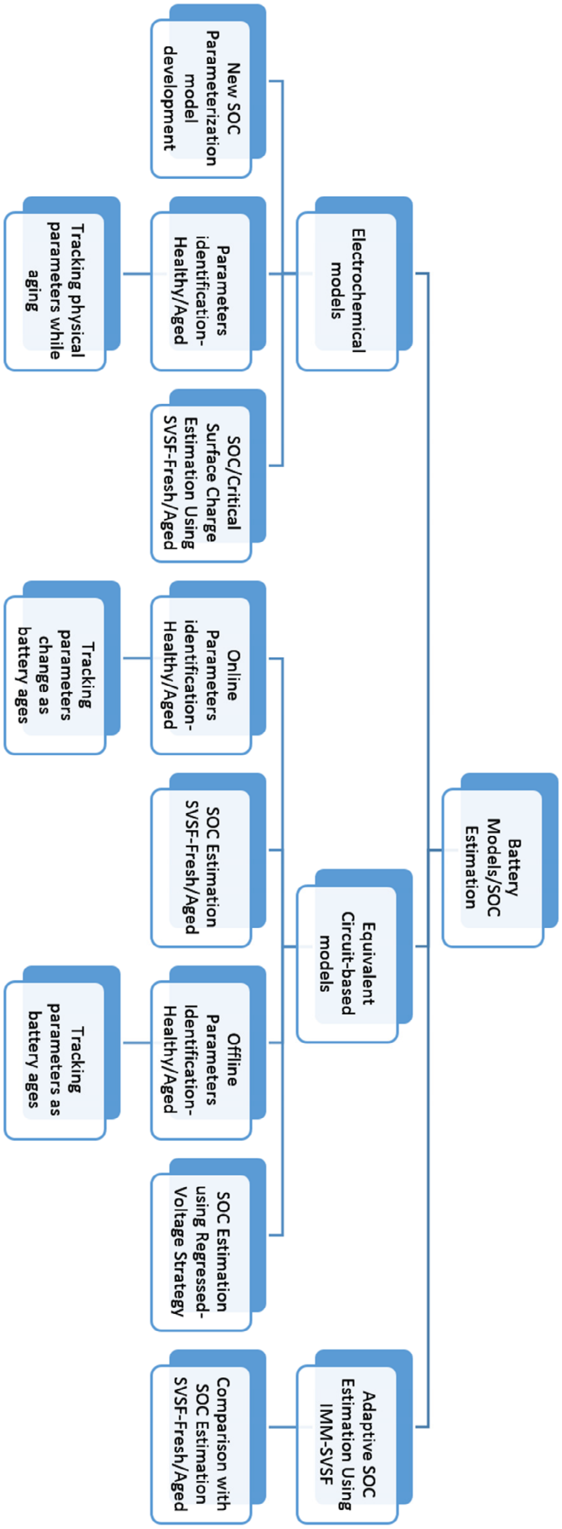

Figure 1.1. Research Flowchart

A robust estimation strategy known as the Smooth Variable Structure Filter (SVSF) has been applied to estimate the electrode critical surface charge and the state of charge at various battery states of life. The strategy works in a predictor-corrector form and is computationally efficient to be implemented on board of a battery management system.

In addition to the aforementioned research conducted in the electrochemical battery modeling, tracking of parametric changes for the equivalent-circuit-based models has been implemented in both online and offline settings. The offline tracking technique utilizes Genetic Algorithm optimization to estimate model parameters while the online tracking methodology uses the Square-Root Recursive Least Square estimation to track model parameters. An extensive array of aging tests has been conducted over the course of 12 months simulating the entire lifetime of a battery in an all-electric vehicle. The tests encompass the driving habits of an average North-American driver in regular weekdays and weekends. A mix of benchmark driving cycles have been used in this study separated by a series of reference performance tests (RPTs) to assess degradation over the lifetime of the vehicle. Furthermore, a state of charge estimation strategy has been applied to estimate the state of charge based on the SVSF and the regressed voltage-based estimation strategy. The techniques have shown robustness to modeling uncertainties and sensor noise and work relatively well at all battery states of life.

Using the developed models at various battery states of life, a technique widely used in radar and tracking applications have been adopted in the battery management field. The technique is known as the interacting multiple models based on the Smooth Variable Structure Filter (IMM-SVSF). Instead of relying on one single battery model in calculating the terminal voltage and estimating the state of charge, the IMM-SVSF works by incorporating multiple models at various states of life. Results indicate the necessity of having an adaptive technique that accounts for battery aging and degradation.

The results of this research represent significant contributions to the area of battery modeling and state of charge estimation, as well as to the body of knowledge in the battery management systems field. In order to provide a summary of research contributions, a list of original research goals presented in this thesis are listed below:

Primary Contributions:

1. Development of a new SOC parameterization strategy based on the number of spherical shells and the final value theorem.
2. Development of an aged battery model based on electrochemistry by varying the effective electrode volume.
3. Estimation of the battery state of charge and the critical surface charge at various states of life based on the developed model.
4. Identification of the full set of the reduced-order model parameters at fresh (healthy) state.
5. Tracking changes of the battery electrochemical model parameters such as the diffusion coefficient, solid-electrolyte interface resistance, open-circuit voltage-state of charge relationship, and the cathode and anode stoichiometry ratio values.
6. Development of an aged battery model based on equivalent-circuit-based models.
7. Application of the Smooth Variable Structure Filter based on the developed models to estimate the state of charge at various states of life.

8. Development of an adaptive method to estimate the SOC and the terminal voltage based on the IMM-SVSF.
9. Estimation of the battery parameters using the Square Root Recursive Least Square estimation at fresh and healthy battery states.
10. Application of the regressed voltage-based strategy to estimate the state of charge at various states of life.

Secondary contributions rely on the attained primary ones as follows:

Secondary Contributions:

1. Identification and quantification of the parameters that contribute to battery aging such as the depth of discharge and temperatures.
2. Estimating the battery effective electrode volume which can provide an indication of the battery state of health.
3. A better understanding of how the SVSF performs in comparison to the IMM-SVSF according to its smoothing boundary layer, and the existence of modeling uncertainties and sensor noise.
4. Estimating the OCV-R-RC battery model parameters provides an indication of the battery state of health.
5. A better understanding of battery aging and failure mechanisms that might occur in traction battery packs.

These contributions have been reported in manuscript submitted or accepted for publication in scientific journals as listed in the next section.

1.3 Organization of the thesis

This thesis presents a combination of analytical and experimental research used to propose advancements in battery mathematical modeling, state of charge, and state of health estimation based on fresh and aged batteries. The thesis is organized as follows:

Chapter 2 provides a literature review of battery models, state of charge, state of health, and aging models.

Chapter 3 proposes a new state of charge parameterization strategy for identifying the full-set of parameters in a reduced-order electrochemical model for a fresh battery. The major contributions of the paper include the development of a new electrochemical model-based SOC parameterization strategy based on the number of spherical shells (model states) and the associated application of the final value theorem. The final value theorem is applied in order to calculate the initial values of lithium concentrations at various shells of the electrode. Then, this value has been used in setting up a constraint for the optimization strategy used in estimating the SOC. The proposed battery models for various battery states of life are computationally efficient and can be utilized in a real-time battery management system.

In addition, the chapter presents a detailed analysis of the proposed models in the context of battery usage in a mid-sized electric vehicle. The vehicle model is used to generate the current profile for the battery according to the velocity profile from driving cycles. Furthermore, the chapter describes the experimental setup that was used for data collection, including battery cyclers and environmental chambers. A detailed analysis of the battery reference performance tests including driving cycles have been presented. These tests have been used for model fitting and validation. Experimental results of the terminal voltage and state of charge, based on the developed parameterization model have been presented.

Chapter 4 includes the development of an aging battery model capable of capturing battery degradation by varying the effective electrode volume. Furthermore, tracking the electrochemical model parameters that contribute to aging as battery degrades is also presented. These parameters include diffusion coefficient, solid-electrolyte interface resistance, and the OCV-SOC relationship.

The chapter summarizes the extensive accelerated aging test that has been conducted on battery cells until the battery reaches the end-of-life (80% of its capacity). In addition, a reference performance test using driving cycles has been conducted on aged batteries. Finally, a battery critical surface charge estimation strategy has been designed to estimate the state of charge based on the identified battery model parameters. A strategy known as the Smooth Variable Structure Filter (SVSF) has been used for battery critical surface charge estimation.

Chapter 5 involves a detailed description of the aging study that simulates the entire lifetime of the electric vehicle. The chapter summarizes the proposed parameter identification and SOC estimation techniques based on equivalent circuit-based models. Two different approaches for battery SOC estimation and model parameters identification have been implemented and compared. Battery model parameters identification using both online and offline techniques at various battery states of life has been conducted. In the first approach, an online recursive least square method has been applied to estimate battery model parameters and to estimate the open circuit voltage (OCV). A square-root version of the recursive least square method (SR-RLS) has been presented in this research with forgetting factor since it represents a robust estimation strategy. Based on the estimated battery OCV, a regressed-voltage method has been applied to map the OCV to the battery SOC thus provides an estimate of the battery SOC at various states of life. In the second approach, a Genetic Algorithm (GA) optimization strategy has been applied offline to estimate the battery model parameters at various states of life. Based on the identified model parameters, a battery SOC estimation strategy has been designed to estimate the SOC based on the identified battery model parameters. The SVSF has been presented for battery SOC estimation. The proposed strategy has been selected since it demonstrates robustness to modeling uncertainties, sensor noise, and to SOC initial conditions. The strategy has been applied to estimate the battery SOC at various battery states of life from fresh (healthy) state (100% capacity) to 80% retained capacity.

Chapter 6 presents a new SOC estimation strategy known as the Interacting Multiple Models using the Smooth Variable Structure Filter (IMM-SVSF). The proposed methodology can adapt to various aging conditions and can provide an accurate approach that can be implemented in a real-time on-board battery management system (BMS). The proposed method presents a proof of concept for the applicability of adaptive techniques in battery SOC estimation. The IMM-SVSF technique is used for extracting the state of charge (SOC) information based on an equivalent circuit-based battery aging model. This technique is capable of tracking the battery SOC and terminal voltage under aging conditions. As battery ages, parameters such as the internal resistance and capacity change overtime and thus, the battery model has to adapt to these variations and provide an accurate SOC estimate over various charging/discharging cycles until the end-of-life (EOL). Computer simulations and experimental results show the effectiveness of the proposed technique for real-time BMS applications.

Chapter 7 provides a summary of the thesis, the major conclusions and the recommendations for future research.

Chapter 2: Literature Review of Battery Models, Aging Models, State of Charge, and State of Health Estimation Strategies

Ryan Ahmed[1], Mohammed El Sayed[1], Saeid Habibi[1]
Centre for Mechatronics and Hybrid Technologies (CHMT), Department of Mechanical Engineering, McMaster University, Hamilton, Canada
Jimi Tjong[2]
[2]Ford Motor Company of Canada, Powertrain Engineering Research and Development Center (PERDC), Windsor, Canada

Abstract

Electric vehicles have received substantial attention in the past few years since they provide a more sustainable, efficient, and greener transportation alternative in comparison to conventional fossil-fuel powered vehicles. Lithium-Ion battery packs are increasingly used and are an important component in the electric vehicle powertrain. Use of batteries pose many challenges in the mass market production of electric vehicles. These include battery cost, range anxiety, safety, and reliability. These challenges can be significantly mitigated by incorporating an efficient battery management system. The battery management system is responsible for estimating, in real-time, the battery state of charge, state of health, and remaining useful life in addition to communicating these parameters with other vehicle components and subsystems. In order for the battery management system to effectively perform these tasks, a high-fidelity battery model along with an accurate, robust estimation strategy must be deployed to work collaboratively at various power demands, temperatures, and states of life. This is a challenging task in safety critical applications such as in the automotive sector. This paper provides a review of the publications related to battery models, aging models, and the associated state of charge, state of health, and remaining useful life estimation strategies. ***Keywords: Battery literature review, battery modeling, state of charge estimation, state of health, lithium-Ion batteries.***

Corresponding Author:

Ryan Ahmed, M.A.Sc, P.Eng., SCPM
Research and Development Engineer

Paper to be submitted to the Journal of Power Sources, 2015

2.1 Introduction

Battery management systems (BMS) play an important role in hybrid and electric vehicles since the battery pack is safety critical and one of the most important and expensive parts of the vehicle. They therefore require accurate monitoring and control. In order to efficiently manage the battery, an accurate estimation of the battery state of charge (SOC), state of health (SOH), and remaining useful life (RUL) is needed. SOC is defined as the remaining battery capacity in comparison to the battery overall capacity, thus providing an indication of the vehicle remaining driving range, [1]. SOH is a measure of the irreversible degradation that occurs in the battery performance due to cycling, [1]. The SOH provides a comparison of the current state of the battery versus the fresh (healthy) battery before any cycling, [1]. SOH is a measure of the battery's capability to respond to the required power demand and thus an indicator of potential need for maintenance or replacement, [1]. Two main critical factors affect the battery SOH, namely: ***battery capacity fade*** and ***power fade***. The battery ***capacity fade*** has a significant impact on the vehicle driving range which is critical since it is associated with customer range anxiety. The second factor is the ***power fade*** which impacts the vehicle performance and drivability. The RUL is used to predict the battery remaining useful time across its predetermined lifetime thus represents a proactive indicator for battery maintenance, [1].

Since the aforementioned parameters cannot be directly measured with a sensor, a high-fidelity mathematical model along with a robust estimation algorithm is necessary. A trade-off between model accuracy and complexity is present in relation to real-time implementations; models must be accurate to capture the system dynamics while being simple to be implemented in real-time embedded microprocessors, [2]. Extensive research has been conducted to achieve accuracy in modeling the dynamic characteristics of the battery while keeping the models simple enough for online implementation in a real-time vehicle BMS, [1]. In this paper, a literature review of the current research advancements in BMS is provided specifically directed to the following areas: ***battery cell and pack-level modeling and parameter identification***, ***techniques for state of charge estimation***, ***state of health estimation, remaining useful life,*** and ***aging models***.

The paper is organized as follows. Section 2 discusses various battery models found in recent literature in addition to various strategies applied for model parameters identification. Section 3 involves various state of charge estimation techniques. Section 4 outlines various aging models that works collaboratively with other techniques for model parameters identification. Section 5 reports on state of health estimation strategies used in BMS. The conclusion are provided in Section 6. An overview of the topics reviewed in this paper is shown in Figure 2.1.

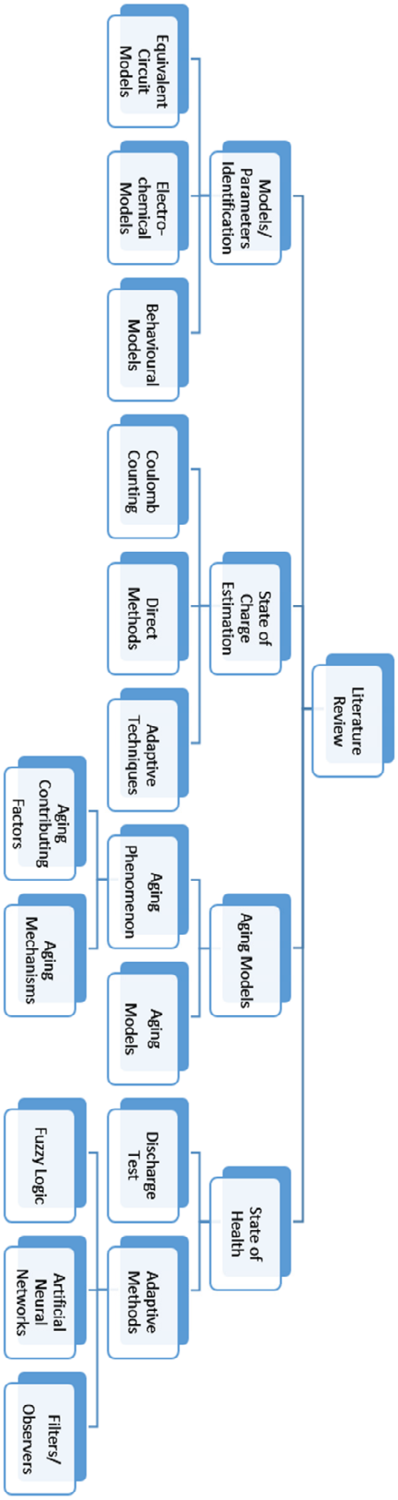

Figure 2.1. Paper (Literature review) Overview

2.2 Battery Models

Battery models are commonly classified under one of the following: (i) equivalent circuit-based models, (ii) electrochemical battery models, (iii) behavioural models (empirical), (iv) hydrodynamic models, (v) tabulated data models, and (vi) black-box battery models (such as artificial neural network and fuzzy logic-based models), [3, 4]. These modeling strategies are reviewed in this section.

2.2.1 Equivalent Circuit-Based Models

Equivalent circuit-based models use simple elements such as resistors and capacitors to model the charging and discharging behavior of Li-ion batteries. Equivalent circuit models are simple to implement, computationally efficient and simple for implementing parameter and model identification. Therefore, equivalent circuit models can be easily implemented in real-time on-board of a vehicle microcontroller. However, model parameters have little or no physical meaning which makes them restrictive for state of health estimation. Equivalent-circuit based models are divided into 5 categories as follows, [1].

2.2.1.1 Thevenin Electrical Model:

The Thevenin model, is shown in

Figure ***2.2***. It consists of one voltage source (V_{oc}), a resistor connected in series (R_1), and a parallel combination of a resistor and a capacitor (R_2C). The output is the battery terminal voltage (V_T), [5]. The resistance (R_1) is used to model the battery internal resistance and the RC branch is used to model the overvoltage. This model has limited capability since it does not take into consideration the variation in the battery parameters as they change with time and according to operating conditions, [5].

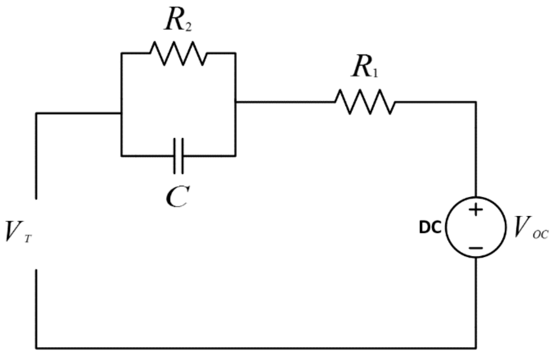

Figure 2.2. Thevenin Battery Model, [5]

2.2.1.2 Linear Electrical Model:

These models represent an improvement over the Thevenin-based models, [5]. These models provide more accuracy as they are capable of modeling the battery self-discharge (R_p) and other overvoltage using different elements as shown in Figure 2.3, [6, 7].

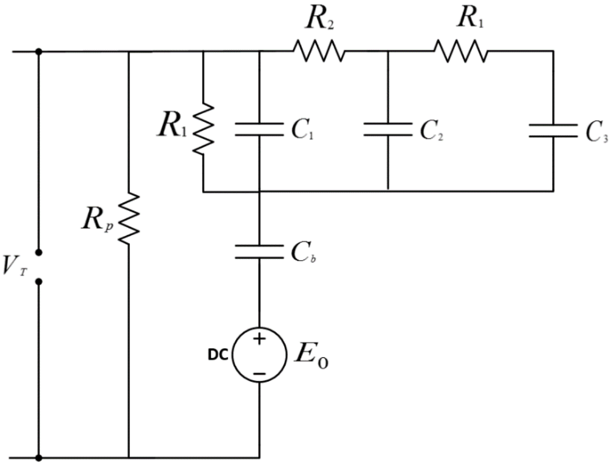

Figure 2.3. Linear Battery Model, [7]

In Figure 2.3, E_0 is the open circuit voltage of a fully-discharged battery cell and C_b is the cell capacitance. These elements add up to the open circuit voltage of the battery cell $V_{OC}(t)$, [7]. R_p is the self-discharge resistance; R_1, R_2, R_3 are the battery resistances; C_1, C_2, C_3 are the battery capacitances that represent the cell dynamics; $i_b(t)$ is the battery current; and $V_T(t)$ represents the battery terminal voltage which is calculated as follows, [7]:

$$v_T(t) = v_{AB} + v_{BC} = V_{oc}(t) + \eta_m(t) \tag{2.1}$$

Note that the battery overvoltage $\eta_m(t)$ represents the difference between the battery terminal voltage and the battery open circuit voltage [7]. This model is not appropriate for real-time implementation as it uses various values for electrical elements to model the variation of the model with the battery state of charge, [5]. Furthermore, it does not take into account temperature dependence and has thus limited accuracy, [5].

2.2.1.3 Non-linear electric model

A more accurate battery model that takes into account temperature variations, self-discharge, internal resistance, overvoltage, and internal storage capacity has been proposed in [5] as shown in Figure 2.4. In this model, , R_p is the self-discharge resistance, C_b is the battery capacity, R_{1C} is the charge overvoltage resistance, R_{1D} is the discharge overvoltage resistance, C_1 is the overvoltage capacitance, R_{sc} is the internal resistance for charge, R_{SD} is the internal resistance for discharge, and V_{oc} is the open circuit voltage, [5].

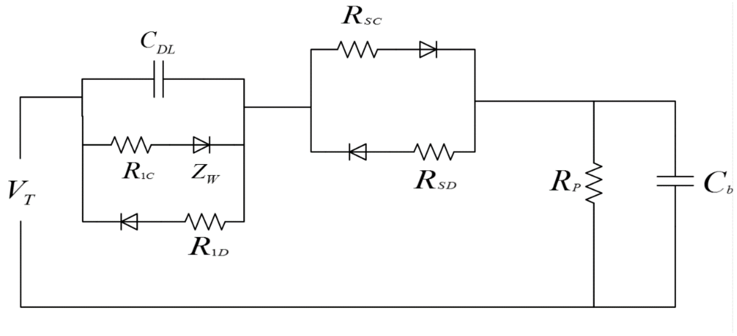

Figure 2.4. Equivalent Circuit-based model with Temperature Dependence, [5]

In nonlinear equivalent circuit based models, battery parameters are not constants and they change according to the battery voltage [5] as follows:

$$MP = ke^{[w_f(V_m - V_{oc})]^{ff}} \tag{2.2}$$

Where MP is the model parameter, k is a gain multiplier, w_f is a width factor, V_m is the mean voltage, V_{OC} is the open circuit voltage, and ff is the flatness factor. The battery resistance elements vary with temperature thus variation due to temperature can be modeled as follows, [5]:

$$TC = \frac{R}{R_{ref}}^{(T_{ref}-T)/T_{ref}} \tag{2.3}$$

Where, TC is the temperature compensation coefficient for the resistance, R is the resistance at temperature T, R_{ref} is the resistance at temperature T_{ref}, [5].

2.2.1.4 First, second, and third-order RC Models

RC models consists of an open circuit voltage source which is a function of the battery state of charge (SOC). R_0 represents the battery internal resistance while RC branches are used to model battery dynamics. The third-order model is as shown below in Figure 2.5, [8].

The terminal voltage relationship from the standalone first, second, and third-order models are as shown below in Table 2.1, [8]. In addition, any of these models can be enhanced by incorporating a hysteresis state to account for battery hysteresis that occurs in charging and discharging, [8].

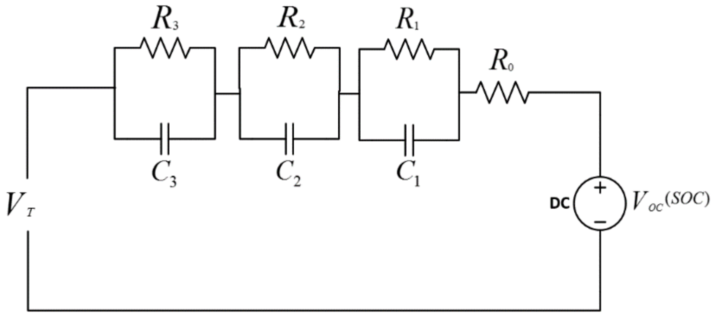

Figure 2.5. Third-Order RC Battery Model, [8]

The parallel RC elements correspond to the dynamic order of the circuit. The equations for the first, second, and third-order models with and without hysteresis are presented in Table 2.1. Here U_1, U_2, U_3 are the voltage of the first, second, and third RC elements, respectively while $\tau_1 = R_1C_1, \tau_2 = R_2C_2, \tau_3 = R_3C_3$ are the associated time constants, [8].

Table 2.1. First, second, and third RC Models with and without hysteresis equations, [8]

Model	Output equations
The first-order RC model [9, 8]	$U_{1,k+1} = \exp(-\Delta t/\tau_1)\, U_{1,k} + R_1[1 - \exp(-\Delta t/\tau_1)]I_k$ $V_k = OCV(z_k) - R_0 I_k - U_{1,k}$

The first-order RC model with hysteresis state [10, 11]	$V_k = OCV(z_k) - R_0 I_k - U_{1,k} + h_k$
The second-order RC model	$V_k = OCV(z_k) - R_0 I_k - U_{1,k} - U_{2,k}$
The second-order RC model with hysteresis state	$V_k = OCV(z_k) - R_0 I_k - U_{1,k} - U_{2,k} + h_k$
The third-order model RC model	$V_k = OCV(z_k) - R_0 I_k - U_{1,k} - U_{2,k} - U_{3,k}$
The third-order model RC model with hysteresis state	$V_k = OCV(z_k) - R_0 I_k - U_{1,k} - U_{2,k} - U_{3,k} + h_k$

2.2.1.5 Randles (Impedance-based) Equivalent circuit models

Randles equivalent circuit based models are macroscopic models that can be developed using data obtained from electrochemical Impedance spectroscopy laboratory experiments, [12]. These models, as shown in Figure 2.6, use a resistance (R_{OHM}) which represents the resistance of the electrolyte and current collector, [13, 12], C_{DL} represents the double layer capacitance at the cathode/electrolyte and lithium/electrolyte interface, R_{CT} is the charge transfer resistance, and z_w is the Warburg impedance which is the impedance due to lithium ion diffusion, [12].

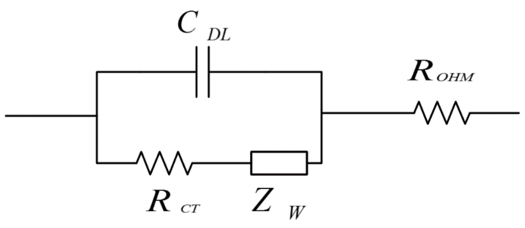

Figure 2.6. Randles Equivalent Circuit-based model, [12]

In general, the battery is excited at frequencies that range from 10^5 to 10^{-2} Hz. The battery model parameters can be obtained using the output from the impedance spectroscopy, [12].

2.2.2 Electrochemical-Based Models

Electrochemical battery models, also known as first-principal models, use partial differential equations to describe lithium diffusion inside both electrodes and the electrolyte, [14]. Electrochemical models are generally complex and require more computational power compared to equivalent-circuit based models, [1]. Even though they are mostly complex, they are preferred since they are capable of modeling the physical phenomenon that occurs in the battery. Therefore, electrochemical models can provide a better indication of the battery state of charge and state of health. In order to implement the electrochemical models on board of a battery management system, model reduction has to be carried out to reduce their computational complexity. Another major difficulty with electrochemical models is that they require numerous number of parameters such as diffusion coefficients and electrode physical dimensions, [8]. In this section, a summary of the full-order electrochemical model is presented followed by a review of the most recent developments.

2.2.2.1 Summary of the Electrochemical Model

The battery model structure and an overview of the electrochemical battery model, as shown in Figure 2.7, is illustrated in this section. The common approach here is to consider the diffusion dynamics in one dimension and only along the X-axis, [15, 16]. At any specified time t and at any location across the x-axis, the following state variables are evaluated:

1. Electric potential in the solid electrode $\phi_s(x,t)$
2. Electric potential in the electrolyte $\phi_e(x,t)$
3. Lithium concentration in the solid phase $c_s(x,r,t)$
4. Lithium concentration in the electrolyte $c_e(x,t)$.

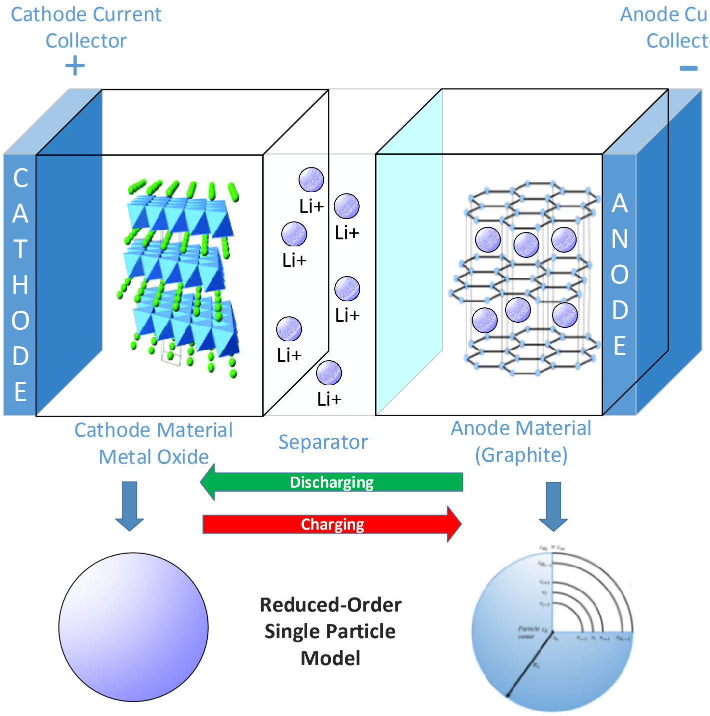

Figure 2.7. Lithium-Ion Battery Structure and the Reduced-Order Model Assumption (Adopted from [17])

The full-order electrochemical model consists mainly of 4 partial differential equations, [18]. The model has one input representing the cell current I and one output representing the terminal voltage V_T. The following equations summarize the relationship between the input and the output, [14]. The solid and electrolyte potentials are described by the following two equations, [17]:

$$\frac{\partial}{\partial x}k^{eff}\frac{\partial}{\partial x}\emptyset_e+\frac{\partial}{\partial x}k_D^{eff}\frac{\partial}{\partial x}\ln c_e=-j^{Li} \tag{2.4}$$

$$\frac{\partial}{\partial x}\sigma^{eff}\frac{\partial}{\partial x}\emptyset_s=j^{Li} \tag{2.5}$$

The diffusion of lithium in the electrolyte is modeled using Fick's law for linear coordinates as shown by equation (2.6), [17],

$$\frac{\partial\varepsilon_e c_e}{\partial t}=\frac{\partial}{\partial x}\left(D_e^{eff}\frac{\partial c_e}{\partial x}\right)+\frac{1-t^0}{F}j^{Li} \tag{2.6}$$

while the solid (electrode) phase diffusion is modeled by Fick's laws of diffusion for spherical coordinates as follows, [17]:

$$\frac{\partial c_s}{\partial t}=\frac{\partial}{\partial r}(D_s\frac{\partial c_s}{\partial r}) \tag{2.7}$$

The Butler-Volmer current density (J^{Li}) is described, [17]:

$$J^{Li}=a_s j_o[exp\left(\frac{\propto_a F}{RT}\eta\right)-exp(\frac{\propto_c F}{RT}\eta)] \tag{2.8}$$

Where R and F are the universal gas constant and Faraday's constant, T is the absolute temperature and η is the over potential, [17].

$$\eta=\emptyset_s-\emptyset_e-U(c_{se}) \tag{2.9}$$

The model output representing the terminal voltage is related to the measured cell solid potential as follows, [17]:

$$V=\emptyset_s(x=L)-\emptyset_s(x=0)-R_f I \tag{2.10}$$

In equation (2.9), U is the open circuit voltage which is a function of the lithium concentration at the solid-electrolyte interface $c_{se}(x,t)=c_s(x,R_s,t)$. The concentration at the interface between the solid and the electrolyte is related to the critical surface charge (CSC), which is lithium concentration at the solid-electrolyte-interface, [17].

$$CSC(t) = \frac{\theta - \theta_{0\%}}{\theta_{100\%} - \theta_{0\%}} \tag{2.11}$$

By defining the normalized solid-electrolyte concentration θ as follows, [17]:

$$\theta = \frac{solid - electrolyte\ concentration}{maximum\ solid\ concentration} = \frac{c_{se}}{c_{s,max}} \tag{2.12}$$

where, $\theta_{0\%}$ and $\theta_{100\%}$ are the normalized concentrations corresponding to 0% (fully discharged) and 100% (fully charged). $\theta_{100\%}$ can be defined by obtaining the concentration corresponding to the maximum fully charged battery. Subsequently, the 0% reference value can be calculated by subtracting the battery capacity Q as, [19]:

$$\theta_{0\%} = \theta_{100\%} - \frac{Q}{\delta}\left(\frac{1}{AF\varepsilon c_{s,max}}\right) \tag{2.13}$$

where R_f is the electrode film resistance at the electrode surface, this resistance increases after charging and discharging cycles (battery aging). As mentioned earlier, the full-order model is relatively complex so further simplifications are necessary to make it useful for control and estimation purposes. The open circuit voltage is obtained from the cathode and anode potentials and is function of the state of charge. An empirical relationship is used to relate the open circuit voltage to the normalized state of charge which is given by [20]:

$$\begin{aligned} U_n(\theta_n) = 8.0029 + 5.064\theta_n - 12.578\theta_n^{0.5} - 8.6322 \times 10^{-4}\theta_n^{-1} + 2.176 \\ \times 10^{-5}\theta_n^{\frac{3}{2}} - 0.46016\,exp[15(0.06 - \theta_n)] \\ - 0.55364exp[-2.4326(\theta_n - 0.92)] \end{aligned} \tag{2.14}$$

For the positive electrode, the empirical equation is as follows, [21]:

$$U_p(\theta_p) = 85.681\theta_p^6 - 357.7\theta_p^5 + 613.89\theta_p^4 - 555.65\theta_p^3 + 281.06\theta_p^2 - 76.648\theta_p + 13.1983 - 0.30987exp(5.657\theta_p^{115}) \quad (2.15)$$

The coefficient j_o depends on the solid and electrolyte concentrations according to the following equations, [17]:

$$j_o = (c_e)^{\alpha_a}(c_{s,max} - c_{se})^{\alpha_a}(c_{se})^{\alpha_c} \quad (2.16)$$

In the following subsections the ongoing research in 4 main areas are reviewed, namely: ***full-order electrochemical model enhancements, reduced-order model enhancements, model parameters identification,*** and ***state of charge estimation.***

2.2.2.2 Full-Order Electrochemical Models Enhancements

Even though equivalent circuit based models are simple and easy to implement, their application is limited to portable electronics. In high power and energy applications such as the automotive field, relying on equivalent circuit based models is questionable since these models do not capture the underlying physical interactions and diffusion processes in the cell and can compromise accuracy and safety, [22]. In order for equivalent circuit-based models to be implemented in high energy and power applications, battery parameters have to be adaptive and change at various states of charge, states of life, and temperatures which significantly increases the complexity of the model to a level comparable to electrochemical models, [22]. Since equivalent circuit-based models provide minimal physical insight to the battery internal states such as solid and electrolyte potentials, extensive research is being conducted on electrochemical models to overcome the problem associated with their computational complexity.

Electrochemical-based battery models have been widely researched in the literature. In 1975, Newman and Tiedemann presented a new development in the theory of flooded porous electrodes. In this theory the electrode was treated as a superposition of the electrolytic solution and the solid matrix, [15]. The solid matrix was modeled as microscopic spherical particles where the lithium ions diffuse and react on the spheres surface. Later in [23], Fuller et al. expanded this model by considering the one dimensional transport of lithium ions from the negative electrode composite through the separator into the positive electrode composite.

The first principals of electrochemical modeling have been presented in [23]. In this paper, the lithium insertion in the active electrodes materials due to galvanostatic charge and discharging process is modeled and simulated, [23]. The main advantage of this model is that it has generic characteristics thus can be applied to any active electrodes and electrolyte materials. This model was further enhanced by Ramadass et al. in [24] by accounting for the cell capacity decay. In 1998, Wang et al [25] introduced a new model that integrates the microscopic concepts of porous electrode theory into a macroscopic battery model, hence reducing the effect of electrode porosity on the model complexity. Wang et al. model was adapted to a wide range of active materials and electrolyte solutions. The model was applied to lithium-ion batteries in [26].

Although electrochemical battery models provide an accurate prediction of lithium concentration across the electrode, a real-time application of full-order electrochemical models is difficult because of their high complexity. Accordingly, to allow real-time battery state of charge (SOC) estimation, approximations to the battery model were introduced in [27, 28].

2.2.2.3 Reduced-Order Electrochemical Model

Full-order models are usually used during the battery design phase since they are capable of predicting the physical interactions inside the cell such as potential distribution and electrochemical species diffusion. In order to implement the electrochemical model for real-time applications on a battery management system for SOC and SOH estimation, a reduced-order form has to be realized. In the literature, two common forms of reduced-order electrochemical models are: the ***electrode average model*** [19], and ***the states value model*** [29]. In the ***electrode average model***, several assumptions have been made for real-time applications, including: (1) high electrolyte lithium concentration (c_e) thus can be assumed constant, and (2) utilizing one representative particle for each electrode instead of having several particles in the spatial x-direction (full-order model). These assumptions result in a computationally efficient model that can be used for real-time estimation and control. This reduction results in some loss of information. However, the model still maintains a connection with the cell physics that cannot be attained using empirical or equivalent circuit-based models, [30].

Regarding the ***states value model***, the full-order model has to be transformed into linear functions that relate the model input current $I(s)$ to model outputs, solid lithium concentration ($c_s(x,s)$), electrolyte concentration ($c_e(x,s)$), solid phase potential ($\emptyset_s(x,s)$), and electrolyte phase potential ($\emptyset_e(x,s)$). Afterwards, by combining the output of sub-models, the battery terminal voltage can be calculated. The key assumptions that have to be made are as follows: (1) Butler-Volmer current $J^{Li}(s)$ is assumed to be decoupled from the electrolyte concentration $c_e(x,s)$, and (2) the model has a linear behaviour.

In [30], a comparison between the electrode average model and the linear states value model is presented. Experiments were conducted on a 37 V 10 Ah lithium-Ion battery cells using multiple driving cycles and pulse tests, [30]. The electrode average model provides various advantages compared to the states value model as follows [30]: (1) The electrode average model provides a better estimate of the state of charge, (2) it requires fewer parameters in comparison to the states value model, (3) it is easier to tune since it requires setting one initial parameter only representing the initial state of charge, [30]. However, its main disadvantages include: (1) high nonlinearity in parameters compared to the linear state value model, and (2) the model parameters are hard to identify, [30]. Reduced order models are mainly used for estimation and control purposes such as state of charge and state of health estimation.

2.2.3 Behavioural Battery Models

Behavioural battery models use various empirical functions and formulas to describe the behaviour of the battery cells. Similar to equivalent circuit-based models, these are simple to implement with less parameters to tune and, therefore can readily be used in real-time applications on a BMS. These models are considered below.

2.2.3.1 Shepherd/Unnewehr/Nernest Equations

The shepherd equation represents a simple approach for battery modeling; it is represented in the following form, [31]:

$$E(t) = E_o + R_\alpha i(t) + \frac{K_1}{q_s(t)} \tag{2.17}$$

where, E_o is the initial cell voltage, R_α is the cell internal resistance, $q_s(t)$ is the instantaneous stored charge, and K_1 is a constant, [31]. Another further approximation is represented in the Unnewehr model, [31]

$$E(t) = E_o + R_\alpha i(t) + K_2 q_s(t) \tag{2.18}$$

Another similar form is known as the Nernest Model as follows, [31]:

$$E(t) = E_o + R_\alpha i(t) + K_3 \, ln\left(\frac{q_s(t)}{Q}\right) - K_4 ln(\frac{Q - q_s(t)}{Q}) \tag{2.19}$$

where, Q is the total charge capacity of the cell and the constants K_1, K_2, K_3, and K_4 can be obtained by fitting experiential data, [32].

In [33], Plett introduced a series of behavioural models based on the previously mentioned models, namely: ***the combined model, the simple model, the zero-state hysteresis model, one state hysteresis model,*** and ***the enhanced-self-correcting model***. These models can account for hysteresis effect, polarization time constants, and ohmic loss effects, [33]. A summary of the abovementioned models is as follows, [33]:

2.2.3.2 The Combined Model

By combining the three above mentioned behavioral models and discretizing them in time, [34], the combined model is obtained as shown below:

$$y_k = K_0 - Ri_k - \frac{K_1}{z_k} - K_2 z_k + K_3 \ln(z_k) + K_4 \ln(1 - z_k) \tag{2.20}$$

$$z_{k+1} = z_k - \left(\frac{\eta_i \Delta t}{C}\right) i_k \tag{2.21}$$

In this model, y_k is the cell terminal voltage, R is the cell internal resistance, representing both charge and discharge resistances. K_1, K_2, K_3, K_4 are tunable constants that can be used to fit experimental data to the model, [34]. The main advantage of this model is that parameters can be easily identified from the current/voltage data using least square optimization.

2.2.3.3 The Simple Model

The simple model is derived from the combined model by grouping all terms that are functions of the state of charge z_k in one group as follows, [34]:

$$f(z_k) = K_0 - \frac{K_1}{z_k} - K_2 z_k + K_3 \ln(z_k) + K_4 \ln(1 - z_k) \tag{2.22}$$

And, by grouping all terms that are functions of the current:

$$f(i_k) = Ri_k$$

Equation (2.22) represents the open circuit potential which is a function of the battery state of charge. Thus the simple model can be formulated as follows, [34]:

$$z_{k+1} = z_k - \left(\frac{\eta_i \Delta t}{C}\right) i_k \tag{2.23}$$

$$y_k = OCV(z_k) - Ri_k \tag{2.24}$$

Where OCV refers to the open circuit voltage.

2.2.3.4 The Zero-State Hysteresis Model

Even though the previous models can capture the terminal voltage dynamics with acceptable accuracy, they do not account for hysteresis effect, [34]. The zero-state hysteresis model is capable of modeling hysteresis by the addition of the following term $s_k M(z_k)$ to the simple model, [34]:

$$y_k = OCV(z_k) - s_k M(z_k) - Ri_k \tag{2.23}$$

where s_k represents the sign of the current and $M(z_k)$ is half the difference between the charge and discharge values (i.e., some value of hysteresis), [34]. For a small and positive value ε, s_k can be defined as follows:

$$s_k = \begin{cases} +1 & i_k > \varepsilon \\ -1 & i_k < -\varepsilon \\ s_{k-1} & |i_k| \leq \varepsilon \end{cases}$$

The zero-state hysteresis model provides a better voltage estimate compared to the simple model, [34].

2.2.3.5 The One-State Hysteresis Model

The hysteresis voltage can be modeled using a separate state $h(z,t)$ which is function of the battery state of charge. The hysteresis voltage can be modeled as follows, [34]:

$$\frac{dh(z,t)}{dz} = \gamma sgn(\dot{z})[M(z,\dot{z}) - h(z,t)] \tag{2.24}$$

$M(z,\dot{z})$ is the maximum polarization due to hysteresis, it is a function of the state of charge and also its rate-of-change. The $sgn(\dot{z})$ is used to model both battery charging and discharging operations, [34]. γ is a positive constant that describes the rate of voltage decay, [34]. $M(z,\dot{z}) - h$ indicates that the rate-of-change of hysteresis voltage which is proportional to the distance away from the main hysteresis loop; leading to a kind of voltage decay in the major loop, [34]. The model can be represented in a state space form as follows, [34]:

$$\begin{bmatrix} h_{k+1} \\ z_{k+1} \end{bmatrix} = \begin{bmatrix} F(i_k) & 0 \\ 0 & 1 \end{bmatrix} \begin{bmatrix} h_k \\ z_k \end{bmatrix} + \begin{bmatrix} 0 & 1 - F(i_k) \\ -\frac{\eta_i \Delta t}{C} & 0 \end{bmatrix} \begin{bmatrix} i_k \\ M(z,\dot{z}) \end{bmatrix} \tag{2.25}$$

$$y_k = OCV(z_k) - Ri_k + h_k \tag{2.26}$$

Where $F(i_k) = \exp(-|\eta_i i(t)\gamma / C_n|)$.

2.2.3.6 The Enhanced Self-Correcting Model

A further enhancement over the one state hysteresis is the enhanced self-correcting model, [34]. The model is capable of capturing the battery dynamics and accommodates for ohmic losses, hysteresis, and polarization time constants, [34]. The model has two inputs, namely: the battery input current i_k, and the maximum polarization due to hysteresis $M(z,\dot{z})$, [34]. The model has one output y_k, which is the terminal voltage. The ESC model in the state space form is as follows, [34]:

$$\begin{bmatrix} f_{k+1} \\ h_{k+1} \\ z_{k+1} \end{bmatrix} = \begin{bmatrix} diag(\propto) & 0 & 0 \\ 0 & F(i_k) & 0 \\ 0 & 0 & 1 \end{bmatrix} \begin{bmatrix} f_k \\ h_k \\ z_k \end{bmatrix} + \begin{bmatrix} 1 & 0 \\ 0 & \left(1 - F(i_k)\right) \\ -\frac{\tau_i \Delta \mathrm{t}}{C_n} & 0 \end{bmatrix} \begin{bmatrix} i_k \\ M(z,\dot{z}) \end{bmatrix} \tag{2.27}$$

$$y_k = OCV(z_k) - Ri_k + h_k + Gf_k \tag{2.28}$$

where z_k is the state of charge, f_k is the states of the low pass filter on i_k which is used to characterize the polarization time constants, h_k is the state representing charging or discharging hysteresis effect, OCV is the open circuit voltage, C_n is the battery nominal capacity, R is the battery internal resistance, G is the output matrix of the low pass filter, and α are the poles of the low pass filter.

2.2.3.7 Hydrodynamic (Kinetic) Battery Models

In this model, filling and draining of fluid in a two-tank reservoir are assumed to be analogous to the process of charging and discharging of the battery, [35, 36, 37]. As shown in Figure 2.8, the fluid pressure, flow, volume, and pipe area in the two-tank reservoir are analogous to the voltage, current, capacity, and resistance, respectively, [35].

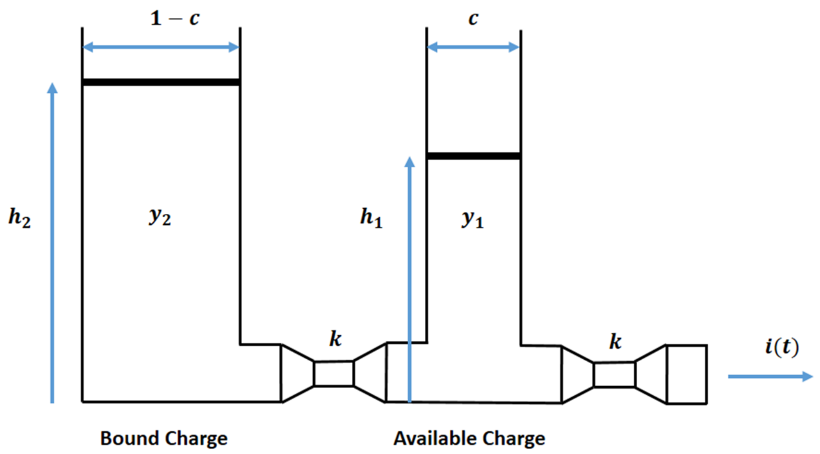

Figure 2.8. Schematic Diagram of Battery Model, [35, 38]

This model has two main advantages: it is capable of modeling two phenomena that occur in most battery chemistries, namely***: rate capacity effect*** and ***recovery effect,*** [38]. The rate capacity effect is the phenomenon of having less battery capacity represented in Ampere-hours that can be drawn from the battery at high C-rates, [38]. This indirectly incorporates the Peukert phenomenon stated earlier in section 1. The recovery effect is that the unattained capacity at high C-rates will be available after a short period of time (after allowing the battery to relax), [38, 39].

The Kinetic battery model is relatively simple, as shown in Figure 8, the overall battery charge is divided into two tanks, namely: the ***bound charge*** and the ***available charge*** tanks, [38]. The two tanks are connected via a pipe and a valve. The charge in the two tanks are divided according to the capacity ratio c $(0 < c < 1)$, [38]. The bound charge is not accessible under high discharge rate thus the model is able to model the rate capacity effect. However, after allowing for some time, fluid from the bound charge tank starts to flow across the valve k to the available charge tank until the height difference h_1 and h_2 are at the same level. Accordingly, the model is able to model the recovery effect.

The rate of charge flow from the bound tank to the available charge tank is controlled by the difference in heights of the two tanks h_1 and h_2 and on the value of the valve k. The change in the charge in both tanks are expressed by the following equations, [40] where y_1 and y_2 are the available and bound charges, respectively:

$$\frac{dy_1(t)}{dt} = -i(t) + k[h_2(t) - h_1(t)] \tag{2.29}$$

$$\frac{dy_2(t)}{dt} = -k[h_2(t) - h_1(t)] \tag{2.30}$$

Assuming the initial conditions of $y_{1,0} = y_1(t_0) = c * C$ and $y_{2,0} = y_2(t_0) = (1 - c) * C$. Where C is the total battery capacity defined in Ampere-hours. The differential equations can be solved as follows, [38] and these equations can be solved for every piecewise constant discharge current I:

$$y_1(t) = y_{1,0}e^{-k'(t-t_0)} + \frac{(y_0k'c - I)[1 - e^{-k'(t-t_0)}]}{k'} - \frac{Ic(k'(t - t_0) - 1 + e^{-k'(t-t_0)}]}{k'} \tag{2.31}$$

$$y_2(t) = y_{2,0}e^{-k'(t-t_0)} + y_0(1 - c)[1 - e^{-k'(t-t_0)}] - \frac{I(1 - c)[k'(t - t_0) - 1 + e^{-k'(t-t_0)}]}{k'} \tag{2.32}$$

$$\delta(t) = h_2(t) - h_1(t) = \frac{y_2(t)}{1 - c} - \frac{y_1(t)}{c}, t_0 \leq t \leq t_1 \tag{2.33}$$

$$u(t) = (1 - c)\delta(t) \tag{2.34}$$

Where, $k' = \frac{k}{[c(1-c)]}$ describes the charge flow diffusion rate, $\delta(t)$ represents the height difference between the two tanks, and $u(t)$ represents the battery unavailable charge. The hydrodynamic battery model has been scarcely researched, it has been applied and expanded in few published papers as follows. In [38], a novel hybrid battery model that combines both the electrical equivalent circuit based models and the hydrodynamic model has been presented. The model has been validated by simulation and experimental data from lithium polymer cells, [38]. The proposed model is computationally effective and can be applied for real-time applications on a battery management systems. In [35], a hydrodynamic battery model has been used as a part of a hybrid vehicle simulation model of a turbo generator-based powertrain. The model has been validated using experimental data from a 14.4 V battery module, [35].

2.2.3.8 Black-Box Models

Artificial neural networks (ANNs) are black box models that are capable of modeling any nonlinear, complex, input-output relationship. ANNs can be used in modeling the behaviour of various battery parameters such as the terminal voltage, state of charge, and to various inputs such as the current, temperatures, and C-rates. Even though ANNs represent an attractive approach in battery modeling and SOC estimation, they require extensive input-output experimental training data which is time consuming to generate. In addition, ANNs generally require high computational power for real-time applications.

In [41], a one-layer ANN has been trained using voltage data from a real-world driving cycles on 60 x 100 Ah lithium polymer battery pack. The ANN is trained using back-propagation technique with a 700 input-output dataset that covers the entire range of battery operating currents and voltages, [41]. Furthermore, a multilayer neural network is trained and the accuracy of the model was significantly enhanced by increasing the number of neurons in the hidden layer. Simulation and experimental results show the accuracy and effectiveness of the proposed model, [41].

In [42], a recurrent ANN has been used to predict the battery state of charge using values of the input current, temperature, and SOC from previous time steps. With this network, a parameter estimation strategy has been developed using the Recursive Least Squares (RLS) algorithm with time-dependant forgetting factor, [42]. This strategy allows for more accurate estimation of the cell terminal voltage. In that research, experimental data from a 4.2 V, 100 Ah lithium polymer cell was used for ANN training, [42]. Currents, voltages, and state of charge data from a European urban driving test has been used for testing, [42].

2.2.3.9 Tabulated Data Models

Across the entire battery range of operation, values of various battery parameters such as internal resistance and open circuit voltage (OCV) can be recorded and tabulated at various states of charge and temperatures, [13]. In [43], the battery pack has been modeled using look-up tables that relates the OCV to the SOC and another column that relates the battery charging and discharging resistance to the SOC, [43, 13]. Tabulated data models can be used onboard of a battery management system.

2.3 Model Parameters Identification

This section reviews the methods that are used for parameter identification for electrochemical (ECM), equivalent circuit, and behavioural models.

2.3.1 ECM Parameters Identification

A challenging task in electrochemical modeling is how to tune model parameters, most manufacturers treat the parameters as being confidential. Accordingly several attempts at obtaining the model parameters for lithium ion batteries have been reported in the literature. Battery parameters were obtained either by conducting a destructive test (i.e.: measuring all parameters by opening the cell) or by non-destructive test using optimization techniques to fit models to experimental data.

In [44], experimental identification of the reduced-order electrochemical model parameters of a lithium-polymer cell is proposed. Using continuous and pulse charging/discharging Experimental data on a 6.8 Ah, 9 model parameters are identified, [44]. The identified model parameters considered included: solid particle diffusion coefficients, electrode surface area, and maximum solid electrode potentials, [44].

In [45], a genetic algorithm has been applied for identifying the full set of parameters of the full-order electrochemical model using experimental data consisting of the input current and the measured terminal voltage. Furthermore, the fisher information technique has been applied to identify the accuracy of the resulting parameters, [45]. The test has been conducted using Lithium Iron Phosphate ($\mathrm{LiFePO_4}$) cells from A123. The cells are used in high power applications such as in an automotive traction battery pack, [45].

2.3.2 Behavioural models parameter identification

In [46], the parameters of behavioural models were estimated by using the extended Kalman filter (EKF). The behavioural models considered included: ***the combined model, the simple model, the zero-state hysteresis model, one state hysteresis model,*** and ***the enhanced-self-correcting model***. A state space representation of these models is formulated as required by the EKF, [46]. Experimental data using a benchmark Urban Dynamometer Driving Schedule (UDDS) cycle in addition to data from a pulsed charge/discharge test have been used for identification.

In [47], a dual estimation strategy was applied to estimate the battery model parameters and SOC for behavioural models. Furthermore, a comparative study of Li-Ion battery models showed that the enhanced self-correcting model is the most accurate model since it is capable of modeling ohmic losses, polarization time constants, and hysteresis effects. Two estimation strategies have been applied for estimation. A new estimation strategy known as the Smooth Variable Structure Filter (SVSF) has been compared to the well-known Kalman filter, [47].

2.3.3 Equivalent circuit-based models Parameter identification

In [48], a multi-objective optimization strategy using genetic algorithms is applied to identify the parameters of a simple RC model. Model parameters such as the resistance and the open circuit potential are assumed to be a polynomial function of the C-rate and the battery cell state of charge, [48]. The multi-objective optimization algorithm is then applied to obtain the polynomial coefficients. The technique has been verified on a 2.5 V, 8 Ah capacity cell and the models show good fit to experimental data at various charge/discharge rates, [48].

In [49], a parameter identification strategy using least squares has been applied to an equivalent circuit-based model. Since the main source of a battery model's nonlinearity arises from the SOC-OCV relationship, this relationship has been divided into 8 piece-wise linear regions and model identification has been applied to each of these regions, [49]. Further to the resulting linear models, an observer has been applied to estimate the state of charge. This technique has been experimentally applied to Lithium polymer cells, [49].

In [50], an identification procedure for an electro-thermal model is presented. The model parameters have been estimated at various states of charge (15% to 90%) and temperature conditions ($-15℃$ to $45℃$). Model parameters are evaluated using a multistep genetic algorithm, [50]. This procedure has been applied to a 2.3Ah, 3.2V lithium-Iron Phosphate cells from A123, [50].

Particle swarm optimization has been used for parameter tuning for 12 different battery models in [11] over several driving cycles including Dynamic Stress Test (DST), Hybrid Pulse Power Characterization test (HPPC), and Federal Urban Dynamic Schedule (FUDS). The technique has been applied and verified on two different battery chemistries including lithium-Iron Phosphate ($\mathrm{LiFePO_4}$) and Lithium Nickel-Manganese-Cobalt oxide (LiNMC), [11]. One of the main conclusions of this research project is that the first-order RC model is the preferred choice for LiNMC, while the one-state hysteresis and the first-order RC model are the best for $\mathrm{LiFePO_4}$, [11].

2.4 State of Charge Estimation

In battery management systems (BMS), three main measurements are readily available, namely: current, voltage, and temperature. The BMS has to utilize these measurements to obtain a robust estimate of the battery pack state of charge, [51]. Estimating battery SOC with high accuracy is a challenging task since various key elements contribute to the change of the SOC including charging and discharging C-rates, temperature, self-discharge, and battery aging, [1]. SOC is extremely important as it helps in optimizing energy consumption in HEVs and BEVs, and avoiding undesirable incidents such as overheating due to overcharging, accelerated aging due to undercharging, or running out of energy due to false estimation (in case of battery electric vehicles), [52]. Several SOC estimation techniques have been presented in the literature, these techniques are classified under one of the following: ***conventional coulomb counting, direct method, Electromotive force (EMF), and adaptive techniques***.

2.4.1 Conventional Coulomb Counting

In this simple method, which is also known as ***book keeping***, current integration is performed and is compared to the nominal battery capacity thus SOC can be calculated. The equation used is as follows:

$$SOC = 1 - \frac{\int idt}{C_n} \tag{2.35}$$

where C_n is the battery nominal capacity for a fresh battery, i is the measured current, and t is the time. The main advantage of coulomb counting is that it is simple to be implemented and it can be applied to all battery chemistries, [1]. Its major disadvantages include the need for regular calibration since error accumulation occurs (due to sensor noise and inaccuracies) over time due to integration, [53]. Another disadvantage is that this method requires an accurate initial SOC in order to provide an acceptable accuracy, [52]. By incorporating further information to the coulomb counting technique such as the cell temperature, charge/discharge efficiency, and capacity degradation due to cycling, the technique can provide an acceptable estimate. However, in order to perform regular calibration, a complete charge and discharge has to be conducted which limits its practical applications.

In the literature, various enhancements to coulomb counting have been proposed. In [54], an enhanced technique that takes into consideration the charging and discharging efficiencies is proposed for compensating for coulomb losses, [54]. Since the initial SOC can significantly affect the accuracy of the coulomb counting technique, the paper presents a strategy to calculate the initial state of charge from the terminal voltage evaluated from the constant current constant voltage (CCCV) charging curve, [54]. Furthermore a state of health estimation technique is presented by evaluating the maximum releasable capacity during the calibration process, [54].

2.4.2 Direct Methods

In these methods, direct measurements of voltages, impedances, and relaxation time are carried out; the SOC is then inferred out of these measurements, [52]. These methods are classified as follows.

2.4.2.1 Peukert Method

Peukert introduced an empirical method to estimate the battery's remaining capacity, [55]. In the literature, many researchers have introduced variants of Peukert's equation in estimating the battery state of charge, [56]. Peukert conducted different experiments using constant discharge test on a battery and proposed the following equation to relate the discharge rate to the remaining capacity (or the remaining discharge time) as follows, [55]:

$$I^{PC}t = Constant \tag{2.36}$$

Where, I is the discharge current, t is the maximum discharge time and PC is the Peukert Coefficient which ranges from 1 to 2, [56]. The battery capacity can be calculated as follows, [56]:

$$C_{n1} = C_n\left(\frac{I_n}{I_{n1}}\right)^{PC-1} \tag{2.37}$$

C_{n1} is the battery remaining capacity at the discharge current of I_{n1}, [56]. One of the main drawbacks of using Peukert equation for state of charge estimation is that it can only be used for constant current discharge profiles and at constant temperatures only, [56]. Therefore, this technique is not suitable for applications such as in hybrid an all-electric vehicles which have aggressive, fast changing current profiles associated with acceleration and deceleration demands.

2.4.2.2 Terminal Voltage-based SOC Calculation

Based on the terminal voltage measurement, SOC can be inferred using look-up tables. This method is extremely simple but it suffers from inaccuracies since SOC varies significantly with temperature, aging, and C-rates, [52]. In addition, this method is inaccurate for a flat voltage curve, in cases where multiple states of charge can have the same terminal voltage.

2.4.2.3 Impedance Measurement-based SOC Calculation

This method needs an electrochemical impedance spectroscopy (EIS) device which is hard to be equipped in-vehicle and is thus limited to laboratory settings. In this method, impedance characterization is carried out by exciting the battery at a range of frequencies. The SOC can then be estimated based on the measured impedance.

A review of various SOC and SOH estimation strategies based on impedance measurements has been presented in [57]. One of the main conclusions presented in this research survey is that the ambient temperature will greatly influence the battery impedance and accordingly its SOC estimate especially at low frequencies. Therefore, in order to estimate the battery SOC and SOH based on impedance measurements in an un-controlled environment, high frequencies (10 Hz to 100 Hz) must be used, [57]. At these high frequencies, the temperature effects are minimized (less than 10%), [57].

The main disadvantages of relying on impedance to estimate the battery SOC is that the changes in the impedance from half charge to fully charge is negligible especially for lithium-Ion batteries, [58]. Therefore, relying on impedance measurement to estimate the battery SOC will induce large errors, [58]. In addition, as battery ages, battery impedance significantly changes therefore expressing the SOC as a function of the impedance will result in SOC errors and misleading estimates, [58]. Furthermore, at high C-rates, the impedance varies in a nonlinear fashion with SOC which results in further errors, [59]. To overcome this problem, current values along with the impedance have to be considered to provide an accurate SOC estimate, [58].

2.4.2.4 OCV Measurement-based SOC Calculation

In this method, SOC can be calculated by measuring the battery open circuit voltage (OCV) since a good agreement exists between SOC and OCV. This relationship is assumed to remain fixed at different C-rates and at various temperatures, [53]. This relationship can be derived by allowing the battery to relax to the OCV after a certain current excitation. This can be done by cycling the battery using full charge/discharge cycles at a very low C-rates and calculating the average of the two curves, [60]. Alternative method is calculating the OCV (or EMF) using Nernest equation (Equation (2.19)). It is a simple method to estimate the SOC by measuring the OCV. However, it requires zero current measurements thus cannot be implemented during vehicle runtime as it requires the battery to rest completely after the relaxation effect.

Even though the OCV-based SOC estimation is extremely simple to implement, it sometimes lead to misleading SOC estimates. This is due to the existence of flat voltage regions where multiple values of SOC can have the same OCV. In order to demonstrate this phenomenon, an experiment has been conducted on a 2.3 Ah lithium Iron Phosphate (LiFePO4) cell as follows. The test has been conducted at a very low C-rate of C/15 in order to obtain the OCV-SOC relationship. The OCV versus time for both charging and discharging is plotted in Figure 2.9. The OCV curves for both charging and discharging are plotted versus SOC as shown in Figure 2.10.

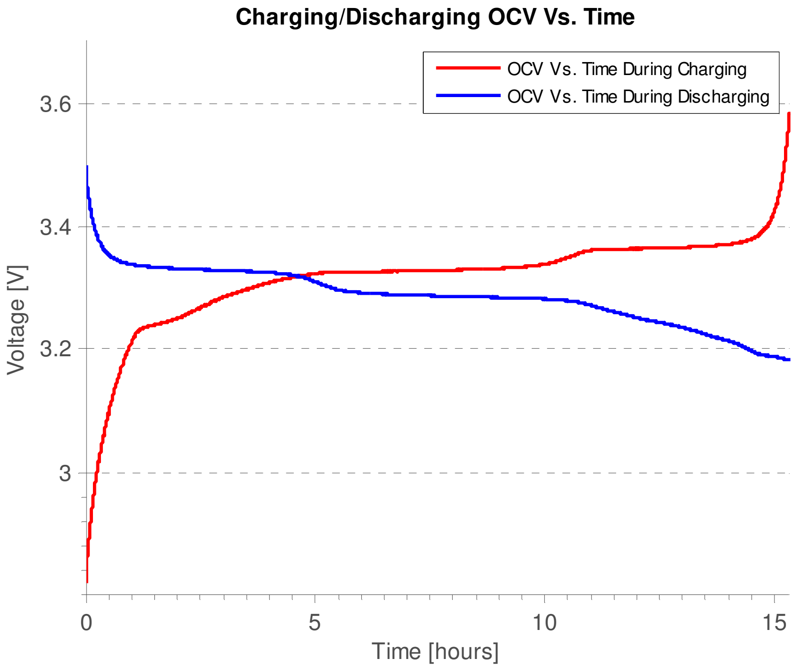

Figure 2.9. Charging/Discharging OCV vs. Time (~C/15)

The very low C-rate (C/20 or C/15) here minimizes the battery dynamics. It is clear from Figure 2.10 that the battery's behaviours during charging and discharging are not identical due to the hysteresis effect. In order to obtain one curve to represent the OCV-SOC relationship, data has been resampled to 50 points for each of the charging/discharging curves and then averaged as shown in Figure 2.11.

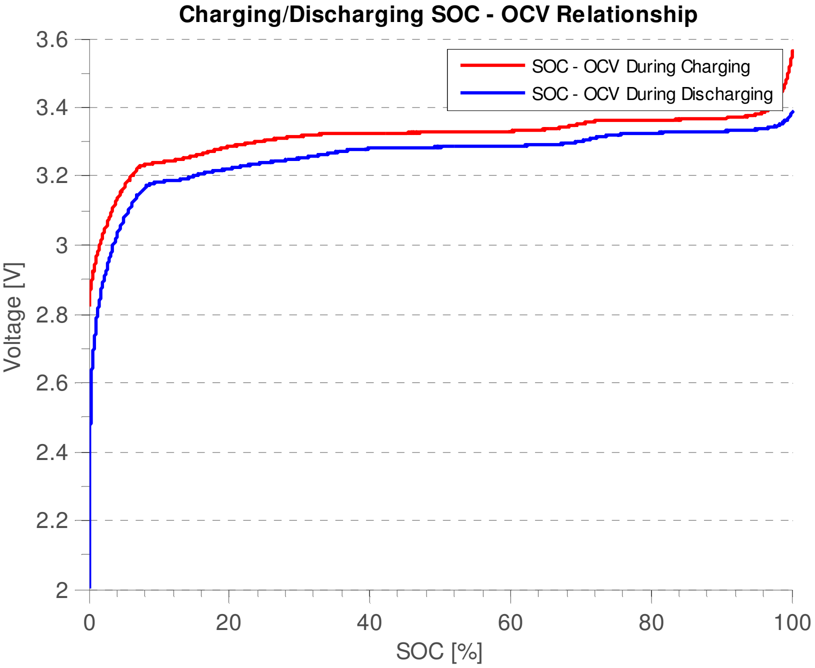

Figure 2.10. SOC-OCV relationship for both charging and discharging

As shown in Figure 2.11, relying on the OCV to estimate the state of charge will lead to misleading SOC estimate since there is a wide flat area between 20% and 90% SOC. Accordingly, this method is relatively challenging for estimating the SOC in case of flat OCV-SOC curves.

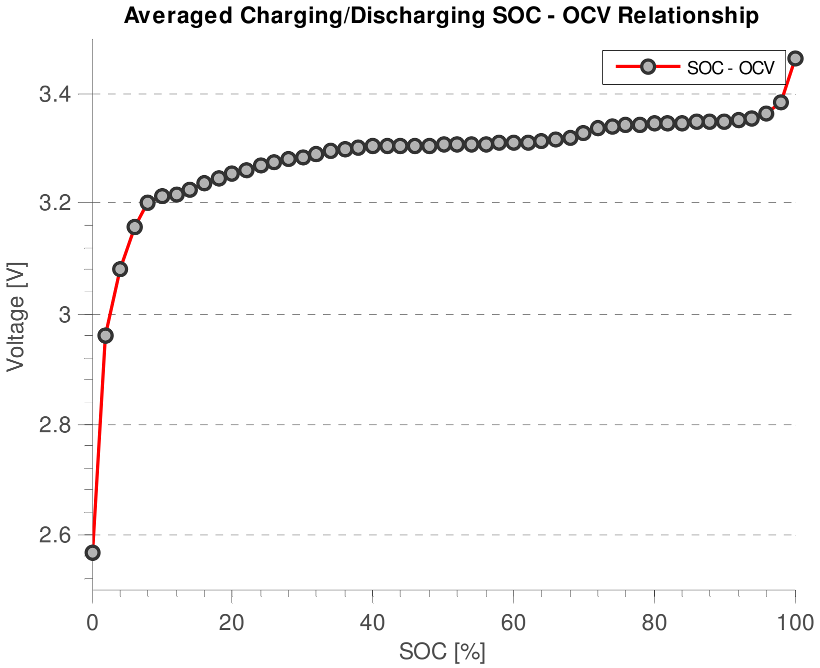

Figure 2.11. Charging and Discharging Averaged SOC-OCV Curve

In order to measure the OCV, the battery has to come to a complete rest which is not practical in real-time applications. In [58], a SOC estimation strategy was developed by estimating the OCV based on currents, voltages, and resistance measurements, and then calculating the SOC by correlating the OCV to the SOC, [54]. The method divides the SOC range into two distinct ranges, namely: the linear and the hyperbolic regions. The rate of change in the hyperbolic region (at extreme values of SOC) varies much faster compared to the linear region, [58].

2.4.3 Adaptive Techniques

Adaptive techniques for SOC estimation are extremely important especially for automotive applications where having an accurate, reliable, and robust estimate is necessary to mitigate the driver range anxiety concerns and ensure safety. In the literature, adaptive SOC estimation techniques are classified as one of the following: ***Fuzzy Logic, Artificial Neural Networks, and filter/observer-based techniques.***

2.4.3.1 Fuzzy Logic-based SOC Estimation

Fuzzy logic techniques rely on approximate functions rather than exact values thus provide the flexibility of estimating the SOC given ambiguities or uncertainties in the collected data, [52]. Fuzzy logic techniques use heuristics that relate factors such as the discharge/charge C-rate, temperatures, and resistances to the battery SOC and SOH. Extensive experimental data, also called qualitative (symbolic) information, is expressed in a form of Boolean or fuzzy if-then rules. The a-priori knowledge is presented in the form of causal relationships between inputs and SOC/SOH.

Fuzzy logic-based SOC estimation techniques have the ability to process data and generate a SOC estimate without having a full understanding of the underlying battery chemical reactions and without the need for a battery model. Furthermore, they may be used in real-time applications and are applicable to all battery chemistries. Their limitation is that membership function characterizations are extremely subjective, [1].

A series of papers have been published to estimate the SOC and SOH using fuzzy logic. A patented methodology has been presented in [61, 62, 63]. In [64, 65], a fuzzy logic-based strategy for SOC and SOH is presented. Training data of measured impedance collected using EIS has been used. These include three inputs representing impedance at three specific frequencies and one output representing the SOC. Furthermore, three frequencies are selected in order to relate impedance to specific values of the SOC. The strategy provides a robust SOC/SOH estimate. Its limitation is that it requires an AC signal generator to excite the battery at various frequencies.

2.4.3.2 Artificial Neural Networks

Artificial Neural Networks (ANNs) are mathematical models inspired by the human brain that are able to learn and recognize patterns. ANNs are capable of mapping input to output datasets using a set of neurons that are interconnected with weights. ANNs can be applied to battery modeling and for state of charge estimation applications. This is an online technique that is appropriate for all battery chemistries but requires training data specific to the battery and is computationally expensive. In [66], an improved ANN model based on Thevenin model presented, capable of predicting the SOC in real-time. The proposed technique is verified by simulation and experimental data, [66].

An ANN-based SOC estimation technique has been presented in [67]. The strategy works by incorporating a series of ANNs. The first network predicts when a specified voltage limit has been reached and then estimating the remaining run time. The other networks work in an adaptive way to modify the first network's weights based on number of cycles, [67]. The technique requires extensive data for network training.

In [42], an ANN has been used to provide a SOC estimate using measurements such as temperature, current, and previous SOC values from a 4.2 V, 100 Ah lithium polymer cell. The technique has been verified using currents, voltages, and state of charge data from a European urban driving test. In this research, a recurrent ANN has been used since it takes into consideration previous input values in addition to current ones in providing an output estimate which is suitable in most battery applications, [42].

In [68], an ANN-based SOC estimation strategy for pulsed input currents has been proposed. The battery SOC is related to the battery chemistry, temperature, load current, and history. The method utilizes a three layered feed forward artificial neural networks to map the inputs to the outputs, [68]. The new method investigates pulse current loads instead of fixed discharge rates, [68]. Experimental data has been used to train the network using the back propagation algorithm. The number of hidden neurons have been optimized to generate the best SOC estimate.

In [69], a three layered ANN has been trained using an evolutionary algorithm. Five inputs have been used as follows: battery terminal voltage, voltage derivative, voltage second derivative, discharge current, and battery temperature. The parallel chaos immune evolutionary algorithm has been selected in order to overcome the local minima problem associated with the back propagation algorithm, [69]. The estimated SOC is compared against the actual battery SOC and the results indicate the effectiveness of the proposed technique, [69].

2.4.3.3 Filters/Observers-based SOC Estimation

State and parameter estimation theories are used to extract information by finding a real-time value of a particular parameter of interest given uncertain observations. States are descriptive of the system dynamics; for example, in battery systems, the battery state of charge and hysteresis represent system states. A filter can be used to estimate one or more of the system states based on a dynamic model and using sensor measurements. The filter can be applied to both linear and nonlinear systems in the presence of uncertain observations and noisy signals.

In order to estimate the battery SOC using filters and observers, an accurate battery model along with a robust estimation strategy is necessary. It is an online technique that can be applied to all battery chemistries, [1]. In this section, a summary of advanced estimators such as the Linear Kalman Filter, the Extended Kalman Filter, the Sigma-point Kalman filter, the Particle Filter, the Smooth Variable Structure Filter, as well as state observers is presented. The above filters are model-based and can estimated the battery SOC using any of the above mentioned models, namely: ***electrochemical, equivalent circuit,*** or ***empirical based models.***

Electrochemical model-based SOC Estimation

As previously mentioned, electrochemical models provide a connection with the physical reactions inside the cell and are thus favoured in comparison to equivalent circuit-based models where minimal or no physical significance is present.

In [70], an estimation strategy for state of charge, potentials, and concentration gradients is presented that uses the Kalman filter in conjunction with a reduced-order electrochemical battery model. Estimates are compared against experimental data from a 6 Ah electric vehicle battery cell, [70]. The filter provides accurate and stable estimates for low current input values. However, at very high C-rates, the estimates exhibit large errors, [70]. The proposed technique is computationally efficient and suitable for real-time applications on board a battery management system, [70].

In [22], a state estimation based on an output error injection observer using a reduced set of partial differential algebraic equations that describe the solid and electrolyte concentrations and potentials is presented. Simulation and experimental results using real-world driving cycles such as the Urban Dynamometer Driving Schedule (UDDS) demonstrate the effectiveness of the proposed technique, [22].

Empirical Model-based SOC Estimation

In [71], an Extended Kalman filter has been applied to estimate model parameters and SOC using 6 behavioural models. A dual state and parameter estimation technique based on the Kalman filter is applied. Quantities that change quickly such as the SOC are considered as a system state while quantities that slowly change such as battery capacity are considered as system parameters, [71]. Two filters were used to estimate both the parameters and the states in a dual form, [71].

In [49], a state of charge estimation technique based on a linearized battery model is presented. In order to overcome the nonlinear behaviour of the battery, the OCV-SOC relationship has been divided into piece-wise linear sections and model parameters are estimated for each section, observers are then applied to estimate the state of charge using this linear model. This technique has been verified using 1.5 Ah lithium-polymer cells, [49].

In [72], Plett proposed a method for SOC estimation using the Sigma-point Kalman filter. The Sigma-point Kalman filter provides more accurate results compared to the standard extended Kalman filter while preserves the computational efficiency which makes it effective for SOC estimation, [72].

Equivalent circuit-based SOC Estimation

A SOC estimation strategy based on equivalent circuit models and using the Extended Kalman filter has been presented in [73]. An added RC element is used to improve the accuracy of the equivalent circuit models. The extra RC element models the concentration polarization and the electrochemical polarization, [73]. A genetic algorithm is used to obtain the model parameters followed by the Extended Kalman Filter for SOC estimation. Five equivalent circuit models have been applied and verified using the Dynamic Stress Test, and the Federal Urban Driving Schedules (FUDS). In addition, the sensitivity of the technique to the initial values of the SOC has been investigated and the initial error in the SOC has been significantly mitigated using the proposed strategy, [73].

In [74], a SOC estimation strategy is proposed using an observer in conjunction with an equivalent circuit-based R-RC-RC model. An adaptive battery parameters/SOC co-estimation strategy is presented where the battery parameters are fed to an optimized observer for estimating the SOC, [74]. A piecewise linear approximation of the OCV-SOC relationship with varying coefficients has been conducted and a moving window least-square parameter identification has been used to obtain model parameters, [74]. The technique was verified using experimental and simulation data sets. Furthermore, the SOC co-estimation algorithm has been compared to a Sliding Mode Observer and the Extended Kalman filter. Results indicate the necessity of updating the parameters while estimating the SOC in order to increase the estimation accuracy and robustness, [74].

2.5 Battery Aging Models

Two important research areas found in literature that relate to battery safety include ***health condition monitoring*** and ***prognostic health monitoring***. The former enables tracking of the aging and degradation effects that occur in the battery due to cycling, [75] ***Prognostic*** helps in predicting the remaining battery life time (run-to-failure) and thus provides an alarm to avoid degradation of performance below a minimum acceptable level, [75]. This section is divided into 2 parts, namely: the description of the ***aging phenomenon***, and the ***aging models*** currently present in the literature.

2.5.1 Aging Phenomenon

The aging phenomenon is considered in relation to ***contributing factors***, ***aging mechanisms, and recent aging studies***.

2.5.1.1 Aging Contributing Factors

Battery aging is a very complex process that depends on multiple factors that interact together and cause degradation. The main factors that contribute to aging are discussed below:

Temperature

At higher temperatures, aging is accelerated due to rapid chemical reactions which exponentially increase with temperature according to the Arrhenius equation, [76]. For every 10℃ rise in temperature, the rate of reactions that contribute to aging are doubled, [76]. Accordingly, the battery capacity is greatly affected by elevated temperatures. For instance, for every temperature increase of 6.85 degC, the capacity loss is doubled assuming 66% loss is due to cycling and the remaining 34% is due to calendar, [77]. Therefore, most electric vehicle manufacturers such as Ford, Tesla, and General Motors (GM) are currently implementing a circulating liquid-based active thermal management system to maintain the battery at an acceptable range of temperatures and thus avoiding accelerated aging due to cycling and temperature.

Overcharging and Excessive Discharging

When a battery is overcharged, irreversible reactions force ions to intercalate after all active solid particles are saturated, [76]. Furthermore, exceeding the allowable maximum battery voltage leads to significant increase in temperature and pressure which might cause cell damage, fires, and short circuits. For Ni-MH batteries, a 0.2 V overcharging results in 40% cycle life capacity loss while 0.3V lead to 66% capacity loss, [78, 76]. Over-discharging also leads to a shortened battery life and even to reversed electrodes.

Depth of Discharge (DOD)

Depth of discharge has a major impact on the battery cycle life, the relationship between the DOD and the cycle life is exponential, [76]. For example, if the DOD for a given cell is 90%, the cell will last for 500 cycles. However, if the same cell is cycled to a 10% DOD, the battery can be cycled up to 5000 cycles, [76]. In order to slow down the battery degradation rate, which is affected mainly by the DOD, most car manufacturers limit the usable range of the battery. For example, General Motors (GM) utilizes about 65% of the Volt's battery capacity, [77]. This is achieved by maintaining the SOC variations between 22% and 87%. The new BMW ActiveE has a 32kWh battery pack, however, the usable capacity is only set at 28kWh in order to prolong the battery life, [79].

Current Severity (C-rates)

Higher C-rates adversely contribute to battery aging. As shown in [80], higher C-rates cause loss of electrode conductivity which in turn result in an uneven charge distribution leading to added stresses and a lowering of cycle life.

2.5.1.2 Battery Aging Mechanisms

A range of studies have been conducted for studying the changes that occur inside a battery as it ages. As reported in many publications, capacity fade and degradation effects are mainly due to two main factors, namely: ***film growth*** and ***carbon retreat,*** [81]. These two phenomenon are found to be changing in a sigmoidal fashion (with sudden changes after a number of cycles), [81]. In [81], the authors suggest that a reaction between the cathode active materials and the electrolyte resulted in the formation of a SEI which in turn changes the particle surface composition leading to the breaking down of the carbon conductive paths. This causes carbon retreat and sudden acceleration of capacity fade.

According to [82], battery aging occurs due to the formation of an insulating layer on the surface of the electrodes (mainly the cathode electrode) which in turn leads to an increase in the impedance of the positive electrode, [82]. In this paper, standard tests conducted at high temperatures ranging from $40\ to\ 70\ ℃$ are used for verifying that the charge-transfer resistance increases on the cathode and is the main contributor to aging and degradation in performance, [82]. X-ray absorption spectroscopy and high-resolution electron microscope (HREM) have been used to identify significant changes in the features of the electrode surface structures and compositions in comparison to the bulk, [82].

Another factor to consider is the loss of electron conductivity in the cathode [83]. This phenomenon is also related to the (carbon retreat) phenomenon which is the disconnection of carbon within the cathode particles due to the formation of a SEI layer. Using images from current-sensing atomic electron microscopy, the cathode surface electronic conductance of nine $LiNi_{0.8}Co_{0.2}O_2$ cells have been significantly decreased, thus contributing to aging. In addition, it has been shown that the rate of decrease in the cell conductance is directly proportional to temperature, [83]. Cells that are cycled at elevated temperatures exhibit a dramatic increase in the surface resistance. In addition, discharging the cells at higher C-rates will lead to a larger loss in conductivity between particles in the active material matrix, [84]. This results in an irregular current distribution which generally imposes more stresses that lead to shorter battery life and to performance degradations, [84].

2.5.1.3 Battery Aging Studies

In [85] and under the MARS Rover program, $LiNio_2$ batteries with 9.2 Ah capacity were subjected to a 100% DOD at $-20°C$ and at $25°C$. In this research, the cycle life performance was fairly good. At $-20°C$, the batteries lost 8% of the capacity after 500 cycles and at $25°C$, the batteries lost about 13%, [85]. Reference tests such as the capacity and DC impedance tests were conducted every 500 cycles, [85]. Regarding calendar life, the batteries exhibited a 9.65% loss in 8 years and 15.87% loss in 15 years, [85]. This study demonstrates a better life performance for batteries at low temperatures and improved robustness to cycling and storage, [85].

In [81], an aging study using a well-defined Dynamic Stress Test (DST) has been conducted on 900 mAh $Li_xNi_{0.8}Co_{0.15}Al_{0.05}O_2$ cells. Reference performance tests have been conducted every 60 DST cycles to evaluate the degradation of performance such as the peak power capability, capacity fade, and impedance measurement. It has been shown that capacity fade is mainly affected by the cell polarization resistance increase, [81]. During testing, a sigmoid change in the capacity were found at two distinct stages of life, namely: capacity loss from 810 to 730 mAh occurred between cycles 225 and 250; and, another one from 730 to 600 mAh between 280 and 320 cycles, [81].

2.5.2 Battery Aging Models

Two approaches are commonly implemented for modeling aging and lifetime prediction, namely: ***performance-based models*** and ***weighted ampere-hour throughput*** models, [86]. Regarding ***performance models***, they can account for the rate of change of model parameters as the battery ages, [86]. For instance, in equivalent circuit-based models, the values of capacitors and resistors can adapt as battery slowly ages and information regarding the end of life (EOL) can be inferred from these values. In the other method of the ***weighted ampere-hour throughput,*** the aging model works by tracking the number of cycles (ampere-hour throughput) that the battery exhibits. These techniques have to consider the conditions where the battery is cycled, such as charging-discharging rates, temperatures, and extreme out-of tolerance aggressive conditions, [1].

In [87], a novel model-based algorithm for battery prognosis bas been developed. The aging model can predict the battery life and keep track of the changing model parameters as battery ages while taking into consideration various factors that contribute to aging such as the DOD, current severity, and temperature, [87]. The model is based on additive damage accumulation law that is similar to the Palmgren-Miner rule used for mechanical fatigue modeling, [87].

In [76], an aging model for HEVs has been developed. Batteries are limited to a DOD of above 50%, [76]. Laboratory experiments from fatigue tests have been transferred to the battery testing field. The developed model relates battery aging to factors such as operating temperature and current history, [76]. The major advantage of this study is the use of real-world test data rather than pre-defined charging and discharging cycles at fixed C-rates. The residual life after a specific amount of discharging events is defined as follows, [76]:

$$Residual\ life\ = 1 - \sum_{i=1}^{N} L_i/L_{tot}(i) \tag{2.38}$$

The $L_{tot}$is defined as the total amount of charge that can be drawn from the battery. The charge life (L_{Ah}) is defined as the life expressed in Ah which is defined as follows, [76]:

$$L_{Ah} = L_{cyc} * DOD * Ah_0 \tag{2.39}$$

For example, the charge life at 10% DOD can be calculated as follows:

$$L_{Ah}(DOD = 10\%) = 5400\, cycles * \frac{10}{100} * 6.5Ah = 3510\, Ah$$

Since aging is affected by the shape of the current profile as well as the DOD, the RMS of the profile must be taken into consideration as a weighting factor to calculate the effective DOD from the actual DOD. Thus the DOD_{eff} can be derived from the measured DOD (DOD_{meas}) as follows, [76]:

$$DOD_{eff} = f\left(\frac{RMS}{RMS_{nom}}, \frac{T}{T_{nom}}\right) * DOD_{meas} \tag{2.40}$$

Where the cycle is defined as the time between successive points when the current is zero, the DOD_{meas} is calculated as follows, [76]:

$$DOD_{meas} = SOC_{start} - \frac{\int Idt}{C_{nom}} \tag{2.41}$$

In [84], a life prediction method was developed to determine the effect of two main parameters on battery aging, namely: depth of discharge and rate of discharge. The effect of the depth of discharge for a given event is described by the following equation, [84]:

$$Ah_{eff} = \left(\frac{D_A}{D_R}\right)^{u_o} e^{u_1(\frac{D_A}{D_R}-1)} Ah_{actual} \tag{2.42}$$

Where, D_R is the percent depth of discharge at which the rated cycle life was determined, D is the actual discharge as a percentage of rated capacity, Ah_{eff} is defined as the effective ampere-hour discharge after depth of discharge and rate of discharge adjustments, Ah_{actual} is the actual ampere-hour throughput. For the rate of discharge, the effective discharge for a certain event is calculated as follows, [84]:

$$Ah_{eff} = \left(\frac{C_R}{C_A}\right)^{v_o} e^{v_1(\frac{C_R}{C_A}-1)} Ah_{actual} \tag{2.43}$$

Where, C_A is defined as the capacity of the cell defined at a given discharge rate, and C_R is defined as the capacity defined at rated discharge rate. By combining both effects through multiplication, [84]:

$$Ah_{eff} = \left(\frac{D_A}{D_R}\right)^{u_o} e^{u_1(\frac{D_A}{D_R}-1)} \left(\frac{C_R}{C_A}\right)^{v_o} e^{v_1(\frac{C_R}{C_A}-1)} Ah_{actual} \tag{2.44}$$

This equation can be used to calculate the effective Ah throughput for a given discharging event. By summing the effective discharges from a series of n discharge events, a battery lifetime prediction can be calculated as follows, [84]:

$$L_{time} = \frac{Ah_{R_{Total}}}{Ah_{A_{Total}}/T} = \frac{L_R D_R C_R}{\sum_{i=1}^{n} Ah_{eff}} T \tag{2.45}$$

Where, $Ah_{R_{Total}}$ is the life of the cell (in Ah) under known, well-defined charging and discharging cycles at a specified depth of discharge and rated discharge current. $Ah_{A_{Total}}$ is defined as the life of the cell under actual operating conditions and T is the operating time, [84].

2.6 SOH Literature Review

SOH is defined as the ability of the battery to store and retrieve electric charge in addition to the ability to keep this charge for long periods in comparison to a fresh, nominal battery [88, 75]. SOH is important in BEVs as they will lead to maximizing the utilized energy from a given battery. Since SOH cannot be physically measured, it must be inferred from other readily available measurements. Two main parameters are generally used to quantify SOH namely; internal resistance and capacity fade, [75]. The main characteristic of the SOH estimation in comparison to the SOC estimation is that SOH dynamics are relatively slow compared to those of the SOC, [75]. SOH dynamics vary after many complete charging/discharging cycles which might take weeks to exhibit in performance. Conversely, SOC varies rapidly within the charging/discharging cycle. Nonetheless the same techniques can be used for both SOC and SOH estimation as shown in this section, [75].

SOH is crucial as it reflects the state of the battery in comparison to a healthy one. A combination of several parameters can be used to conclude the SOH such as: ***cell conductance, cell impedance, capacity, internal resistance, self-discharge, charge acceptance, cycle counting, mobility of electrolyte, and discharge capabilities,*** [1]. In order to come up with a collective decision out of all these parameters, a weighting factor has to be assigned to each parameter depending on its importance and based on prior knowledge and experience, [1]. The battery might exhibit a high rate of self-discharge or high internal resistance thus indicating an aged battery. A number based on all these factors is generated and compared to the one based on a healthy fresh battery, [1]. The following subsections summarize the techniques used for SOH estimation.

2.6.1 Discharge test

The discharge test is used for capacity calculation by completely discharging the battery from a fully charged state (after a constant current-constant voltage (CCCV) charge). The test is widely known as the static capacity test. Even though the test is accurate for calculating the available discharge capacity, it cannot be conducted online on board a battery management system. This is due to the fact that the test alters the battery state and in addition, it is a time consuming and results in loss of energy, [1].

2.6.2 Fuzzy Logic SOH Estimation

Fuzzy logic is a powerful tool in battery health monitoring as they are able to map complex input-output data without the need of an explicit mathematical model, [89]. Singh et al. presented a SOC and SOH estimation strategy based on fuzzy logic in [90] using data from impedance spectroscopy at different battery states of charge (from SOC = 0% to 100%) over 100 cycles. Three frequencies were used to excite the battery. Features from this data set (real and imaginary parts) were used to develop fuzzy logic models, [90]. Experimental results demonstrated the effectiveness of the proposed technique for SOC estimation to within ±5% accuracy, [90].

Salkind et al. also developed a practical method for SOC and SOH estimation based on fuzzy logic, [89]. The technique has been verified on two different battery chemistries, namely Lithium/sulfur dioxide and Nickel Metal Hydride, [89]. One of the main drawbacks of this technique is that an external source is necessary to excite the battery at specific frequencies, thus limiting its applicability when considering real-time, practical, in-vehicle implementations, [75].

2.6.3 Artificial Neural Networks (ANNs)-based SOH Estimation:

As previously mentioned, ANNs have been widely used in battery SOC estimation since they are capable of mapping any inputs to outputs with potentially high accuracy. This mapping can be attained given a reasonable number of neurons and a sufficient number of training datasets.

Besides their applicability in SOC estimation, ANNs can also be used for SOH estimation. In [91], a method for SOH estimation based on ANNs by deducing the battery available capacity has been presented. In this research, a three layered ANN has been used with the discharge current as the input to the network and the available capacity as the network output, [91]. Thus the network was able to map the discharge current to the available battery capacity, [91]. The performance of the proposed methodology has been compared to the conventional Peukert equation which relates the available capacity to the discharge current as follows, [92]:

$$C_a = K/I_d^{(n-1)}$$

Where K and n are constants that depend on the temperature and the concentration of the electrolyte, [91].

In [93], artificial neural Networks were trained on fuzzified data and the outputs were then correspondingly defuzzified, [93]. The SOH estimation of the battery using this method were obtained under 3 minutes as documented in [93]. One of the main advantages of neural networks is the ability to adapt and self-learn through experience. The accuracy of the technique can be significantly enhanced by incorporating more experimental data,

[93]. The technique has been commercially available in the Cadex QuickTest C700 battery analyzer platform, [93]. The system can read the battery configuration code and adapt to different battery chemistries, [93].

2.6.4 Filters/Observer-based SOH Estimation

For practical applications and real-time implementation on board of a vehicle controller, Kalman filters are applied for both SOC and SOH estimation, [75]. As previously mentioned, an extended Kalman filter-based state estimation strategy has been applied to estimate model parameters and SOC based on 6 behavioural models in [71]. Furthermore, estimating battery parameters that provide an indication of the battery state of health and state of power have been presented in the same paper, [71]. The method works by estimating the battery capacity and the internal resistance thus provide an indication of both capacity and power fade [71]. Experimental results indicate the effectiveness of the proposed strategy.

In [94], SOC and capacity estimation based on equivalent circuit models in conjunction with the EKF are presented. This paper reports a comparatively improved accuracy for capacity estimation. The presented technique incorporates a state projection methodology for stable and increased capacity estimation accuracy, [94]. Furthermore, since capacity is a slowly varying parameter, a time-scale separation has been implemented thus producing an SOC estimate at a faster rate compared to the SOH thus resulting in reduced computational complexity, [94]. In general, one of the major drawbacks of the EKF is that the algorithm's stability and convergence are not guaranteed, [52].

A SOH technique based on the Extended Kalman filter (EKF) has been presented in [95]. In this research, EKF has been used to estimate the bulk capacitance thus providing an indication of the battery SOH. Experimental results demonstrate the better accuracy (2%) of the proposed technique compared to other techniques in estimating the SOC and SOH, [95].

A real-time, impedance-based parameter identification method for SOC and SOH estimation has been proposed in [96]. The EKF can estimate the battery model parameters based on Randles' model, [96]. More RC blocks are used to model the Warburg impedance but this modification has led to over-parameterization, thus causing divergence problems for the EKF. The technique has been verified using the UDDS Cycle, [96].

Saha et al. [97] proposed an estimation of battery SOC, SOH, and RUL using Bayesian frameworks based on Relevance Vector Machines (RVMs) and particle filters. A combination between equivalent-circuit based models and statistical models of state-transitions and aging processes has been applied to experimental batteries, [97]. Experimental results indicate the effectiveness of the proposed strategy, [97].

2.7 Conclusion

This paper provides a summary of published literature on battery modeling, model parameters identification and extraction, and state of charge and state of health estimation. It is specifically intended for batteries used for energy storage in electric and hybrid vehicles. The following models are considered: equivalent circuit-based models, electrochemical battery models, behavioural models (empirical), hydrodynamic models, tabulated data models, and black-box battery models.

Equivalent circuit and behavioural models are easy to implement and require less parameters to tune. However, they have little or no physical significance. On the other hand, electrochemical models relate to physical reactions in cells and are capable of modeling lithium intercalation dynamics inside the electrodes and the electrolyte. They are thus favoured in state of health estimation. Full-order electrochemical models are complex and require reduction before online implementations in battery management systems. Even though the reduction process results in loss of information, the reduced order models are still able to provide an accurate measure of physical effects inside the cell.

For model and parameter identification, optimization and estimation strategies can be effectively applied on any of the above mentioned battery models. However, it has been shown that identifying model parameters offline using optimization techniques provide more robust estimates and greater stability in comparison to online strategies.

For the battery SOC and SOH, these can be estimated using conventional coulomb counting, Artificial Neural Networks, Fuzzy logic techniques, and filters/observers. The conventional coulomb counting is accurate provided that a known initial SOC is provided and while maintaining a periodic calibration, these are difficult to realize on board of a BMS. Filters and observers for SOC and SOH estimation are the most favoured techniques since they can be effectively utilized on any of the above-mentioned models and can provide a relatively high degree of accuracy.

References

[1] B. Pattipati, C. Sankavaram and K. R. Pattipati, "System Identification and Estimation Framework for Pivotal Automotive Battery Management System Characteristics," 2010.

[2] C. S. K. P. B. Pattipati, "B. Pattipati, C. Sankavaram, K.R. Pattipati," *IEEE Trans. Syst. Man Cybern,* p. 869–884, 2011.

[3] M. Doyle, T. Fuller and J. Newman, "Modeling of galvanostatic charge and discharge of the lithium/polymer/insertion cell," *J. Electrochemical Society,* pp. 1526-1533, 1993.

[4] FullerT., M. Doyle and J. Newman, "Simulation and optimization of the dual lithium ion insertion cell," *J. Electrochemical Society,* pp. 1-10, 1994.

[5] Z. M. Salameh, M. Casacca and W. Lynch, "A Mathematical Model for Lead-Acid Batteries," vol. 7, no. 1, 1992.

[6] J. Appelbaum and R. Weiss, "An Electrical Model of the Lead-Acid Battery," 1982.

[7] R. Weiss and J. Appelbaum, "Battery State of Charge Determination in Photovoltaic systems," vol. 129, no. 9, 1982.

[8] X. Hua, S. Lia and H. Penga, "A comparative study of equivalent circuit models for Li-ion batteries," vol. 198 , no. 359– 367, 2012.

[9] Y.-H. Chiang, W.-Y. Sean and J.-C. Ke, "Online estimation of internal resistance and open-circuit voltage of lithium-ion batteries in electric vehicles," vol. 196, 2011.

[10] M. Verbrugge and E. Tate, "Adaptive state of charge algorithm for nickel metal hydride batteries including hysteresis phenomena," vol. 126, Febrary 16, 2004.

[11] X. Hu, S. Li and P. Huei, "A comparative study of equivalent circuit models for Li-ion batteries," vol. 198, 2012.

[12] P. Baudry, M. Neri, M. Gueguen and G. Lonchampt, "Electro-thermal modelling of polymer lithium batteries for starting period and pulse power," vol. 54, no. 393-396, 1995.

[13] "http://www.thermoanalytics.com/docs/batteries.html," 2012. [Online].

[14] N. Chaturvedi, R. Klein, J. Christensen, J. Ahmed and A. Kojic, "Algorithms for Advanced Battery-Management Systems Modeling, Estimation and Control Challenges for Lithium-ion Batteries," *IEEE CONTROL SYSTEMS MAGAZINE,* pp. 49-68, 2010.

[15] J. Newman and W. Tiedemann, "Porous-electrode theory with battery applications," *AIChE Journal,* vol. 21, no. 1, pp. 25-41, 1975.

[16] A. J. Bard and L. R. Faulkner, "Electrochemical Methods: Fundamentals and Applications," *Russian Journal of Electrochemistry,* vol. 38, no. 12, 2002.

[17] D. Domenico, S. Anna and F. Giovanni, "Lithium-Ion Battery State of Charge and Critical Surface Charge Estimation Using an Electrochemical Model-Based Extended Kalman Filter," *Journal of Dynamic Systems, Measurement, and Control,* vol. 132, pp. 1-11, 2010.

[18] K. Smith and C.-Y. Wang, "Solid-state diffusion limitations on pulse operation of a lithium ion cell for hybrid electric vehicles," *Journal of Power Sources,* vol. 161, no. 1, pp. 628-639, 2006.

[19] D. D. Domenico, G. Fiengo and A. Stefanopoulou, "Lithium-Ion battery State of Charge estimation with a Kalman Filter based on a electrochemical model," *IEEE Interantional Conference on control Applications (CCA),* pp. 702-707, 2008.

[20] M. Doyle and Y. and Fuentes, "Computer Simulations of a Lithium-Ion Polymer Battery and Implications for Higher Capacity Next-Generation Battery Designs," *Journal of Electrochemistry Society,* p. A706–A713, 2003.

[21] C. W. K. Smith, "Solid-state diffusion limitations on pulse operation of a lithium-ion cell for hybrid electric vehicles," *Journal of Power Sources,* p. 161:628–639, 2006.

[22] R. Klein, N. A. Chaturvedi, J. Christensen, J. Ahmed, R. Findeisen and A. Kojic , "Electrochemical Model Based Observer Design for a Lithium-Ion Battery," vol. 21, no. 2, 2013.

[23] FullerT., M. Doyle and J. Newman, "Simulation and optimization of the dual lithium ion insertion cell," *J. Electrochemical Society,* pp. 1-10, 1994.

[24] P. Ramadass, Haran, B., Gomadam, P. M., White, R. and Popov, "Development of First Principles Capacity Fade Model for Li-Ion Cells," vol. 151, no. pp. A196–A203, 2004.

[25] C. Y. Wang and W. B. Gu, "Micro-Macroscopic Coupled Modeling of Batteries and Fuel Cells Part 1 . Model Development," *J. Electrochemical Society,* pp. 1-25, 1998.

[26] K. Smith and C. Y. Wang, "Solid-State Diffusion Limitations on Pulse Operation of a Lithium-Ion Cell for Hybrid Electric Vehicles," *Journal of Power Sources,* p. 628–639, 2006.

[27] B. Paxton and Newmann, J., "Modeling of Nickel Metal Hydride," vol. 144, no. pp. 3818–3831, 1997.

[28] O. V. F. a. G. L. Barbarisi, "State of Charge Kalman Filter Estimator for Automotive Batteries," vol. 14, no. pp. 267–275, 2006 .

[29] K. Smith, C. Rahn and C. Wang., "Control oriented 1D electrochemical model of lithium ion battery," no. 48, 2007.

[30] C. Speltino, D. D. Domenico, G. Fiengo and A. Stefanopoulou, "Comparison of Reduced Order Lithium-Ion Battery Models for Control Applications," Shanghai, P.R. China, December 16-18, 2009.

[31] G. Plett, "Extended Kalman filtering for battery management systems of LiPB-based HEV battery packs," *Journal of Power Sources,* p. 252–261, 2004.

[32] R. L. H. II, "An Aging Model for Lithium-Ion Cells," Ph.D. Thesis, University of Akron, December, 2008.

[33] "Extended Kalman filtering for battery management systems of LiPB-based HEV battery packs Part 2. Modeling and identificatio," vol. 134, 2004.

[34] G. L. Plett, "Extended Kalman Filtering for Battery Management Systems of LiPB-Based HEV Battery Packs: Part 2. Modeling and Identification," *Journal of Power Sources,* vol. 134, no. 2, pp. 262-276, 2004.

[35] C. Leontopoulos, M. Etemad, K. Pullen and M. Lamperth, "Hybrid vehicle Simulation for Turbogenerator-based Power-train," vol. 212:317, 1998.

[36] D. Mayer and S. Biscaglia, "Modeling and Analysis of Lead Acid battery," 1989.

[37] D. Mayer and S. Biscaglia, "Use of the Modeling of Lead-acid Battery Operation for the Development of the State of Charge Meter," 1991.

[38] T. Kim and W. Qiao, "A Hybrid Battery Model Capable of Capturing Dynamic Circuit Characteristics and Nonlinear Capacity Effects," vol. 26, no. 4, December, 2011.

[39] V. Rao, G. Singhal, A. Kumar and N. Navet, "Battery modeling for embedded systems," 2005.

[40] M. R. Jongerden and B. R. Haverkort, "Which battery model to use?," vol. vol. 3 , no. 6, December, 2009.

[41] A. Eddahech, O. Briat and J.-M. Vinassa, "Neural Networks Based Model and Voltage Control for Lithium Polymer Batteries," 2011.

[42] O. B. a. J. V. A. EDDAHECH, "Adaptive Voltage Estimation for EV Li-ion Cell Based on Artificial Neural Networks State-of- Charge Meter," 2012 IEEE International Symposium on Industrial Electronics, ISIE 2012.

[43] M. A. Merkle, "Variable Bus Voltage Modeling for Series Hybrid Electric Vehicle Simulation," M.A.Sc Thesis, Virginia Polytechnic Institute and State University , 1997.

[44] C. Speltino, D. D. Domenico, G. Fiengo and A. Stefanopoulou, "Experimental identification and validation of an electrochemical model of a Lithium-Ion Battery," 2009.

[45] J. C. Formana, S. J. Moura, J. L. Steina and H. K. Fathy, "Genetic identification and fisher identifiability analysis of the Doyle–Fuller–Newman model from experimental cycling of a LiFePO4 cell," vol. 210, 2012.

[46] G. L. Plett, "Extended Kalman filtering for battery management systems of LiPB-based HEV battery packs: Part 3. State and parameter estimation," vol. 277–292, no. 134, 2004.

[47] M. Farag, R. Ahmed, A. Gadsden, J. JTjong and S. Habibi, "A Comparative Study of Li-Ion Battery Models and Nonlinear Estimation Techniques," Dearborn, Michigan, 2012.

[48] P. Kumar and P. Bauer, "Parameter Extraction of Battery Models Using Multiobjective Optimization Genetic Algorithms," 2010.

[49] H. Rahimi-Eichi, F. Baronti and M.-Y. Chow, "Modeling and Online Parameter Identification of Li-Polymer Battery Cells for SOC estimation," 2012 .

[50] Y. Hu, S. Yurkovich, Y. Guezennec and B. Yurkovich, "Electro-thermal battery model identification for automotive applications," vol. 196, 2011.

[51] e. a. D. Domenico, "Lithium-Ion Battery State of Charge Estimation with a Kalman Filter Based on a Electrochemical Model," San Antonio, TX, 2008.

[52] S. E. Samadani, R. A. Fraser and M. Fowler, "A Review Study of Methods for Lithium-ion Battery Health Monitoring and Remaining Life Estimation in Hybrid Electric Vehicles," Detroit, Michigan, United States, 2012.

[53] H. Bergveld, W. S. Kruijt and P. Notten, Battery Management Systems: Design by Modelling, Springer, 2002.

[54] K. S. Ng, C.-S. Moo, Y.-P. Chen and Y.-C. Hsieh, "Enhanced coulomb counting method for estimating state-of-charge and state-of-health of lithium-ion batteries," 2009.

[55] W. Peukert, "Elektrotechnische Zeitschrift," 20–21, 1997.

[56] D. Doerffel and S. Abu Sharkh, "A critical review of using the Peukert equation for determining the remaining capacity of lead-acid and lithium-ion batteries," vol. 155 , no. 395–400, 2006.

[57] F. Huet, "A review of Impedance Meausurements for Determination of the State of Charge or State of Health of Secondary Batteries," *Journal of Power Sources,* vol. 70, pp. 59-69, 1998.

[58] M. Coleman, C. K. Lee, C. Zhu and W. G. Hurley, "State of Charge Determination from EMF Voltage Estiamtion: Using Impedance, Terminial Voltage, and Current for Lead-Acid and Lithium-Ion Batteries," *IEEE Transactions of Industrial Eleectronics,* vol. 54, no. 5, 2007.

[59] K. E. and R. De Doncker, "The Nonlinear low frequency impedance of lead/acid batteries during discharge, charge, and float operation," *Interanational Telecommunications Energy Conference INTELEC 2001 (IEE Conference Publications),* pp. 65-72, 2001.

[60] V. Pop, H. J. Bergveld, N. P. H. L. and P. Regtien, "State-of-the-art of battery state-of-charge determination," *Measurement Science and Technology,* 2005.

[61] C. Fennie, P. Singh and D. Reisner, "A Method for Determining Battery State-of- Health Using Intelligent Systems,". U.S. and Taiwan Patent Appls. 12 March 1997.

[62] P. Singh and J. C. Fennie, "A Method for Determining Battery State of Charge Using Intelligent Systems," U.S. Patent No. 6,011,379, Jan 4, 2000". Patent 6011379, 2000.

[63] P. Singh and C. Fennie, "A Method for Determining Battery State-of-Charge Using Intelligent Systems". Taiwan Patent Patent 106,353 , 3 January 2000.

[64] P. Singh and David E. Reisner, "Development of Fuzzy Logic-Based Lead Acid Battery Management Techniques with Applications to 42V Systems," 1998.

[65] P. Singh, C. F. Jr. and D. Reisner, "Fuzzy logic modelling of state-of-charge and available capacity of nickel/metal hydride batteries," vol. 136, 2004.

[66] C. Piao, X. Yang, C. Teng and H. Yang, "An improved model based on artificial neural networks and Thevenin model for nickel metal hydride power battery," 2010.

[67] J.-N. Patillon and O. Gerard, "System for monitoring charging/ discharging cycles of a rechargeable battery, and host device including a smart battery". New York, NY Patent Patent 5825156, 1998.

[68] S. Grewal and D. Grant, "A Novel Technique for Modeling the State of Charge of Lithium Ion Batteries Using Artificial Neural Networks," *INTELEC Conference ,* vol. 484, 2001.

[69] C. Bo, B. Zhifeng and C. Binggang, "State of Charge Estimation based on Evolutionary Neural Network," *Energy Conversion and Management ,* vol. 49, pp. 2788-2794, 2008.

[70] K. A. Smith, C. D. Rahn and C.-Y. Wang, "Model-Based Electrochemical Estimation of Lithium-Ion Batteries," San Antonio, Texas, USA, September 3-5, 2008.

[71] G.L.Plett, "Extended Kalman filtering for battery management systems of LiPB-based HEV battery packs: Part 3. State and parameter estimation," vol. 134, no. 2, August 2004.

[72] G. L. Plett, "Sigma-point Kalman filtering for battery management systems of LiPB-based HEV battery packs," *Journal of Power Sources,* vol. 2, no. 161, p. 1369–1384, 2006.

[73] H. He, R. Xiong and J. Fan, "Evaluation of Lithium-Ion Battery Equivalent Circuit Models for State of Charge Estimation by an Experimental Approach," *Energies ,* vol. 4, pp. 582-598, 2011.

[74] H. Rahimi-Eichi, F. Baronti and M.-Y. Chow, "Online Adaptive Parameter Identification and State of Charge Coestimation for Lithium-Polymer Battery Cells," *IEEE Transactions on Industrial Electronics ,* vol. 61, no. 4, 2014.

[75] S. E. Samadani, R. A. Fraser and M. Fowler, "A Review Study of Methods for Lithium-ion Battery Health Monitoring and Remaining Life Estimation in Hybrid Electric Vehicles," *SAE International ,* 2012.

[76] L. Serrao, Z. Chehab, Y. Guezenne and G. Rizzoni, "An Aging Model of Ni-MH Batteries for Hybrid Electric Vehicles," in *Vehicle Power and Propulsion, 2005 IEEE Conference*, 2005.

[77] "www.mynissanleaf.com/wiki/," [Online].

[78] "http://www.mpoweruk.com/," MPower Solutions Ltd. [Online].

[79] T. Moloughney, "understanding Battery Capacity Loss," www.Bmwblog.com.

[80] "http://www.peve.panasonic.co.jp/catalog/e_kaku.html," Panasonic EV Energy Co.. [Online].

[81] M. Dubarry, V. Svoboda, R. Hwu and B. Y. Liaw, "Capacity and power fading mechanism identification from a commercial cell evaluation," *Journal of Power Sources,* 2006.

[82] D. Abraham, T. R.D. , B. M. , P. I., J. McBreen and K. Amine, "Surface changes on LiNi0:8Co0:2O2 particles during testing of high-power lithium-ion cells," *Electrochemistry Communications,* vol. 4, pp. 620-625, 2002.

[83] R. Kostecki and F. McLarnon, "Degradation of LiNi0.8Co0.2O2 Cathode Surfaces in High-Power Lithium-Ion Batteries," *Electrochemical and Solid-State Letters,* vol. 5, pp. A164-A166, 2002.

[84] S. Drouilhet and B. Johnson, "A battery life prediction method for hybrid power applications," in *35th AIAA Aerospace Sciences Meeting and Exhibit Reno*, Nevada , 1997.

[85] H. Croft, B. Staniewicz, M. Smart and B. Ratnakumar, "Cycling and Low Temperature Performance of Li Ion Cells," in *Energy Conversion Engineering Conference and Exhibit, 2000. (IECEC) 35th Intersociety (Volume:1)*, Las Vegas, NV, 2000.

[86] S. Onori, S. Pierfrancesco, V. Marano, Y. Guezennec and G. Rizzoni, "A new life estimation method for lithium-ion batteries in plug-in hybrid electric vehicles applications," *International Journal of Power Electronics ,* vol. 4, no. 3, 2012.

[87] L. Serrao, S. Onori, G. Rizzoni and Y. Guezennec, "A Novel Model-Based Algorithm for Battery Prognosis," in *Proceedings of the 7th IFAC Symposium on Fault Detection, Supervision and Safety of Technical Processes*, Barcelona, Spain, 2009.

[88] B. S. Bhangu, P. Stone and D. A. Bingham, "Nonlinear observers for predicting state-of-charge and state-of-health of lead-acid batteries for hybrid-electric vehicles," *IEEE Transactions on Vehicular Technology,* vol. 54, pp. 783-794, 2005.

[89] A. J. Salkind, C. Fennie, P. Singh, T. Atwater and D. Reisner, "Determination of state-of-charge and state-of-health of batteries by fuzzy logic methodology," *Journal of Power Sources ,* vol. 80, p. 293–300, 1999 .

[90] P. Singha, C. F. Jr. b and D. Reisner, "Fuzzy logic modelling of state-of-charge and available capacity of nickel/metal hydride batteries," *Journal of Power Sources ,* vol. 136, p. 322–333, 2004.

[91] C. C. Chan, E. W. C. Lo and S. Weixiang, "The available capacity computation model based on artificial neural network for lead-acid batteries in electric vehicles," *Journal of Power Sources,* vol. 87, pp. 201-204, 2000.

[92] W. Peukert, "An equation for relating capacity to discharge rate," *Electrotech, Z. 18 ,* p. 1897 287.

[93] I. Buchmann, "Artificial Intelligence Reads Battery State-of-Health in Three Minutes," Cadex Elextronics Inc., 22000 Fraserwood Way, Richmond B.C. Canada V6W 156, 2001.

[94] C. Hua, B. D. Younb and J. Chung, "A multiscale framework with extended Kalman filter for lithium-ion battery SOC and capacity estimation," *Journal of Applied Energy,* vol. 92, p. 694–704 , 2012.

[95] B. S. Bhangu, P. Bentley, D. A. Stone and C. M. Bingham, "Nonlinear Observers for Predicting State-of-Charge and State-of-Health of Lead-Acid Batteries for Hybrid-Electric Vehicles," vol. 54, no. 3, May, 2005.

[96] D. V. Do, . C. Forgez, K. El Kadri Benkara and G. Friedrich, "Impedance Observer for a Li-Ion Battery Using Kalman Filter," vol. 58, no. 8, 2009.

[97] M. I. Bhaskar Saha, K. Goebel, S. Poll and J. Christophersen, "Prognostics Methods for Battery Health Monitoring Using a Bayesian Framework," vol. 58, no. 2, Feb, 2009.

Chapter 3: Reduced-Order Electrochemical Model Parameters Identification and SOC Estimation for Healthy and Aged Li-Ion Batteries

Part I: Parameterization Model Development for Healthy Batteries

Ryan Ahmed[1], Mohammed El Sayed[1], Jimi Tjong[2], Saeid Habibi[1]

[1]McMaster Automotive Resource Center (MARC), Department of Mechanical Engineering, McMaster University, Hamilton, Canada
[2]Ford Motor Company of Canada, Powertrain Engineering Research and Development Center (PERDC), Windsor, Canada

Abstract

Our mode of transportation is undergoing a paradigm shift from conventional, fossil-fuel-based vehicles to a second generation electric and hybrid vehicles. Electric vehicles have many benefits and are in general more efficient, sustainable, greener, and cleaner. The commercial market penetration and success of electric vehicles are tied to the efficiency, safety, cost, and lifetime of the traction battery pack. One of the current key electrification challenges is to accurately estimate the battery pack state of charge and state of health and therefore provide an estimate of the remaining driving range at various battery states of life. In order to estimate the battery state of charge, a high-fidelity battery model along with a robust, accurate estimation strategy are necessary. This paper provides three main contributions: (1) introduction of a new state of charge parameterization strategy, (2) identification of the full-set of reduced-order electrochemical battery model parameters using non-invasive genetic algorithm and its implementation on a fresh battery, (3) model validation using real-world driving cycles. Extensive tests have been conducted on Lithium Iron Phosphate-based cells widely utilized in high power automotive applications. Models can be effectively utilized onboard of battery management system.

Keywords: Lithium-Ion Batteries, electric vehicles, genetic Algorithm optimization, electrochemical battery model, parameters identification.

- **Corresponding Author:**

  Ryan Ahmed, M.A.Sc, P.Eng., SCPM
  Research and Development Engineer, McMaster University

This paper has been accepted for publication at the IEEE Journal of Emerging Technologies and Selected Topics in Power Electronics (*Special issue on Transportation and Electrification, 2014*)

3.1 Introduction

In a series of two papers, the authors propose a complete solution for electrochemical battery modeling, parameter identification, and state of charge estimation at all battery states of life. The technique has been effectively applied to Lithium Iron Phosphate (LiFePO4) cells and is applicable to any other lithium ion battery chemistry.

This paper (*Part I*) considers the derivation of reduced-order electrochemical models and investigates parameter identification by using a genetic optimization algorithm. The paper includes a new parameterization strategy for state of charge calculation. The proposed methods have been applied and validated on lithium ion battery cells. A detailed description of the experimental setup and data are provided. The paper also includes description of an electric vehicle simulation model developed to generate current profiles from vehicle driving profile and velocity. *Part II* of this set of papers presents the development of an aging and degradation model based on electrochemistry. This latter model accommodates for battery aging and provides an accurate estimate of the battery state of charge even at the end-of-life. The model works by changing the electrode effective volume along with tracking changes in the model parameters such as the diffusion coefficients and solid-electrolyte interface resistance. The model has been validated using real-world driving cycles for both fresh and aged battery cells. Furthermore, a state of charge and critical surface charge estimation strategy based on the reduced-order electrochemical model has been implemented and described.

3.1.1 Motivation and Technical Challenges

Electric Vehicles (EVs) have received substantial attention in the last decade since they promise a more sustainable transportation system compared to their petroleum-based counterparts. EVs have advantages as electricity can be obtained from numerous energy sources such as nuclear, renewables (e.g.: solar, wind, and tidal), and fossil-fuels. Furthermore, EVs can recapture a portion of the energy lost during regenerative braking for later re-use thus increasing their overall efficiency. Electrified vehicle do not need to have an engine idling when they stop and can have simpler mechanical structures, [1].

Electric vehicles are increasingly driven by an on-board lithium-Ion battery pack which is one of the most important elements of the powertrain and requires precise monitoring and control. A battery management system (BMS) is used and made responsible for their real-time monitoring and control, including their State of Charge (SOC), State of Health (SOH), and Remaining Useful Life (RUL). The main limitations of EV penetration in the automotive market are: ***cost, range anxiety, safety concerns, and resale value***. Regarding ***cost,*** the battery represents the most expensive component in the entire electric vehicle powertrain thus the price of an electric vehicle can be significantly reduced by economies of scale; for example, the cost of 1kWh is estimated to be approximately $1000 for a lithium-Ion battery pack and the objective is to bring it down to $250, [2]. Price can also be reduced by implementing an accurate SOC estimation strategy which could help reduce any extra overdesign in battery power. As for ***range anxiety***, application of an accurate onboard SOC estimation strategy is extremely important; this will facilitate commercialization and wide-acceptance of electric vehicles which will eventually bring down their cost. In terms of ***safety*** and ***resale value*** concerns, these can be mitigated by incorporating a SOC estimation strategy to avoid battery over charge and under discharge, as these significantly reduce the life time of battery packs. Furthermore, accurate SOH estimation techniques and battery lifetime prediction (prognosis) approaches are necessary to assess battery degradation. SOH provides the driver with information regarding the remaining useful life (RUL) which increases reliability and customer satisfaction.

In order to monitor the battery SOC and SOH, an accurate, high-fidelity mathematical model has to work collaboratively with an accurate and robust estimation strategy. However, SOC and SOH monitoring are challenging tasks as degradation is reflected in changes in numerous parameters of the battery model. Batteries run under a dynamic environment involving acceleration and deceleration depending on the driving cycle; These and many factors also affect battery models and monitoring accuracy such as imbalance between cells, self-discharge, aging effects, capacity fade, and temperature effects, [3].

3.1.2 Literature Review

Electrochemical battery models (ECMs) have been widely researched in recent literature since they are capable of modeling the diffusion of lithium inside the electrolyte and the electrodes. In contrast to equivalent circuit-based models and lumped-parameters models, ECMs represent a more attractive approach since they can provide an insight into the internal physical states and limitations of the battery; these are important in automotive applications since batteries are exposed to high transient current loads under various driving cycles, [4].

Various attempts have been reported in the literature for estimating the electrochemical model parameters for both reduced and full-order models. In general, electrochemical battery model parameters such as diffusion coefficient and maximum solid lithium concentration are proprietary information and are not generally provided by manufacturers. ECM parameters can be experimentally measured by examining the cells. This approach is however costly, time consuming, and cannot obtain all parameters. Another approach as proposed in this paper, is to use non-destructive tests and using optimization to tune model parameters to experimental data.

In [4], a parameter identification strategy for reduced-order electrochemical models for lithium-polymer cells is proposed. Using continuous and pulse charging/discharging experimental data on a 6.8 Ah cell, 9 model parameters are identified, [4]. These include: solid particle diffusion coefficients, electrode surface area, and maximum solid electrode potentials, [4]. In [5], a genetic algorithm has been applied to identify the parameters of the full-order electrochemical model using non-invasive experimental data from the input current and measured voltage, [5]. Furthermore, fisher information technique has been applied to identify the accuracy of the resulting parameters, [5]. The test has been conducted using $LiFePO_4$ cells from A123, [5]. The cells are used for high power applications which is the case in electric vehicles, [5].

3.1.3 Contributions

This paper presents a generic technique that can be used to estimate the electrochemical battery model parameters using a non-invasive optimization strategy for any battery state of life. Based on the current literature and up to the authors' best knowledge, the full-set of the reduced-order electrochemical model parameters have not been identified using a real-world driving cycle while calculating the state of charge. Furthermore, no state of charge parameterization model has been developed to adjust the spherical volume-based state of charge calculation accordingly. The technique has been used to estimate the full-set of the reduced-order electrochemical model parameters for 3.3 V, 2.3 Ah Lithium Iron Phosphate ($LiFePO_4$) batteries at various states of life. The technique can be applied to other battery chemistries provided that parameters upper and lower bounds are provided by the manufacturer. Furthermore, the paper introduces a new electrochemical model-based SOC parameterization strategy based on the number of spherical shells (model states) and on the final value theorem. The final value theorem is applied in order to calculate the initial values of lithium concentrations at various shells of the electrode. Then, this value is used for setting up a constraint for the optimizer in order to achieve an accurate SOC estimation.

In order to fit ECM parameters, electric current input from an Urban Dynamometer Driving Schedule (UDDS) has been used. This current has been selected since it includes fast changing and therefore a demand signal that is rich in its frequency content and thus favorable to information extraction. Battery models have been validated using a variety of aggressive driving cycles such as the light duty drive cycle for high speed and high load (US06) and the highway fuel economy test (HWFET). In order to generate the current profile from driving cycles, an electric vehicle model (based on SimScape) has been used in a modified form, [6].

3.1.4 Paper Outline

Section 3.2 of this paper describes the reduced-order electrochemical battery model. Section 3.3 illustrates the demand-current generation process from the velocity. Section 3.4 describes the performance tests conducted on fresh and aged battery cells. Section 3.5 details the proposed model parameterization and optimization strategies. Section 3.6 describes the parameter identification technique using genetic algorithm. Finally, section 3.7 presents conclusions, limitations, and future work.

3.2 Reduced-Order Electrochemical Model

The derivation of the reduced-order electrochemical battery model is summarized in this section, [7]. This reduced-order model is an approximation of the full-order Doyle-Fuller Newman Model that is briefly summarised in **APPENDIX A**, [8, 5]**.** The reduced-order form of the model is generally preferred in estimation and control applications, since full-order models are computationally expensive, making them impractical for online applications in BMS, [8].

As shown in Figure 3.1, a typical lithium-Ion battery comprises of two electrodes and a separator immersed in an electrolyte solution. The negative electrode (anode) is made of carbon and the positive electrode (cathode) consists of a metal oxide. Battery charging and discharging processes occur by transferring lithium ions between the anode and the cathode across the solution and, electrons through the current collectors, [9]. The negative electrode half reaction is, [8]:

$$\mathrm{Li_xC_6} \leftrightarrows \mathrm{C_6} + \mathrm{xLi^+} + \mathrm{xe^-}$$

The half reaction for the positive electrode is as follows, [8]:

$$\mathrm{Li_{y-x}Mn_2O_4 + xLi^+ + xe^- \leftrightarrows Li_yMn_2O_4}$$

The overall battery reaction is described by the flowing equation, [8]:

$$\mathrm{Li_{y-x}Mn_2O_4 + Li_xC_6 \leftrightarrows Li_yMn_2O_4 + C_6}$$

The battery discharging reaction is represented by the right arrow direction and the charging process is presented by the left arrow, [8]. Modeling the entire battery diffusion dynamics across both electrodes and the electrolyte, which is known as the Full-order model, is a computationally expensive task. Therefore, in order to implement the model onboard of a BMS, model reduction has to be conducted. As shown in Figure 3.1, a single particle is selected to represent each electrode and spherical diffusion inside this particular particle is considered.

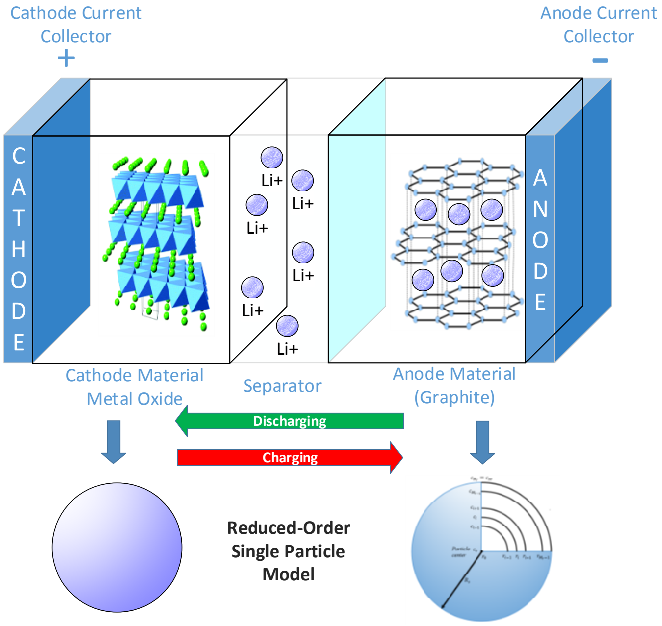

Figure 3.1. Lithium-Ion Battery Structure and the Reduced-Order Model Assumption (Adopted from [8])

The reduced-order model used in this paper is known as the average model, [8]. Several assumptions are made which results in a reduction in model accuracy. However, the model is still applicable to control and monitoring, such as for state of charge and state of health control and estimation. The following assumptions have been made, [8]:

- Each lithium-ion electrode is assumed to be a single sphere whose surface area is scaled to that of the porous electrode as shown in Figure 3.1.
- Lithium concentration in the electrolyte and all model parameters are assumed to be constant.
- No aging or capacity fade has been accounted for and all thermal effects are ignored.

Any of the above assumptions can be accommodated for at the expense of an increase in model complexity and computational requirements. The algorithm of the simplified averaged electrochemical model can be divided into 3 sub-models, namely: ***spherical diffusion sub-model***, ***solid electrolyte interface concentration to terminal voltage sub-model***, and ***solid concentration to SOC sub-model***. These sub-models are discussed in details below:

3.2.1 Spherical diffusion sub-model

A single particle of radius R_s representing the entire electrode is chosen as shown in Figure 3.2. Accordingly, the spatial dimension x across the electrode is ignored. A summary of the model parameters are summarized in Table 3.1, [8]. The reduced-order model utilizes only one representative particle for each of the anode and the cathode. The sphere is divided into a number of equal thickness shells. The single spherical particle is divided into $M_r - 1$ shells each of size Δr with $i = 1, \ldots, M_r - 1$ and $r_i = i\Delta r$, where:

$$\Delta r = \frac{R_s}{M_r} \tag{3.1}$$

As shown in Figure 3.2, the outer shell (M_r) is exposed to the input current on the solid-electrolyte interface. The diffusion inside the particle is described using Fick's law of spherical diffusion as follows, [9]:

Table 3.1. Electrochemical Battery Model Parameters Nomenclature and Units, [8]

Symbol	Name	Unit
$\boldsymbol{i_e}$	Electrolyte current density	$A\ cm^{-2}$
$\boldsymbol{i_e}$	Solid current density	$A\ cm^{-2}$
$\emptyset_e$	Electrolyte potential	V
$\emptyset_s$	Solid potential	V
$\boldsymbol{c_e}$	Electrolyte concentration	$mol\ cm^{-3}$
$\boldsymbol{c_s}$	Solid concentration	$mol\ cm^{-3}$
$\boldsymbol{c_{se}}$	Concentration at the solid electrolyte interface	$mol\ cm^{-3}$
$\boldsymbol{J_{Li}}$	Butler-Volmer current	$A\ cm^{-3}$
$\boldsymbol{\theta_n}$	Anode Normalized solid concentration	-
$\boldsymbol{\theta_p}$	Cathode Normalized solid concentration	-
$\boldsymbol{U}$	Open circuit potential	V
$\boldsymbol{U_n}$	Anode open circuit voltage	V
$\boldsymbol{U_p}$	Cathode open circuit voltage	V
$\boldsymbol{\eta}$	Overpotential	V
$\boldsymbol{F}$	Faraday's constant	$C\ mol^{-1}$
$\boldsymbol{I}$	Applied battery cell current	A
$\boldsymbol{R}$	Universal Gas constant	$J\ K^{-1}\ mol^{-1}$
$\boldsymbol{T}$	Temperature	K

$$\frac{\partial c_s}{\partial t} = \frac{\partial}{\partial r}(D_s \frac{\partial c_s}{\partial r}) \tag{3.2}$$

Where, c_s is the solid concentration at time t, and D_s is the diffusion coefficient. In order to discretize the above equation, consider the spherical particle as shown in Figure 3.2 and shell i that is of interest. In order to define the net flux diffusing from and into the shell, let the mole number N_2 from shell i to shell $i + 1$ be defined as, [8]:

$$\delta N_2 = D_s \delta t A_i [c_{s_{i+1}} - c_{s_i}]/\delta r \tag{3.3}$$

Similarly, the mole number N_1 from shell $i - 1$ to i can be expressed as follows, [8]:

$$\delta N_1 = D_s \delta t A_{i-1}\left[c_{s_i} - c_{s_{i-1}}\right]/\delta r \tag{3.4}$$

The net mole flux (per volume) into shell i can be obtained by subtracting equations (3.3) and (3.4) and dividing by the sphere volume V_i, [8]:

$$c_{s_i} = \frac{D_s \delta t}{\delta r}\left\{A_i\left[c_{s_{i+1}} - c_{s_i}\right] - A_{i-1}\left[c_{s_i} - c_{s_{i-1}}\right]\right\}/V_i \tag{3.5}$$

Substituting $A_i = 4\pi r_i^2$, $A_{i-1} = 4\pi r_{i-1}^2$, and $V_i = 4\pi\delta r\left[\frac{r_{i+1}+r_i}{2}\right]^2$ into equation (3.5) results in, [8]:

$$c_i = \frac{4D_s\delta t}{\delta r^2 (r_{i-1} + r_i)^2}\left\{r_i^2\left[c_{s_{i+1}} - c_{s_i}\right] - r_{i-1}^2\left[c_{s_i} - c_{s_{i-1}}\right]\right\} \tag{3.6}$$

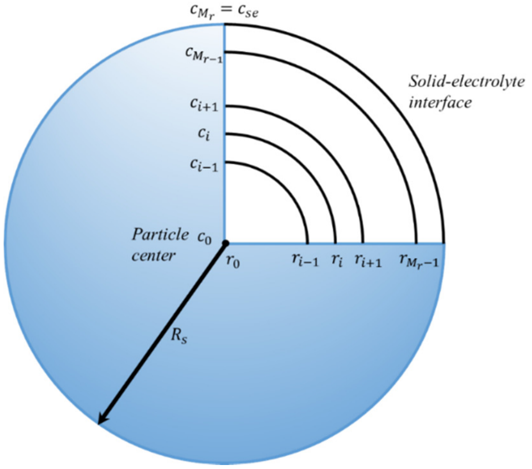

Figure 3.2. Spherical Particle of Radius R_s discretized into M_r shells, [8]

By using the approximations $r_i^2 \cong r_{i-1}r_{i+1}$ and $(r_{i-1} + r_i)^2 \cong 4r_{i-1}r_i$ and substituting in equation (3.6), the following is obtained, [8]:

$$\delta c_{s_i} = \frac{D_s\delta t}{\delta r^2}\left\{c_{s_{i-1}} - 2c_{s_i} + c_{s_{i+1}} + (\delta r/r_i)\left(c_{s_{i+1}} - c_{s_{i-1}}\right)\right\} \tag{3.7}$$

Thus the rate of change of lithium concentration $(\delta c_{s_i}/\delta t)$ in shell i can be described by the following equation, [8]:

$$\frac{\delta c_{s_i}}{\delta t} = \frac{D_s}{\delta r^2}\{c_{s_{i-1}} - 2c_{s_i} + c_{s_{i+1}} + (\delta r/r_i)\,(c_{s_{i+1}} - c_{s_{i-1}})\} \tag{3.8}$$

Substituting $r_i = i\delta r$ into equation (3.8) and re-arranging terms gives:

$$\dot{c}_{s_i} = \frac{D_s}{\delta r^2}\left\{\left(\frac{i-1}{i}\right)c_{s_{i-1}} - 2c_{s_i} + \left(\frac{i+1}{i}\right)c_{s_{i+1}}\right\} \tag{3.9}$$

Equation (3.9) describes the rate of change of lithium concentration in any shell i, and can be used to specify the concentrations at various shells in addition to application of boundary conditions. By setting $i = 1, 2, .., M_{r-2}, M_{r-1}$ and defining $\alpha_1 = D_s/\delta r^2$ results in, [8]:

$$\dot{c}_1 = \alpha_1[-2c_{s_1} + 2c_{s_2}] \tag{3.10}$$

$$\dot{c}_{s_2} = \alpha_1\left[\frac{1}{2}c_{s_1} - 2c_{s_2} + 3/2c_{s_3}\right] \tag{3.11}$$

$$\dot{c}_{s_{M_r-2}} = \alpha_1\left[\left(\frac{M_r-3}{M_r-2}\right)c_{s_{M_r-3}} - 2c_{s_{M_r-2}} + \left(\frac{M_r-1}{M_r-2}\right)c_{s_{M_r-1}}\right] \tag{3.12}$$

$$\dot{c}_{s_{M_r-1}} = \alpha_1\left[\left(\frac{M_r-2}{M_r-1}\right)c_{s_{M_r-2}} - 2c_{s_{M_r-1}} + \left(\frac{M_r}{M_r-1}\right)c_{s_{M_r}}\right] \tag{3.13}$$

Two boundary conditions are set for the problem, one on the surface of the sphere as follows, [8]:

$$D_s\left.\frac{\partial c_s}{\partial r}\right|_{r=R_s} = \frac{-J_{Li}}{a_s F}$$

And the other at the center of the sphere:

$$D_s\left.\frac{\partial c_s}{\partial r}\right|_{r=0} = 0$$

The two boundary conditions at the sphere surface and the core, respectively can be re-written as follows, [8]:

$$D_s\left[(c_{s_{M_r}}-c_{s_{M_r-1}})/\delta r\right]=\frac{-J_{Li}}{a_s F} \tag{3.14}$$

$$D_s\left[(c_{s_1}\_c_{s_0})/\delta r\right]=0 \tag{3.15}$$

Re-arranging the previous equations results in, [8]:

$$c_{s_{M_r}}=c_{s_{se}}=c_{s_{M_r-1}}-\delta r\frac{J_{Li}}{F a_s D_s} \tag{3.16}$$

$$c_{s_0}=c_{s_1} \tag{3.17}$$

Where $c_{s_{M_r}}$ is the solid concentration at the sphere outermost shell in contact with the electrolyte, and is thus referred to as the solid electrolyte interface concentration (c_{se}). Substituting with the solid concentration at the core and at the surface in equations (3.10) and (3.13) and defining $\alpha_2=1/(F a_s \delta r)$ and re-arranging, [8]:

$$\dot{c}_{s_{M_r-1}}=\alpha_1\left[\left(\frac{M_r-2}{M_r-1}\right)c_{s_{M_r-2}}-\left(\frac{M_r-2}{M_r-1}\right)c_{s_{M_r-1}}-\frac{\alpha_2}{\alpha_1}\left(\frac{M_r}{M_r-1}\right)J_{Li}\right] \tag{3.18}$$

Equations (3.10-3.12) along with equation (3.18) represent the single particle model and can be written in a state-space representation form as follows, [8]:

<u>System equation:</u>

$$\dot{c}_s=Ac_s+Bu \tag{3.19}$$

<u>Output equation:</u>

$$c_{se}=c_{s_{M_r}}=c_{s_{M_r-1}}-\frac{\alpha_2}{\alpha_1}J_{Li} \tag{3.20}$$

Where, matrices *A* and *B* can be written as follows, [8]:

$$A = \alpha_1 \begin{bmatrix} -2 & 2 & 0 & & & 0 & \\ 1/2 & -2 & 3/2 & \cdots & & 0 & \\ 0 & 2/3 & -2 & & & 0 & \\ & \vdots & & \ddots & & \vdots & \\ & & & & -2 & \frac{M_r-2}{M_r-3} & 0 \\ 0 & 0 & 0 & \cdots & \frac{M_r-3}{M_r-2} & -2 & \frac{M_r-1}{M_r-2} \\ & & & & 0 & \frac{M_r-2}{M_r-1} & \frac{2-M_r}{M_r-1} \end{bmatrix}, \qquad B = \alpha_2 \begin{bmatrix} 0 \\ 0 \\ \vdots \\ -\left(\frac{M_r}{M_r-1}\right) \end{bmatrix}$$

This sub-model has one input, one output, and M_{r-1} states representing the shells surface concentrations. The model input u is the butler-Volmer current (J^{Li}) which is a function of the solid electrolyte surface concentration $(\mathrm{c_{se}})$ and the total current (I). The output of this sub-model is the solid concentration at the solid-electrolyte interface $(\mathrm{c_{se}})$. This output is fed into another sub-model that calculates the terminal voltage.

3.2.2 Solid electrolyte interface-Terminal voltage sub-model:

Detailed description of the derivation of the following equations is discussed in [8]. A summary of the equations that use the solid concentration at the solid-electrolyte interface to generate the terminal voltage is provided in this subsection. The battery terminal voltage (from the full-order model) is calculated using equation (A18) in **APPENDIX A** and repeated here, [8]:

$$V = \emptyset_s(x = L) - \emptyset_s(x = 0) - R_{SEI} I \tag{3.21}$$

The over-potential for the positive and negative electrodes η_p, and η_n is described by the following equations, [8]:

$$\eta_p = \emptyset_{s,p} - \emptyset_{e.p} - U_p(c_{se,p}) \tag{3.22}$$

$$\eta_n = \emptyset_{s,n} - \emptyset_{e.n} - U_n(c_{se,n}) \tag{3.23}$$

Substituting equations (3.22) and (3.23) into equation (3.21) results in [8]:

$$V(t) = (\eta_p + \emptyset_{e.p} + U_p(c_{se,p})) - (\eta_n + \emptyset_{e.n} + U_n(c_{se,n})) \tag{3.24}$$

Grouping similar elements together results in [8]:

$$V(t) = (\bar{\eta}_p - \bar{\eta}_n) + (\overline{\emptyset}_{e.p} - \overline{\emptyset}_{e.n}) + \left(U_P(c_{se,p}) - U_n(c_{se,n})\right) - R_f I \tag{3.25}$$

The four terms in equation (3.25) are obtained separately as follows:

3.2.2.1 Open circuit Potential $\left(\boldsymbol{U_P(c_{se,p}) - U_n(c_{se,n})}\right)$

The $c_{se,p}$ for the positive electrode is used to calculate the solid concentration at the solid-electrolyte interface for the negative electrode $c_{se,n}$ using the following equation, [8]:

$$\bar{c}_{se,n} = c_{s,max,n}\left(\theta_{n0\%} + \frac{\bar{c}_{se,p} - \theta_{p0\%}c_{s,max,p}}{(\theta_{p100\%} - \theta_{p0\%})c_{s,max,p}}(\theta_{n100\%} - \theta_{n0\%})\right) \tag{3.26}$$

Where $\theta_{n0\%}$, $\theta_{n100\%}$, $\theta_{p0\%}$, $\theta_{p100\%}$ are the stoichiometry points for the negative and positive electrodes respectively, [10]. The solid concentrations at the electrode-electrolyte interface for the positive and negative particles are normalized as follows, [8]:

$$\theta_p = \frac{solid - electrolyte\ interface\ concentration\ (positive\ )}{maximum\ solid\ concentration} = \frac{c_{se,p}}{c_{s,max,p}} \tag{3.27}$$

$$\theta_n = \frac{solid - electrolyte\ interface\ concentration\ (negative)}{maximum\ solid\ concentration} = \frac{c_{se,n}}{c_{s,max,n}} \tag{3.28}$$

Normalized concentration values in equations (3.27) and (3.28) range from 0 to 1 and are further used to obtain the open circuit potential equations for the cathode (Up) and for the anode (U_n). The experimental derivation of U_p and U_n is described in details in section 3.4.

3.2.2.2 The Overpotential $\left(\bar{\boldsymbol{\eta}}_{\boldsymbol{p}} - \bar{\boldsymbol{\eta}}_{\boldsymbol{n}}\right)$

The difference between the anode and cathode overpotentials can be calculated using the following equations (details of the equations derivations can be found in [8]):

$$\bar{\eta}_n = \frac{RT}{\alpha_a F}\ln(\xi_n + \sqrt{\xi_n^2 + 1}) \tag{3.29}$$

$$\bar{\eta}_p = \frac{RT}{\alpha_a F}\ln(\xi_p + \sqrt{\xi_p^2 + 1}) \tag{3.30}$$

where,

$$\xi_n = \frac{\bar{j}_n^{Li}}{2a_s j_o} \tag{3.31}$$

$$\xi_p = \frac{\bar{j}_p^{Li}}{2a_s j_o} \tag{3.32}$$

Where $\bar{j}_n^{Li}$ and $\bar{j}_n^{Li}$ are the Butler-Volmer currents defined as follows:

$$\bar{j}_n^{Li} = \frac{I}{A\delta_n} = a_s j_o[exp\left(\frac{\propto_a F}{RT}\bar{\eta}_n\right) - exp(\frac{\propto_c F}{RT}\bar{\eta}_n)] \tag{3.33}$$

$$\bar{j}_p^{Li} = \frac{I}{A\delta_p} = a_s j_o[exp\left(\frac{\propto_a F}{RT}\bar{\eta}_p\right) - exp(\frac{\propto_c F}{RT}\bar{\eta}_p)] \tag{3.34}$$

j_o can be calculated as:

$$j_o = (c_e)^{\alpha_a}\left(c_{s,max} - c_{se}\right)^{\alpha_a}(c_{se})^{\alpha_c} \tag{3.35}$$

3.2.2.3 The electrolyte potential $(\bar{\boldsymbol{\emptyset}}_{\boldsymbol{e.p}} - \bar{\boldsymbol{\emptyset}}_{\boldsymbol{e.n}})$

An approximate of the difference can be calculated using the following equation, [8]:

$$(\bar{\emptyset}_{e.p} - \bar{\emptyset}_{e.n}) = -\frac{I}{2A}(\frac{\delta_n}{k^{eff}} + \frac{\delta_n}{k^{eff}} + \frac{\delta_n}{k^{eff}}) \tag{3.36}$$

3.2.3 Solid Particle Concentration - SOC sub-model

The critical surface charge (CSC) for the positive electrode is calculated from the solid-electrolyte interface ($c_{se,p}$). Normalized solid-electrolyte concentration θ is obtained first using equation (3.27); the critical surface charge is calculated based on the positive electrode lithium concentration only using the following equation, [8]:

$$CSC = \frac{\theta_p - \theta_{p0\%}}{\theta_{p100\%} - \theta_{p0\%}} \tag{3.37}$$

The battery state of charge (SOC) is calculated based on the spherical average concentration ($c_{s,p_{avg}}$) inside the positive electrode. The SOC is calculated as, [8]:

$$\theta_{p_{avg}} = \frac{average\ positive\ sphere\ concentration}{maximum\ solid\ concentration} = \frac{c_{s,p_{avg}}}{c_{s,max,p}} \tag{3.38}$$

Where, the average solid particle concentration for the positive electrode ($c_{s,p_{avg}}$) is calculated by integrating the concentrations of electrode shells and dividing by the sphere volume as, [8]:

$$c_{s,p_{avg}} = \frac{c_T}{V} = \frac{total\ lithium\ concetration}{particle\ volume} = \frac{\sum_{i=1}^{M_r-1} r_i^2 4\pi\Delta r c_i}{\frac{4}{3}\pi(R_s - \Delta r)^3} \tag{3.39}$$

Then the SOC is calculated as, [8]:

$$SOC = 100 * (\frac{\theta_{p_{avg}} - \theta_{p0\%}}{\theta_{p100\%} - \theta_{p0\%}}) \tag{3.40}$$

Note that the critical surface charge (i.e.: the charge at the solid-electrolyte interface) is not used in the calculation of the total battery state of charge. Alternatively, the solid electrolyte interface concentration is used for terminal voltage calculation. This explains the fact that when a zero current is applied to the battery, battery voltage exhibits relaxation effect, since lithium ions on the outer surface diffuse to lower concentration shells inside the particle thus voltage decreases until lithium concentration in all shells are equalized and no further diffusion takes place. On the other hand, the battery state of charge does not change upon applying a zero current input. Since the same lithium concentration is contained inside the sphere and averaged to obtain the overall battery SOC as given in equation (3.40). The overall ECM Models can be simulated using the collection of equations (3.1) to (3.40). The coefficient values for a $LiFePO_4$ battery cell can be obtained from manufacturers and through experimental parameter identification using drive cycles as explained in the following sections.

3.3 Current Generation and Experimental Setup

This section summarizes the process of current generation from the velocity profiles of various driving cycles. Then a summary of the experimental setup including cyclers, environmental chambers, data acquisition systems, and battery cells is provided. The experimental data is then used for extracting parametric values for a reduced order ECM for a $LiFePO_4$ battery cell.

3.3.1 Current Generation

In order to generate the current profiles needed for experimentation, an electric vehicle battery model has been modified from an existing hybrid vehicle model, [6]. The model has been simulated using SimScape in Matlab environment in order to obtain the current profile from the velocity profile. Loading conditions such as heating and air conditioning have been ignored in this study. A model of a mid-size sedan (Battery Electric Vehicle Ford Focus) has been used with an approximate driving range of 200 kilometers per full charge. The simulation model, as shown in Figure 3.3, consists of a vehicle dynamic model, DC electric motor, DC-DC convertor, lithium-Ion battery pack, and vehicle speed controller.

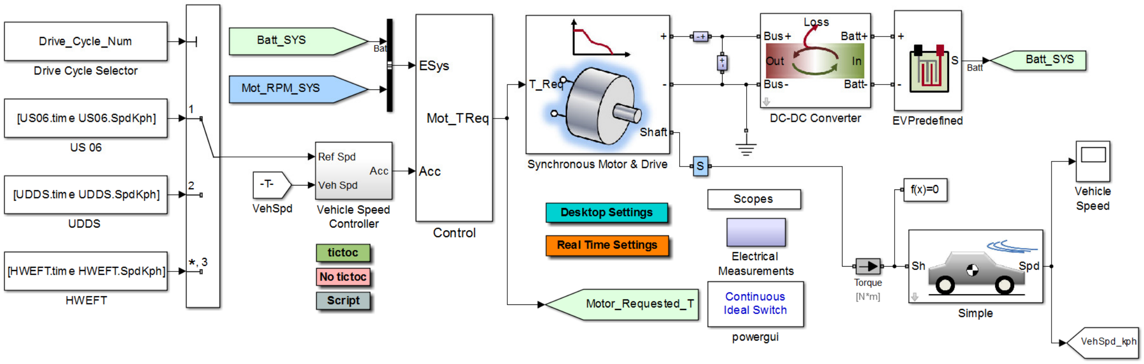

Figure 3.3. All-Electric Mid-size Sedan Simulation Model in SimScape (Adopted from [6])

Three benchmark driving schedules have been used in the simulation; namely, an Urban Dynamometer Driving Schedule (UDDS), a light duty drive cycle for high speed and high load (US06), and a High fuel Economy Test (HWFET), [11]. Even though the driving behaviour of an average driver may likely vary, these driving cycles have been widely used in both industrial and academic settings to simulate various driving patterns.

Table 3.2. Characteristics of UDDS, US06, and HWFET Driving Schedules, [11]

	Length	Distance	Avg Speed (mph)
UDDS	1,369	7.45	19.59
US06	596	8.01	48.37
HWFET	765	10.26	48.30

The UDDS driving cycle represents a city driving condition, the UDDS cycle (commonly known as “LA4” or “the city test” or Federal Test Procedure “FTP-72”) was originally used for light duty fossil-fueled vehicle testing, [11]. It has been developed to imitate average speed, idle time, and number of stops that the average driver performs in practice, [12].

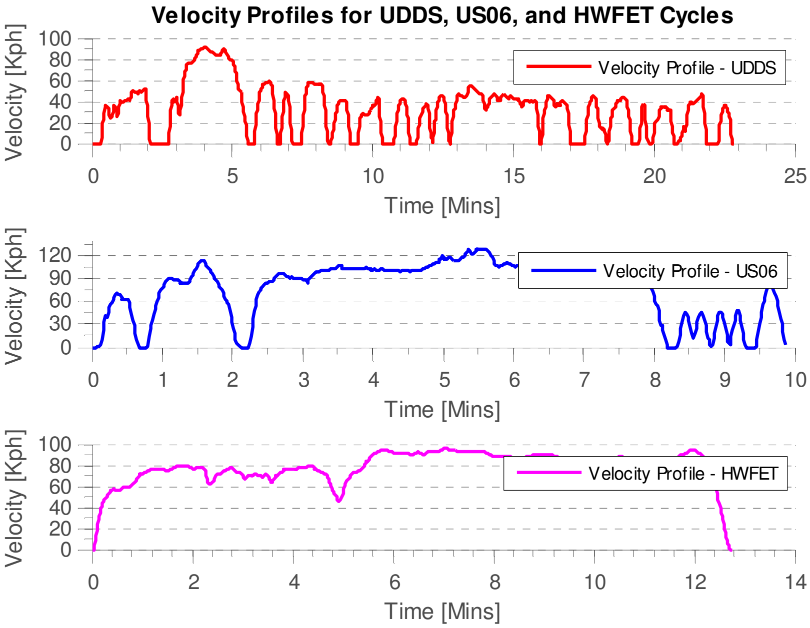

Figure 3.4. Velocity Profiles for the UDDS (upper figure), US06 (middle), and HWFET (lower) Cycles [11]

The test profile is recommended by the U.S. Environmental Protection Agency to estimate the fuel economy in city driving conditions, [11]. For electric vehicles, the profile has been extensively used to estimate the driving range in miles per full charge, [13, 14]. The US06 cycle is a high acceleration, aggressive driving cycle, and the HWFET represents a highway driving conditions with speeds below 60 miles/hours, [15]. The three aforementioned driving cycles are as shown in Figure 3.4 below. An exclusive summary of these driving cycle characteristics such as distance, time, and average speeds is as shown in Table 3.2, [16].

The pack current profiles from these driving cycles are as shown in Figure 3.5. Since the US06 driving cycle is an aggressive driving cycle, the current demand by the motor is quite high compared to current profiles from the HWFET and the UDDS cycles.

Current profiles have been scaled down to the cell level and used for model parameters fitting. The pack consists of 100 cells connected in series for voltage buildup and 15 cells connected in parallel. Cell balancing has been ignored in this study.

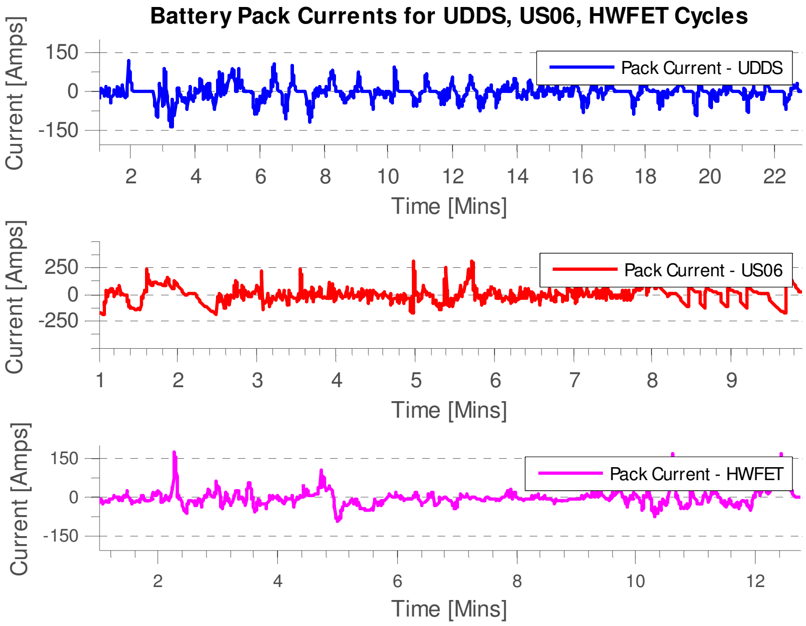

Figure 3.5. Pack Current Profiles for the UDDS (Upper figure), US06 (middle figure), and HWFET (lower figure) Cycles

3.3.2 Experimental Setup

The experimental setup is as shown in Figure 3.6, the setup includes 3 channel Arbin BT2000 tester, 3 lithium Iron Phosphate cells, 3 environmental chambers, AVL Lynx data acquisition system, and AVL Lynx user-interface software. AVL Lynx software is used for setting up the test procedure and for data acquisition. Various variables such as battery current, voltage, and temperatures during charging, discharging, and rest phases are acquired at a maximum frequency of 50 Hz. Battery test cells are placed in environmental chambers in order perform the test at controlled temperature conditions. Two different environmental chambers provided by two different companies are used for testing namely, Thermotron and Espec.

Figure 3.6. Experimental Setup including Cyclers, Environmental Chambers, and Data Acquisition Systems

Figure 3.7. Arbin BT2000 Cycler with Espec/Thermotron Environmental Chambers

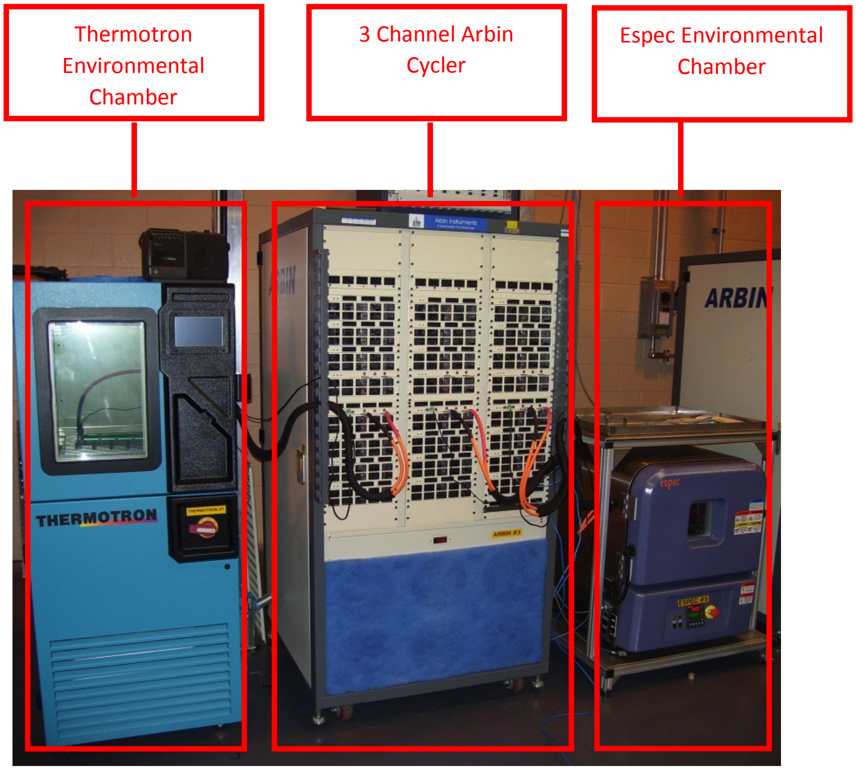

These units can change the temperature from -70 to 180 ℃ and are able to change the temperatures at a rate of $3.5\ ℃/min$. This kind of heating and cooling capability is necessary for stressing samples and accelerating battery aging and therefore saving total test time.

Each battery is independently tested using separate tester channel. The Arbin tester, as shown in Figure 3.7 and Figure 3.8, has 3 independent channels. The cycler can operate in two voltage ranges namely, low: 0-5 V and high: 0-20 V, and 3 different current ranges, high: 0 - ±400 Amps, medium: 0 - ±40 Amps, and low: 0 - ±5 Amps.

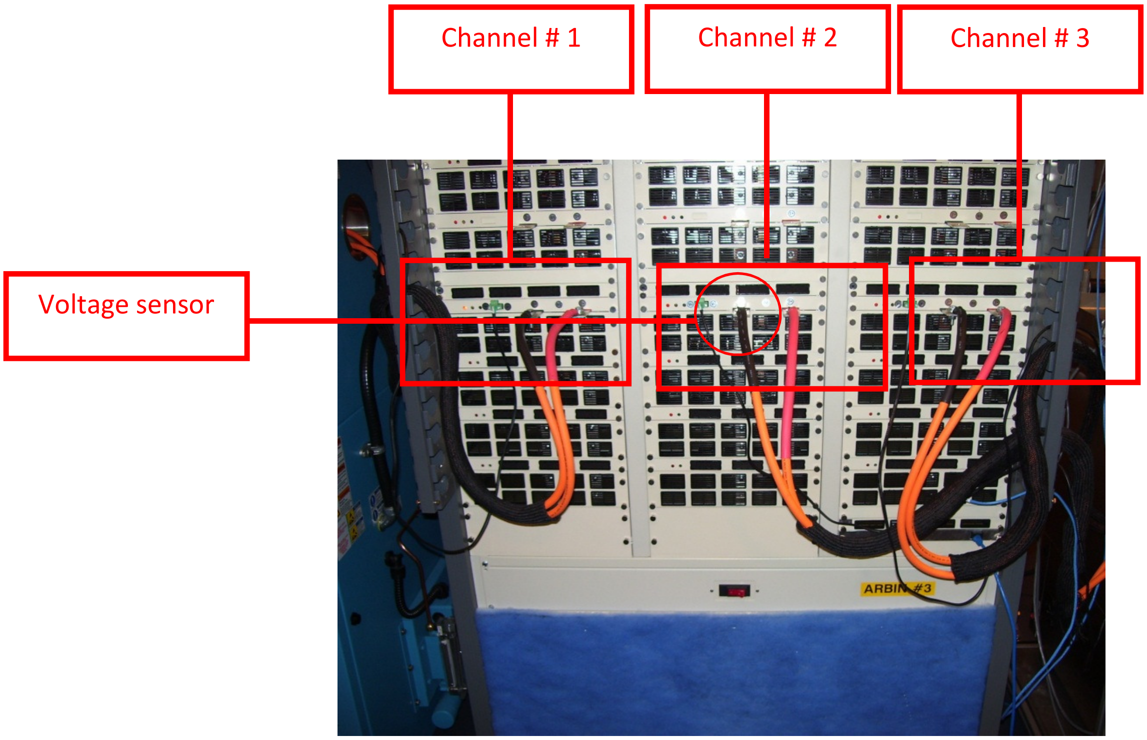

Figure 3.8. Arbin Cycler channels: channels equipped with voltage sensor and status indicator light

3.4 Reference Performance Tests and Experimental Data Analysis

A summary of the reference performance tests (RPT) conducted on fresh battery cells is presented in subsection 3.4.1. In subsection 3.4.2, an illustration of the data analysis conducted to generate the cathode and anode equilibrium potentials (U_p and U_n) is provided.

3.4.1 Characterization/RPT tests

Extensive characterization tests have been conducted on a fresh and aged batteries at controlled room temperature of 25℃, 4 main experiments include: ***A static capacity test at 1C rate, SOC-OCV characterization test, pulse charge/Discharge test, and Driving Cycle tests (e.g.: Urban Dynamometer Driving schedule) test.*** Characterization tests are conducted to specify battery cell baseline performance characteristics such as cell power capability, internal resistance, capacity, and time constants. The following tests were selected for this study.

3.4.1.1 Static Capacity Test – PNGV, 2001

This test is used to measure the battery cell capacity in Ampere-hours at a constant current (CC) discharge rate. This test is conducted in order to provide a baseline for a fresh battery cell capacity. The test procedure follows the constant current constant voltage (CCCV) protocol and is summarized in the following steps, [17]:

A. *Charge the battery at 1C rate (2.3 A) to fully charged state in a constant current constant voltage (CCCV) mode. The battery is fully charged at 3.6 V and when the current end point is at 0.02 C (0.046 A).*
B. *Leave the battery to rest for one hour in order to allow for voltage and current stabilization,* [17].

C. *Discharge sequence at a constant current 1C rate until the voltage reaches the battery minimum voltage limit (2 V) recommended by the manufacturer,* [17].
D. *Battery is left at rest with no load for one hour.*

3.4.1.2 OCV-SOC Relationship:

This test is used to characterize the open-circuit voltage (OCV) - state of charge (SOC) relationship. Very small C-rates (C/20, C/15) are used for OCV-SOC characterization in order to minimize cell dynamics and to minimize ohmic loss effects due to battery internal resistances, [18]. Accordingly, by conducting this experiment, the measured terminal voltage is assumed to be the open circuit voltage. This test is important since the cathode and anode electrode potentials (U_p and U_n), which are used in the electrochemical model, are being derived from this test as discussed in subsection 3.4.3. The OCV-SOC relationship is obtained as follows (this test is similar to the capacity test but is conducted at a very low C-rate):

A. *Fully charge the battery in a CCCV mode until maximum voltage (3.6V).*
B. *Fully discharge the battery at constant current (CC) mode with 1C-rate until the voltage hits the minimum voltage (2V).*
C. *All cycler current accumulators are reset to zero. At this moment, the battery is at zero state of charge (SOC).*
D. *Charge the battery at a very small C-rate of C/15 (0.06*2.3=0.15A) in a CCCV mode until it hits the maximum voltage of 3.6V. The cell is left to rest for one hour to relax.*
E. *Discharge the cell at the same rate of C/15 until and the battery hits the minimum voltage of 2 V.*

The charging and discharging curves are averaged to obtain a single fixed relationship between OCV and SOC.

3.4.1.3 Driving cycles

Current profiles generated from the electric vehicle model as illustrated in section 3.3 are used to excite the cells. The pack current profile is scaled down to the cell level and is fed to the cycler. These driving cycles are very rich in their frequency content, since they include fast variations and will be used for model parameters fitting. The cell current is generated from the pack current by assuming no cell balancing (i.e.: all cells are held at the same state of charge) and by assuming equal current distributions among parallel cell branches.

3.4.2 Fresh Battery - Cathode/Anode Electrode Potential Derivation

The separate cathode and anode electrodes potential can be estimated from the SOC-OCV relationship. The OCV vs. time for both charging and discharging of a fresh battery is as shown in Figure 3.9. The test has been conducted at C/15 rate. In order to obtain the OCV-SOC relationship, the OCV curves for both charging and discharging are plotted vs. SOC as shown in Figure 3.10. This relationship, as previously mentioned, is obtained by cycling the battery at a very low C-rate (C/20 or C/15) to minimize battery dynamics and use the measured terminal voltage as the open circuit voltage (i.e.: assuming negligible voltage drop on the internal resistance due to very low current), [18].

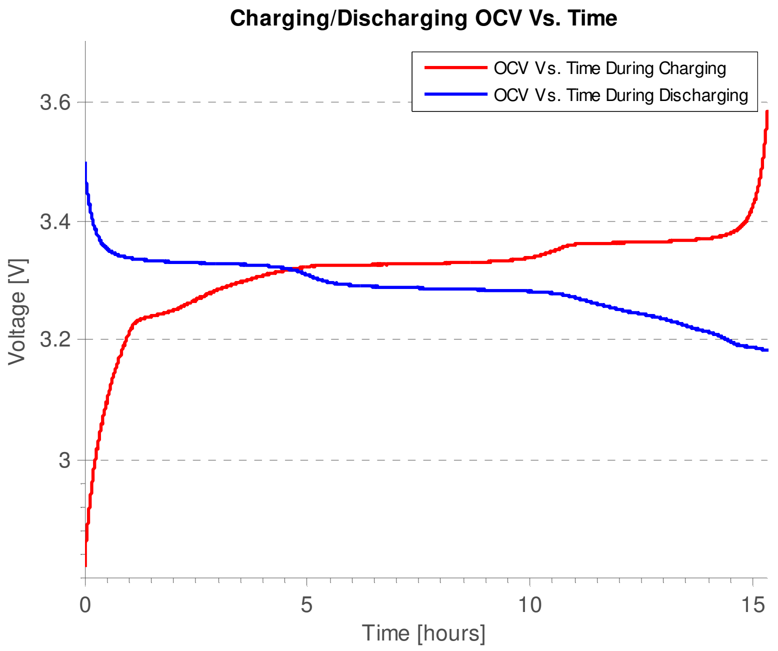

Figure 3.9. Charging/Discharging OCV vs. Time (~C/15)

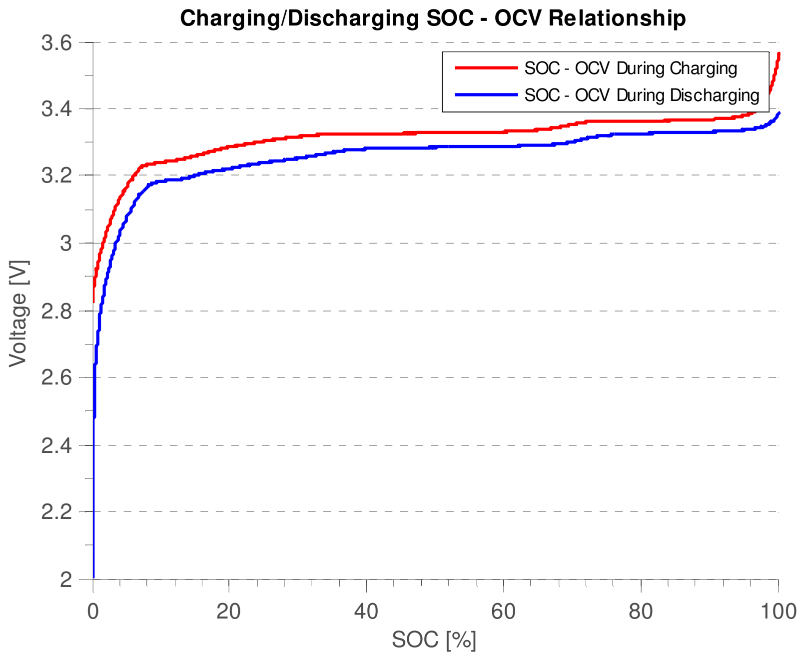

Figure 3.10. SOC-OCV relationship for both charging and discharging

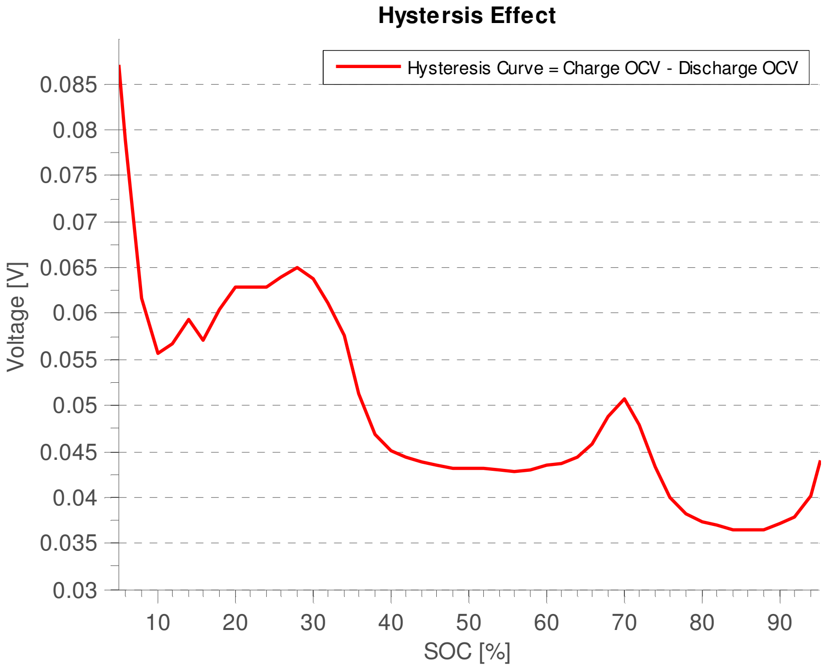

Figure 3.11. Hysteresis Effect - Obtained by subtracting Charging and Discharging Curves

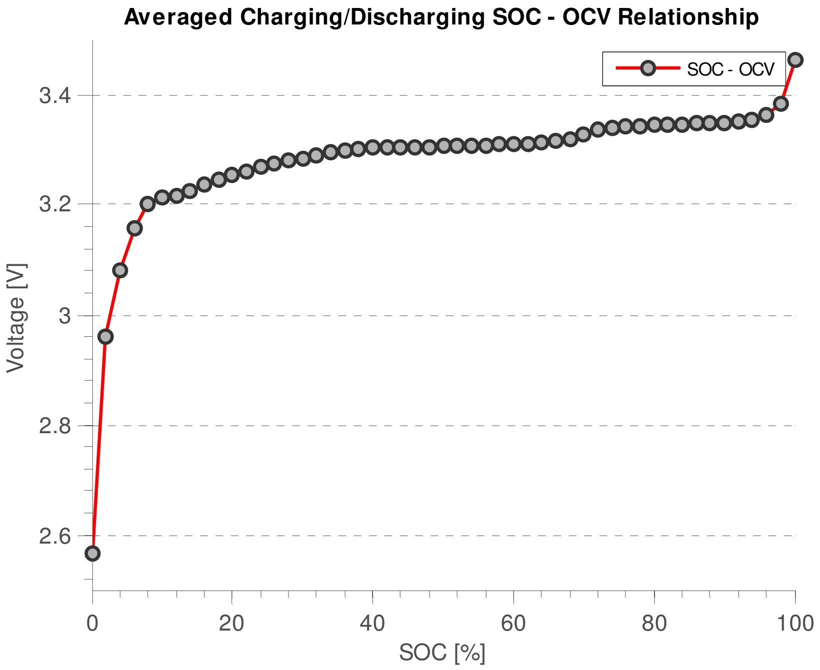

Figure 3.12. Charging and Discharging Averaged SOC-OCV Curve

It is clear that the battery behaviour during charging and discharging are not identical due to hysteresis effects which is obtained by subtracting both curves is shown in Figure 3.11. In order to obtain one curve to represent the OCV-SOC relationship, data has been resampled to 50 points for each of the charging/discharging curves then they have been averaged as shown in Figure 3.12.

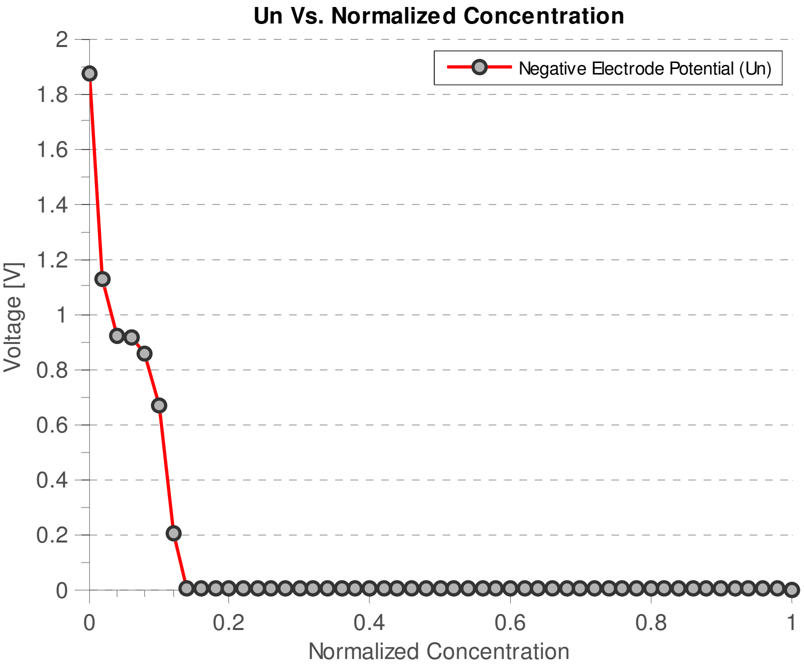

Figure 3.13. Anode Equilibrium Potential Vs. Normalized Concentration [5]

In order to obtain the open circuit potential for the positive electrode (U_p) and the negative electrode (U_n) from the OCV-SOC relationship shown in Figure 3.13, one of the two electrode potentials has to be independently calculated and then subtracted from the OCV-SOC relationship to derive the other. In this paper, since the negative electrode active material is made of graphite (Li_xC_6), the empirical relationship below [19] can be derived from the literature, [20]. The anode electrode potential (U_n) as function of the normalized lithium concentration is as shown in Figure 3.13, [5]. The empirical relationship is as follows, [19]:

$$U_n(x) = C_1 + C_2 x + C_3 x^{1/2} - C_4 x^{-1} + C_5 x^{\frac{3}{2}} + C_6 \exp[\,15(0.06 - x)] - C_7 \exp[C_8(x - 0.92)]$$

Where, x is defined as the lithium concentration in the solid active material divided by the maximum permissible solid concentration, [19]. The constants C_1 to C_8 values are as follows:

$$C_1 = 8.002296379,\ C_2 = 5.064722977,\ C_3 = -12.57808059,\ C_4 = 8.632208755e - 4,\ C_5 = 2.179498281e - 5,\ C_6 = -0.4601573522,\ C_7 = 0.5536351675,\ C_8 = -2.432630003$$

The cathode potential (U_p) is obtained from the anode potential by subtracting U_n from the OCV-SOC curve as shown in Figure 3.14 below, [5]. In each electrode, curves have been discretized to 50 control points and a Piecewise Cubic Hermite Interpolating Polynomial (PCHIP) is used perform interpolation between control points, [5].

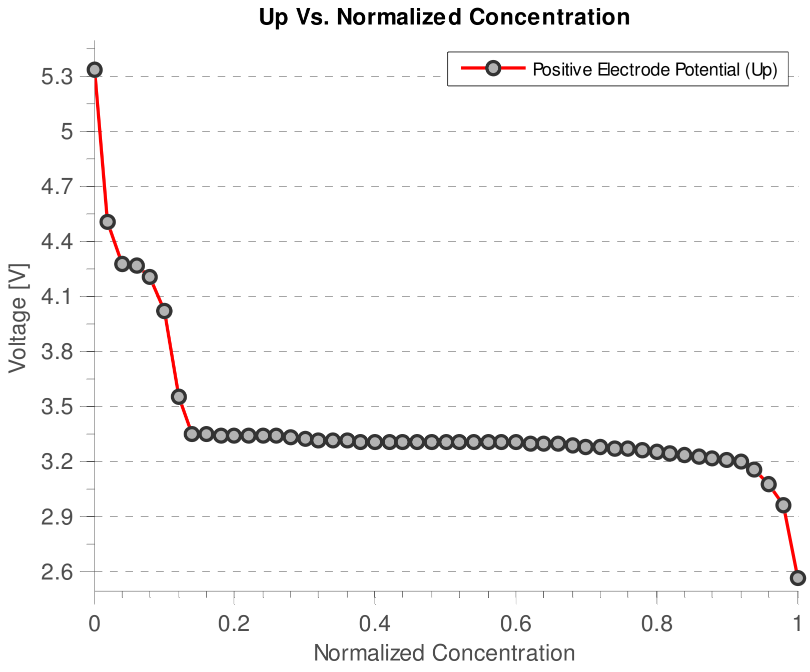

Figure 3.14. Cathode Equilibrium Potential as function of Normalized concentration

3.5 Parameterization Model Development

In order to identify the electrochemical battery model parameters, an objective function has to be set in order to fit the model output voltage to experimental data. In order to optimize the battery voltage while maintaining an accurate SOC estimate, model parameterization has to be conducted in order to scale the input current to the Butler-Volmer current values. This value is further applied as an input to the spherical particle for each electrode. This section provides a new parameterization model which is a function of the number of spherical shells (M_r). The model is further used as a constraint during parameters optimization. The following subsections illustrate the parameterization procedure by considering the reversed process of obtaining the initial lithium concentration from the initial SOC followed by deriving the parameterization equation.

3.5.1 Total sphere concentration from initial SOC

In order to start simulating the model, the initial lithium concentration values have to be calculated from the initial SOC. First, assuming a known battery SOC, an inverse SOC calculation has to be conducted as follows. Recall that the battery SOC is calculated based on the spherical average concentration ($c_{s,p_{avg}}$) inside the positive electrode (equations 3.39-3.40). Equations are repeated here for readability, the SOC is calculated as follows, [8]:

$$SOC = 100 * \left(\frac{\frac{c_{s,p_{avg}}}{c_{s,max,p}} - \theta_{p0\%}}{\theta_{p100\%} - \theta_{p0\%}}\right) \tag{3.39}$$

Where, the average solid particle concentration for the positive electrode ($c_{s,p_{avg}}$) is calculated by integrating the concentrations of electrode shells and dividing by the sphere volume as follows, [8]:

$$c_{s,p_{avg}} = \frac{c_T}{V} = \frac{total\ lithium\ concetration}{particle\ volume} = \frac{\sum_{i=1}^{M_r-1} r_i^2 4\pi\Delta r c_i}{\frac{4}{3}\pi(R_s - \Delta r)^3} \tag{3.40}$$

Thus assuming a known initial state of charge, the total solid concentration in the particle can be calculated by re-arranging the previous equations as follows:

$$c_T = c_{s,p_{avg}} * \frac{4}{3}\pi(R_s - \Delta r)^3 = \left(\frac{SOC}{100} * \left(\theta_{p100\%} - \theta_{p0\%}\right) + \theta_{p0\%}\right) * c_{s,max,p} * \frac{4}{3}\pi(R_s - \Delta r)^3 \tag{3.41}$$

The next step is to evaluate lithium concentration values at various shells at steady state conditions (i.e.: assuming no diffusion). The total lithium concentration is divided equally among all shells as follows:

$$c_T = \sum_{i=1}^{M_r-1} r_i^2 4\pi\Delta r c_i = r_1^2 * 4\pi\Delta r c_1 + r_2^2 * 4\pi\Delta r c_2 + r_3^2 * 4\pi\Delta r c_3 \ldots r_{M_r-1}^2 * 4\pi\Delta r c_{M_r-1} \tag{3.42}$$

In order to evaluate the values of lithium concentrations at various shells $[c_1\ c_2\ c_3 \ldots c_{Mr-1}]$, we use the final value theorem to evaluate the steady state concentration values. The technique is described in details in the following subsections.

3.5.2 Initial concentration using Final Value Theorem

Given a dynamic system representing the lithium diffusion in the solid particle defined in state-space which is previously defined in equations (3.19-3.20), matrices A and B can be written as follows:

$$A = \alpha_1 \begin{bmatrix} -2 & 2 & 0 & & & 0 & \\ 1/2 & -2 & 3/2 & \cdots & & 0 & \\ 0 & 2/3 & -2 & & & 0 & \\ & \vdots & & \ddots & & \vdots & \\ & & & & -2 & \frac{M_r-2}{M_r-3} & 0 \\ 0 & 0 & 0 & \cdots & \frac{M_r-3}{M_r-2} & -2 & \frac{M_r-1}{M_r-2} \\ & & & & 0 & \frac{M_r-2}{M_r-1} & \frac{2-M_r}{M_r-1} \end{bmatrix}, \qquad B = \alpha_2 \begin{bmatrix} 0 \\ 0 \\ \vdots \\ -\left(\frac{M_r}{M_r-1}\right) \end{bmatrix}$$

Assuming a zero input $u(t) = 0$, the zero-input solution can be formulated as:

$$\frac{dc}{dt} = Ac(t) \tag{3.43}$$

Taking unilateral Laplace transform,

$$sc(s) - c(0) = Ac(s) \tag{3.44}$$

Where $c(0) = c(t)$ at $t = 0$. Thus,

$$(sI - A)c(s) = c(0) \tag{3.45}$$

By applying the inverse, the states $c(s)$ can be evaluated as follows:

$$c(s) = (sI - A)^{-1}c(0) \tag{3.46}$$

By applying the Final Value theorem for a unilateral transfer function $F(s)$ as follows:

$$Final\,Value = \lim_{t\to\infty} f(t) = \lim_{s\to 0} sF(s) \tag{3.47}$$

Thus substituting equation (3.46) into equation (3.47), get:

$$Final\,Value = \lim_{t\to\infty} f(t) = \lim_{s\to 0} s((sI - A)^{-1}c(0)) \tag{3.48}$$

The final value calculated above is a function of the matrix *A*. It is clear that the matrix depends solely on the number of spherical shells M_r thus the final value depends on the number of shells. The final value achieved using the final value theorem represents the fraction by which the concentration will be equally divided amongst all shells. In this paper, this value is referred to as the $c_{s_{factor}}$. Accordingly, in order to evaluate the solid concentration in each spherical shell, assume that all lithium contained in the sphere is concentrated at the outermost shell. Then the following equation can be used:

$$\begin{aligned} c_i = c_T/(r_{M_{r-1}}^2 * 4\pi\Delta r) * \ c_{s_{factor}} &= \sum_{i=1}^{M_r-1} r_i^2 4\pi\Delta r c_i \,/(r_{M_{r-1}}^2 * 4\pi\Delta r) * \ c_{s_{factor}} \\ &= (r_1^2 * 4\pi\Delta r c_1 + r_2^2 * 4\pi\Delta r c_2 + r_3^2 * 4\pi\Delta r c_3 \ldots + r_{M_{r-1}}^2 \\ &\quad * 4\pi\Delta r c_{M_r-1})/(r_{M_{r-1}}^2 * 4\pi\Delta r) * \ c_{s_{factor}} \end{aligned} \tag{3.49}$$

Where c_i represents the steady state initial concentration at every shell, for a given state of charge and the number of shells in the spherical particle.

3.5.3 Number of shells, SOC slope, and $c_{s_{factor}}$ relationship

By examining the state transition matrix A, a relationship between the number of electrode spherical shells (M_r) and the $c_{s_{factor}}$ can be derived. Assume that the number of spherical shells is $M_r = 3$, the state transition matrix can be formulated as function of M_r as follows:

$$A|_{M_r=3} = \begin{bmatrix} -2 & (M_r-1)/(M_r-2) \\ (M_r-2)/(M_r-1) & -(M_r-2)/(M_r-1) \end{bmatrix} \tag{3.50}$$

By converting from the state space to the transfer function representation and assuming zero input current, the transfer function (TF) for the outermost shell that relates the input butler-Volmer current to the subsequent inner shell can be written as follows:

$$TF|_{M_r=3} = \frac{(M_r-1)(s+2)}{(M_r-1)s^2 + (3M_r-4)s + M_r - 3} \tag{3.51}$$

By applying the final value theorem (equation (3.47)) and simplify:

$$Final\ Value|_{M_r=3} = c_{s_{factor}}|_{M_r=3} = 1 - \frac{M_r - 2}{3M_r - 4} \tag{3.52}$$

Similarly, by repeating the same procedure for the number of spherical shells $M_r = 4$, the state transition matrix can be formulated as a function of M_r as follows:

$$A|_{M_r=4} = \begin{bmatrix} -2 & \frac{(M_r-2)}{(M_r-3)} & 0 \\ \frac{(M_r-3)}{(M_r-2)} & -2 & \frac{(M_r-1)}{(M_r-2)} \\ 0 & \frac{(M_r-2)}{(M_r-1)} & -\frac{(M_r-2)}{(M_r-1)} \end{bmatrix} \tag{3.53}$$

The transfer function (TF) for the outermost shell that relates the input current to the subsequent inner shell is as follows:

$$TF|_{M_r=4} = \frac{(M_r-1)(s^2+4s+3)}{(M_r-1)s^3 + (5M_r{-}6)s^2 + (6M_r-10)s + M_r - 4} \tag{3.54}$$

By applying the final value theorem and simplifying:

$$Final\ Value|_{M_r=4} = c_{s_{factor}}|_{M_r=4} = 1 - \frac{3M_r - 7}{6M_r - 10} \tag{3.55}$$

Finally, for the number of spherical shells $M_r = 5$, the state transition matrix is:

$$A|_{M_r=5} = \begin{bmatrix} -2 & \frac{(M_r-3)}{(M_r-4)} & 0 & 0 \\ \frac{(M_r-4)}{(M_r-3)} & -2 & \frac{(M_r-2)}{(M_r-3)} & 0 \\ 0 & \frac{(M_r-3)}{(M_r-2)} & -2 & \frac{(M_r-1)}{(M_r-2)} \\ 0 & 0 & \frac{(M_r-2)}{(M_r-1)} & -\frac{(M_r-2)}{(M_r-1)} \end{bmatrix} \tag{3.56}$$

And the transfer function (TF) for is as follows:

$$TF|_{M_r=5} = \frac{(M_r-1)(s^3+6s^2+10s+4)}{(M_r-1)s^4+(7M_r-8)s^3+(15M_r-21)s^2+(10M_r-20)s+M_r-5} \tag{3.57}$$

By applying the final value theorem and simplify:

$$Final\ Value|_{M_r=5} = c_{s_{factor}}|_{M_r=3} = 1-\frac{6M_r-16}{10M_r-20} \tag{3.58}$$

By further examining the $c_{s_{factor}}$ values for various number of shells, the following relationship can be formulated:

$$c_{s_{factor}} = \frac{\left(\frac{M_r^2-3M_r+2}{2}\right)(M_r)-\left(\frac{M_r^3-7M_r+6}{6}\right)}{\left(\frac{M_r^2-M_r}{2}\right)(M_r)-\left(\frac{M_r^3-M_r}{6}\right)} \tag{3.59}$$

Therefore the closed form of the relationship can be simplified to:

$$c_{s_{factor}} = 1-\frac{2M_r^3-9M_r^2+13M_r-6}{2M_r^3-3M_r^2+M_r} \tag{3.60}$$

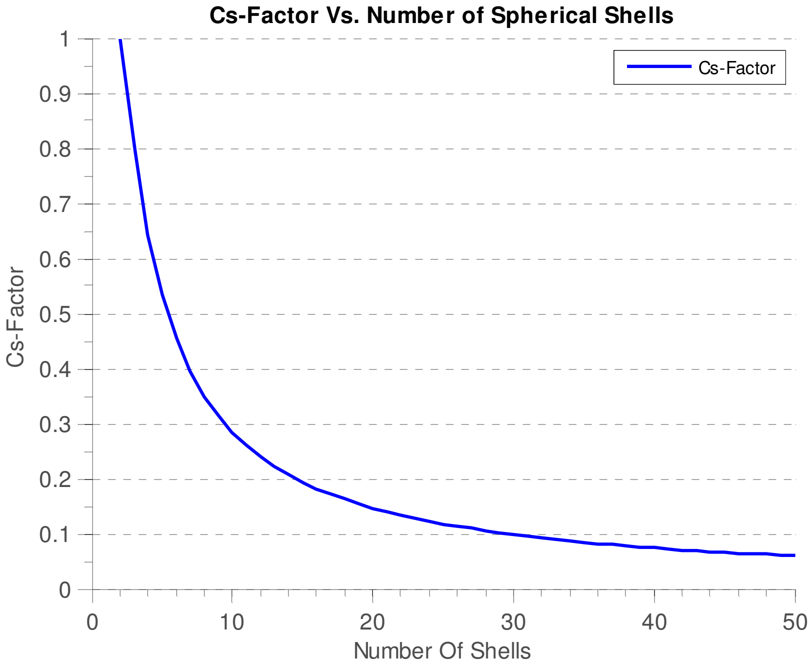

Figure 3.15. Relationship between the $c_{s_{factor}}$ and the number of electrode spherical shells

The relationship between the $c_{s_{factor}}$ and the number of spherical shells (M_r) is as shown in Figure 3.15. By simulating the model using various number of shells, we can derive a relationship between the number of shells (M_r), the $c_{s_{factor}}$, and the slope of the SOC $(\Delta SOC/\Delta t)$ curve as summarized in the following table:

Table 3.3. Model Simulation parameters using various number of shells

$c_{s_{factor}}$	M_r	$\Delta SOC/\Delta t$	$(\Delta SOC/\Delta t) / c_{s_{factor}}$
0.26	11	2.72	10.5
0.13	21	2.85	20.5
0.12	25	2.88	24.5
0.09	31	2.90	30.5

As shown in Table 3.3, by dividing $c_{s_{factor}}$ by the SOC slope $(\Delta SOC/\Delta t)$**,** a relationship which depends solely on the number of shells can be derived as follows:

$$(\Delta SOC/\Delta t)\Big/c_{s_{factor}} = (2M_r - 1)/2 \tag{3.61}$$

The previous relationship is of critical importance to scale the battery input current (I) to the Butler -Volmer current (J_p). This relationship is expanded upon to include dependence on the battery capacity (Q_{max}) in Ampere-second, normalized concentrations ($\theta_{p_{0\%}}, \theta_{p_{100\%}}$), particle radius ($R_s$), maximum positive solid concentration ($c_{s_{max}}$), and α_2.

$$(\Delta SOC/\Delta t)\Big/c_{s_{factor}} = (\frac{2M_r - 1}{2} * \alpha_2 * \Delta r)/(c_{s_{max}} * R_s * Q_{max} * (\theta_{p_{100\%}} - \theta_{p_{0\%}}) \tag{3.62}$$

Where,

$$\alpha_1 = D_s/\delta r^2 \text{ and } \alpha_2 = 1/(Fa_s\Delta r)$$

The relation is further expanded to involve volumetric average used for SOC calculation:

$$\left(\frac{\Delta SOC}{\Delta t}\right)\Big/c_{s_{factor}} = ((\frac{2M_r - 1}{2}) * \left(\frac{M_r}{M_r - 1}\right)^3 * \alpha_2 * \Delta r)/(c_{s_{max}} * R_s * Q_{max} * (\theta_{p_{100\%}} - \theta_{p_{0\%}}) \tag{3.63}$$

The aforementioned relationship is used as an optimization constraint. The optimizer is used to identify the electrode area (A) and then using the previous constraint to calculate the electrode thickness δ as follows:

$$\delta = \left(\frac{1}{A}\right) * \left(\left(\frac{2M_r - 1}{2}\right) * \left(\frac{M_r}{M_r - 1}\right)^3 * \alpha_2 * \Delta r * \ c_{s_{factor}}\right)/(c_{s_{max}} * R_s * Q_{max} * (\theta_{p_{100\%}} - \theta_{p_{0\%}}) \tag{3.64}$$

This relationship indicates that capacity degradation due to battery aging is attributed to a decreased sphere effective volume.

3.6 Parameters Optimization

A benchmark Urban Dynamometer Driving Schedule has been used for data fitting. Experimental data from $LiFePO_4$ cells have been collected and fitted to the reduced-order model. Even though the reduced-order model has fewer parameters compared to the full-order model, model parameters are still difficult to identify. Accordingly, in this work, the full-set of the reduced-order model parameters are being attained using genetic algorithm optimization.

3.6.1 Parameters to be identified

The full-set of the reduced-order electrochemical battery model parameters have been identified. The 18 parameters are as follows: the solid maximum particle concentration in the anode and cathode $(c_{s,max,p}, c_{s,max,n})$, positive and negative diffusion coefficients $(D_{s,p}, D_{s,n})$, positive and negative active surface area per electrode $(a_{s,p}, a_{s,n})$, positive and negative electrode area (A), electrode film resistance (R_{SEI}) (also known as the solid electrolyte interface resistance), maximum positive and negative solid normalized concentrations (stoichiometry values) $(\theta_{p_{100}}, \theta_{n_{100}})$, minimum positive and negative normalized solid concentration $(\theta_{p_0}, \theta_{n_0})$, anode and cathode particle radiuses (R_{s_p}, R_{s_n}), active material volume fraction $(e_{s,p}, e_{s,n})$, average electrolyte concentration $(\bar{c}_e)$, and positive and negative current coefficient or reaction rate (k_0). Some parameters are held constant as shown in Table 3.4.

Table 3.4. Fixed Model Parameters (held constant during optimization)

Parameter name (unit)	*Parameter value*
Change transfers coefficient $\boldsymbol{\alpha}_{\mathbf{a}}$, $\boldsymbol{\alpha}_{\mathbf{c}}$	0.5,0.5
Universal gas constant ($\boldsymbol{J\,K^{-1}\,mol^{-1}}$)	8.3144 e+4
Temperature (°$\boldsymbol{K}$)	298.15
Faraday's constant ($\boldsymbol{C\,mol^{-1}}$)	96485

3.6.2 Genetic Algorithm optimization Technique

Genetic algorithms are search techniques based on the evolutionary model. They are best suited for complex problems in which obtaining a gradient is rather difficult. In addition, GA is a global optimization search algorithm for complex, non-unimodal objective functions. A detailed description of genetic algorithms can be found in references, [21, 22]. A brief summary of the method used in this paper is summarized below, [23].

A. *Creation of random initial population*

In this work, 1000 individuals have been used for every population. The initial range is set as illustrated in Table 5. An initial guess based on literature for parametric values and according to the authors' best knowledge has been adopted in this work.

B. *Generating a sequence of new populations as follows:*

- *The fitness value of each population member is valuated and the raw fitness values are scaled to generate an operational range of values.*
- *Individuals are selected based on their fitness function, these individuals are called parents.*
- *Off springs are generated from the population by crossover or mutation.*

- *Low fitness individuals are replaced from current population by new off-springs to for the next generation.*

C. *The steps are repeated until the stopping criteria is reached. This include a maximum number of iterations of 10 or a minimum RMSE of 1e-5.*

3.6.3 Results and Discussions

During optimization, bounds have been set on all 18 parameters, as given in Table 5. In order to identify the electrochemical model parameters using the Genetic Algorithm (GA), an objective function has to be selected. The parameter identification objective function used in this research is targeted at minimizing the error between the model output terminal voltage $\hat{V}(t)$ and the experimentally measured terminal voltage $V(t)$. The objective function is a cumulative sum of the squared voltage error as follows:

$$min \int_0^T \left(V(t) - \hat{V}(t)\right)^2 dt \tag{3.65}$$

The Urban Dynamometer Driving Schedule (UDDS) has been used for parameter fitting. The UDDS driving cycle has been selected since it entails fast changing signal, rich in its frequency content thus favoured when optimization strategies are applied. The driving cycle includes resting periods thus captures the battery relaxation effects. In addition, the cycle includes charging current that represents regenerative braking in addition to discharging currents representing vehicle acceleration. The driving cycle has been previously used to get the electrochemical battery model parameters for the full-order electrochemical model in previous publication, [5]. As shown in the paper, the model will be validated using other driving cycles (HWFET, US06) that has never been used during parameter extraction process and the model exhibits good accuracy. The Genetic Algorithm

(GA) starts varying the 18 model parameters to be identified. The GA is best suited in this application since gradient information is hard to evaluate for the electrochemical model.

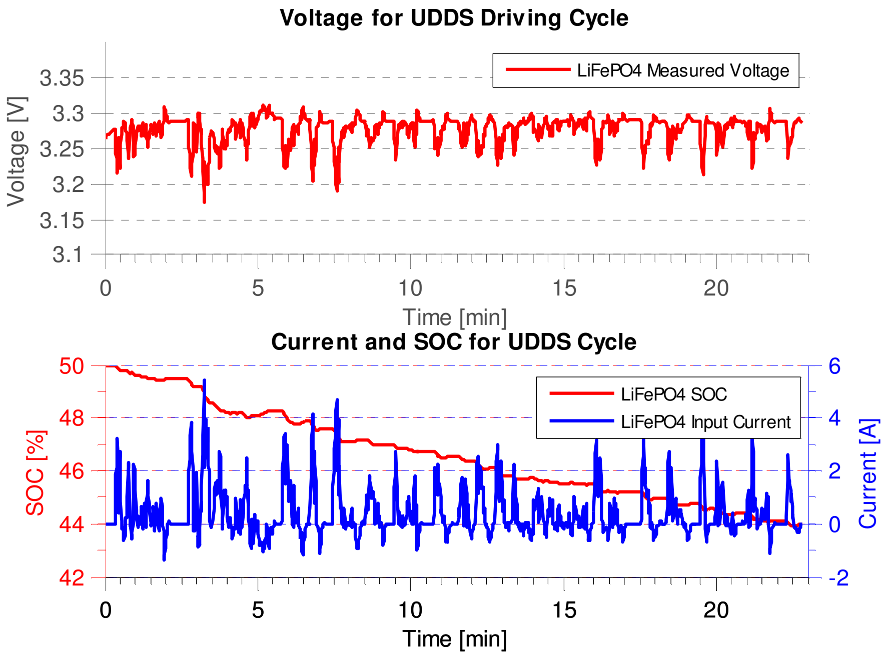

Figure 3.16. Battery Voltage (Upper Figure), SOC and Current (Bottom Figure) for one UDDS Cycle

The scaled current input from an Urban Dynamometer Driving cycle has been used as an input to the model along with the parameter guess generated by the GA.

Table 3.5. Electrochemical Battery Model Optimizer Bounds

Parameter name (electrode) (symbol) (unit)	*Lower Bound*	*Upper Bound*
Maximum solid-phase concentration (Positive) ($\boldsymbol{C_{s,max,p}}$) ($\boldsymbol{mol/cm^3}$)	1e-4	0.1
Maximum solid-phase concentration (Negative) ($\boldsymbol{C_{s,max,n}}$) ($\boldsymbol{mol/cm^3}$)	1e-4	0.1
Solid phase diffusion coefficient (Positive) ($\boldsymbol{D_{s,p}}$) ($\boldsymbol{cm^2/sec}$)	1e-15	1e-8
Solid phase diffusion coefficient (Negative) ($\boldsymbol{D_{s,n}}$) ($\boldsymbol{cm^2/sec}$)	1e-15	1e-8
Active surface area per electrode unit volume (Positive) ($\boldsymbol{a_{s,p}}$)	10000	180000

Active surface area per electrode unit volume (Negative) ($a_{s,n}$)	10000	130000
Maximum solid concentration (Positive) ($\theta_{p_{100\%}}$)	0	1
Minimum solid concentration (Positive) ($\theta_{p_{0\%}}$)	0	1
Maximum solid concentration (Negative) ($\theta_{n_{100\%}}$)	0	1
Minimum solid concentration (Negative) ($\theta_{n_{0\%}}$)	0	1
Particle radius (Positive) ($R_{s,p}$) (cm)	1e-7	1e-1
Particle radius (Negative) ($R_{s,n}$) (cm)	1e-7	1e-1
Active material volume fraction (Positive) ($e_{s,p}$)	0	1
Active material volume fraction (Negative) ($e_{s,p}$)	0	1
Reaction rate (k_0)	1000	12000
Solid Electrolyte interface Resistance (R_{SEI}) (Ω)	0	1
Average electrolyte concentration ($\bar{c}_e$) (mol/cm^3)	1e-5	1e-1
Electrode plate area (Positive, Negative) (A) (cm^2)	100	20000

The current is scaled down by a factor of 15 assuming 15 cells are connected in parallel, also, cell balancing is ignored in this context. Current, voltage, and SOC data from a UDDS cycle are shown in Figure 3.16 (assuming positive current for discharge and negative current for charge). The model is simulated once for every member of the population and the terminal voltage is further compared with the experimental terminal voltage. Since over-potential equations (3.29) and (3.30) used for terminal voltage calculation involve square root calculation, it might generate complex numbers. Therefore, when setting up the cost function, if any population generates complex terminal voltage, it is penalized by setting the terminal voltage to a very large number.

The GA optimization has been set to 10 runs and to 1000 population size due to extensive computational complexity required by the algorithm. The algorithm has been conducted on a mobile workstation with 3.0 GHz, quad Core i7-3940XM Extreme Edition processor.

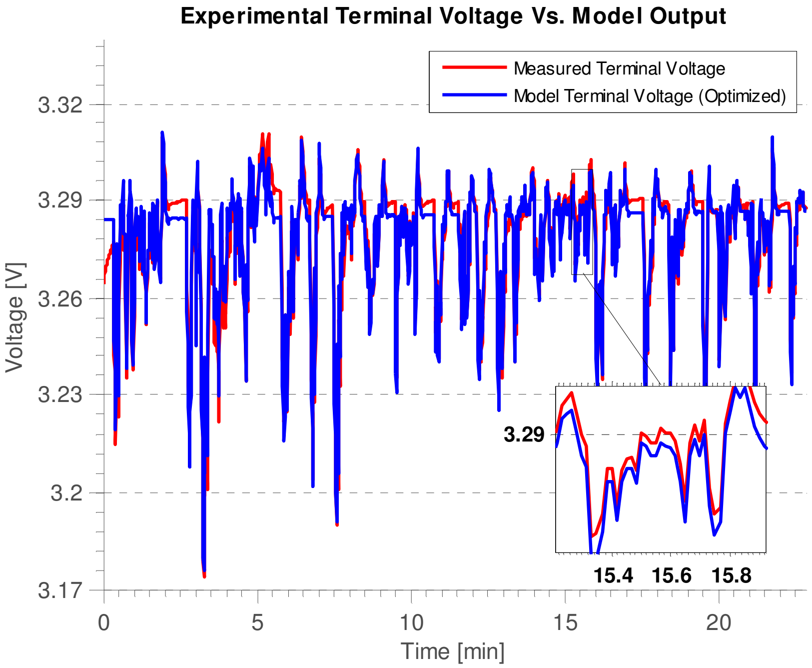

Figure 3.17. Electrochemical Battery Model vs. Experimental Data from a UDDS Driving Cycle

The estimated value of the R_{SEI} inherently includes current collectors and electrolyte resistance. The algorithm requires approximately 6 hours to generate the optimized parameters.

Table 3.6. Electrochemical Battery Model Optimized Parameters

Parameter name (electrode) (symbol) (unit)	*Optimized Parameters*
Maximum solid-phase concentration (Positive) ($C_{s,max,p}$) (mol/cm^3)	0.04782
Maximum solid-phase concentration (Negative) ($C_{s,max,n}$) (mol/cm^3)	0.08147
Solid phase diffusion coefficient (Positive) ($D_{s,p}$) (cm^2/sec)	7.432474 e-09
Solid phase diffusion coefficient (Negative) ($D_{s,n}$) (cm^2/sec)	1.139458 e-09
Active surface area per electrode unit volume (Positive) ($a_{s,p}$)	164083.82
Active surface area per electrode unit volume (Negative) ($a_{s,n}$)	65588.80
Maximum solid concentration (Positive) ($\theta_{p_{100\%}}$)	0.9149
Minimum solid concentration (Positive) ($\theta_{p_{0\%}}$)	0.6976
Maximum solid concentration (Negative) ($\theta_{n_{100\%}}$)	0.3101
Minimum solid concentration (Negative) ($\theta_{n_{0\%}}$)	0.1535
Particle radius (Positive) ($R_{s,p}$) (cm)	0.0015
Particle radius (Negative) ($R_{s,n}$) (cm)	0.0264
Active material volume fraction (Positive) ($e_{s,p}$)	0.1646
Active material volume fraction (Negative) ($e_{s,n}$)	0.7970
Reaction rate (k_0)	10016.583
Solid Electrolyte interface Resistance (R_{SEI}) (Ω)	0.0104
Average electrolyte concentration ($\bar{c}_e$) (mol/cm^3)	0.0851
Electrode plate area (Positive, Negative) (**A**) (cm^2)	16524.27

The identified values generated by the GA are summarized in Table 3.6. As shown in Figure 3.17, the optimized electrochemical battery model output fits the experimental data quite well. The slight shift is due to the averaging of the OCV and SOC relationship and due to the approximations from the full-order to the reduced-order form. Recall that the model assumes constant electrolyte concentration and only one representative particle for each electrode. The root mean square error (RMSE) between the measured terminal voltage ($V(t)$) and the electrochemical model output ($\widehat{\boldsymbol{V}}(\boldsymbol{t})$) for n number of samples can be calculated as follows:

$$\boldsymbol{RMSE} = \sqrt{\frac{\sum_{t=1}^{n} \boldsymbol{V}(\boldsymbol{t}) - \widehat{\boldsymbol{V}}(\boldsymbol{t})}{\boldsymbol{n}}} \tag{3.66}$$

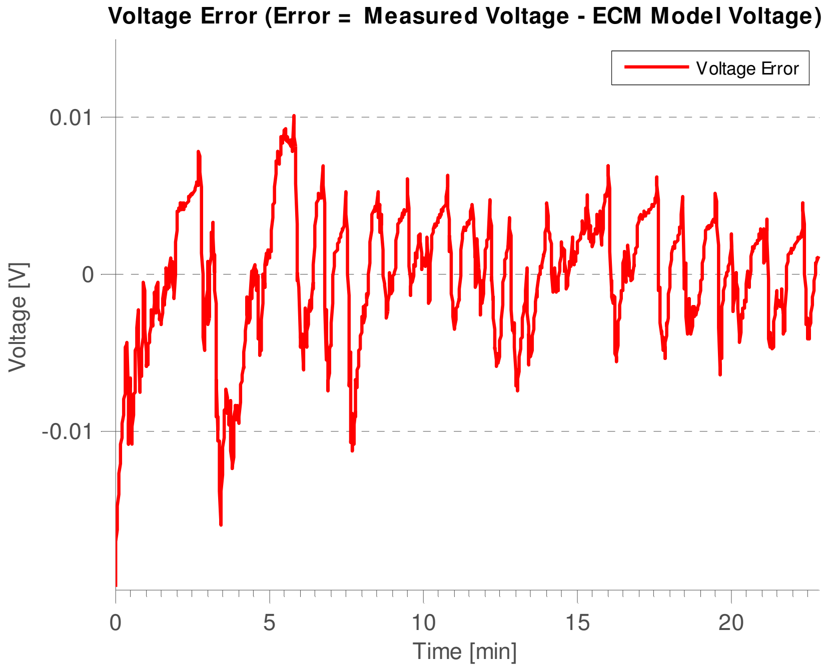

Figure 3.18. Voltage Error between experimental and ECM Output

The error between experimental and the ECM model output is shown in Figure 3.18. Using the optimized battery model parameters, the RMSE for a UDDS cycle is 0.22057 mV. The actual battery SOC Vs. electrochemical battery model output SOC based on spherical average are shown in Figure 3.19. The actual SOC is calculated using coulomb counting provided by the Arbin cycler.

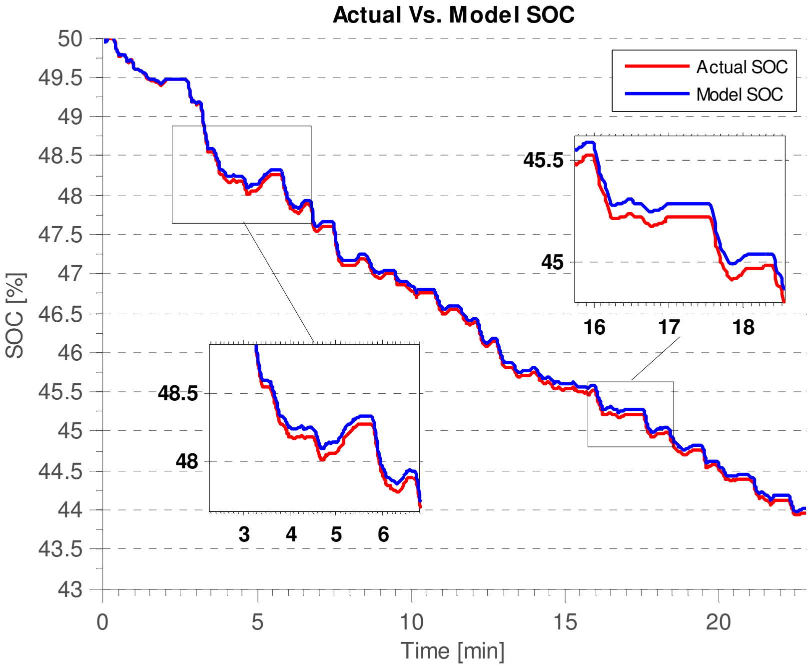

Figure 3.19. Actual SOC (using Coulomb Counting) Vs. Model SOC

The SOC has been reset before conducting the test to minimize accumulated error due to integration. The histogram of the voltage error is shown in Figure 3.20.

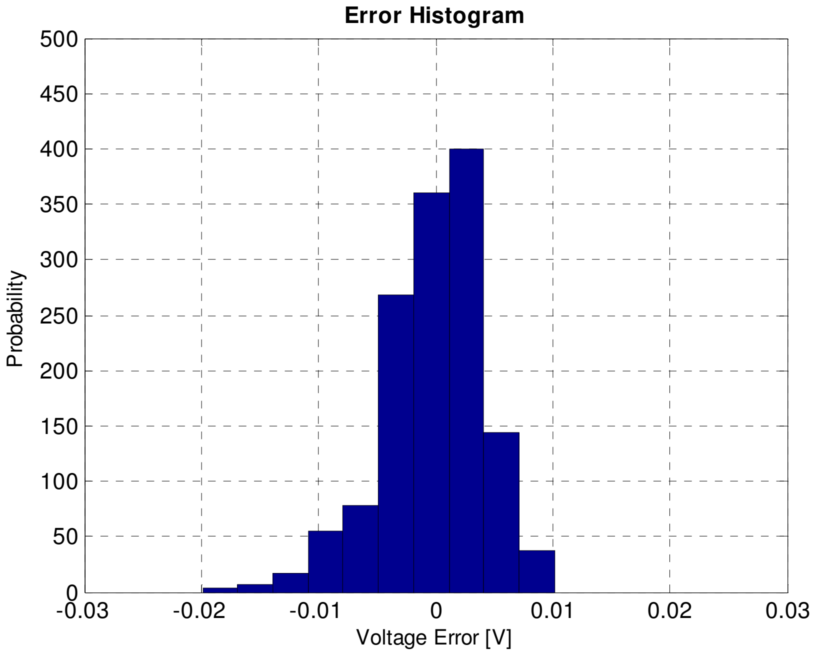

Figure 3.20. Probability density plot of voltage error for UDDS cycle

As shown, the maximum absolute error is within 0.02 V which indicates that the model is very accurate using the optimized parameter values at this specific state of life. As battery ages, model parameters will significantly change and will result in model deviation. One of the major advantages of electrochemical modeling in comparison to the equivalent circuit-based models is that a further insight into lithium concentrations in both electrodes can be monitored. As shown in Figure 3.21, the solid-electrolyte interface concentration in the cathode and the anode for a UDDS cycle is presented.

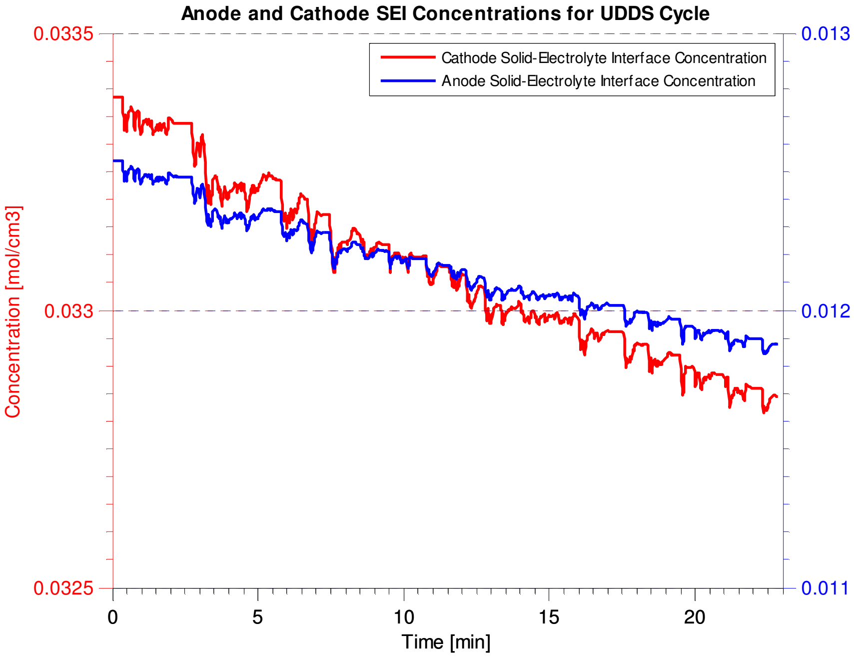

Figure 3.21. Anode and Cathode Lithium Concentrations at the Solid-Electrolyte Interface

Furthermore, Figure 3.22 shows the variations of lithium concentrations across various shells (10 shells) in the cathode for the UDDS cycle. It is clear that the solid-electrolyte interface concentration is rapidly varying since it is directly related to the terminal voltage concentrations, while the other inner shells are slowly varying since they are not directly exposed to the Butler-Volmer current. This describes the fact that the battery exhibits relaxation effects for zero current input which is related to the variation of lithium concentration at the surface, as it decays to the inner shells over time. The total sphere concentration is held constant for zero input current and accordingly the battery state of charge is fixed.

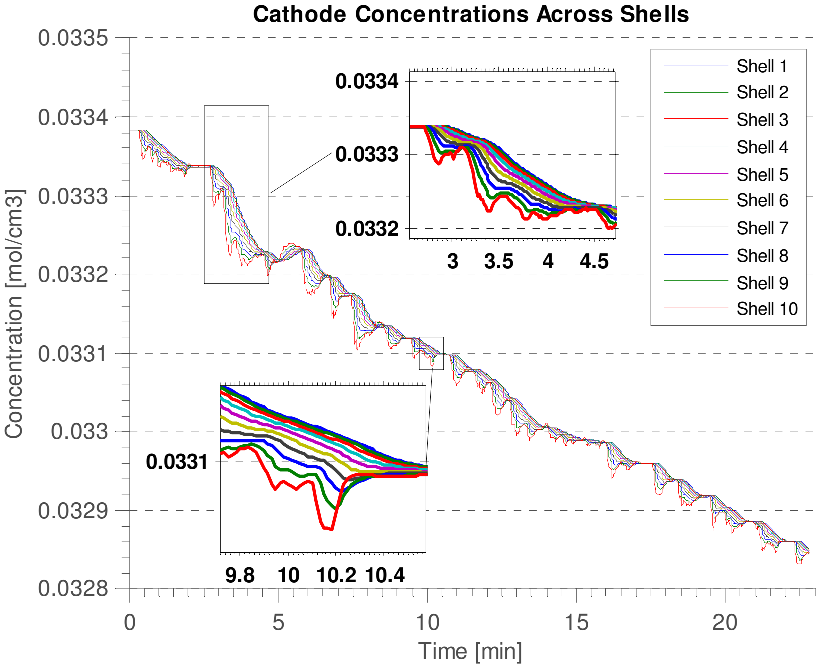

Figure 3.22. Lithium Concentration in the Cathode across Various Shells

3.6.4 Model validation

The optimized model along with the developed SOC parameterization strategy has been validated using other real-world driving cycles that have never been seen by the model. Current profiles from highway fuel economy test (HWFET) and a light duty drive cycle for high speed and high load (US06) driving cycles have been used. As shown in Figure 3.23 and 3.24, the identified model parameters using UDDS cycle still generates good results. The RMSE for terminal voltage and SOC using the US06 driving cycle are 0.0041531 V and 0.2932 % respectively.

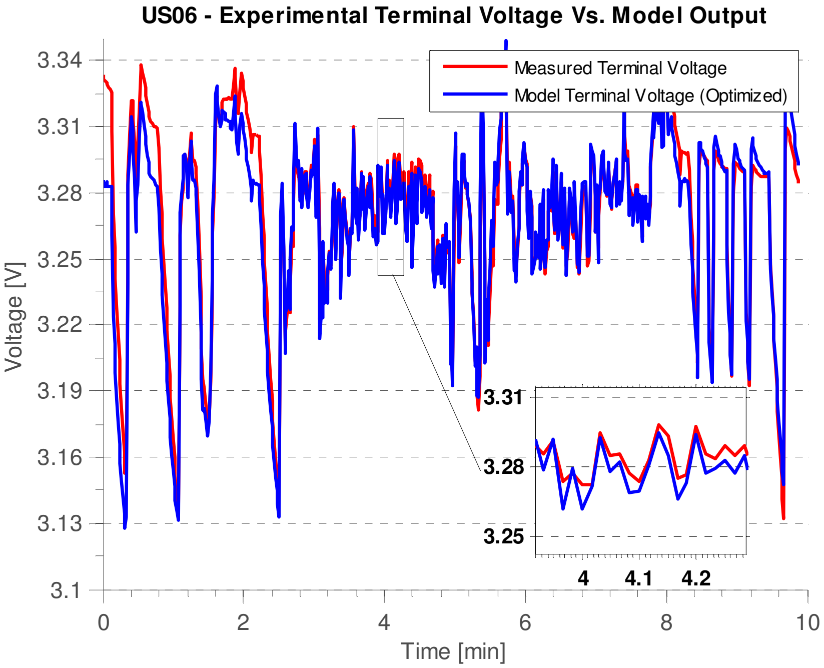

Figure 3.23. Electrochemical Battery Model vs. Experimental Data from a US06 Driving Cycle

As shown in Figure 3.25, the model has also been validated using a HWFET driving cycle, since this driving cycle has never been seen during model fitting, a slight offset between the model and the measured voltage has been exhibited. This is also due to the approximation done during model reduction process from a full-order to a reduced-order form. The offset is due to the averaging process of both charging/discharging SOC-OCV curves. The maximum voltage offset is approximately 0.03 V and the RMSE across the entire driving cycle is 0.0154 V which is relatively small. The ECM model SOC Vs. actual SOC (from the Arbin cycler) are as shown in Figure 3.26, The RMSE for the SOC using the HWFET driving cycle is 0.161 %.

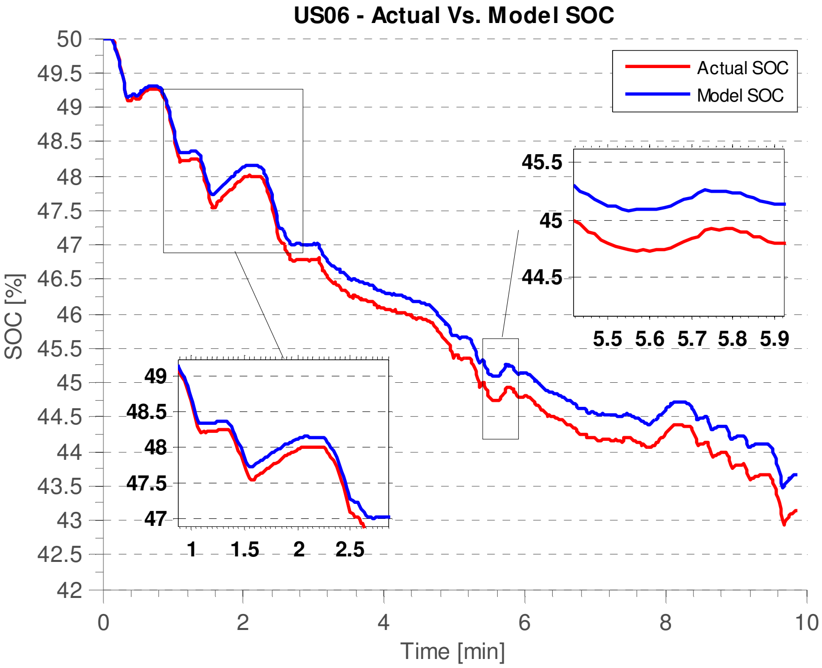

Figure 3.24. Actual SOC (using Coulomb Counting) Vs. Model SOC for US06 Driving Cycle

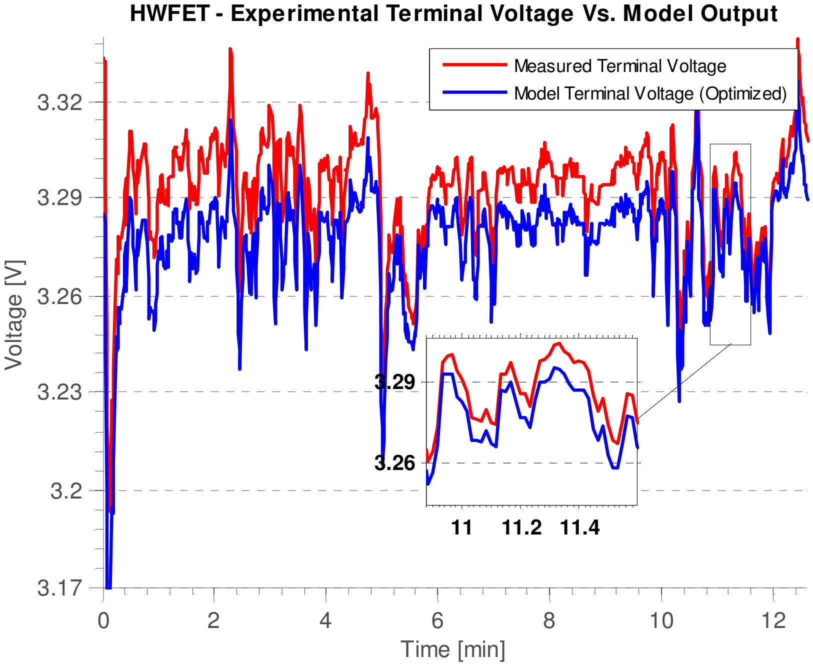

Figure 3.25. Electrochemical Battery Model vs. Experimental Data from a HWFET Driving Cycle

Since these driving cycles have never been utilized during optimization, the RMSE is slightly higher compared to the UDDS cycle. However, the results for terminal voltage and SOC are within the acceptable range of operation. A summary of the terminal voltage and SOC RMSE for all driving cycles used are shown in Figure 3.27. It is clear that since the UDDS cycle has been used for parameter fitting, it generates the least error for both the voltage and the SOC. The HWFET exhibits the highest voltage error while the US06 demonstrates the highest error on SOC.

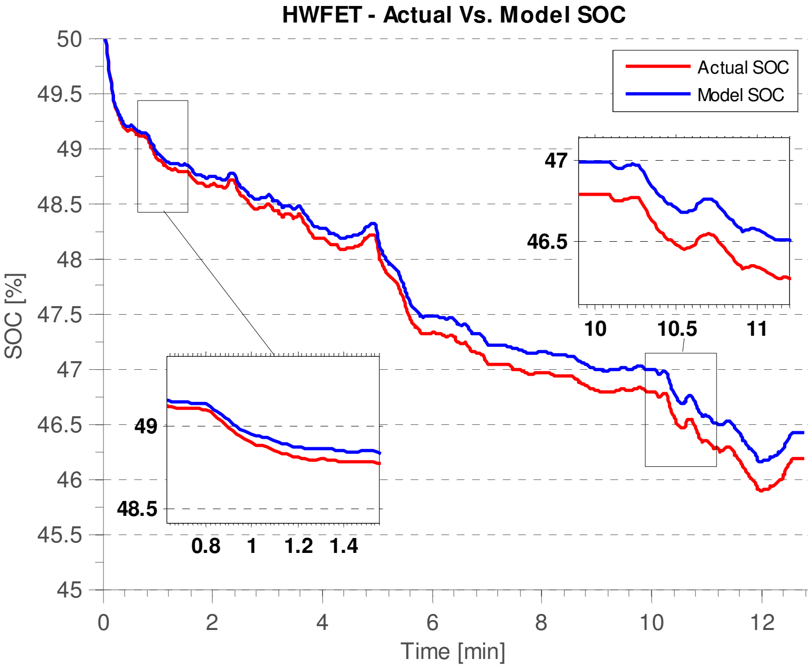

Figure 3.26. Actual SOC (using Coulomb Counting) Vs. Model SOC for HWFET Driving Cycle

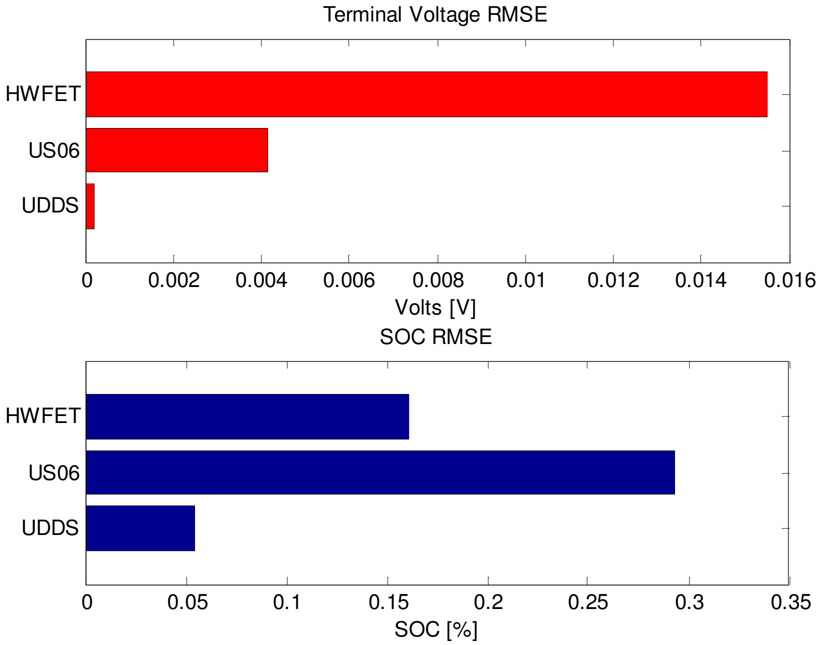

Figure 3.27. Terminal voltage (upper) and SOC RMSE (lower) for all driving cycles

3.7 Conclusions

In this paper, identification of 18 model parameters of the reduced-order electrochemical model using genetic algorithms has been conducted. The technique can be used for a non-invasive determination of the electrochemical model parameters for any battery chemistry. Furthermore, a SOC parameterization model has been developed and effectively utilized as a constraint during the parameter optimization process. The electrochemical model with optimized parameters fits voltage experimental data very well with an RMSE of approximately 0.2 mV over one UDDS cycle. Moreover, spherical average concentration can be effectively used for SOC calculation provided that the initial SOC is known.

The reduced-order model results in heavy loss of information from the full-order model. However, it still maintains a strong connection to the internal battery potential and diffusion dynamics which are beneficial for the state of health estimation. Future research involves extension of the proposed methodology to incorporate changes of aging parameters using correlation with ampere-hour throughput and other aging parameters such as battery discharge rate, temperatures, and depth of discharge.

Acknowledgments

Financial support from Ford Motor Company and NSERC (National Sciences and Engineering Research Council of Canada) is gratefully acknowledged. The authors would also like to thank researchers and engineers: Robyn Jackey, Javier Gazzarri, and Kevin Rzemien from MathWorks Inc. for their help with the electric vehicle model development and tuning.

APPENDIX

Full-Order Electrochemical Battery Model

The full order electrochemical battery model is described in this section. Diffusion dynamics in one dimensional (1-D), single axis (X-axis) is only considered while diffusion dynamics in both dimensions (Y-axis and Z-axis) are ignored, [24, 25]. The state variables required to describe the 1D-spatial model at any x, t are the electric potential in the solid electrode $\phi_s(x,t)$, the electric potential in the electrolyte $\phi_e(x,t)$, the lithium concentration in the solid phase $c_s(x,r,t)$ and the lithium concentration in the electrolyte $c_e(x,t)$. Mathematical equations to model the electrochemical behavior of a Li-ion battery is presented below, the input to the model is the external current I applied to the battery, and the output of the model is the corresponding output voltage V [26]. The 1D-spatial electrochemical model consists of four PDEs [27], the solid and electrolyte potentials are described by the following two equations [24, 25]:

$$\frac{\partial}{\partial x} k^{eff} \frac{\partial}{\partial x} \emptyset_e + \frac{\partial}{\partial x} k_D^{eff} \frac{\partial}{\partial x} \ln c_e = -j^{Li} \tag{A1}$$

$$\frac{\partial}{\partial x} \sigma^{eff} \frac{\partial}{\partial x} \emptyset_s = j^{Li} \tag{A2}$$

The diffusion of lithium in the electrolyte is modeled using Fick's law for linear coordinates as shown by equation (A3) [24, 25],

$$\frac{\partial \varepsilon_e c_e}{\partial t} = \frac{\partial}{\partial x}\left(D_e^{eff} \frac{\partial c_e}{\partial x}\right) + \frac{1-t^0}{F} j^{Li} \tag{A3}$$

While the solid (electrode) phase diffusion is modeled by Fick's laws of diffusion for spherical coordinates as shown in equation (A4), [24, 25]:

$$\frac{\partial c_s}{\partial t} = \frac{\partial}{\partial r}(D_s \frac{\partial c_s}{\partial r}) \tag{A4}$$

In order to simplify the model, the electrolyte concentration (c_e) is assumed to be constant. This approximation will greatly simplify the model while preserving accuracy of <5% compared to the detailed model [9]. After simplification, equation (A3) is removed, equations (A2) and (A4) remain unchanged, and equation (A1) is being simplified as follows, [24, 25]:

$$\frac{\partial}{\partial \mathrm{x}} \mathrm{k}^{\mathrm{eff}} \frac{\partial}{\partial \mathrm{x}} \emptyset_{\mathrm{e}} = -\mathrm{j}^{\mathrm{Li}} \tag{A5}$$

Equations (A6) and (A7) introduce the solid current density (i_s) $(\mathrm{A/cm^2})$ and the electrolyte current density (i_e) $(\mathrm{A/cm^2})$, [24, 25]:

$$i_e(x) = -k^{eff} \frac{\partial}{\partial x} \emptyset_e \tag{A6}$$

$$i_s(x) = -\sigma^{eff} \frac{\partial}{\partial x} \emptyset_s \tag{A7}$$

Thus, the solid and electrolyte potential equations (A1) and (A2) can be re-written as follows, [24, 25]:

$$\frac{\partial}{\partial x} i_e(x) = j^{Li} \tag{A8}$$

$$\frac{\partial}{\partial x} i_s(x) = -j^{Li} \tag{A9}$$

The Butler-Volmer current density is described [24, 25]:

$$J^{Li} = a_s j_o [exp\left(\frac{\propto_a F}{RT}\eta\right) - exp(\frac{\propto_c F}{RT}\eta)] \tag{A10}$$

Where R and F are the universal gas constant and Faraday's constant, T is the absolute temperature and η is the over potential [24, 25].

$$\eta = \emptyset_s - \emptyset_e - U(c_{se}) \tag{A11}$$

In equation (A11), U is the open circuit voltage which is a function of the lithium concentration at the solid-electrolyte interface $c_{se}(x,t) = c_s(x, R_s, t)$. The concentration at the interface between the solid and the electrolyte is related to the critical surface charge (CSC), [24, 25]:

$$CSC(t) = \frac{\theta - \theta_{0\%}}{\theta_{100\%} - \theta_{0\%}} \tag{A12}$$

By defining the normalized solid-electrolyte concentration θ as follows, [24, 25]:

$$\theta = \frac{solid - electrolyte\ concentration}{maximum\ solid\ concentration} = \frac{c_{se}}{c_{s,max}} \tag{A13}$$

Where, $\theta_{0\%}$ and $\theta_{100\%}$ are the normalized concentrations corresponding to 0% (fully discharged) and 100% (fully charged). $\theta_{100\%}$ can be defined by obtaining the concentration corresponding to the maximum fully charged battery. Subsequently, the 0% reference value can be calculated by subtracting the battery capacity Q as, [10]:

$$\theta_{0\%} = \theta_{100\%} - \frac{Q}{\delta}(\frac{1}{AF\varepsilon c_{s,max}}) \tag{A14}$$

The open circuit voltage varies from the cathode and the anode. An empirical relationship is used to relate the open circuit voltage to the normalized state of charge which is given by, [28]:

$$\begin{aligned} U_n(\theta_n) = {} & 8.0029 + 5.064\theta_n - 12.578\theta_n^{0.5} - 8.6322 \times 10^{-4}\theta_n^{-1} + 2.176 \times 10^{-5}\theta_n^{\frac{3}{2}} \\ & - 0.46016\, exp[15(0.06 - \theta_n)] - 0.55364 exp[-2.4326(\theta_n - 0.92)] \end{aligned} \tag{A15}$$

For the positive electrode, the empirical equation is as follows [9]:

$$\begin{aligned} U_p(\theta_p) = {} & 85.681\theta_p^6 - 357.7\theta_p^5 + 613.89\theta_p^4 - 555.65\theta_p^3 + 281.06\theta_p^2 - 76.648\theta_p + 13.1983 \\ & - 0.30987 exp(5.657\theta_p^{115}) \end{aligned} \tag{A16}$$

The coefficient j_o depends on the solid and electrolyte concentrations according to the following equations, [24, 25]:

$$j_o = (c_e)^{\alpha_a} (c_{s,max} - c_{se})^{\alpha_a} (c_{se})^{\alpha_c} \tag{A17}$$

The solid potential is related to the measured cell potential as follows, [24, 25]:

$$V = \emptyset_s(x = L) - \emptyset_s(x = 0) - R_{SEI} I \tag{A18}$$

where R_{SEI} is the solid electrolyte interface (film) resistance at the electrode surface, this resistance increases after charging and discharging cycles (battery aging). As mentioned earlier, the full order model is relatively complex so further simplification is necessary for its real-time applications such as in control and condition monitoring.

References

[1] J. LeSage, "Long-term maintenance costs show benefit of electric vehicles over ICEs," Green Auto Blog, 2012.

[2] C. Shiau, C. Samaras, R. Hauffe and J. Michalek, "Impact of battery weight and charging patterns on the economic and environmental benefits of plug-in hybrid vehicles," *Energy Policy,* vol. 37, no. 7, p. 2653–2663, 2009.

[3] S. E. Samadani, R. A. Fraser and M. Fowler, "A Review Study of Methods for Lithium-ion Battery Health Monitoring and Remaining Life Estimation in Hybrid Electric Vehicles," *SAE International ,* 2012.

[4] C. Speltino, D. D. Domenico, G. Fiengo and A. Stefanopoulou, "Experimental identification and validation of an electrochemical model of a Lithium-Ion Battery," 2009.

[5] J. C. Forman, S. J. Moura, J. L. Stein and H. K. Fathy, "Genetic identification and fisher identifiability analysis of the Doyle–Fuller–Newman model from experimental cycling of a LiFePO4 cell," *Journal of Power Sources,* no. 210, pp. 263-275, 2012.

[6] "www.MathWorks.com/Matlabcentral/fileexchange," [Online].

[7] M. Doyle, T. Fuller and J. Newman, "Modeling of Galvanostatic Charge and Discharge of the Lithium/Polymer/insertion Cell," *Journal of Electrochemical Society ,* vol. 140, pp. 1526-1533, 1993.

[8] D. Domenico, S. Anna and F. Giovanni, "Lithium-Ion Battery State of Charge and Critical Surface Charge Estimation Using an Electrochemical Model-Based Extended Kalman Filter," *Journal of Dynamic Systems, Measurement, and Control,* vol. 132, pp. 1-11, 2010.

[9] K. Smith and C. Y. Wang, "Solid-State Diffusion Limitations on Pulse Operation of a Lithium-Ion Cell for Hybrid Electric Vehicles," *Journal of Power Sources,* p. 628–639, 2006.

[10] D. D. Domenico, G. Fiengo and A. Stefanopoulou, "Lithium-Ion battery State of Charge estimation with a Kalman Filter based on a electrochemical model," *IEEE Interantional Conference on control Applications (CCA),* pp. 702-707, 2008.

[11] "http://www.epa.gov/nvfel/testing/dynamometer.htm," U.S. EPA. [Online].

[12] R. E. Kruse and T. A. Huls, "Development of the Federal Urban Driving Schedule," May 14, 1973.

[13] "http://www.wired.com/autopia/2010/11/honda-finds-evs-a-perfect-fit," [Online].

[14] C. Hua, B. D. Younb and J. Chung, "A multiscale framework with extended Kalman filter for lithium-ion battery SOC and capacity estimation," 2012.

[15] "www.epa.gov/nvfel/testing/dynamometer.htm," EPA United States Environmental Protection Agency. [Online].

[16] U. D. o. Energy, "Plug-In Hybrid Electric Vehicle Value Proposition Study," U.S. Department of Energy, ORNL/TM-2010/46, July, 2010.

[17] "Battery Test Manual for Plug-In Hybrid Electric Vehicles," U.S. Department of Energy, Idaho National Laboratory, Idaho Falls, Idaho 83415, March 2008.

[18] G. L. Plett, "Extended Kalman filtering for battery management systems of LiPB-based HEV battery packs: Part 3. State and parameter estimation," *Journal of Power Sources,* no. 134, p. 277–292, 2004.

[19] Y. Fuentes. and M. Doyle , "Computer simulations of a lithium-ion polymer battery and implications for higher capacity next-generation battery designs," *Journal of Electrochemical Society,* vol. 150, p. A706–A713, 2003.

[20] C. Speltino, D. D. Domenico , F. Giovanni and A. Stefanopoulou, "Experimental identification and validation of an electrochemical model of a Lithium-Ion Battery".

[21] J. Holland, "Adaptation in Natural and Artificial Systems," *University of Michigan Press, Ann Arbor,* 1975.

[22] D. Goldberg, "Genetic Algorithms in search, Optimization, and MAchine Learning," *Addison-Wesley, Reading, Massachusetts,* 1989.

[23] M. Inc, "www.mathworks.com/help/grads/how-the-genetic-algorithm-works.html," 2013. [Online].

[24] J. Newman and W. Tiedemann, "Porous-electrode theory with battery applications," *AIChE Journal,* vol. 21, no. 1, pp. 25-41, 1975.

[25] A. J. Bard and L. R. Faulkner, "Electrochemical Methods: Fundamentals and Applications," *Russian Journal of Electrochemistry,* vol. 38, no. 12, 2002.

[26] N. Chaturvedi, R. Klein, J. Christensen, J. Ahmed and A. Kojic, "Algorithms for Advanced Battery-Management Systems Modeling, Estimation and Control Challenges for Lithium-ion Batteries," *IEEE CONTROL SYSTEMS MAGAZINE,* pp. 49-68, 2010.

[27] K. Smith and C.-Y. Wang, "Solid-state diffusion limitations on pulse operation of a lithium ion cell for hybrid electric vehicles," *Journal of Power Sources,* vol. 161, no. 1, pp. 628-639, 2006.

[28] M. Doyle and Y. and Fuentes, "Computer Simulations of a Lithium-Ion Polymer Battery and Implications for Higher Capacity Next-Generation Battery Designs," *Journal of Electrochemistry Society,* p. A706–A713, 2003.

Chapter 4: Reduced-Order Electrochemical Model Parameter Identification and SOC Estimation for Healthy and Aged Li-Ion Batteries

Part II: Aged Battery Model and State of Charge Estimation

Ryan Ahmed[1], Mohammed El Sayed[1], Jimi Tjong[2], Saeid Habibi[1]

[1]McMaster Automotive Resource Center (MARC), Department of Mechanical Engineering, McMaster University, Hamilton, Canada
[2]Ford Motor Company of Canada, Powertrain Engineering Research and Development Center (PERDC), Windsor, Canada

Abstract

Recently, extensive research has been conducted in the field of battery management systems due to increased interest in vehicles electrification. Parameters such as battery state of charge and state of health are of critical importance to ensure safety, reliability, and prolong battery life. This paper includes the following contributions: (1) tracking reduced-order electrochemical battery model parameter variations as battery ages, using genetic algorithm optimization technique, (2) the development of an aged battery model capable of capturing battery degradation by varying the electrode effective volume, (3) estimation of the battery critical surface state of charge using a new estimation strategy known as the Smooth Variable Structure Filter. The proposed filter is used for state of charge estimation, and demonstrates strong robustness to modeling uncertainties which is relatively high in case of reduced-order electrochemical models. Batteries used in this research are lithium-Iron Phosphate cells widely used in automotive applications. Extensive testing using real-world driving cycles are used for State of Health and State of Charge estimation and for conducting aging tests.

Keywords: Lithium-Ion Batteries, state of charge estimation, state of health estimation, electrochemical battery model, smooth variable structure filter.

- **Corresponding Author:**

  Ryan Ahmed, M.A.Sc, P.Eng., SCPM
  Research and Development Engineer, McMaster University
  Stanford Certified Project Manager

- **This paper has been accepted for publication at the IEEE Journal of Emerging Technologies and Selected Topics in Power Electronics (*Special issue on Transportation and Electrification, 2014*)**

4.1 Introduction

This paper considers strategies pertaining to battery state of charge (SOC) estimation and parameter identification for reduced-order electrochemical models in relation to aging. The paper presents an extension to previous research reported in [1], in which battery model parameters for fresh batteries were obtained by using genetic algorithms. In this paper, an aging model for lithium-Ion batteries that are increasingly used in electrified vehicles is developed. Here, battery aging is captured by changing the effective volume of the electrode.

4.1.1 Motivation and Technical Challenges

Battery State of Charge (SOC) and State of Health (SOH) estimation are challenging tasks, given that automotive batteries are designed to meet fast transient demands resulting from vehicle acceleration and deceleration according to driving profiles. In order to ensure a reliable electric vehicle performance, precise estimation of lithium-Ion battery SOC and SOH is necessary, [2]. SOC is defined as the remaining pack capacity thus provides an indication of the vehicle remaining driving range, [3]. SOH is a measure of the irreversible degradation that occurs in the battery performance due to cycling, [3]. SOH provides an indication of the current state of the battery compared to its new or fresh state before cycling, [3]. SOH is a measure of the battery capability to respond to the required power demand and is an indicator for triggering maintenance or replacement. In general, two main critical factors are considered when addressing the battery SOH, namely: ***capacity fade*** and ***power capability***. The battery ***capacity fade*** has a large impact on the vehicle range and relates to range anxiety. The second factor is the ***power capability*** which impact the vehicle performance and drivability. The remaining useful life (RUL) is used to predict the battery remaining useful time during its life time thus it represents a predictive measure for battery maintenance, [3].

Battery SOC and SOH are highly correlated, and a trade-off exists between extending the life-time of the battery and extending the range of the vehicle, [2]. Discharging the battery to a high level of Depth of Discharge (DOD) (i.e.: low SOC) is generally not recommended as it will significantly shorten the lifetime of the battery. However, this will lead to shorter driving range as only partial charge is being utilized from the entire stored charge. In contrast, charging the battery beyond the acceptable range of operation results in high temperatures and shortens the battery life, [2]. Consequently, an accurate SOC estimate is extremely important in electric vehicles; any deviation in SOC estimation might result in an irreversible loss of capacity or even premature and permanent damage to the battery, [2].

Since electric and hybrid vehicles are relatively new to the market, it will require some time to assess their performance in real-world operation. In particular, the battery might suffer from irreversible degradation due to cycling; a matter that will adversely affect the SOC estimation accuracy. Battery Management Systems (BMS) are used to control energy management in electric vehicles. A BMS has to be adaptive in order to account for aging and degradation in performance that might affect the vehicle range of operation and charging efficiency. For instance, as per October, 2012, there are 112 documented cases of customers complaining of capacity loss in their electric vehicles, [4]. In addition, around

11.8% of the total number of Nissan Leaf vehicles sold in Arizona have exhibited a loss in capacity gauge bars, [4].

4.1.2 Literature Review

Adaptive techniques for SOC estimation are important especially for automotive applications where having an accurate, reliable, and robust estimate is necessary to mitigate the driver range anxiety concerns and ensure safety. In the literature, adaptive SOC estimation techniques are classified under one of the following: ***Fuzzy Logic, Artificial Neural Networks, and filter/observer-based techniques (such as Kalman Filters)***. The work in this paper will focus on filter/observer based methods.

In [5], an estimation strategy based on reduced-order electrochemical battery model is presented. It uses a Kalman filter to estimate the SOC, terminal potentials, and concentration gradients. Estimates are compared against experimental data from a 6 Ah electric vehicle battery cell, [5]. The filter provides accurate and stable estimates for low currents. However, at very high discharge rates (C-rates) large errors are exhibited due to the methods inability to account for large changes in electrolyte concentration near electrodes, [5]. The filter model is of low order and complexity (7 states) that is comparable to equivalent circuit-based models, [5]. The technique is computationally efficient and suitable for real-time applications such as in on-board battery management system, [5].

In [6], a state estimation strategy based on an output error injection observer is proposed. This strategy uses a reduced set of partial differential algebraic equations describing the solid and electrolyte concentrations and potentials. Simulation and experimental results using real-world driving cycles such as the urban dynamometer driving schedule (UDDS) demonstrate the effectiveness of the proposed technique. In [7], a state of charge estimation technique based on a linearized battery model is presented. In order to overcome the nonlinear behaviour of battery models, the Open Circuit Voltage-State of Charge (OCV-SOC) relationship has been divided into linear sections and model parameters are estimated for each section individually, [7]. Then, based on the resultant linear model, an observer is used to estimate the SOC. The technique has been verified on 1.5 Ah lithium-polymer cells, [7].

4.1.3 Contributions

The electrochemical models reported in literature do not commonly account for aging and degradation effects; they have been applied to fresh, healthy batteries only. As batteries age with time, these models become inaccurate and the SOC estimator could diverge or become unstable. Accordingly, developing an adaptive model that can account for cycling effects is therefore important. Such an adaptive model can significantly enhance the existing SOH estimation techniques and can provide an estimate for the battery RUL. Furthermore, published reduced-order electrochemical models are not generally tuned or verified by using SOC and aging experimental data.

This paper presents an aging model that can account for battery degradation at various battery states of life. The model works by varying the effective electrode volume, OCV-SOC relationship, solid-electrolyte interface resistance, and the solid diffusion coefficient to account for aging. The model can be practically implemented in a real-time microprocessor for terminal voltage and state of charge estimation. A strategy for the tuning of model parameters is presented for aged batteries. This strategy is supported and verified by using experimental data from extensive accelerated aging tests conducted on lithium ion battery cells at high depth of discharge and elevated temperatures. The aging tests were continued until the battery cells reached end-of-life (80% of capacity). The method used for SOC estimation is known as the Smooth Variable Structure Filter (SVSF). The SVSF was selected as it demonstrates robustness to modeling uncertainties, sensor noise, and to state of charge initial conditions, [8, 9].

4.1.4 Paper Outline

This paper is organized as follows. Section 4.2 provides a summary of aging tests conducted for experimental data generation. Section 4.3 presents a battery aging model and a strategy for model parameter identification for aged batteries. Section 4.4 describes the SOC estimation using the Smooth Variable Structure Filter (SVSF). Section 4.5 contains the conclusions.

4.2 Aging/Reference Performance Test Experiments

Battery testing procedures vary depending on the country and the application, i.e.: for HEVs, PHEV, or BEVs, [10]. In U.S., battery test procedures are generally classified into 3 main categories: characterization, life, and reference tests, [11].

- **Characterization tests** are conducted to specify battery cell/pack baseline performance characteristics, [11]. Examples of these tests include: static capacity, hybrid pulse power characterization (HPPC), self-discharge, cold cranking, thermal performance, and efficiency tests, [11].

- **Life tests** are conducted to determine battery degradation (aging) effects that take place in both cycle life and calendar life, [11]. Calendar life (shelf life) means the life of the battery during storage (with no cycling involved) while cycle life is the life of the battery after multiple charging/discharging cycles, [10]. The main purpose of these tests is to perform accelerated battery aging for acquiring data in a relatively short time in order to predict the performance of the battery. In addition, these tests can be used for battery warranty estimates.
- **Reference performance tests (RPT):** are conducted periodically to track changes that might occur in the battery baseline characteristics. Reference tests are performed after conducting a certain number of life tests to measure the capacity fade and degradation in performance throughout the entire battery life cycle, [12]. These tests are performed at the beginning (fresh battery) and at the end of life.

This paper reports on a range of experiments that have been conducted on three Lithium Iron Phosphate (LiFePO4) battery cells. Characterization/RPT tests have been conducted at two different states of life, namely: fresh battery (at 100% capacity) and at 80% capacity. A summary of these tests are as follows.

4.2.1 Characterization/RPT tests

Extensive characterization tests have been conducted on fresh and aged batteries at the controlled room temperature of 25℃. Three RPT experiments were conducted as follows: ***A static capacity test at 1C rate, SOC-OCV characterization test, and a driving scenario.*** The scenario includes a mix of driving schedules for an average North American driver.

The data is used for validating the SOC estimation strategy and the associated aging model. A detailed description of the reference performance tests (OCV-SOC, static capacity test) in addition to the experimental setup used in data generation can be found in part I of this paper, [1].

4.2.2 Fast Charge/Discharge Aging (Life) Tests

Aging test using well-defined charging/discharging cycles at elevated temperature (55℃) and high C-rates have been conducted. This accelerated test was conducted to track changes in battery electrochemical model parameters. These tests were conducted 24 hours a day and 7 days a week over a period of 6 months. The test procedure is as follows:

A. *Fully charge the battery in a Constant Current Constant Voltage (CCCV) mode until maximum voltage (3.6V).*
B. *Fully discharge the battery at constant current (CC) mode with 1C-rate until the voltage hits the minimum voltage (2V).*
C. *All cycler current accumulators are reset to zero. At this moment, the battery is at zero state of charge (SOC).*
D. *Charge the battery to 90% SOC.*
E. *Discharge the battery at 10 C-rate until the battery hits the minimum voltage (2V)*
F. *Allow for voltage relaxation for 5 minutes.*
G. *Charge the battery at 4C-rate for 20 minutes. If the battery hits the maximum voltage, CCCV charge mode is maintained.*
H. *Repeat the procedure from D to G for approximately 200 cycles (till capacity hits 80%).*

A summary of one fast charge aging cycle is illustrated in Figure 4.1.

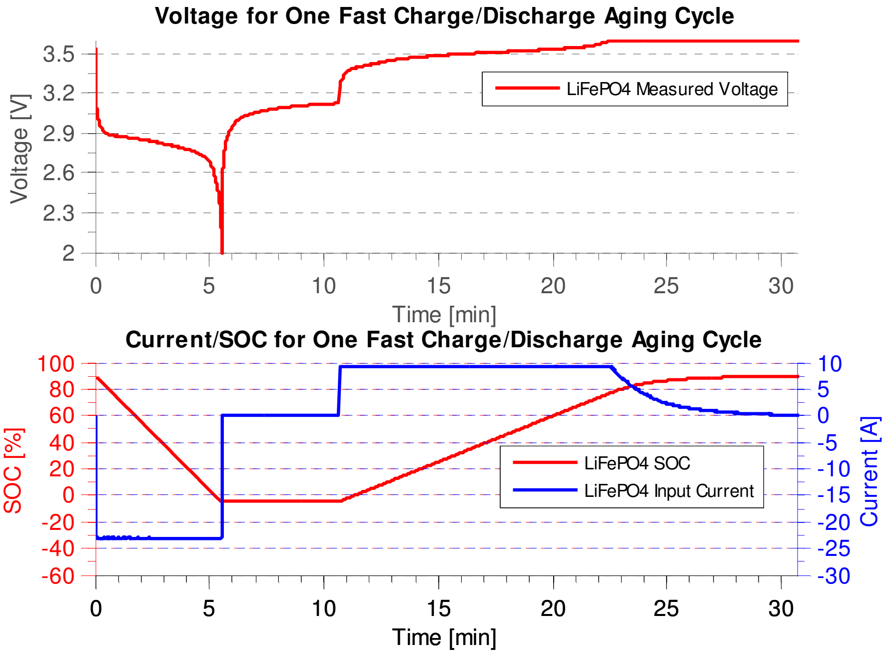

Figure 4.1. Voltage, Current and SOC for One Fast Charge/Discharge Aging Test

4.3 Battery Aging Model Development and Parameters Fitting

In this section, an electrochemical aging model is developed and model parameters for aged batteries at 80% capacity are estimated. Subsection 4.3.1 provides a brief summary of the reduced-order electrochemical battery model. Subsection 4.3.2 illustrates the necessity of having updated model parameters as battery ages. This is done by assessing the performance of a model developed from a fresh battery vs. data from aged battery. Subsection 4.3.3 demonstrates the process of aging model development and model parameter evaluation as battery ages.

4.3.1 Reduced-Order Electrochemical Battery Model

A detailed description of the reduced-order electrochemical battery model and its parameterization can be found in [1]. A summary of the reduced-order model equations is provided here for improving the readability and the completeness of this paper. Recall that each electrode can be modeled as a sphere with a particle radius R_s. The single spherical particle is divided into $M_r - 1$ shells each of size Δr with $i = 1, \dots, M_r - 1$ and $r_i = i\Delta r$, where:

$$\Delta r = \frac{R_s}{M_r} \tag{4.1}$$

The particle outer shell (M_r) is exposed to the input current on the solid-electrolyte interface. The system, which has one input, one output, and M_{r-1} states representing the shells surface concentrations, can be summarized in the following state-space representation form, [13]:

System equation:

$$\dot{c}_s = \alpha_1 \begin{bmatrix} -2 & 2 & 0 & & & 0 & \\ 1/2 & -2 & 3/2 & \cdots & & 0 & \\ 0 & 2/3 & -2 & & & 0 & \\ & \vdots & & \ddots & & \vdots & \\ & & & & -2 & \dfrac{M_r - 2}{M_r - 3} & 0 \\ 0 & 0 & 0 & \cdots & \dfrac{M_r - 3}{M_r - 2} & -2 & \dfrac{M_r - 1}{M_r - 2} \\ & & & & 0 & \dfrac{M_r - 2}{M_r - 1} & \dfrac{2 - M_r}{M_r - 1} \end{bmatrix} c_s + \alpha_2 \begin{bmatrix} 0 \\ 0 \\ \vdots \\ -\left(\dfrac{M_r}{M_r - 1}\right) \end{bmatrix} u \tag{4.2}$$

Output equation:

$$c_{se} = c_{s_{M_r}} = c_{s_{M_{r-1}}} - \frac{\alpha_2}{\alpha_1} J^{Li} \tag{4.3}$$

The model input u is the butler-Volmer current (J^{Li}) which is a function of the solid-electrolyte surface concentration ($\mathrm{c_{se}}$) and the total current (I). The output of this sub-model is the solid concentration at the solid-electrolyte interface ($\mathrm{c_{se}}$). This output is fed into another sub-model that calculates the terminal voltage and the SOC. The solid-electrolyte interface concentration from the negative electrode ($c_{se,n}$) is calculated from the positive one ($c_{se,p}$) using the following equation, [13]:

$$\bar{c}_{se,n} = c_{s,max,n}\left(\theta_{n0\%} + \frac{\bar{c}_{se,p} - \theta_{p0\%}c_{s,max,p}}{(\theta_{p100\%} - \theta_{p0\%})c_{s,max,p}}(\theta_{n100\%} - \theta_{n0\%})\right) \tag{4.4}$$

Where $\theta_{n0\%}$, $\theta_{n100\%}$, $\theta_{p0\%}$, $\theta_{p100\%}$ are the stoichiometry points for the negative and positive electrodes, respectively, [14]. The terminal voltage can be calculated based on the solid-electrolyte-interface concentrations (c_{se}) from the anode and the cathode as follows, [13]:

$$V(t) = (\bar{\eta}_p - \bar{\eta}_n) + (\bar{\emptyset}_{e.p} - \bar{\emptyset}_{e.n}) + \left(U_P(c_{se,p}) - U_n(c_{se,n})\right) - R_f I \tag{4.5}$$

Note that the state of charge can be calculated as, [13]:

$$SOC = 100 * \left(\frac{\frac{c_{s,p_{avg}}}{c_{s,max,p}} - \theta_{p0\%}}{\theta_{p100\%} - \theta_{p0\%}}\right) \tag{4.6}$$

Where the average concentrations can be calculated as, [13]:

$$c_{s,p_{avg}} = \frac{c_T}{V} = \frac{total\ lithium\ concetration}{particle\ volume} = \frac{\sum_{i=1}^{M_r-1} r_i^2 4\pi\Delta r c_i}{\frac{4}{3}\pi(R_s - \Delta r)^3} \tag{4.7}$$

4.3.2 Aged Battery vs. Optimized ECM Model (Fresh)

In order to demonstrate the importance of having multiple battery models at various battery states of life, a current profile from a UDDS driving cycle is applied to an aged battery (at 80% capacity fade).

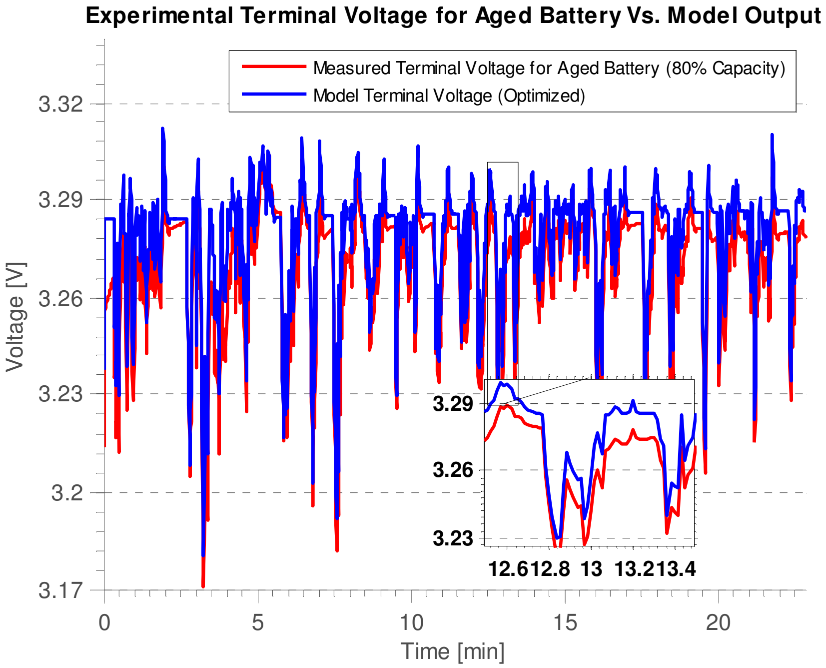

Figure 4.2. Electrochemical Battery Model vs. Experimental Data from a UDDS Driving Cycle (Aged Battery)

The measured experimental voltage is compared against the voltage from an electrochemical battery model for a fresh battery [1]. The actual SOC in Figure 4.1 is obtained experimentally by using coulomb counting with an Arbin cycler. The estimated battery SOC is calculated based on the battery discharge capacity test conducted as a reference performance test at the beginning of the experiment. The battery discharge capacity for the battery after the aging test is 1.74 Ah. As shown in Figure 4.2 and 4.3, it is clear that the ECM at 100% capacity (fresh battery) will significantly deviated in both terminal voltage and SOC from what is exhibited by an aged battery.

As shown in Figure 4.3, it is important to update model parameters as battery ages since the ECM estimate of the SOC for a fresh battery is higher than the actual SOC of an aged battery, thus giving a false SOC estimate. For example, at the end of the UDDS driving cycle, the model SOC is at approximately 44% while the actual SOC is at 41.5%; this is a relatively significant error. It is also important to highlight that other factors such as temperature and cell-balancing have not been accounted for in the scope of this paper. These factors will further contribute to modeling errors and worsen the terminal voltage and SOC estimate.

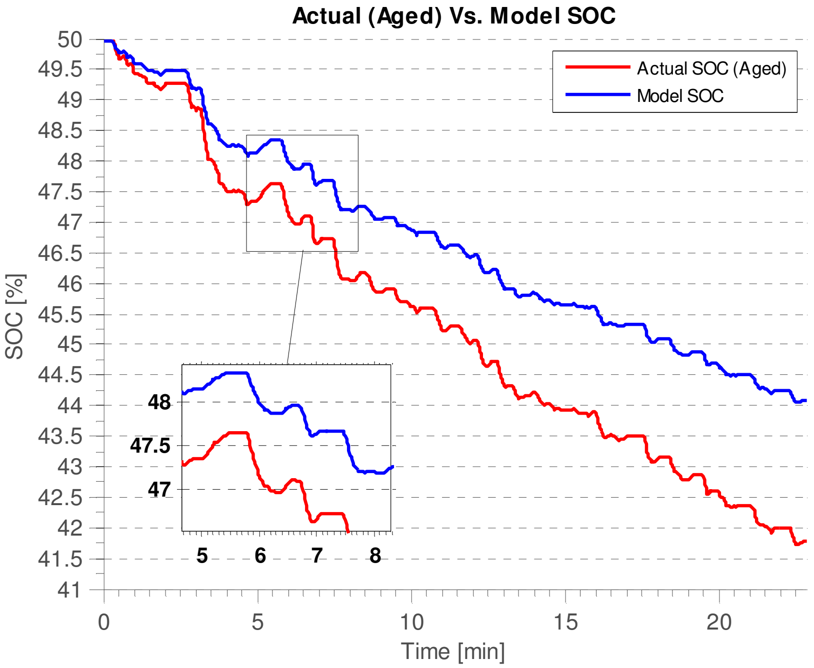

Figure 4.3. Actual SOC for Aged Battery (using Coulomb Counting) vs. Model SOC

The root mean square error (RMSE) between the measured terminal voltage ($V(t)$) and the electrochemical model output ($\boldsymbol{\hat{V}(t)}$) for *n* number of samples can be calculated as follows:

$$\boldsymbol{RMSE} = \sqrt{\frac{\boldsymbol{\sum_{t=1}^{n} V(t) - \hat{V}(t)}}{\boldsymbol{n}}} \tag{4.8}$$

The RMSE associated with using an ECM developed for fresh battery cells for estimating the terminal voltage and the SOC for an aged battery cell are 0.0087 V and

1.4694 %, respectively. However, the model performs really well with data from fresh (healthy) batteries; the associated RMSE for the terminal voltage and the SOC are 0.22057 mV and 0.1%. It is important to highlight that this error is over a single driving cycle which depletes the battery from 50% to approximately 40%. This error will worsen for extended driving cycles that might deplete the battery from 90% to 10%. A summary of the RMSE for the UDDS driving cycle for ECM on fresh and aged batteries is shown in Figure 4.4. In the following section, the ECM is modified and a strategy is applied to effectively overcome this problem and account for battery aging and degradation.

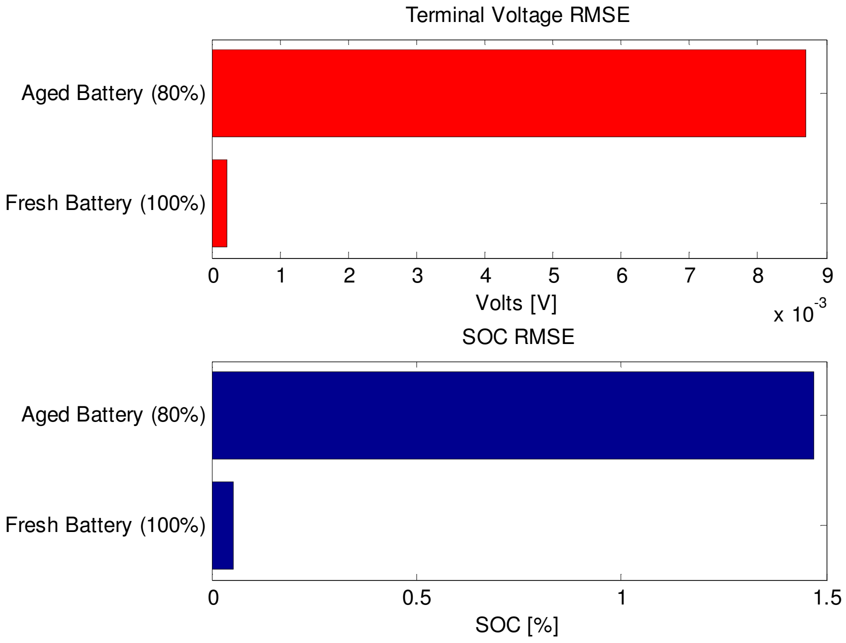

Figure 4.4. Terminal Voltage RMSE for Fresh vs. Aged Battery (Upper), SOC RMSE for Fresh vs. Aged (Lower)

4.3.3 Battery Aging Model Development

Battery aging and performance degradation occur due to two main effects, namely: ***film growth*** and ***carbon retreat,*** [15]. These two phenomena are found to be changing in a sigmoidal fashion (with sudden changes after a number of cycles), [15]. Aging occurs due to the reaction between the cathode active materials and the electrolyte, resulting in the formation of a solid-electrolyte interface (SEI) layer. This in turn changes the particle surface composition leading to breaking down of the carbon conductive paths which cause carbon retreat and sudden acceleration of capacity fade, [15]. Furthermore, battery aging occurs due to the formation of an insulating layer on the surface of the electrode particles (mainly the cathode electrode) which in turn leads to an increase in the impedance of the positive electrode, [16].

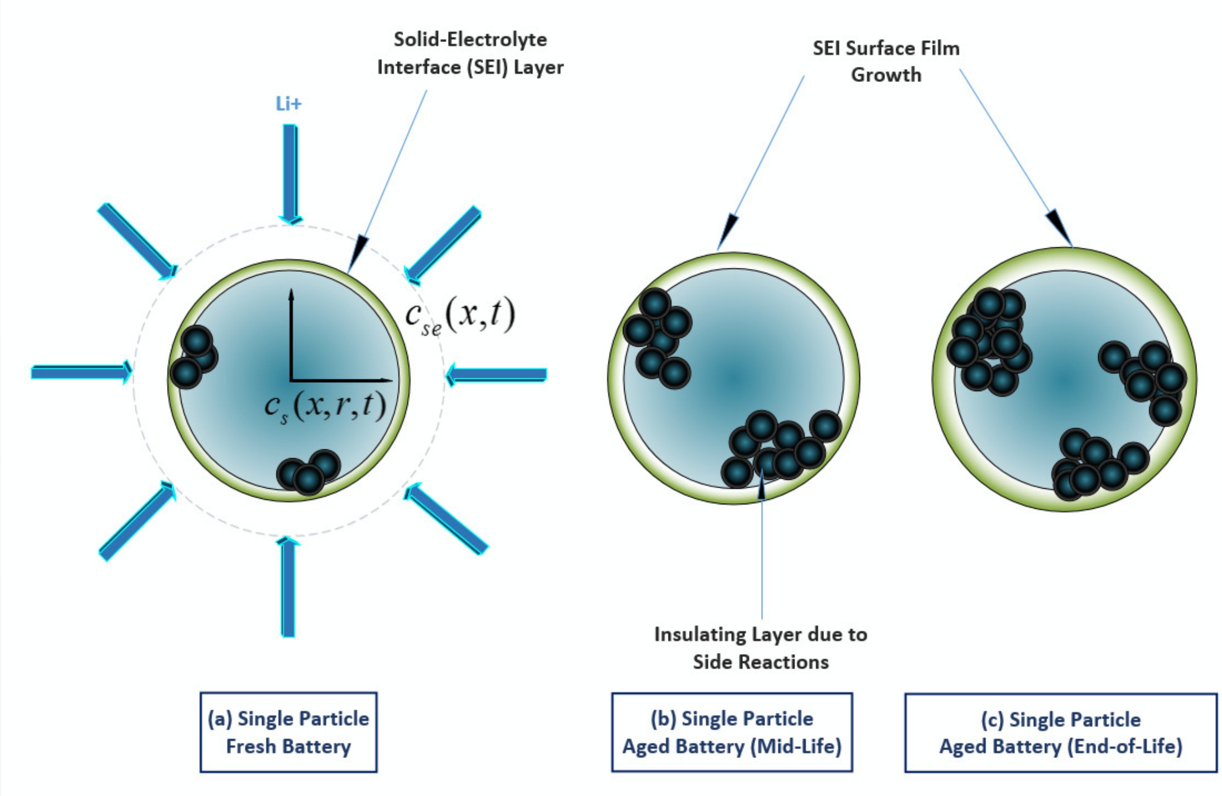

(a) Single Particle Fresh Battery

(b) Single Particle Aged Battery (Mid-Life)

(c) Single Particle Aged Battery (End-of-Life)

Figure 4.5. Battery Reduced-order Electrochemical Model at 3 States of Life; (a) Fresh (healthy state), (b) Mid-life, and (c) End-of-life. Aging is modeled by increase in the SEI layer and decrease in the Effective Electrode Volume.

The other factor is likely due to loss of electron conductivity of the cathode particles, [17]. This phenomenon is also related to the (carbon retreat) phenomenon which is the disconnection of carbon within the particles due to the formation of a SEI layer. The reduced-order Electrochemical Model (ECM) needs to be modified and augmented in order to account for aging. Figure 4.5 depicts a representation of the battery as it related to the reduced-order electrochemical model at 3 distinct states of life, namely: fresh (healthy state), mid-life, and end-of-life. The proposed battery aging model works by modeling the increase in the SEI layer and the decrease in the electrode volume due to side reactions. As battery ages, the electrode resistance to accept further lithium ions increases and this results in capacity degradation and aging.

In ECM, it is assumed that at steady state, no lithium diffusion occurs inside the spherical particle representing the electrode, [1] . All lithium concentrations in every shell reaches a steady state condition according to the following equation, [1]:

$$\begin{aligned} c_i = c_T/(r_{M_r-1}^2 * 4\pi\Delta r) * \; c_{s_{factor}} &= \sum_{i=1}^{M_r-1} r_i^2 4\pi\Delta r c_i \,/(r_{M_r-1}^2 * 4\pi\Delta r) * \; c_{s_{factor}} \\ &= (r_1^2 * 4\pi\Delta r c_1 + r_2^2 * 4\pi\Delta r c_2 + r_3^2 * 4\pi\Delta r c_3 \ldots + r_{M_r-1}^2 * 4\pi\Delta r c_{M_r-1})/(r_{M_r-1}^2 \\ &\quad * 4\pi\Delta r) * \; c_{s_{factor}} \end{aligned} \tag{4.9}$$

where c_i represents the steady state initial concentration at every shell of the spherical particle for a given state of charge and number of shells in the particle.

In order to demonstrate the previous equation, consider a spherical particle of radius 0.0015 cm with 11 spherical discretization segments (spherical shells) and assume that the total lithium concentration is concentrated at the outermost shell. Further, assume that the maximum lithium concentration is 0.04782 mol/cm^3, and the initial SOC is 50%. The stoichiometry values of 0.6976 and 0.9149 have been selected. By substituting with the SOC in the following equation, average lithium concentration at the specified state of charge is calculated as follows, [1]:

$$c_{s,p_{avg}} = \left(\frac{SOC}{100} * \left(\theta_{p100\%} - \theta_{p0\%}\right) + \theta_{p0\%}\right) * c_{s,max,p} = 0.0386\, mol/cm^3 \tag{4.10}$$

Assuming the total lithium concentration is concentrated at the outermost shell, lithium concentration at the outermost shell $c_{s_{p_{M_r-1}}}$ can be calculated as follows:

$$c_{s_{p_{M_r-1}}} = c_{s,p_{avg}} * \frac{4}{3}\pi(R_s - \Delta r)^3/(r_{M_r-1}^2 * 4\pi\Delta r) = 0.1285\, mol/cm^3$$

As shown in Figure 4.6, assuming no input current is applied at the solid-electrolyte interface layer, lithium at the outermost shell (starting from 0.1285 mol/cm^3) will diffuse inside the sphere according to Fick's second law of diffusion until all lithium concentrations are equalized. Then on, no further lithium diffusion would occur inside the sphere. The final concentration value in which all shells settle is related to the $c_{s_{factor}}$ according to equation (4.11).

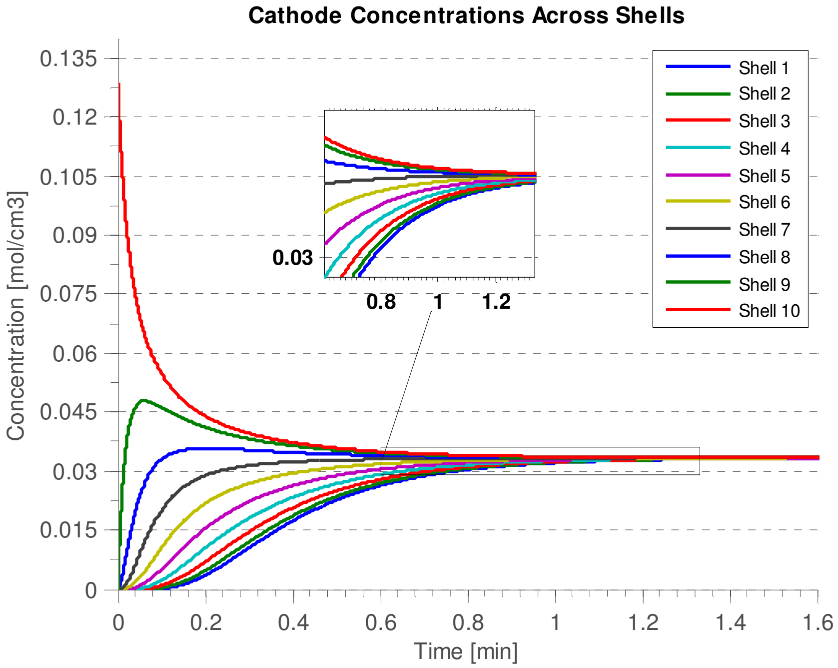

Figure 4.6. Lithium concentrations across shells assuming total lithium concentration is concentrated at the outermost shell

Lithium concentrations in every shell can be calculated by applying the final value theorem below:

$$c_{s_{factor}} = final\ value = \lim_{t\to\infty} f(t) = \lim_{s\to 0} s((sI - A)^{-1}c(0)) = 0.2597 \tag{4.11}$$

The final value, which is dependent on the state transition matrix A is 0.259. It is important to highlight that this value solely depends on the number of discretization segments M_r which is 11 in this example. The steady state value of lithium concentrations, as shown in Figure 4.6, can be calculated as follows:

$$c_i = c_{s_{p_{M_r-1}}} * \ c_{s_{factor}} = c_T/(r_{M_r-1}^2 * 4\pi\Delta r) * \ c_{s_{factor}} = 0.1285 * 0.2597 = 0.033 mol/cm^3 \tag{4.12}$$

Recall that an optimizer is used to optimize the electrode area (A) and then further to constraints, to calculate the electrode thickness δ as follows, [1]:

$$\delta = \left(\frac{1}{A}\right) * \left(\left(\frac{2M_r - 1}{2}\right) * \left(\frac{M_r}{M_r - 1}\right)^3 * \alpha_2 * \Delta r * \ c_{s_{factor}}\right) / (c_{s_{max}} * R_s * Q_{max} * (\theta_{p_{100\%}} - \theta_{p_{0\%}}) \tag{4.13}$$

This relationship is important since as battery ages, the effective volume of the sphere representing the electrode is decreased. This results in capacity degradation and battery aging. In this paper, the definition "$Electrode\ Aging\ Factor\ (\tau)$" is introduced as follows:

$$Electrode\ Aging\ Factor\ (\tau) = \frac{I}{J * \delta * A} =$$

$$= (I) / \left(J * \left(\frac{2M_r - 1}{2}\right) * \left(\frac{M_r}{M_r - 1}\right)^3 * \alpha_2 * \Delta r * \ c_{s_{factor}}\right) / (c_{s_{max}} * R_s * Q_{max} * (\theta_{p_{100\%}} - \theta_{p_{0\%}}) \tag{4.14}$$

In other words, the battery input current is scaled down to the Butler-Volmer current by dividing the input current by the effective electrode volume (V_{eff}). As battery ages, the effective electrode volume is reduced and thus lithium ions are prevented from further diffusion inside the particle representing the electrode. The effective electrode volume can be calculated as follows:

$$V_{eff} = \delta * A * \tau \tag{4.15}$$

In order to demonstrate the accuracy of this model, assume that an input discharge current of 1C (-2.3 A) is applied for 15 minutes on the outermost shell of the sphere with the same parameters as previously discussed. Then a resting period of 15 minutes, followed by a charging current of +2.3A, and then a 15 minutes resting period is applied as shown in Figure 4.7.

Assume that the electrode plate area is 16524.27 cm^2, the battery capacity Q_{max} is 2.3 Ah and $\alpha_2 = 1/(Fa_s\Delta r)$ is 4.632e-7. Lithium ion concentrations across the particle spherical shells due to the input current are as shown in Figure 4.8. It is clear that during the first 15 minutes when a discharging current is applied to the battery, lithium ion concentration across shells decrease uniformly until a steady state condition occurs. During the resting period, when no current is applied to the battery, lithium concentration equalizes across spherical shells. Lithium values is approximately 0.0356 mol/cm^3.

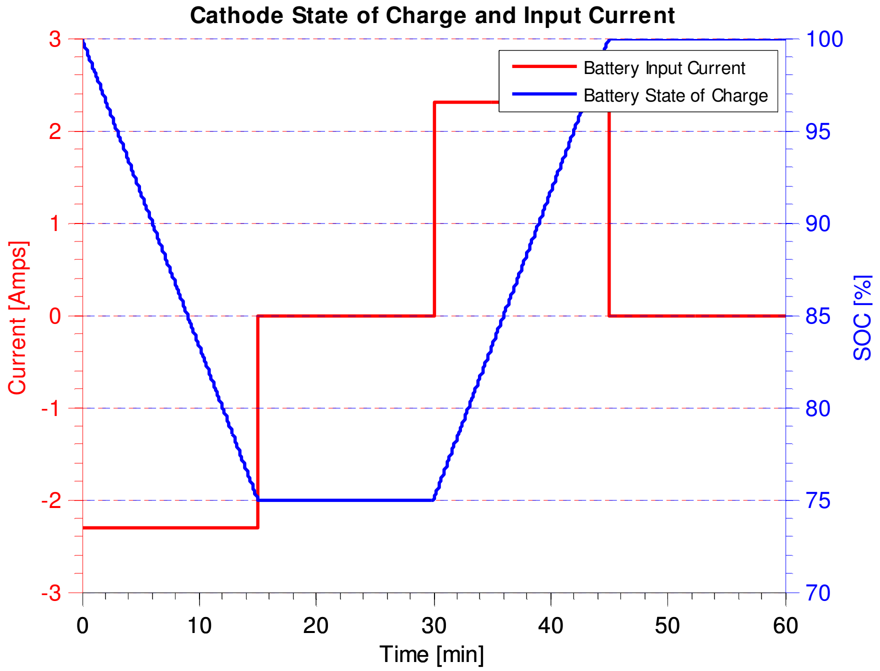

Figure 4.7. Cathode Input Current and State of Charge for healthy battery (100% capacity)

During the charging period, lithium ion concentration across shells increases uniformly as shown in Figure 4.8 followed. For the fresh battery, the SOC changes from 100% to 75% using the specified charging/discharging input current.

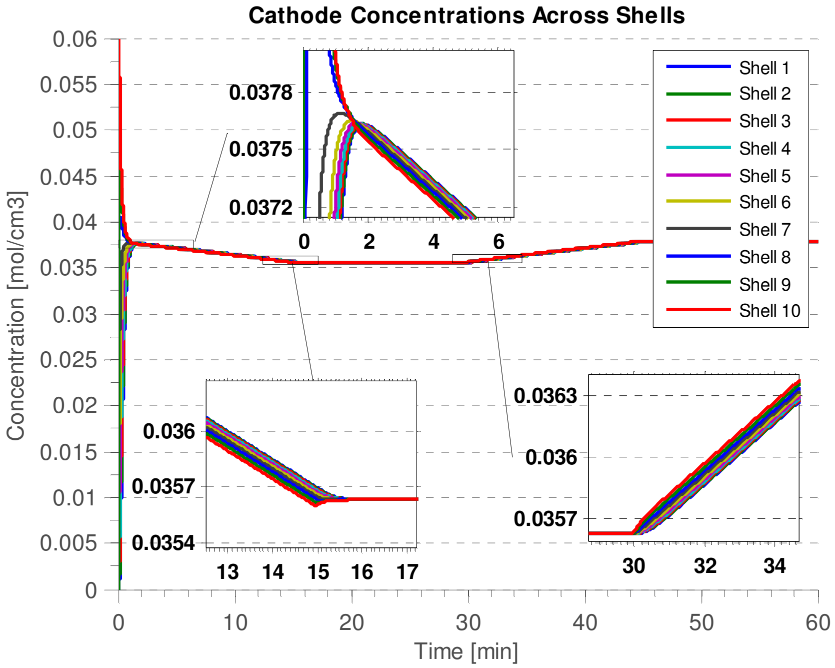

Figure 4.8. Lithium Concentration variations vs. time for healthy battery (100% capacity)

As battery degrades, the battery effective volume is decreased which in turn changes the electrode aging factor (τ). Battery aging is attributed to cycling and calendar aging effects. Calendar aging is not considered within the scope of this paper. Assume that the aging factor decreased from 1 for a fresh (healthy) battery state to 0.7 at its end of life. Other parameters such as the solid diffusion coefficient (D_{s_p}) changes as battery degrades. Changes in these parameters reflect the increased electrode resistance to accept further charges. In this example, the diffusion coefficient decreases from $7.4324\text{e}-9$ to $5.34479\text{e}-9\ cm^2/sec$. Battery state of charge, as shown below in Figure 4.9, varies from 100% to 64% using the same input current. This indicates that the electrode no longer accepts further charges due to the change in its effective volume and decreased diffusion coefficient.

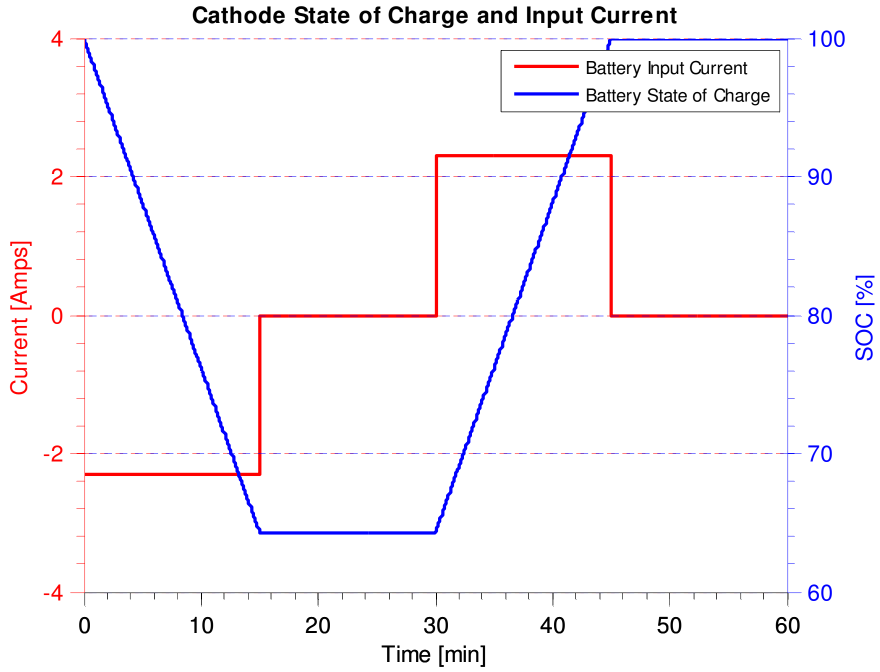

Figure 4.9. Battery input current and SOC for aged battery ($\tau = \mathbf{0.7}$)

As shown in Figure 4.10, lithium concentrations for aged batteries are generally below those of a fresh battery. The steady state values of lithium concentration for a fresh battery is 0.03563 mol/cm^3, however for the aged battery, lithium concentrations at steady state is approximately 0.0346 mol/cm^3. This describes the lower state of charge values for the same current input. Regarding the battery terminal voltage, the OCV-SOC relationship changes as battery ages in addition to other parameters such as the solid-electrolyte interface resistance and the stoichiometry values for both the cathode and the anode.

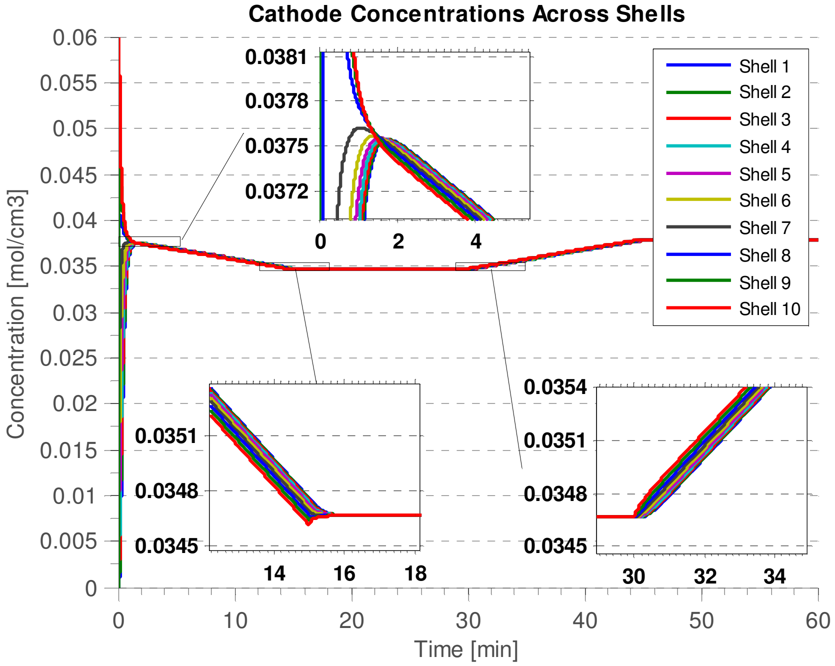

Figure 4.10. Lithium Concentration variations vs. time for aged battery ($\tau = 0.7$)

Variations in these parameters will be tracked using genetic algorithm optimization technique as discussed next in subsection 4.3.4.

4.3.4 Aging Model Parameter Optimization

In order to optimize battery model parameters as well as the electrode aging factor τ, the same optimization procedure conducted on fresh cells has been conducted on aged LiFePO4 batteries at 20% capacity fade. As shown in Figure 4.11, it is clear that the OCV-SOC relationship changes at various battery states of life. Since the SOC for aged batteries is now revised and defined based on the updated capacity, a shift in the SOC-OCV curve is exhibited as shown below. In order to fit the electrochemical model to aged batteries, the battery discharge capacity is updated from 2.3Ah to 1.76Ah based on the static capacity test. The genetic algorithm procedure discussed is conducted again to update model parameters for aged batteries, [1].

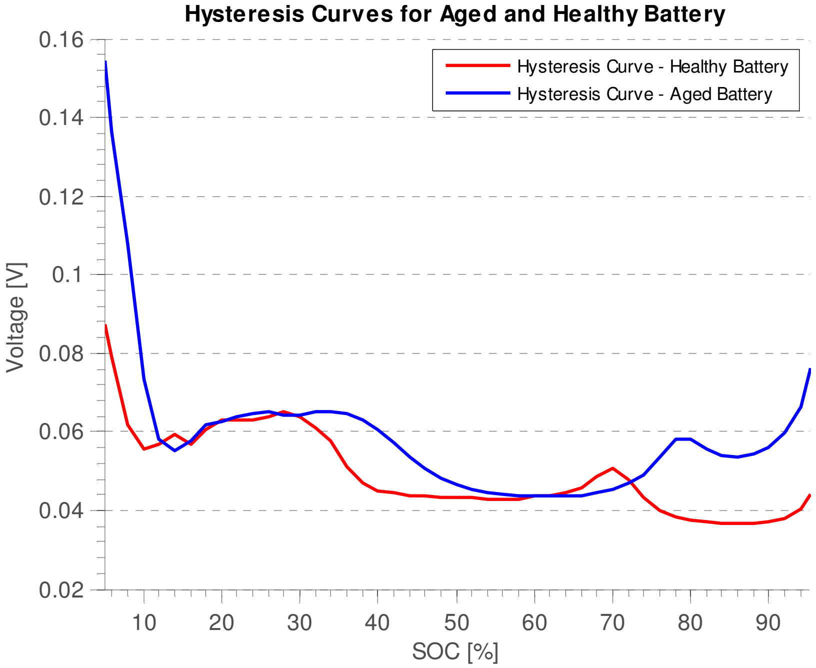

Figure 4.11. SOC-OCV Hysteresis Curve for Healthy and Aged Batteries

Results for optimized battery parameters are summarized in Table 4.1. The terminal voltage and SOC for the updated model vs. experimental data from aged batteries are shown in Figure 4.12 and 4.13. At the start of the optimization process, the model parameters are initially set to those of fresh batteries with the same range. Some parameters are held constant as follows: the solid maximum particle concentration in the anode and cathode ($c_{s,max,p}, c_{s,max,n}$), positive and negative electrode area (A), anode and cathode particle radius (R_{s_p}, R_{s_n}), active material volume fraction ($e_{s,p}, e_{s,n}$), positive and negative active surface area per electrode ($a_{s,p}, a_{s,n}$), positive and negative current coefficient or reaction rate (k_0), and average electrolyte concentration ($\bar{c}_e$).

Table 4.1. Electrochemical Battery Model Optimized Parameters for Aged Batteries

Parameter name (electrode) (symbol) (unit)	*Optimized Parameters*
Electrode aging factor ($\boldsymbol{\tau}$)	*0.69*
Solid phase diffusion coefficient (Positive) ($\boldsymbol{D_{s,p}}$) ($\boldsymbol{cm^2/sec}$)	5.34479 e-09
Solid phase diffusion coefficient (Negative) ($\boldsymbol{D_{s,n}}$) ($\boldsymbol{cm^2/sec}$)	1.139458 e-09
Maximum solid concentration (Positive) ($\boldsymbol{\theta_{p_{100\%}}}$)	0.91496
Minimum solid concentration (Positive) ($\boldsymbol{\theta_{p_{0\%}}}$)	0.685320
Maximum solid concentration (Negative) ($\boldsymbol{\theta_{n_{100\%}}}$)	0.499761
Minimum solid concentration (Negative) ($\boldsymbol{\theta_{n_{0\%}}}$)	0.153574
Solid Electrolyte interface Resistance ($\boldsymbol{R_{SEI}}$) ($\boldsymbol{\Omega}$)	0.011

The following parameters are adjusted by the optimizer for aged batteries: electrode aging factor (τ), positive and negative diffusion coefficients ($D_{s,p}, D_{s,n}$), electrode film resistance (R_{SEI}) (also known as the solid electrolyte interface resistance), maximum positive and negative solid normalized concentrations (stoichiometry values) ($\theta_{p_{100}}$, $\theta_{n_{100}}$), minimum positive and negative normalized solid concentration (θ_{p_0}, θ_{n_0}).

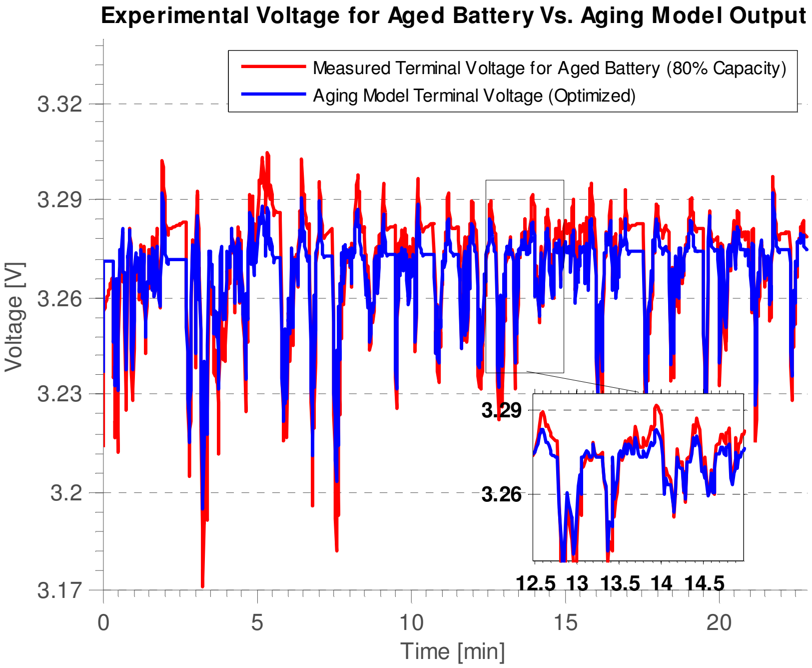

Figure 4.12. Electrochemical Battery Aging Model vs. Experimental Data from a UDDS Driving Cycle (Aged Battery)

The overall RMSE using UDDS driving cycle is 0.166 mV and the SOC RMSE is 0.2029 %. As shown in Table 4.1, the optimized electrode aging factor is less than one indicating a reduced effective electrode volume. The solid-electrolyte interface resistance increases as battery ages which indicates more resistance to lithium diffusion inside the representative particle. Stoichiometry values for both the cathode and the anode change since the OCV-SOC relationship changes with aging. The positive solid particle diffusion coefficient decreases indicating decreased rate of lithium diffusion inside the particle.

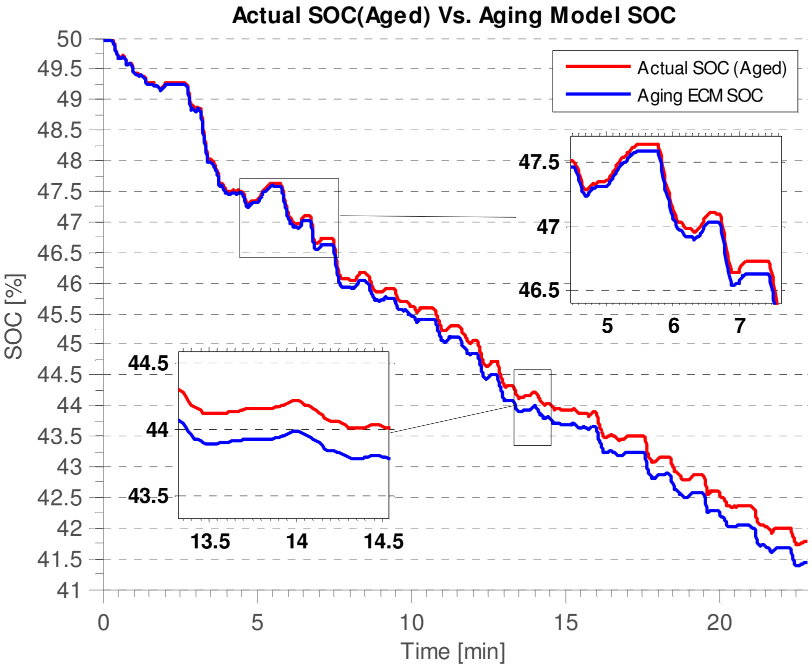

Figure 4.13. Electrochemical Battery Aging Model SOC vs. Experimental Data from a UDDS Driving Cycle (Aged Battery)

4.4 Battery Critical Surface Charge Estimation

In this section, an estimation strategy known as the Smooth Variable Structure Filter (SVSF) which was introduced in 2007 is used for estimating the battery critical surface charge based on the reduced-order electrochemical battery model. A brief overview of the SVSF is first provided, followed by its application for critical surface charge estimation.

4.4.1 The Smooth Variable Structure Filter

Similarly to the Kalman filter, the SVSF works in a predictor-corrector fashion, [18]. The filter is based on the sliding mode concept and has demonstrated robustness to modeling uncertainties and sensor noise, [18, 8]. The SVSF can be applied to both linear and non-linear systems. It works by using an SVSF gain that forces the states to converge to a neighborhood the actual or true value, [18]. The gain forces the states to switch back and forth across the state trajectory within a region referred to as the existence subspace which is function of modeling uncertainties. The width of the existence space β is a function of the uncertain dynamics associated with the inaccuracy of the internal model of the filter as well as the measurement model, and varies with time, [18]. The SVSF can be applied to systems that are differentiable and observable, [18, 19]. The original form of the SVSF as presented in [18] did not include covariance derivations. An augmented form of the SVSF that includes the derivation of an error covariance matrix has been presented in, [20]. Here, the latter is summarized.

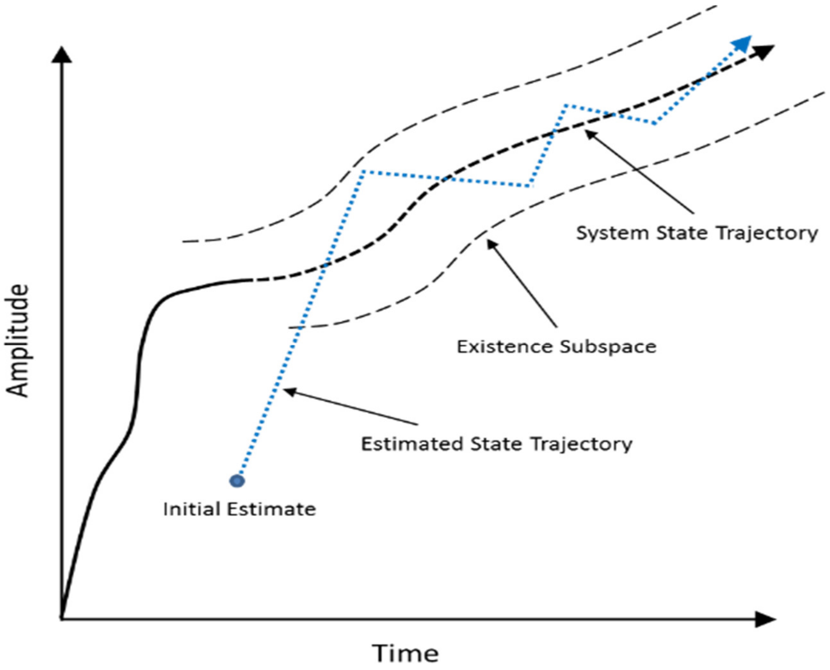

Figure 4.14. The SVSF estimation strategy starting from some initial value, the state estimate is forced by a switching gain to within a region referred to as the existence subspace, [18].

Consider a nonlinear system with a linear output (measurement) equation. The filter runs by generating a prediction of the state estimate (which represents the solid-electrolyte interface concentration) as follows:

$$\hat{x}_{k+1|k} = \hat{f}\left(\hat{x}_{k|k}, u_k\right) \tag{4.16}$$

The predicted estimates are then used to generate a predicted measurements $\hat{z}_{k+1|k}$ as follows [18]:

$$\hat{z}_{k+1|k} = C_{k|linearized}\hat{x}_{k+1|k} \tag{4.17}$$

Where $C_{k|linearized}$ is the measurement matrix. Then the measurement error $e_{z,k+1|k}$ can be calculated as follows, [18]:

$$e_{z,k+1|k} = z_{k+1} - \hat{z}_{k+1|k} \tag{4.18}$$

The SVSF has predictor-corrector form. Its gain is a function of the a-priori and the a-posteriori measurement errors $e_{z_{k+1|k}}$ and $e_{z_{k|k}}$. It has a smoothing boundary layer widths ψ, a memory or convergence rate γ, as well as the linear measurement matrix $C_{k|linearized}$. For the derivation of the SVSF gain K_{k+1}, refer to [18, 20]. The SVSF gain is defined as follows, [18]:

$$K_{k+1} = {C_{k|linearized}}^{+} diag\left[\left(\left|e_{z_{k+1|k}}\right| + \gamma\left|e_{z_{k|k}}\right|\right) \circ sat\left(\frac{e_{z_{k+1|k}}}{\psi}\right)\right] diag\left(e_{z_{k+1|k}}\right)^{-1} \tag{4.19}$$

The updated states $\hat{x}_{k+1|k+1}$ are calculated as follows, [18]:

$$\hat{x}_{k+1|k+1} = \hat{x}_{k+1|k} + K_{k+1}e_{z_{k+1|k}} \tag{4.20}$$

The output estimates and the a posteriori measurement errors are then calculated respectively as follows, [18]:

$$\hat{z}_{k+1|k+1} = C_{k|linearized}\widehat{w}_{k+1|k+1} \tag{4.21}$$

$$e_{z_{k+1|k+1}} = z_{k+1} - \hat{z}_{k+1|k+1} \tag{4.22}$$

Equations 4.17 to 4.22 are iteratively repeated until a certain threshold is attained. As per [18], the estimation process is stable and convergent if the following lemma is satisfied:

$$|e_{k|k}| > |e_{k+1|k+1}| \tag{4.23}$$

The proof, as defined in [18], yields the derivation of the SVSF gain. The standard SVSF gain yields the following:

$$e_{z,k+1|k+1} = e_{z,k+1|k} - HK_{k+1} \tag{4.24}$$

Substitution of (4.24) into (4.23) yields:

$$|e_{z,k|k}| > |e_{z,k+1|k} - HK_{k+1}| \tag{4.25}$$

Simplifying and rearranging (4.28):

$$|HK_{k+1}| > |e_{z,k+1|k}| + \gamma|e_{z,k|k}| \tag{4.26}$$

Based on the fact that $|HK_{k+1}| = HK_{k+1} \circ sign(HK_{k+1})$, the standard SVSF gain can be derived as follows, [18]:

$$K_{k+1} = H^{-1}\left(|e_{z,k+1|k}| + \gamma|e_{z,k|k}|\right) \circ sign(HK_{k+1}) \tag{4.27}$$

Equation (4.27) may be further expanded based on the fact that $sign(HK_{k+1}) = sign(e_{z,k+1|k})$, as per [18], such that:

$$K_{k+1} = H^{-1}\left(|e_{z,k+1|k}| + \gamma|e_{z,k|k}|\right) \circ sign\left(e_{z,k+1|k}\right) \tag{4.28}$$

The SVSF switching may be smoothed out by the use of a saturation function, accordingly, equation (4.28) becomes, [18]:

$$K_{k+1} = H^{-1}\left(|e_{z,k+1|k}| + \gamma|e_{z,k|k}|\right) \circ sat\left(e_{z,k+1|k}\right) \tag{4.29}$$

where the saturation function is defined by, [18]:

$$sat\left(e_{z,k+1|k}\right) = \begin{cases} 1, & e_{z,k+1|k} \geq 1 \\ e_{z,k+1|k}, & -1 < e_{z,k+1|k} < 1 \\ -1, & e_{z,k+1|k} \leq -1 \end{cases} \tag{4.30}$$

Finally, a smoothing boundary layer ψ may be added to further reduce the magnitude of chattering, leading to, [18]:

$$K_{k+1} = H^{-1}\left(|e_{z,k+1|k}| + \gamma|e_{z,k|k}|\right) \circ sat\left(e_{z,k+1|k}/\psi\right) \tag{4.31}$$

Note that the gain described in equation (4.31) is slightly different than that presented earlier in (4.19). A diagonalized form was created, as described in [20, 21], to formulate an SVSF derivation that included a covariance function. The form shown as (4.31) was presented as the original or ‘standard’ SVSF in [18].

4.4.2 SVSF-based Critical Surface Charge Estimation-fresh battery

The SVSF has been used to estimate the critical surface charge based on the reduced-order model. The state space representation indicating the diffusion of lithium into the solid particle consists of a linear system equation (4.3) and a nonlinear measurement (output) equation (4.5). The terminal voltage is function of the solid-electrolyte interface concentrations $c_{se,p}$ and $c_{se,n}$. The model has one input current (I), $M_r - 1$ states and, one output representing the terminal voltage (V_T). The measured voltage is compared to the model output to calculate the error signal that is fed back to the SVSF estimator to calculate the gain and update the states. The output equation is linearized with respect to the current state as follows:

$$C_{k|linearized} = \frac{\partial V}{\partial x} = \frac{\partial \mathrm{V}}{\partial \bar{\mathrm{c}}_{\mathrm{s,p}(\mathrm{M_r}-1)}} \tag{4.32}$$

Due to the complexity of the output equation, complex differentiation has been conducted to linearize the output equation then to generate the $C_{k|linearized}$ matrix. The $C_{k|linearized}$ matrix consists of zero elements except for the last element thus when used to update the states, only the solid electrolyte interface concentration is updated.

The filter can estimate the solid-electrolyte interface concentration $c_{se,p}$ and since at steady state conditions, all lithium concentrations are equalized (no further diffusion occurs), the filter can estimate all the spherical shell concentrations and thus provides an estimate of the initial SOC. Accordingly, the filter can be used to estimate the SOC at steady state conditions to correct the initial SOC; then after the model takes over as shown below.

It is important to discuss computational issues that may occur when calculating the pseudoinverse of the linearized measurement matrix in (4.19). Numerous authors have experienced abrupt and unexpected instabilities with the pseudoinverse, [22, 23]. A sudden growth of the Jacobian matrix elements when calculating the pseudoinverse during the SVSF gain calculation occurs at each iteration. Consequently, the estimator outputs and thus the mean square error between the measured terminal voltage and model output increases significantly. A stabilizing adjustment is performed to avoid this problem. The problem has been extensively analyzed in [22], and occurs due to the presence of singularities. Singularities occur when the Jacobian matrix loses rank. Small singular values of H might arise in the vicinity of these singularities. Consequently, larger values occur when obtaining the pseudoinverse of the Jacobian H^+ thus creating larger error values which leads to instability. According to [24], it is rather difficult to detect these singularities. A traditional method of solving this instability problem is by replacing the pseudoinverse H^+ with the following equation, [24]:

$$C_d^+ = C^T(CC^T + \rho^2 I)^{-1} \tag{4.36}$$

where, ρ is called the damping parameter. The effect of the added damping is that it mitigates the effect of small singular values when computing the inverse, [24]. On the other hand, a slightly small error is introduced when calculating the inverse. In this paper, ρ is set to 0.4, and is shown to have a negligible effect on the accuracy. As shown in Figure 4.15, 4.16 and 4.17, the SVSF has been applied to estimate the critical surface concentration, the battery state of charge, and the battery terminal voltage for zero input current. The battery actual state of charge is held at 34% and the estimator is initialized at 50% SOC which is a relatively large deviation. Since all battery states are held at steady state conditions, the battery SOC and terminal voltage can be estimated accordingly with high accuracy.

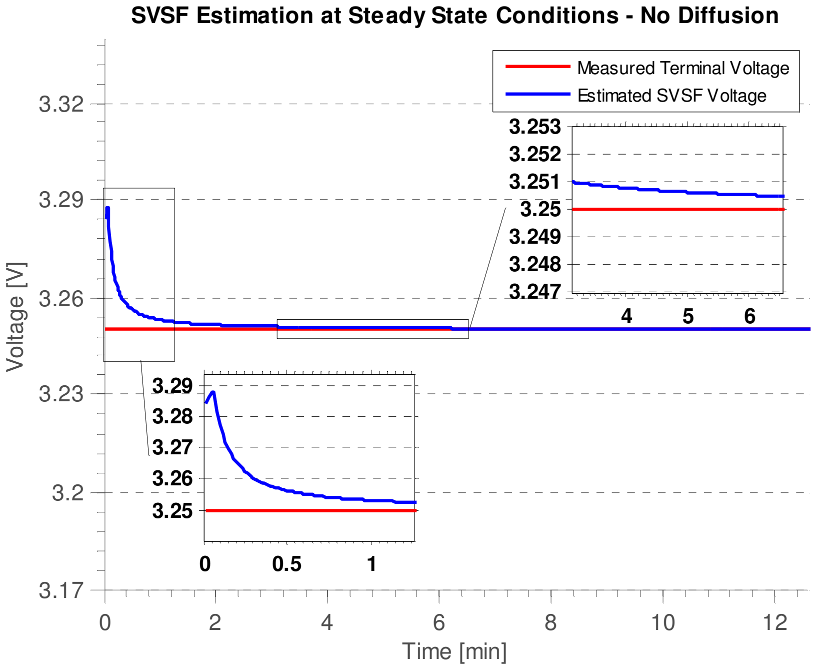

Figure 4.15. SVSF Voltage Estimation at steady state conditions - equal lithium concentrations across shells

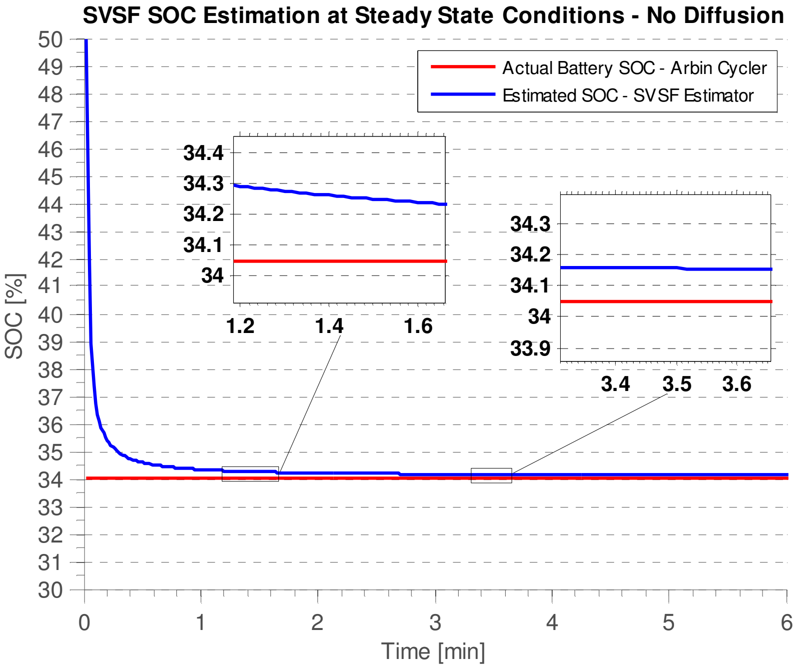

Figure 4.16. SVSF SOC Estimation at steady state conditions - equal lithium concentrations

The estimation error for both the terminal voltage and the SOC are as shown in Figure 4.17. It is clear that the SOC estimator converges to the actual SOC value within a relatively short period of time assuming the initial SOC is at 47% error from the actual SOC which is a significantly large error. The estimator converges much faster if the initial SOC is close to the actual SOC values.

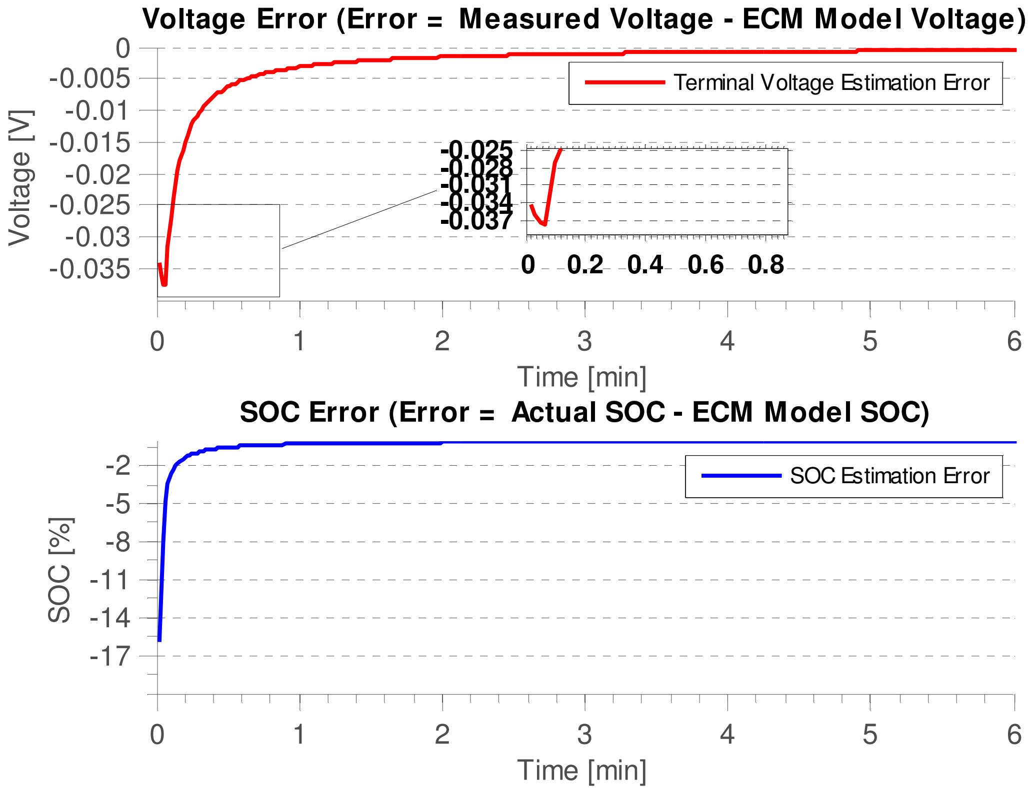

Figure 4.17. Terminal Voltage Estimation Error (Upper) and the SOC Estimation Error (Lower)

Furthermore, the SVSF capabilities were tested by using an aggressive driving cycle that entails fast acceleration and regenerative braking. Current profile from a US06 driving cycle has been used for testing. Estimated vs. experimental voltages are as shown in Figure 4.18.

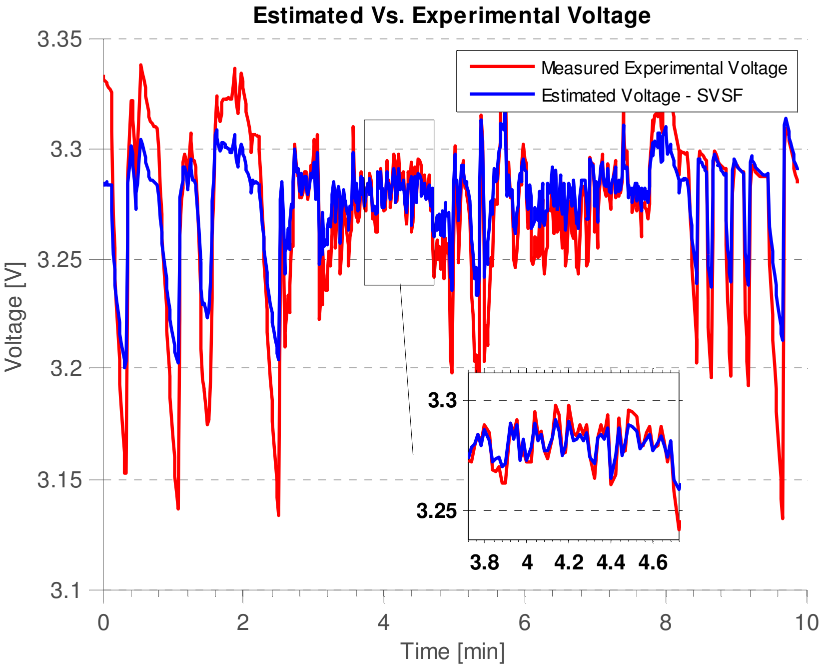

Figure 4.18. SVSF Estimated Voltage Vs. Experimental Data

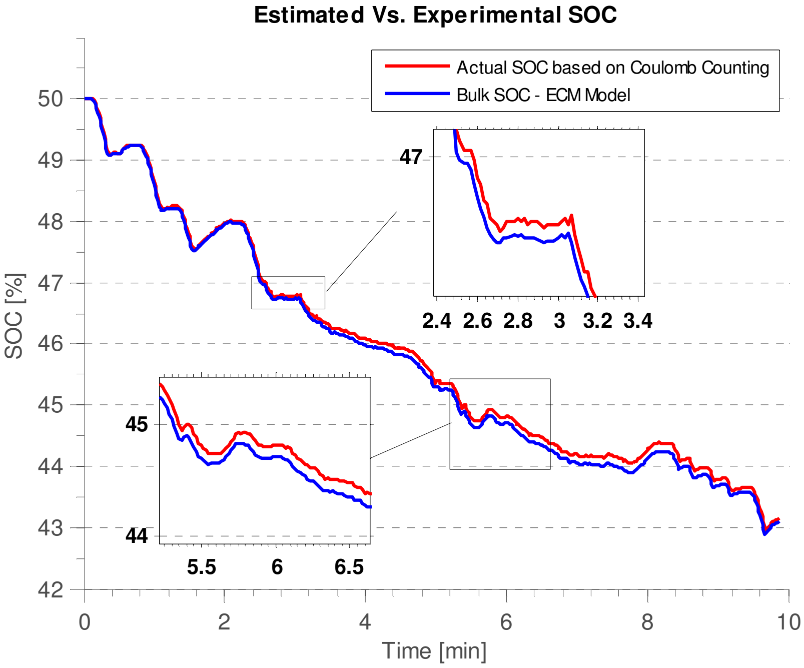

Figure 4.19. ECM Model SOC vs. Experimental (Coulomb Counting) SOC

The electrochemical model SOC vs. experimental SOC (using coulomb counting from Arbin Cycler) is as shown below in Figure 4.19. The terminal voltage and SOC estimation error for US06 driving cycle are as shown below in Figure 4.20. The maximum error in the SOC is within 0.2 % and within 0.05V for the terminal voltage. The RMSE for the SOC is 0.0989% and 0.0207V for the terminal voltage, respectively.

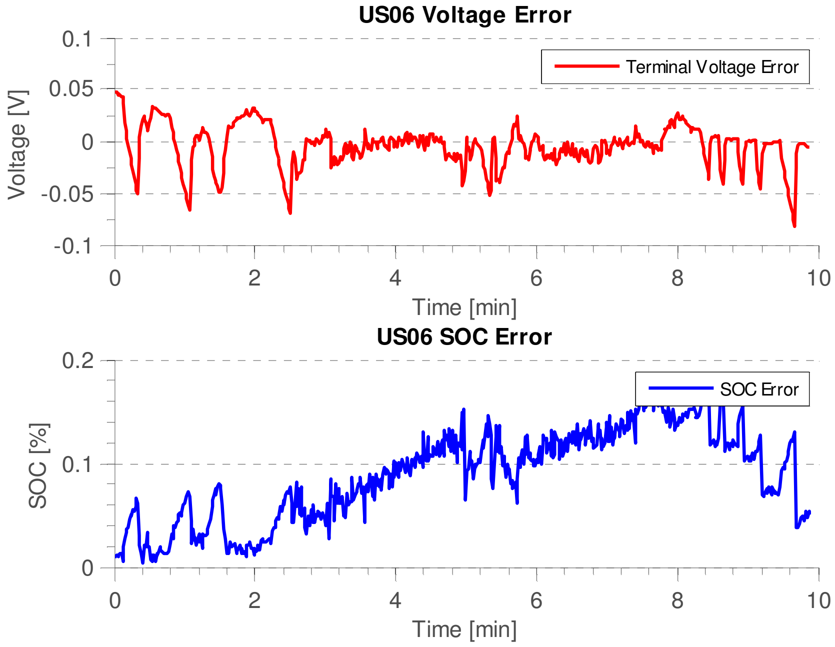

Figure 4.20. US06 Voltage (Upper) and SOC (Lower) Error

4.5 Conclusion

The paper extends on the existing electrochemical battery models to accommodate for aging and degradation that occurs overtime. An aging battery model is developed by changing the effective electrode volume to model capacity degradation. A non-invasive genetic algorithm has been applied to estimate model parameters for aged batteries. Main parameters that contribute to battery aging are: the OCV-SOC relationship, the solid-electrolyte interface resistance (R_{SEI}), the solid diffusion coefficient (D_s), the electrode effective volume (τ), and the minimum and maximum stoichiometry values ($\theta_{p_{0\%}}$) and ($\theta_{p_{100\%}}$). The battery loss of capacity due to aging is attributed to the increase in the battery solid electrolyte interface resistance, the decrease in diffusion coefficient, and the decrease in the battery electrode effective volume, those changes reflect the electrode tendency to resist further lithium diffusion as battery degrades.

Extensive accelerated aging and reference performance tests have been conducted on lithium-iron phosphate cells. Reference tests have been conducted at two distinct states of life, namely: 100% and 80% capacity. Furthermore, a critical state of charge estimation strategy has been implemented using the SVSF methodology. Results indicate that the SVSF is robust, and can be used for real-time applications on board of an electric vehicle battery management system. The SVSF can be used to estimate the critical surface charge and the battery overall state of charge at steady state conditions. An open circuit voltage measurement can also be used along with the estimator for more accurate SOC estimation.

Acknowledgments

Financial support from Ford Motor Company and NSERC (National Sciences and Engineering Research Council of Canada) is gratefully acknowledged.

Table 4.2. Electrochemical Battery Model Parameters Nomenclature and Units

Symbol	Name	Unit
$\boldsymbol{i_e}$	Electrolyte current density	$A\ cm^{-2}$
$\boldsymbol{i_e}$	Solid current density	$A\ cm^{-2}$
$\emptyset_{\boldsymbol{e}}$	Electrolyte potential	V
$\emptyset_{\boldsymbol{s}}$	Solid potential	V
$\boldsymbol{c_e}$	Electrolyte concentration	$mol\ cm^{-3}$
$\boldsymbol{c_s}$	Solid concentration	$mol\ cm^{-3}$
$\boldsymbol{c_{se}}$	Concentration at the solid electrolyte interface	$mol\ cm^{-3}$
$\boldsymbol{J_{Li}}$	Butler-Volmer current	$A\ cm^{-3}$
$\boldsymbol{\theta_n}$	Anode Normalized solid concentration	-
$\boldsymbol{\theta_p}$	Cathode Normalized solid concentration	-
$\boldsymbol{U}$	Open circuit potential	V
$\boldsymbol{U_n}$	Anode open circuit voltage	V
$\boldsymbol{U_p}$	Cathode open circuit voltage	V
$\boldsymbol{\eta}$	Overpotential	V
$\boldsymbol{F}$	Faraday's constant	$C\ mol^{-1}$
$\boldsymbol{I}$	Applied battery cell current	A
$\boldsymbol{R}$	Universal Gas constant	$J\ K^{-1}\ mol^{-1}$
$\boldsymbol{T}$	Temperature	K

References

[1] R. Ahmed, M. El Sayed, J. Tjong and S. Habibi, "Reduced-Order Electrochemical Model Parameters Identification and Critical Surface Charge Estimation for Healthy and Aged Li-Ion Batteries, Part I: Parameterization Model Development for Healthy Battery," *Journal of Emerging Technologies,* 2014.

[2] S. E. Samadani, R. A. Fraser and M. Fowler, "A Review Study of Methods for Lithium-ion Battery Health Monitoring and Remaining Life Estimation in Hybrid Electric Vehicles," *SAE International ,* 2012.

[3] B. Pattipati, C. Sankavaram and K. R. Pattipati, "System Identification and Estimation Framework for Pivotal Automotive Battery Management System Characteristics," *IEEE Transactions on Systems, Man, and Cybernetics,* vol. 41, no. 6, 2010.

[4] "www.mynissanleaf.com/wiki/," [Online].

[5] K. A. Smith, C. D. Rahn and C.-Y. Wang, "Model-Based Electrochemical Estimation of Lithium-Ion Batteries," in *IEEE International Conference on Control Applications*, San Antonio, Texas, USA, September 3-5, 2008.

[6] R. Klein, N. A. Chaturvedi, J. Christensen, J. Ahmed, R. Findeisen and A. Kojic , "Electrochemical Model Based Observer Design for a Lithium-Ion Battery," *IEEE Transactions on Control Systems Technology,* vol. 21, no. 2, 2013.

[7] H. Rahimi-Eichi, F. Baronti and M.-Y. Chow, "Modeling and Online Parameter Identification of Li-Polymer Battery Cells for SOC estimation," in *IEEE International Symposium on Industrial Electronics (ISIE)*, Hangzhou, 2012.

[8] S. R. Habibi and R. Burton, "The Variable Structure Filter," *Journal of Dynamic Systems, Measurement, and Control (ASME),* vol. 125, pp. 287-293, September 2003.

[9] S. R. Habibi and R. Burton, "Parameter Identification for a High Performance Hydrostatic Actuation System using the Variable Structure Filter Concept," *ASME Journal of Dynamic Systems, Measurement, and Control,* 2007.

[10] M. Conte, V. C. Fiorentino , I. D. Bloom, K. Morita, T. Ikeya and J. R. Belt, "Ageing Testing Procedures on Lithium Batteries in an International Collaboration Context," China, November, 2010.

[11] "Battery Test Manual for Plug-In Hybrid Electric Vehicles," U.S. Department of Energy, Idaho National Laboratory, Idaho Falls, Idaho 83415, March 2008.

[12] G. Pistoia, Electric and Hybrid Vehicles, Rome, Italy: Elsevier, 2010.

[13] D. Domenico, S. Anna and F. Giovanni, "Lithium-Ion Battery State of Charge and Critical Surface Charge Estimation Using an Electrochemical Model-Based Extended Kalman Filter," *Journal of Dynamic Systems, Measurement, and Control,* vol. 132, pp. 1-11, 2010.

[14] D. D. Domenico, G. Fiengo and A. Stefanopoulou, "Lithium-Ion battery State of Charge estimation with a Kalman Filter based on a electrochemical model," *IEEE Interantional Conference on control Applications (CCA),* pp. 702-707, 2008.

[15] M. Dubarry, V. Svoboda, R. Hwu and B. Y. Liaw, "Capacity and power fading mechanism identification from a commercial cell evaluation," *Journal of Power Sources,* 2006.

[16] D. Abraham, R. Twesten, M. Balasubramanian, I. Petrov, J. McBreen and K. Amine, "Surface changes on LiNi0:8Co0:2O2 particles during testing of high-power lithium-ion cells," *Electrochemistry Communications,* vol. 4, pp. 620 - 625, 2002.

[17] R. Kostecki and F. McLarnon, "Degradation of LiNi0.8Co0.2O2 Cathode Surfaces in High-Power Lithium-Ion Batteries," *Electrochemical and Solid-State Letters,* vol. 5, pp. A164-A166, 2002.

[18] S. R. Habibi, "The Smooth Variable Structure Filter," *Proceedings of the IEEE,* vol. 95, no. 5, pp. 1026-1059, 2007.

[19] M. Al-Shabi, "The General Toeplitz/Observability SVSF," Hamilton, Ontario, 2011.

[20] S. A. Gadsden and S. R. Habibi, "A New Form of the Smooth Variable Structure Filter with a Covariance Derivation," in *IEEE Conference on Decision and Control*, Atlanta, Georgia, 2010.

[21] S. A. Gadsden, "Smooth Variable Structure Filtering: Theory and Applications," Hamilton, Ontario, 2011.

[22] K. O'Neil and C. Y.-C, "Instability of Pseudinverse Acceleration Control of Redundant Mechanisms," *Proceedings of the IEEE International Conference on Robotocs and Automation* , April 2000.

[23] K. Doty, C. Melchiorri and C. Bonivento, "A theory oof generalized inverses applied to robotics," *International Robotics Journal,* vol. 12, pp. 1-19, 1993.

[24] H. Lipkin and P. E. , "Enumeration of singular configuration for robotic manipulators," *journal of Mech. Design* , vol. 113, no. 3, pp. 272-279, 1991.

Chapter 5: Online and Offline Parameters Identification and SOC Estimation for Healthy and Aged Electric Vehicle Batteries Based on Equivalent Circuit Models

Ryan Ahmed[1], Ienkaran Arasaratnam[1], Mohamed El-Sayed[1], Jimi Tjong[2], Saeid Habibi[1]

[1]McMaster Automotive Resource Center (MARC), Department of Mechanical Engineering,
McMaster University, Hamilton, Canada
[2]Ford Motor Company of Canada, Powertrain Engineering Research and Development Center
(PERDC), Windsor, Canada

Abstract

Recently, extensive research has been conducted in the field of hybrid (HEVs) and battery electric vehicles (BEVs) since they represent a more sustainable alternative compared to conventional, fossil fuel-based vehicles. The battery pack is one the most expensive and important elements of the EV powertrain. It requires accurate, real-time monitoring and control. Parameters such as battery state of charge (SOC) and state of health (SOH) have to be accurately monitored in real-time to ensure battery safety and reliability and avoid overcharge or under-discharge conditions. These conditions can cause irreversible capacity degradation and power fade. For battery condition monitoring, an accurate battery model is needed in conjunction with a robust estimation strategy for extracting battery health information from a limited set of measurements. In this paper, online and offline battery model parameters identification and state of charge estimation at various states of life have been implemented. An extensive aging test has been conducted over a period of 12 months using real-world driving scenarios. This paper provides the following contributions: (1) tracking changes in the battery OCV-R-RC model parameters as battery ages using genetic algorithm optimization, (2) estimation of the battery SOC using a relatively new estimation strategy known as the Smooth Variable Structure Filter, (3) online estimation of the battery model parameters using square-root recursive least square (SR-RLS) with forgetting factor methodology, (4) estimation of the battery state of charge using regressed-voltage-based estimation strategy at various states of life, (5) model validation using a series of real-world driving cycles. The limitations and benefits of the proposed strategies are discussed.

Keywords: Lithium-Ion Batteries, genetic algorithm optimization, recursive least square, equivalent circuit-based battery model, parameter identification, smooth variable structure filter, state of charge estimation.

- **Corresponding Author:**

Ryan Ahmed, M.A.Sc, P.Eng., SCPM
Research and Development Engineer, McMaster University
Stanford Certified Project Manager

5.1 Introduction

Recently, HEVs and EVs have received considerable attention due to increased price of non-renewable resources and the impact of fossil fuels on climate, [1]. Batteries are one of the most important and expensive components of the electric vehicle powertrain. Therefore, their accurate monitoring and control is critically important in order to avoid battery overcharge or under-discharge that might lead to battery degradation and impact safety.

Electric vehicles have been on the market for quite a short period of time thus possible malfunction of batteries is of great concern. Therefore, adaptive control of batteries is necessary to account for aging and degradation in performance that might affect vehicle range of operation and charging efficiency, [2]. Furthermore, safety is of great concern; since EVs are relatively new, more time is needed to assess their performance in real-world operations (until odometer reaches 150,000 miles), [3]. Any severe fires due to battery overcharge or short circuits would result in loss of market share and in a move away from electric vehicles. Accordingly, health monitoring in battery systems is extremely important.

The battery management system (BMS) is responsible for several tasks, monitoring the battery state-of-charge (SOC), state-of-health (SOH), state-of-power (SOP), and remaining useful life. In addition, the BMS ensures cell balancing and performs thermal management in order to avoid battery overcharge or under discharge which might affect the driver safety and shorten the battery life. SOC, SOH, and SOP are three key variables used in battery control and energy management. The SOC is defined as a ratio of the remaining capacity to the nominal capacity. The performance and safety of hybrid and pure electric vehicles is highly dependent on the accurate and immediate assessment of the amount of charge available for use by the vehicle at any time. The range, fuel economy and other critical, calculated performance criteria rely greatly on the SOC. Consequently, estimating the SOC accurately will ultimately improve both vehicle safety and customer satisfaction. The SOH is often related to the loss of battery's rated capacity. When the capacity reduces to 80% of the beginning of life capacity, the battery is considered to have reached its end of life. Cycling and calendar aging cause the battery to lose its capacity.

Recently, several incidents of battery degradation have been reported. For instance, as per October, 2012, there were 112 documented cases of customers complaining of capacity loss in electric vehicles, [4]. In addition, around 11.8% of the total number of Nissan Leaf vehicles sold in Arizona have exhibited a loss in capacity gauge bars (Note: first capacity bar represents 15% capacity loss and 6.25 in the subsequent bars), [4]. Manufacturers generally have lifetime data on batteries, but these are generated using predefined charging/discharging cycles at fixed temperatures and fixed charging/discharging rates referred to as C-rate. Relying on this data in model development will result in inaccuracies and errors in SOC and SOH estimations. This because in EV applications, the battery is exposed to various driving cycles with fast transients and aggressive current demands. Accordingly, these transients have to be captured in the model and the model degradation with aging tracked accordingly.

In this paper, extensive aging test results using real-world driving cycles for an average North American driving profile are reported. These tests were conducted over 12 months period and involved accelerated testing of battery lifetime. Model parameters such as the capacity and internal resistance have been tracked in both online and offline modes. A relatively new estimation strategy has been applied to estimate the battery SOC at various states of life.

5.1.1 Battery Models Literature Review

In the literature, battery models are classified to one of the following: ***equivalent circuit-based models, behavioral models,*** and ***electrochemical models.*** **Equivalent circuit-based models** use RC circuit elements such as resistors and capacitors to model the charge and discharge behavior of Li-ion batteries. Due to their simplicity, equivalent circuit-based models require less computational power and thus can be easily implemented onboard of a battery management system. **Behavioural models** are empirical and utilize various functions to model battery dynamics. In [5], Plett has introduced a series of behavioural models, namely: ***the combined model, the simple model, the zero-state hysteresis model, one state hysteresis model,*** and ***the enhanced-self-correcting model***. These models can account for hysteresis effect, polarization time constants, and ohmic loss effects. **Electrochemical battery models** utilize partial differential equations to model lithium intercalation inside the electrolyte and both electrodes. Since electrochemical models provide a physical insight of the battery chemistry, they are favoured in state of health estimation and in tracking battery degradation. However, in general, electrochemical models are complex and require more computational power. Therefore for their application in real-time battery management systems, these models need to be simplified and reduced to their correct level of dynamic significance, [6]. Various strategies for battery modeling are summarised in the following sections, starting with equivalent circuit-based and lumped parameters models.

5.1.1.1 Equivalent Circuit-based models

All published RC models include an open circuit voltage source which is a function of the battery SOC. R_0 represents the battery internal resistance while RC branches are used to model battery dynamics. The third-order model is as shown below in Figure 5.1. The terminal voltage relationship from the standalone first, second, and third-order models are listed in Table 5.1, [7, 8].

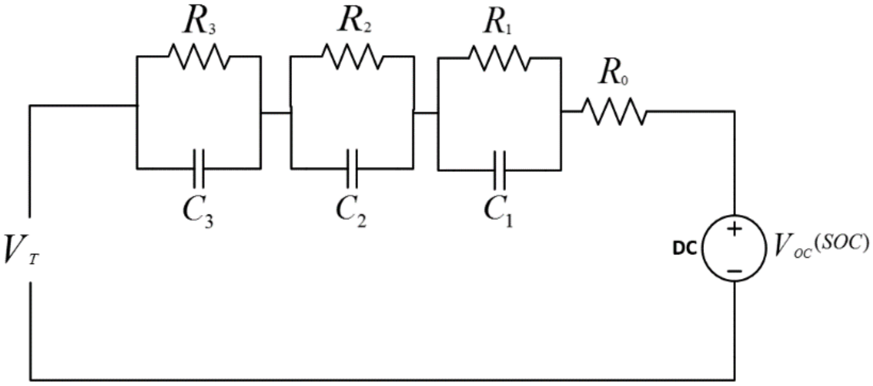

Figure 5.1. Third-order RC battery model [7, 8]

In addition, any of these models can be enhanced by incorporating hysteresis to account for the battery's hysteresis that occurs during charging/discharging cycles.

Table 5.1. First, second, and third RC models with and without hysteresis equations, [7, 8]

Model	**Output equations**
The first-order RC model [9, 10]	$U_{1,k+1} = \exp(-\Delta t/\tau_1)\, U_{1,k} + R_1[1 - \exp(-\Delta t/\tau_1)]I_k$ $V_k = OCV(z_k) - R_0 I_k - U_{1,k}$
The first-order RC model with hysteresis state [7, 8]	$V_k = OCV(z_k) - R_0 I_k - U_{1,k} + h_k$
The second-order RC model	$V_k = OCV(z_k) - R_0 I_k - U_{1,k} - U_{2,k}$
The second-order RC model with a hysteresis state	$V_k = OCV(z_k) - R_0 I_k - U_{1,k} - U_{2,k} + h_k$
The third-order model RC model	$V_k = OCV(z_k) - R_0 I_k - U_{1,k} - U_{2,k} - U_{3,k}$
The third-order model RC model with hysteresis state	$V_k = OCV(z_k) - R_0 I_k - U_{1,k} - U_{2,k} - U_{3,k} + h_k$

Equations for the first, second, and third-order models with and without hysteresis are presented in Table 5.1. Where U_1, U_2, U_3 are the voltage of the first, second, and third order RC network, respectively and while $\tau_1 = R_1C_1, \tau_2 = R_2C_2, \tau_3 = R_3C_3$ are their corresponding time constants.

5.1.1.2 Behavioural Battery Models

Behavioural battery models use various empirical functions and formulas to describe the behaviour of the battery cells. Similar to equivalent circuit-based models, these models are simple to implement with less parameters to tune and are therefore easy to be implemented in real-time applications on a BMS. Examples are as follows.

Shepherd/Unnewehr/Nernest Equations

The shepherd equation represents a simple approach for battery modeling; it is represented in the following form, [11]:

$$E(t) = E_o + R_\alpha i(t) + \frac{K_1}{q_s(t)} \tag{5.1}$$

where, E_o is the initial cell voltage, R_α is the cell internal resistance, $q_s(t)$ is the instantaneous stored charge, and K_1 is a constant, [11]. Another further approximation is represented in the Unnewehr model:

$$E(t) = E_o + R_\alpha i(t) + K_2 q_s(t) \tag{5.2}$$

Another model which has a similar form is known as the Nernest Model as follows, [11]:

$$E(t) = E_o + R_\alpha i(t) + K_3\, ln\left(\frac{q_s(t)}{Q}\right) - K_4 ln(\frac{Q - q_s(t)}{Q}) \tag{5.3}$$

where, Q is the total charge capacity of the cell and the constants K_1, K_2, K_3, and K_4 can be obtained by fitting experiential data, [12].

In [5], Plett has introduced a series of behavioural models based on the previously mentioned models, namely: ***the combined model, the simple model, the zero-state hysteresis model, one state hysteresis model,*** and ***the enhanced-self-correcting model***. These models can account for hysteresis effect, polarization time constants, and ohmic loss effects. A summary of these models is provided below.

The Combined Model

By combining the three abovementioned models and discretizing them in time [13], the combined model is obtained, [13]:

$$y_k = K_0 - Ri_k - \frac{K_1}{z_k} - K_2 z_k + K_3 \ln(z_k) + K_4 \ln(1 - z_k) \tag{5.4}$$

$$z_{k+1} = z_k - \left(\frac{\eta_i \Delta t}{C}\right) i_k \tag{5.5}$$

In this model, y_k is the cell terminal voltage, R is the cell internal resistance, representing both charge and discharge resistances. K_1, K_2, K_3, K_4 are tunable constants that can be used to fit experimental data to the model, [13]. Model parameters can be easily identified from the current/voltage data by using least square optimization.

The Simple Model

The simple model is derived from the combined model by grouping all terms that are functions of SOC (z_k) in one group as follows, [13]:

$$f(z_k) = K_0 - \frac{K_1}{z_k} - K_2 z_k + K_3 \ln(z_k) + K_4 \ln(1 - z_k) \tag{5.6}$$

And by grouping all terms that are function of the current:

$$f(i_k) = Ri_k$$

Equation (5.6) represents the open circuit potential which is a function of the battery SOC. The simple model can thus be formulated as follows, [13]:

$$z_{k+1} = z_k - \left(\frac{\eta_i \Delta t}{C}\right) i_k \tag{5.7}$$

$$y_k = OCV(z_k) - Ri_k \tag{5.8}$$

Where OCV refers to the open circuit voltage.

The Zero-State Hysteresis Model

Even though the previous models can model the terminal voltage dynamics with acceptable accuracy, they do not account for the hysteresis effect. The zero-state hysteresis model is capable of modeling hysteresis by adding the following term $s_k M(z_k)$ to the simple model, [13]:

$$y_k = OCV(z_k) - s_k M(z_k) - R i_k \tag{5.9}$$

where s_k represents the sign of the current and $M(z_k)$ is half the difference between the charge and discharge values, [13]. For a small and positive value ε, s_k can be defined as follows:

$$s_k = \begin{cases} +1 & i_k > \varepsilon \\ -1 & i_k < -\varepsilon \\ s_{k-1} & |i_k| \le \varepsilon \end{cases}$$

The zero-state hysteresis model provides a better voltage estimate compared to the simple model, [13].

The One-State Hysteresis Model

The hysteresis voltage can be modeled using a separate state $h(z,t)$ which is function of the battery SOC. The hysteresis voltage can be modeled as follows, [13]:

$$\frac{dh(z,t)}{dz} = \gamma sgn(\dot{z})[M(z,\dot{z}) - h(z,t)] \tag{5.10}$$

$M(z,\dot{z})$ is the maximum polarization due to hysteresis. It is a function of the SOC and also its rate-of-change. The $sgn(\dot{z})$ is used to model both battery charging and discharging operations, [13]. γ is a positive constant that describes the rate of voltage decay, [13]. $M(z,\dot{z}) - h$ indicates that the rate-of-change of hysteresis voltage is proportional to the distance away from the main hysteresis loop; leading to a kind of voltage decay in the major loop, [13]. The model can be represented in a state space form as follows [13]:

$$\begin{bmatrix} h_{k+1} \\ z_{k+1} \end{bmatrix} = \begin{bmatrix} F(i_k) & 0 \\ 0 & 1 \end{bmatrix} \begin{bmatrix} h_k \\ z_k \end{bmatrix} + \begin{bmatrix} 0 & 1 - F(i_k) \\ -\frac{\eta_i \Delta t}{C} & 0 \end{bmatrix} \begin{bmatrix} i_k \\ M(z, \dot{z}) \end{bmatrix} \tag{5.11}$$

$$y_k = OCV(z_k) - Ri_k + h_k \tag{5.12}$$

Where $F(i_k) = \exp(-|\eta_i i(t) \gamma / C_n|)$.

The Enhanced Self-Correcting Model

A further enhancement over the one state hysteresis is the enhanced self-correcting model. The model is capable of capturing the battery dynamics and accommodates for ohmic losses, hysteresis, and polarization time constants, [13]. The model has two inputs, namely: the battery input current i_k, and the maximum polarization due to hysteresis $M(z, \dot{z})$. The model has one output y_k, which is the terminal voltage. The ESC model in the state space form is as follows, [13]:

$$\begin{bmatrix} f_{k+1} \\ h_{k+1} \\ z_{k+1} \end{bmatrix} = \begin{bmatrix} diag(\propto) & 0 & 0 \\ 0 & F(i_k) & 0 \\ 0 & 0 & 1 \end{bmatrix} \begin{bmatrix} f_k \\ h_k \\ z_k \end{bmatrix} + \begin{bmatrix} 1 & 0 \\ 0 & \left(1 - F(i_k)\right) \\ -\frac{\tau_i \Delta \mathrm{t}}{C_n} & 0 \end{bmatrix} \begin{bmatrix} i_k \\ M(z, \dot{z}) \end{bmatrix} \tag{5.13}$$

$$y_k = OCV(z_k) - Ri_k + h_k + Gf_k \tag{5.14}$$

where z_k is the state of charge, f_k is the states of the low pass filter on i_k which is used to characterize the polarization time constants, h_k is the state representing charging or discharging hysteresis effect, OCV is the open circuit voltage, C_n is the battery nominal capacity, R is the battery internal resistance, G is the output matrix of the low pass filter, and α's are the poles of the low pass filter.

5.1.2 Model Parameters Identification and SOC Estimation

Several papers have been published on parameter identification for the abovementioned model categories. In [14], parameter estimation using the extended Kalman filter (EKF) has been reported for behavioural models. Experimental data using a benchmark Urban Dynamometer Driving Schedule (UDDS) cycle in addition to data from a pulsed charge/discharge test have been used.

In [15], a dual strategy was applied for estimating the battery parameters and SOC for behavioural models. Furthermore, a comparative study of Li-Ion battery models showed the enhanced self-correcting model is the most accurate since it is capable of modeling ohmic losses, polarization time constants, and hysteresis effects. Two estimation strategies were used, namely the well-known Kalman filter and the more recent Smooth Variable Structure Filter (SVSF), [15].

In [16], a multi-objective optimization using genetic algorithms is applied for identifying the parameters of a simple RRC model. Model parameters such as the resistance and the open circuit potential are assumed to be a polynomial function of the C-rate and the SOC. The multi-objective optimization is then applied to obtain the polynomial coefficients. The technique has been verified on a 2.5 V, 8 Ah capacity cell and the models show good fit to experimental data at various charge/discharge rates.

In [17], a parameter identification strategy using least squares has been applied to an equivalent circuit-based model. Since the main source of nonlinearity for battery models arises from the SOC-OCV relationship, this relationship has been divided into 8 piece wise linear regions and the technique has been applied to estimate the parameters of each individual region. Then based on the resultant linear model, an observer has been applied to estimate the state of charge. The technique has been experimentally verified on Lithium polymer cells.

A parameter identification procedure using multi-swarm particle optimization on 12 different battery models has been presented in [8]. Several driving cycles including the Dynamic Stress Test (DST), the Hybrid Pulse Power Characterization test (HPPC), and the Federal Urban Dynamic Schedule (FUDS). The technique has been verified on two different battery chemistries including the lithium-Iron Phosphate ($\mathrm{LiFePO_4}$) and the Lithium Nickel-Manganese-Cobalt oxide (LiNMC). One of the main conclusions of this research project is that the first order RC model is preferred for LiNMC, while the one-state hysteresis and the first-order RC model are the best for $\mathrm{LiFePO_4}$. In most of the existing literature, model parameters have been obtained based on fresh, healthy batteries at 100% capacity. However, as battery ages, model parameters will change and thus this will affect the accuracy of the terminal voltage prediction and the SOC estimation accuracy.

5.1.3 Paper Outline and Contributions

From the literature, most battery aging studies conducted to date use charging/discharging profiles at fixed C-rates to age the battery which is not what happens in real-world driving conditions. Automotive batteries are subjected to high transients resulting from vehicle acceleration and regenerative braking. Accordingly, this research addresses this issue by conducting various aging scenarios assuming an average North-American driver. Current profiles from real-world driving cycles such as the Urban Dynamometer Driving Schedule

(UDDS) have been used. Various parameters that contribute to battery aging such as the discharge rate, temperatures, and depth of discharge have been considered. A first-order OCV-R-RC battery model widely used in the literature has been considered in this research since it provides a good compromise between model accuracy and simplicity for real-time implementation on-board of a BMS.

In this paper, two different approaches for battery SOC estimation and model parameter identification have been implemented and compared. Battery model parameters identification using both online and offline techniques at various battery states of life have been conducted. In the first approach, an online recursive least square method has been applied to estimate battery model parameters and to estimate the open circuit voltage (OCV). A square-root version of the recursive least square method (SR-RLS) has been presented in this research with a forgetting factor since it represents a robust estimation strategy. Based on the estimated battery OCV, a regressed-voltage method has been applied to map the OCV to the battery SOC and provides an estimate of the battery SOC at various states of life.

In the second approach, a Genetic Algorithm (GA) optimization strategy has been applied offline to estimate the battery model parameters at various states of life. Based on the optimized model parameters, a battery SOC estimation strategy has been designed to estimate the SOC based on the identified battery model parameters. A relatively new strategy known as the Smooth Variable Structure Filter (SVSF) has been presented for battery SOC estimation. The proposed strategy has been selected since it demonstrates robustness to modeling uncertainties, sensor noise, and to SOC initial conditions, [18, 19].

The strategy has been applied for estimating the battery SOC at various battery states of life from fresh (healthy) state (100% capacity) to 80% retained capacity.

This paper is organized as follows: section 5.2 describes the electric vehicle model development to generate the current profile required for experimentation. Section 5.3 of this paper provides a summary of the aging experiments. Section 5.4 describes the experimental setup used for data gathering. Section 5.5 contains illustrations of battery performance under various aging conditions. Section 5.6 provides illustration of parameters and SOC estimation strategies using RLS and Regressed-voltage based methods. Section 5.7 contains offline parameter identification and SOC estimation based on the SVSF. The conclusions and limitations of the above strategy are presented in Section 5.8.

5.2 Electric Vehicle Model and Current Generation

This section summarizes the process of current generation from the velocity profiles of various driving cycles. In order to conduct the aging study, a cell-level current profile from the velocity profile of various benchmark driving cycles is required. Therefore, a mid-size all-electric vehicle (EV) model as shown in Figure 5.2 has been modified from an existing hybrid vehicle model, [20]. The model has been simulated in Matlab/SimScape environment. The driving range of the simulated EV is approximately 200 Kms when the battery is fully charged. As shown in Figure 5.2, the EV model consists of a lithium-Ion battery pack, vehicle dynamic model, DC electric motor, DC-DC convertor, and vehicle speed controller.

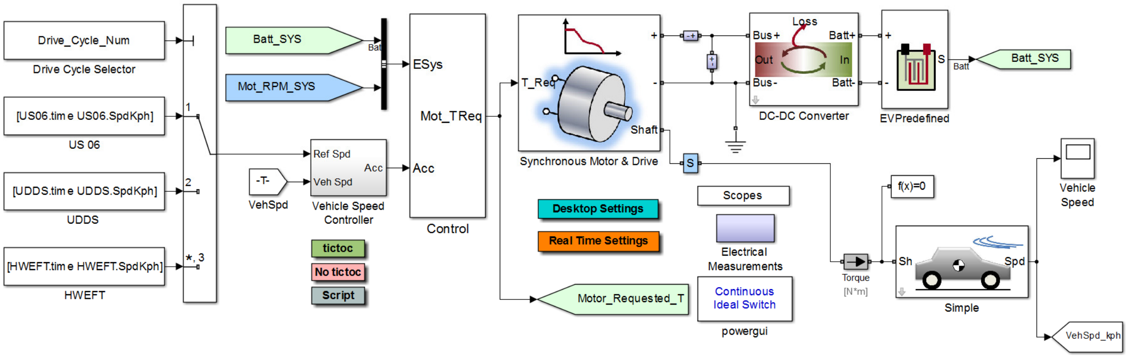

Figure 5.2. All-Electric Mid-size Sedan Simulation Model in SimScape (Adopted from [20])

Three benchmark driving schedules have been considered in this study; namely, an Urban Dynamometer Driving Schedule (UDDS), a light duty drive cycle for high speed and high load (US06), and a High fuel Economy Test (HWFET), [21].

These driving cycles have been used during the aging study in addition to model fitting and validation. While driving behaviours of drivers might vary, these driving cycles are generally adopted to conduct powertrain durability testing and to provide an estimate of fuel economy. The UDDS driving cycle is used to characterise a city driving condition. It has been established to replicate average speed, idle time, and number of stops that the average driver performs in practice, [22]. The test profile is recommended by the U.S. Environmental Protection Agency for estimating the fuel economy in city driving conditions, [21]. For electric vehicles, the profile has been extensively used to estimate the driving range in miles per full charge, [23, 24].

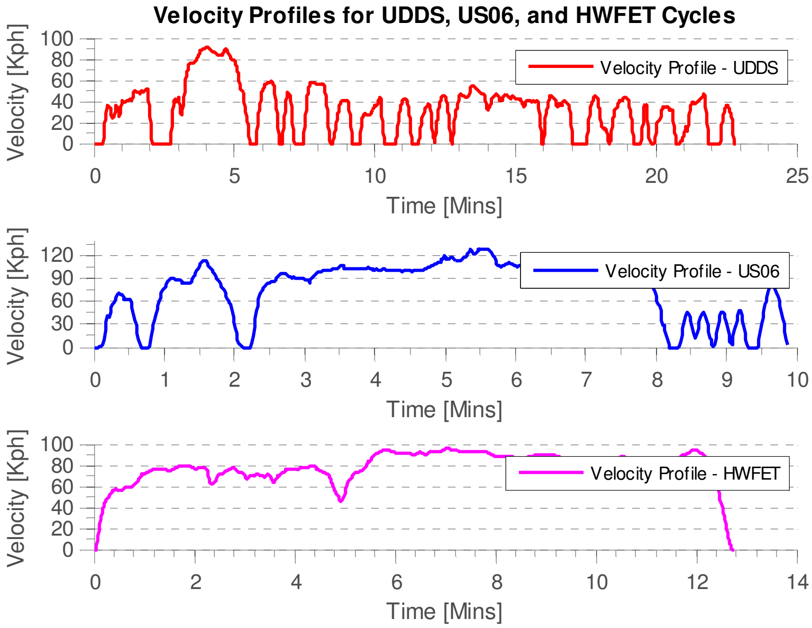

Figure 5.3. Velocity Profiles for the UDDS (upper figure), US06 (middle), and HWFET (lower) Cycles [11]

The US06 cycle is a high acceleration, aggressive driving cycle, and the HWFET embodies a highway driving conditions with speeds below 60 miles/hours, [25]. The three abovementioned driving cycles are shown in Figure 5.3. A summary of these driving cycle characteristics such as distance, time, and average speed is provided in Table 5.2, [26].

Table 5.2. Characteristics of UDDS, US06, and HWFET Driving Schedules, [11]

	Length (sec)	Distance (miles)	Avg Speed (mph)
UDDS	1,369	7.45	19.59
US06	596	8.01	48.37
HWFET	765	10.26	48.30

The pack current profiles from these driving cycles are as shown in Figure 5.4. As shown below, the US06 driving cycle current demand by the motor is relatively high compared to other driving cycles since it is an aggressive driving cycle. The pack-level current profiles have been scaled down to the cell-level and used for model parameters identification in the aging study.

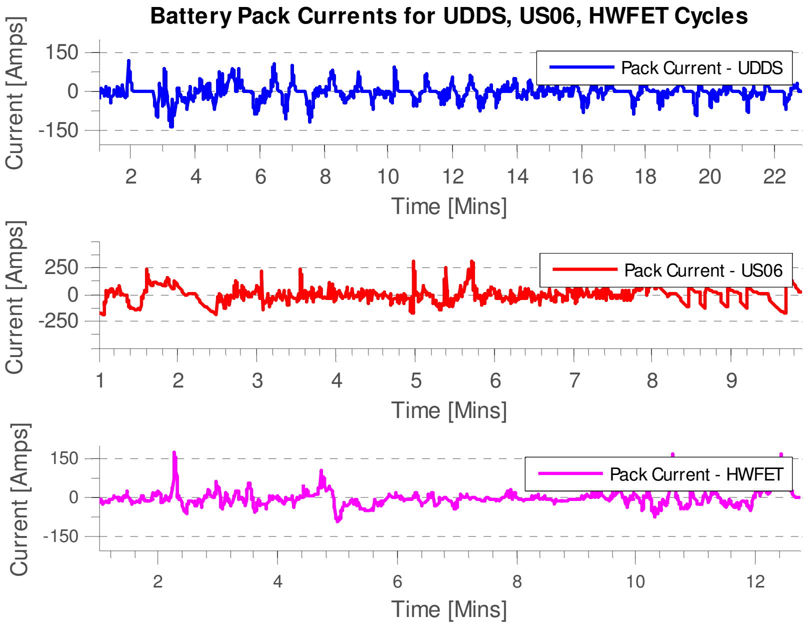

Figure 5.4. Pack current profiles for the UDDS (Upper figure), US06 (middle figure), and HWFET (lower figure) cycles

5.3 Aging Study Overview

Battery cells, modules, and packs have to undergo laboratory testing in order to assess their performance under various load and temperature conditions, [27]. In addition, data collected during these tests can be used to train and validate various battery models which are essential for State of Charge (SOC) and State of Health (SOH) estimation. In order to standardize these tests and to set a common basis for OEMs and battery manufactures, the test procedures have been documented in numerous reports, [27], such as the “USABC EV battery Test Procedures Manual” produced by the U.S. DOE/Argonne National Laboratory in 1996, [28, 27], the “PNGV Battery Test Manual” published by the U.S. DOE/INEEL in

2000, [29, 27], and the "Battery Test Manual For Plug-In HEVs" published in 2008 by the U.S. DOE/Idaho National Laboratory, [30, 27].

Battery test procedures might vary depending on the country and the application, i.e.: for HEVs, PHEV, or BEVs, [31]. This research focuses on test procedures used for PHEVs and BEVs. In U.S., battery test procedures are generally classified into 3 main categories: characterization, life, and reference tests, [30].

- **Characterization tests** are conducted to specify battery cell (or pack) baseline performance characteristics. Examples of these tests include: static capacity, hybrid pulse power characterization (HPPC), self-discharge, cold cranking, thermal performance, and efficiency tests, [30].
- **Life tests** are conducted to determine battery degradation (aging) effects that take place in both cycle life and calendar life, [30]. Calendar life means the life of the battery during storage (with no cycling involved) while cycle life is the life of the battery after multiple charging/discharging cycles, [31]. The main purpose of these tests is to perform an accelerated battery aging by acquiring data in a relatively short time therefore be able to predict the performance of the battery cell in practice. In addition, these tests can be used for battery warranty estimates.
- **Reference performance tests (RPT):** are conducted periodically to track changes that might occur in the battery baseline characteristics. Reference tests are performed after conducting a certain number of life tests to measure the capacity fade and degradation in performance through the entire progress of battery life

cycle, [27]. In addition, these tests are performed at the beginning (fresh battery) and at the end of life state.

In this paper, two test schedules are considered. **Schedule A** which represents the reference performance tests (RPTs) and **Schedule B** which represents the aging test. Regarding **Schedule A**, reference performance tests are selected, namely:

- **Static capacity test at 1C, 2C, 3C, and 4C;**
- **Open circuit voltage-state of charge (OCV-SOC) relationship test;**
- **A series of UDDS, US06, and HWFET driving cycles (that scans the entire SOC range from 90% to approximately 20%);**

These tests are selected since they can provide information regarding aging effects and the test results are expected to significantly vary as battery ages. All aging tests are conducted at elevated temperatures (ranging from $35\ to\ 40$℃) to simulate electric vehicle driving in hot weather conditions such as in Arizona and to obtain the experimental data in a realistic period of time. Regarding **Schedule B** cycling (aging) tests, 3 driving scenarios are considered. The first test schedule,

- **Schedule B1 - Real driving conditions at low C-rates/high DOD:** is used to perform battery aging which simulates the real driving cycle for an all-electric vehicle (EV) at high depth of discharges of approximately 20% to 25% and low C rates of approximately 2C.
- **Schedule B2 - Fixed Current Demand:** is used to apply a well-defined charging and discharging cycles at 1C rate to age the battery. According to the manufacturer

datasheet, the battery will last for approximately 500 charging and discharging cycles at room temperature. Schedule B3 is used to perform battery aging using the same well defined cycles but at elevated temperature, the test is conducted at elevated temperatures in the range of $35-45$℃.

- **Schedule B3 - Real driving conditions at high C-rates/high DOD:** is used to age the battery using high C-rate currents up to 10C assuming fewer parallel cells in the entire pack which leads to higher C-rate values. Batteries are subject to high depth of discharge of approximately 20%.

A reference performance test is conducted after a specific number of aging tests depending on the schedule. For **Schedule B1 and Schedule B3,** a reference performance test is conducted every 5 aging cycles. For **Schedule B2**, a reference performance is conducted every 50 full charging/discharging aging cycles. In the following subsections, a detailed description of the reference performance tests (***Schedule A***) and aging tests (***Schedule B***) is presented.

5.3.1 Schedule A – Characterization/RPT tests

Characterization tests are conducted to capture battery cell baseline performance characteristics such as cell power capability, internal resistance, capacity, and time constants. Tests selected for the study include the following.

5.3.1.1 Static Capacity Test

This test is used to measure the battery cell capacity in Ampere-hours at a constant current (CC) discharge rate. This test is conducted in order to provide a baseline for a fresh battery cell capacity. The test procedure follows the Constant Current-Constant Voltage (CCCV) protocol and is summarized in the following steps, [30]:

A. *Charge the battery at 1C rate (5.4 A) to the fully charged state in a CCCV mode. The battery is fully charged to 4.2 V and when the current end point is at 0.02 C (0.108 A).*
B. *Leave the battery to rest for one hour in order to allow for voltage and current stabilization,* [30].
C. *Discharge sequence at a constant current 1C rate until the voltage reaches the battery minimum voltage limit (2.8 V) as recommended by the manufacturer,* [30].
D. *Battery is left at rest with no load for one hour.*

The test has been repeated at various C-rates of 2C, 3C and 4C. These tests are important since the battery capacity is inversely proportional to the current C-rate.

5.3.1.2 OCV-SOC Relationship:

This test is used to characterize the Open-Circuit Voltage (OCV)-State of Charge (SOC) relationship, [32]. Very small C-rates (C/20, C/15) are used for OCV-SOC characterization in order to minimize cell dynamics and to minimize ohmic loss effects due to battery internal resistances. Accordingly, by conducting this experiment, the measured terminal voltage is assumed to be the open circuit voltage. This test is important since the cathode and anode electrode potentials (U_p and U_n), which are used in the electrochemical model, are being derived from this test as discussed in subsection 5.4.2. The OCV-SOC relationship is obtained as follows (this test is similar to the capacity test but conducted at very low C-rates), [32]:

A. *Fully charge the battery in a CCCV mode until maximum voltage (4.2).*

B. *Fully discharge the battery at constant current (CC) mode with 1C-rate until the voltage hits the minimum voltage (2.8V).*
C. *All cycler current accumulators are reset to zero. At this moment, the battery is at zero SOC.*
D. *Charge the battery at a very small C-rate of C/15 (0.06*5.4=0.324A) in a CCCV mode until it hits the maximum voltage of 4.2V. The cell is left to rest for one hour to relax.*
E. *Discharge the cell at the same rate of C/15 until and the battery hits the minimum voltage of 2.8 V.*

The charging and discharging curves are averaged to obtain a single fixed relationship between OCV and SOC.

5.3.1.3 Model Fitting and Validation Driving Cycles

Current profiles generated from the electric vehicle model as illustrated in section 5.3 are used to excite the cells. The pack-level current profile is scaled down to the cell-level and fed to the cycler. These driving cycles are used for model parameter fitting since they include fast variations thus rich in their frequency content. The cell current is generated from the pack current by assuming no cell balancing (i.e. all cells are held at the same SOC) and by assuming equal current distributions among parallel cell branches. Two driving schedules for model validation and fitting have been conducted in this study; namely: ***Schedule A1*** and ***Schedule A2***.

The first driving cycle ***(Driving Schedule A1)*** consists of current ranges from $-2C$ to $2C$ and lasts for approximately 290 minutes of driving. The driving schedule consists of a mix of UDDS, US06, and HWFET test schedules. The first validation driving cycle is as shown below in Figure 5.5.

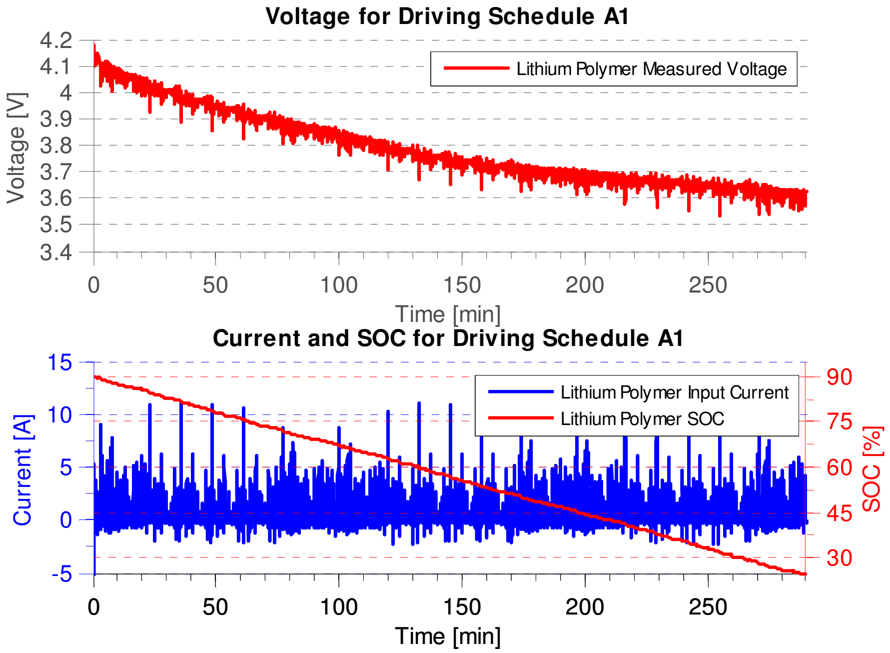
Voltage for Driving Schedule A1

Current and SOC for Driving Schedule A1

Figure 5.5. Voltage (Upper), current, and SOC (lower) for driving Schedule A1

Regarding ***Driving Schedule A2***, it is similar to driving Schedule A1 since it scans the entire state of charge range from 90% to approximately 20% and contains a mix of UDDS, US06, and HWFET driving cycles. However, as shown in Figure 5.6, driving ***Schedule A2*** consists of higher C-rate currents of up to $10C$ compared to schedule 1 which represents a more challenging driving cycle for the OCV-R-RC model to capture. Driving Schedule 2 lasts for approximately 65 minutes before the battery SOC reaches approximately 20%.

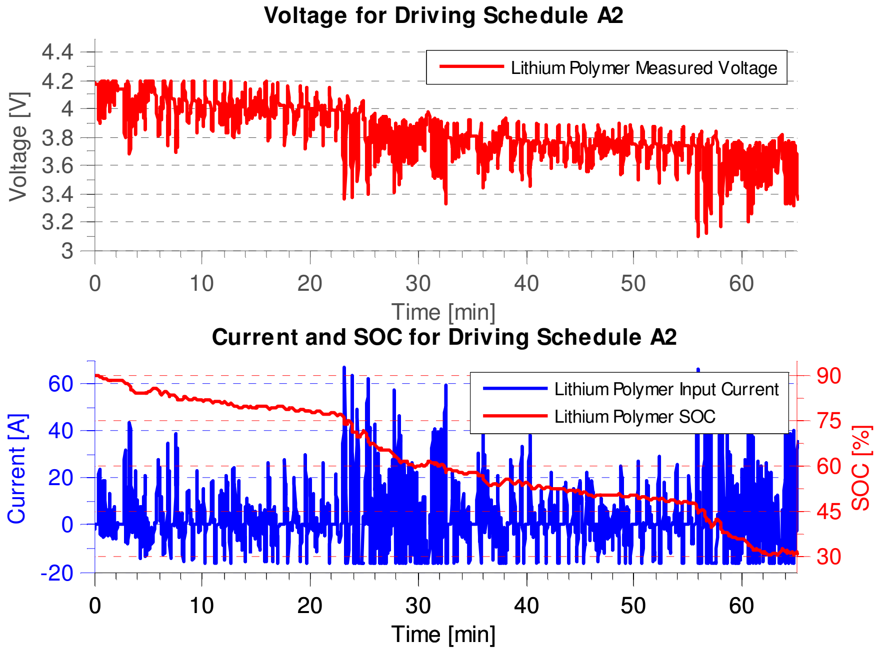

Figure 5.6. Voltage (Upper), Current, and SOC (lower) for driving Schedule A2

5.3.2 Schedule B – Aging (Cycle life) test

Two aging factors are generally involved, namely: ***calendar life*** and ***cycle life***. Calendar life means the life of the battery during storage (with no cycling involved) while cycle life is the life of the battery after multiple charging/discharging cycles, [31]. This study focuses only on aging due to cycling. Aging tests have been iteratively conducted to study the effect of battery degradation (aging) due to multiple charging/discharging cycles, [30]. Two types of aging tests are considered (3 cells each):

- Aging due to normal driving operating conditions which consists of a mix of highway, urban, and aggressive high acceleration driving conditions. Schedule B1 and B3 belongs to this test category.

- Aging due to well-defined charging/discharging (square-shaped) cycle - 500 Cycles. Schedule B2 fits in to this category.

These two types of aging conditions are implemented in this research study in order to characterize degradation in performance as a function of life and to detect pertinent failure mechanisms, [28]. A mix of driving schedules that are commonly used has been implemented, these test schedules have been adopted from [33] and are as follows.

5.3.2.1 Schedule B1: Aging due to real driving conditions (low C-rates/high DOD):

This aging test is used to simulate battery aging due to an average driver in real-world driving conditions. A mix of UDDS, US06, and HWFET driving schedules previously mentioned has been selected in this study.

Table 5.3. Aging Schedule B1 Scenario, [33]

Trip	Drive Cycles Combination	Frequency	Description
Work	$UDDS_l+US06_l+UDDS_l+US06_l$	Twice Daily, 5 days/week, 48 weeks/year	Starting from a fully charged state, a commute from home to work and back with no charge at work
Weekend/ Vacation	$UDDS_l+HWFET_l+HWFET_l+HWFET_l+HWFET_l+UDDS_l+UDDS_l+HWFET_l+HWFET_l+HWFET_l+HWFET_l+UDDS_l$	2 days/week 124 days/year	Starting from a fully charged state, assuming no charging station at the weekend destination

These tests are defined based on a velocity profile and used for deriving the current profile from the velocity for an all-electric, mid-size sedan vehicle simulated in a Matlab/SimScape environment.

Schedule B1 consists of a mix of driving cycles but used to age the battery at lower depth of discharges of approximately 25%. This will age the battery at a much accelerated rate compared to cycling at 50 DOD. The assumption is that the driver will be driving to farther destinations with no available charger thus driving to a lower DOD. No evening errand has been considered in this scenario. The test is conducted at elevated temperatures in the range of $35\ to\ 40℃$ to accelerate aging and to simulate driving in hot weather conditions such as occurring in Arizona. The description of schedule B2 for both weekday and weekend is as shown in Table 5.3 and in Figure 5.7 and Figure 5.8, respectively, [26].

Current profile, voltage, and SOC from one aging week is as shown in Figure 5.9. The SOC varies from 25% to 90% every day. The battery is then is fully charged at the end of every day. Currents range from -2C to 2C and voltages from 3.6V to a maximum of 4.2V. Current, SOC, and voltage from one weekday of driving are shown in Figure 5.10, and for one weekend of driving are shown in Figure 5.11.

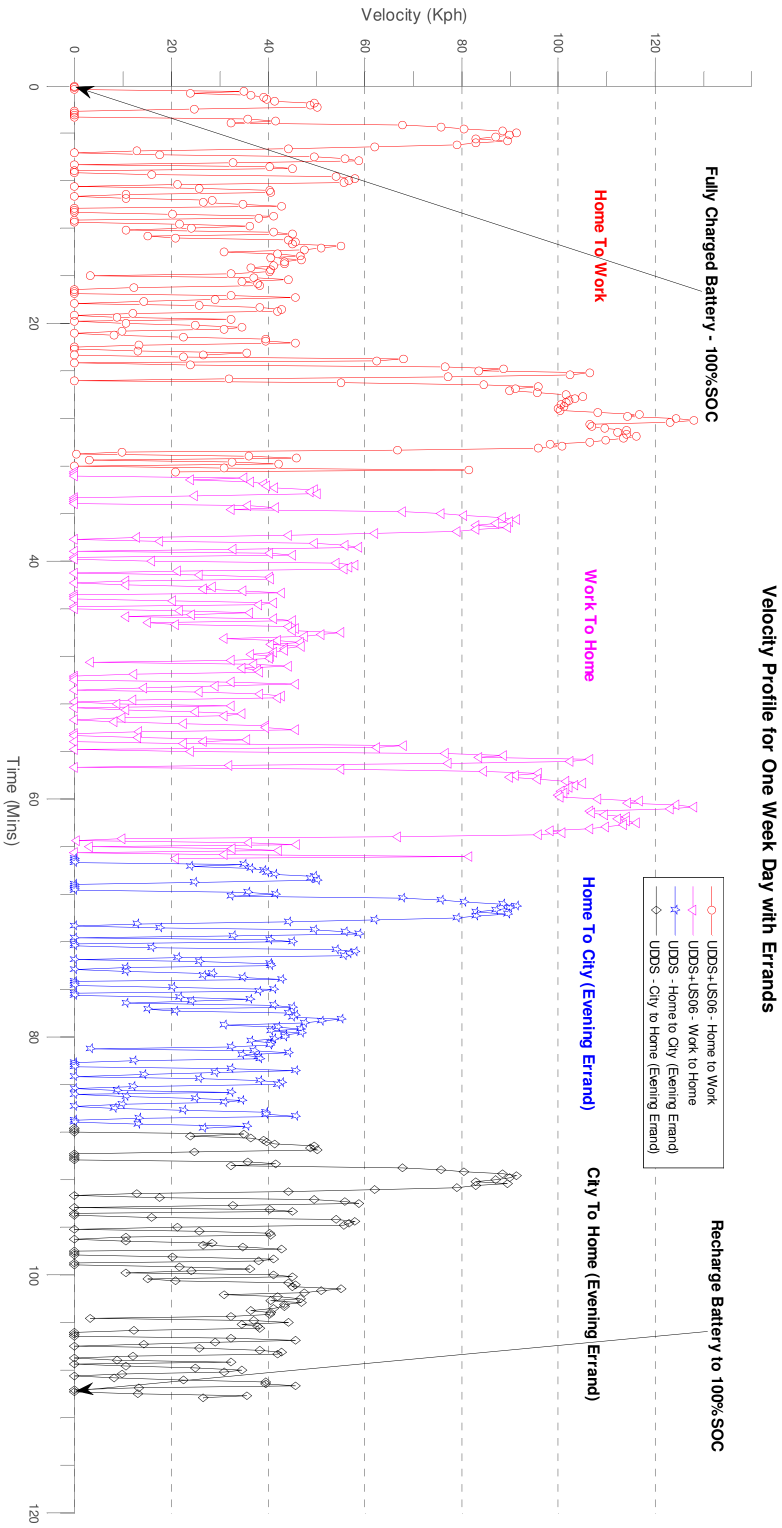

Figure 5.7. Schedule B1: One week day of driving with Errand

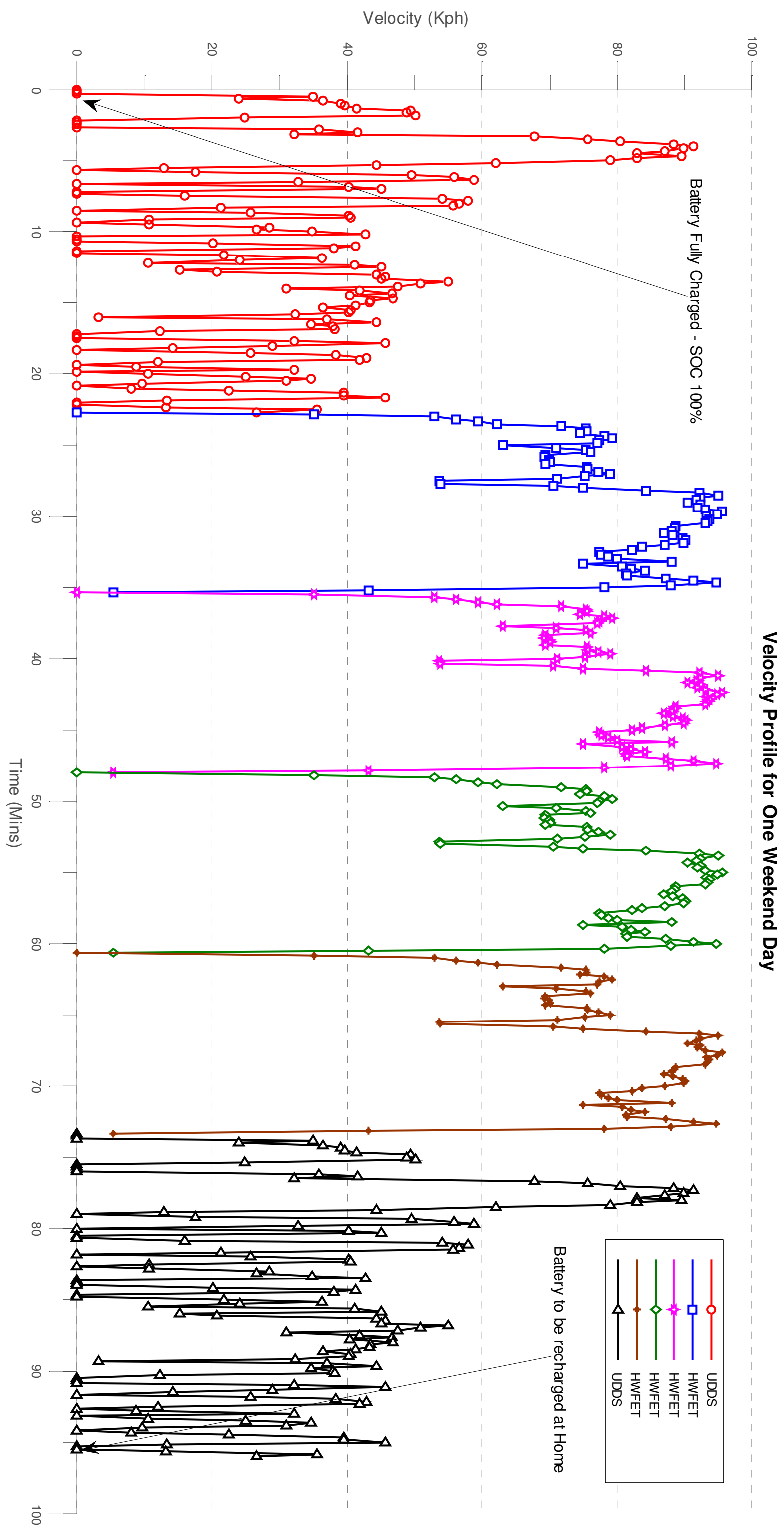

Figure 5.8. Schedule B1: One Weekend driving

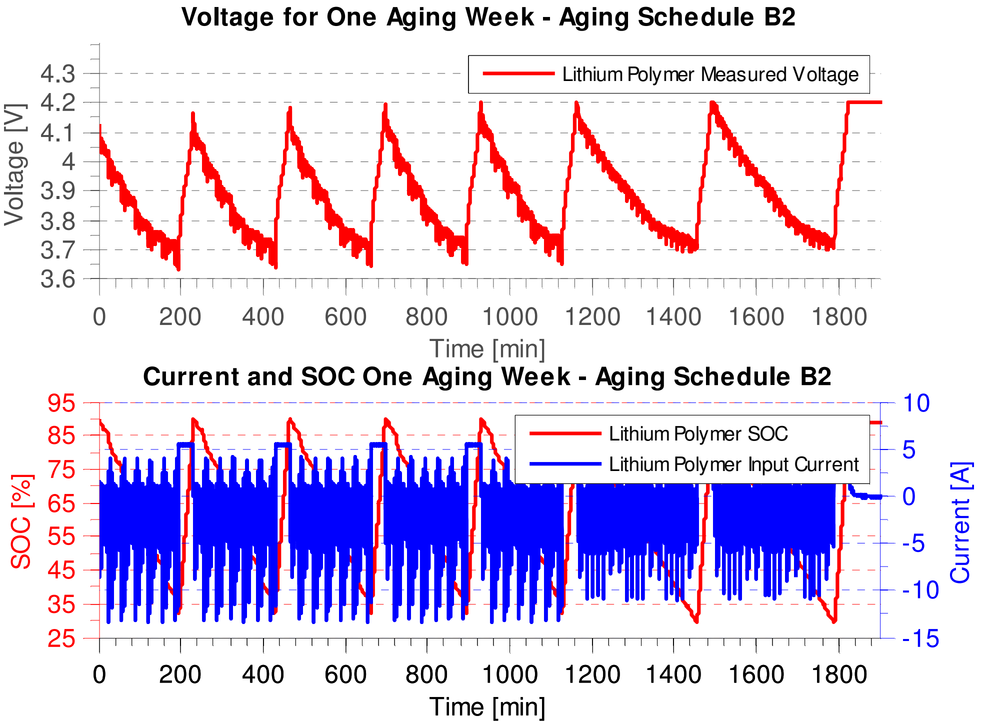

Figure 5.9. Voltage (Upper), Current, and SOC (lower) for one aging week - Schedule B1

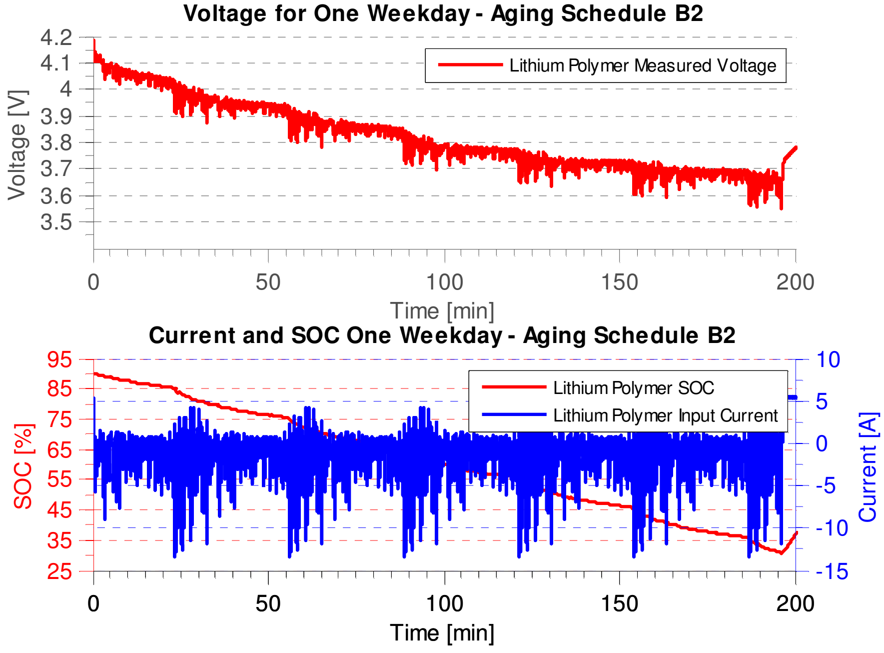

Figure 5.10. Voltage (Upper), Current, and SOC (lower) for one weekday - Schedule B1

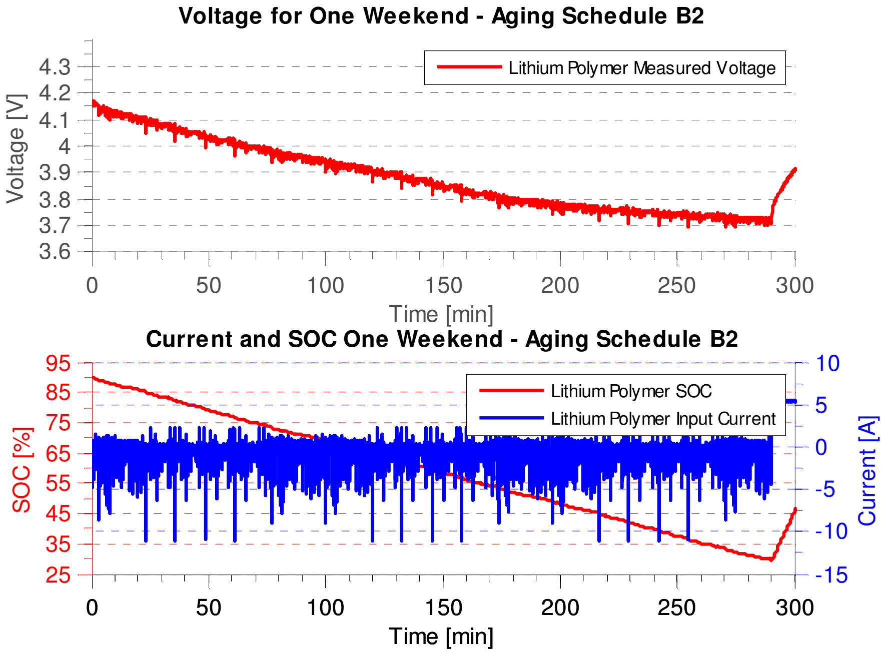

Figure 5.11. Voltage (Upper), Current, and SOC (lower) for one weekend - Schedule B1

5.3.2.2 Schedule B2: Aging at fixed charging/discharging C-rates

The test involves a repeated capacity cycle test at 1C. Reference performance tests are conducted every 50 cycles to assess cell degradation and to be used for model parameterization. **Schedule B2** is used to apply a well-defined charging/discharging cycles at 1C rate to age the battery. According to the manufacturer datasheet, the battery will last for approximately 500 charging and discharging cycles at room temperature. **Schedule B2** is used to perform battery aging using the same well defined cycles but at elevated temperatures in the range of $35 - 45°\mathrm{C}$. The current profile from one day of driving is shown in Figure 5.12.

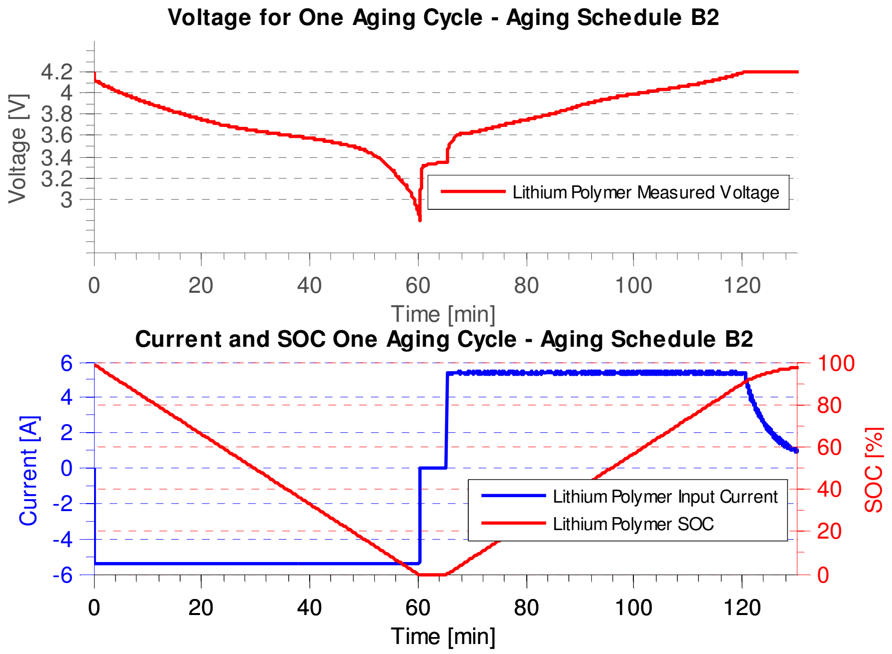

Figure 5.12. Voltage (Upper), current, and SOC (lower) for one aging cycle - Schedule B2

5.3.2.3 Schedule B3: Aging due to real driving conditions (high C-rates/high DOD):

Schedule B3 is used to age the battery using high C-rate currents of up to 10C, assuming fewer parallel cells in the entire pack. A mix of driving cycles such as the UDDS, HWFET, and the US06 have been used in this study. In this paper, a subscript “h” will be used to indicate higher C-rates as shown in Table 5.4. Batteries are subjected to a low depth of discharge of approximately 20%. Similar to Schedule B1 and B2, Schedule B3 is conducted at elevated temperatures.

Current profile from one aging week of driving is shown in Figure 5.13. Since the maximum charging rate on these batteries was 3C (i.e.: 3*5.4A = 16.2A), the maximum regenerative (charging) current was set to this value. Regarding discharging current, maximum discharge current rates of up to 12C may be observed.

Table 5.4. Aging Schedule B3 Scenario, [33]

Trip	Drive Cycles Combination	Frequency	Description
Work	$UDDS_h$+$HWFET_h$	Twice Daily, 5 days/week, 48 weeks/year	Starting from a full charge, a commute from home to work and back with no charge at work, at high C-rates
Weekend/ Vacation	$UDDS_h$+$HWFET_h$+ $HWFET_h$+ $HWFET_h$+ $HWFET_h$+$UDDS_h$	2 days/week 124 days/year	Starting from a fully charged state, assuming no charging station at the weekend destination, at high C-rates

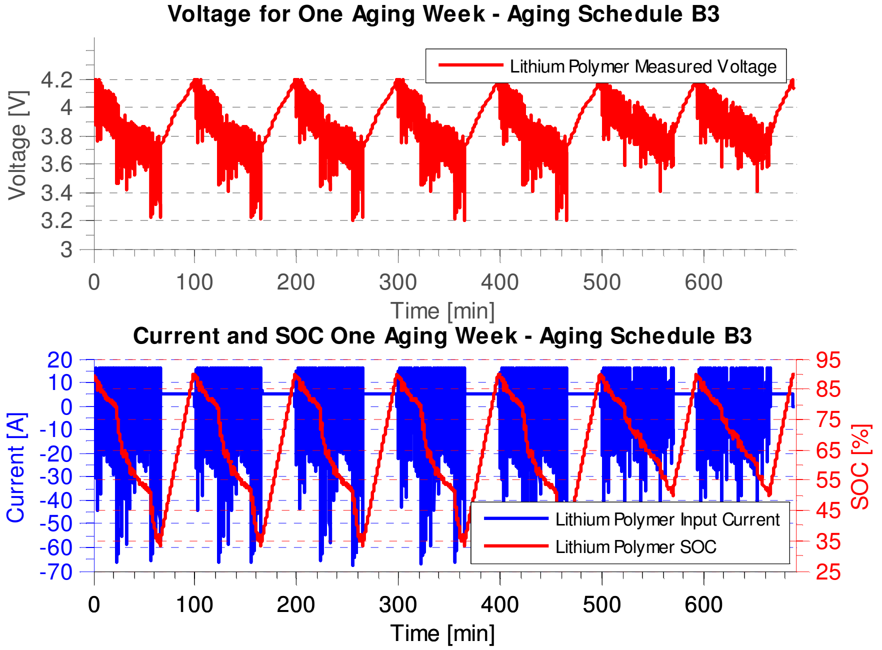
Voltage for One Aging Week - Aging Schedule B3

Current and SOC One Aging Week - Aging Schedule B3

Figure 5.13. Voltage (Upper), Current, and SOC (lower) for one aging week - Schedule B3

Data for one weekend and one weekday of driving are shown in Figure 5.14 and Figure 5.15, respectively.

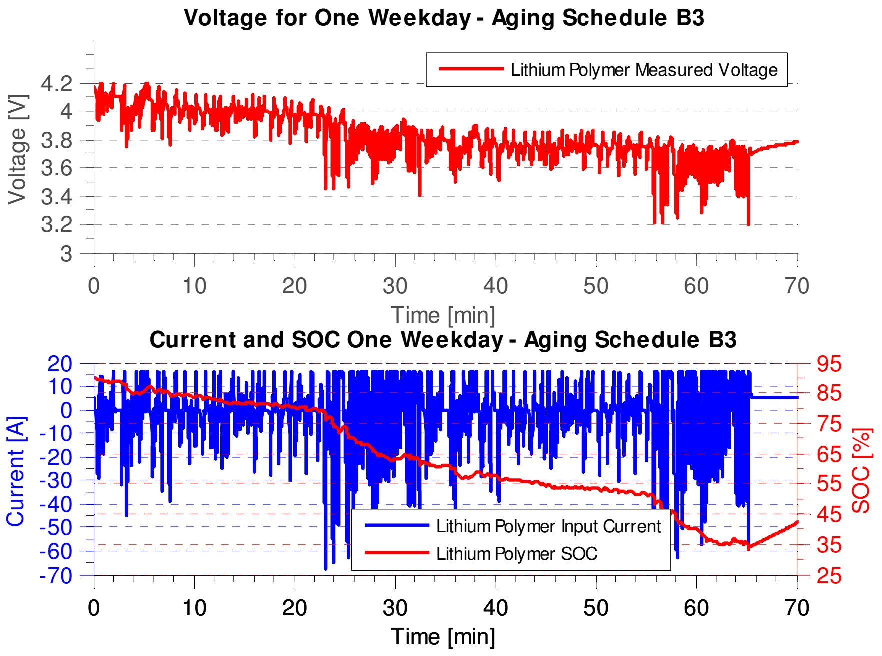

Figure 5.14. Voltage (Upper), Current, and SOC (lower) for one weekday - Schedule B3

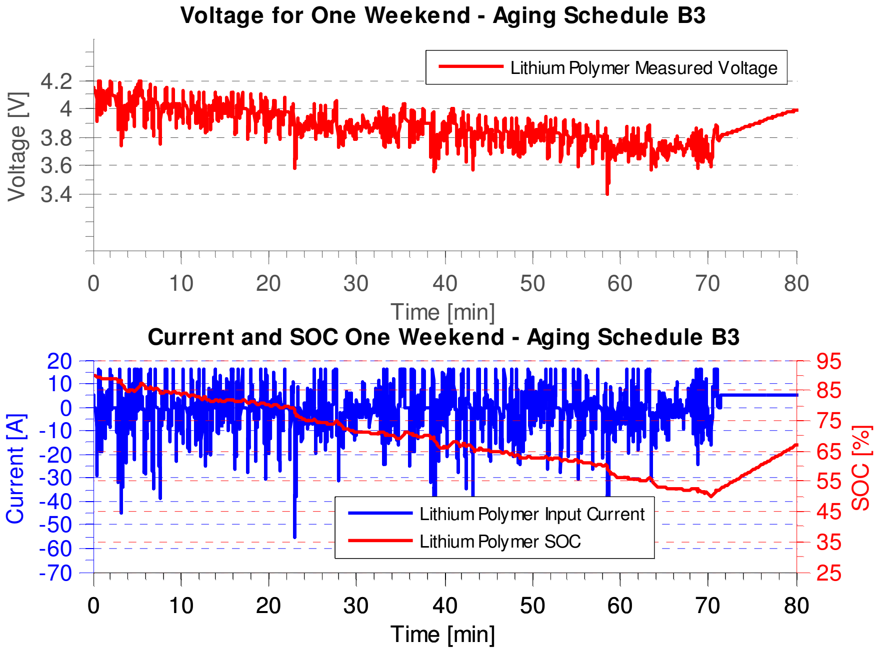

Figure 5.15. Voltage (Upper), Current, and SOC (lower) for one weekend - Schedule B3

5.4 Experimental Setup

In this section, a summary of the experimental setup used in this study including cyclers, environmental chambers, data acquisition systems, and battery cells is provided. The experimental data is then used for extracting parametric values for an OCV-R-RC model for a NMC lithium polymer battery cell. The experimental setup is as shown in Figure 5.16 and 5.17, the setup includes 3 channel Arbin BT2000 tester, 6 NMC lithium polymer battery cell, 3 environmental chambers, AVL Lynx data acquisition system, and AVL Lynx user-interface software. AVL Lynx software is used for setting up the test procedure and for data acquisition. Various variables such as battery current, voltage, and temperatures during charging, discharging, and rest phases are acquired at a maximum frequency of 50 Hz.

Figure 5.16. Arbin BT2000 Cycler along with Espec and Thermotron Environmental Chambers

Battery test cells are placed in environmental chambers in order perform the test at controlled temperature conditions. Two different environmental chambers provided by two different companies are used for testing namely, Thermotron and Espec. These units can change the temperature from -70 to 180 ℃ and are able to change the temperatures at a rate of $3.5\ ℃/min$. This kind of heating and cooling capability is necessary for stressing samples and accelerating battery aging and therefore saving total test time.

Figure 5.17. Experimental Setup including Cyclers, Environmental Chambers, and Data Acquisition Systems

Each battery is independently tested using separate tester channel. A close up look to the Arbin tester is as shown in Figure 5.18.

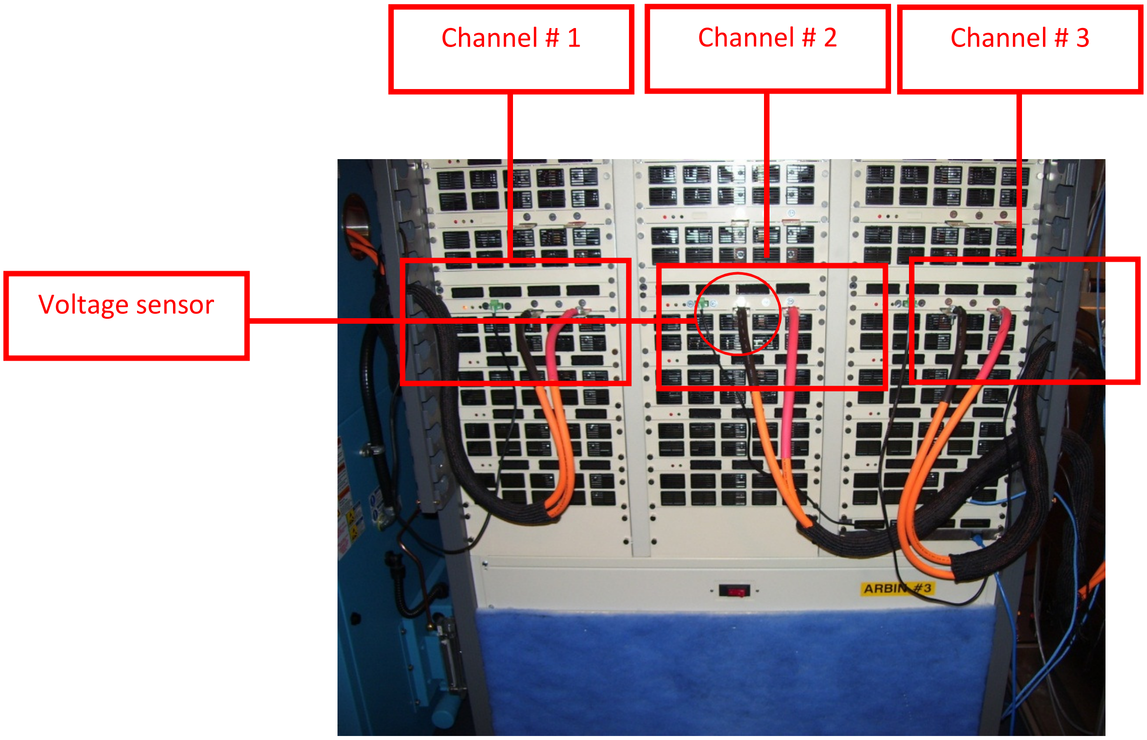

Figure 5.18. Arbin Cycler channels: channels equipped with voltage sensor and status indicator light

The tester has 3 independent channels. The cycler can operate in two voltage operations ranges namely, High operation voltage: 0-5 V and low operation voltage: 0-20 V and 3 different current ranges: High operation range: 0 - ± 400 Amps, Medium operation range: 0 - ± 40 Amps, and Low operation range: 0 - ± 5 Amps.

5.5 Experimental Results – Aging Schedules

In this section, a summary of degradation mechanisms observed using the 3 aging scenarios is represented. As mentioned earlier, a series of reference performance test is conducted every certain number of charging and discharging cycles. This section explores different battery aging behaviours according to the aforementioned aging schedules; namely: Schedule B1, Schedule B2, and Schedule B3. In addition, a comparison between current, voltage, and SOC behaviour under the model fitting driving schedules – Schedule A1 and A2 at various battery states of life is presented.

5.5.1 Capacity Degradation

As shown below in Figure 5.19, the battery discharge capacity for aging schedule B2 is plotted versus number of aging charging/discharging cycles at fixed C-rate. As per the manufacturer data sheet, the expected number of charging/discharging cycles is approximately 500 cycles if the test is conducted at room temperature. As previously mentioned, all aging schedules in this study have been conducted at elevated temperatures of $35°\mathrm{C}\ to\ 40°\mathrm{C}$. Test results are in support with the battery manufacturer data sheet. Since at higher temperatures, aging is accelerated due to rapid chemical reactions which exponentially increase with temperature according to the Arrhenius equation, [34]. For every 10°C rise in temperature, the rate of reactions that contribute to aging are doubled, [34].

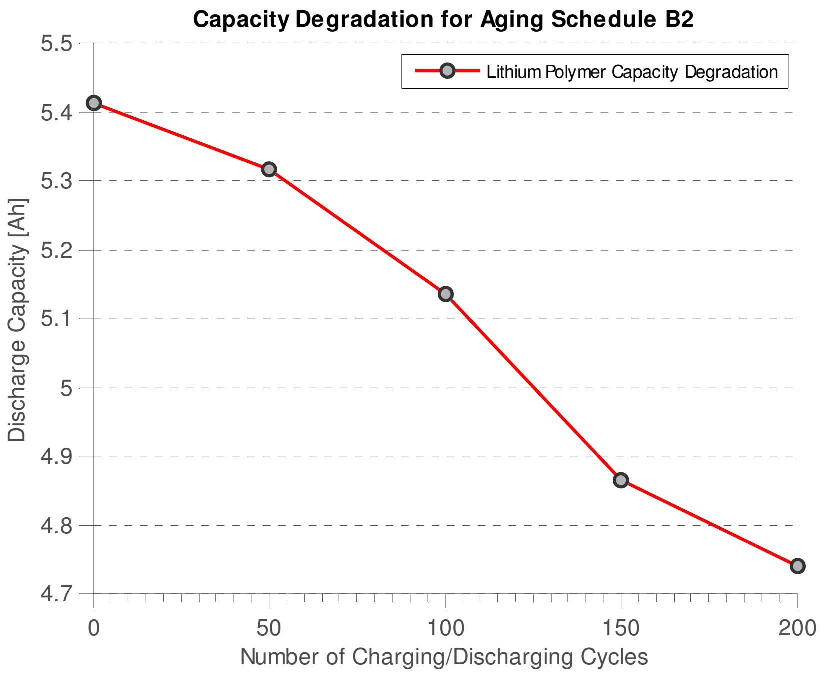

Figure 5.19. Discharge capacity vs. number of cycles for aging Schedule B2

Capacity degradation vs. number of aging weeks for aging schedules B1 and B3 are as shown in Figure 5.20. Since aging schedule B3 includes higher current C-rates compared to Schedule B1, aging is significantly accelerated. Both aging schedules scan the SOC range from 90% to 20% and are conducted at elevated temperatures.

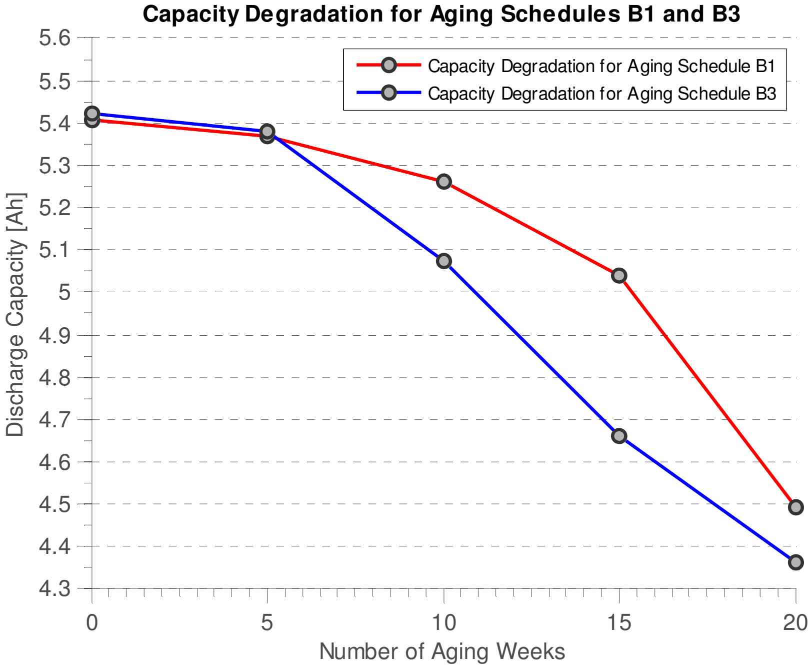

Figure 5.20. Discharge Capacity Vs. number of aging weeks for aging Schedules B1 and B3

5.5.2 Healthy and Aged Driving Schedules

In order to show the difference in terminal voltage and SOC using the same driving schedule at different states of life, both voltage and SOC data for fresh (healthy) and aged battery at approximately 80% capacity for driving Schedule A1 are plotted as shown in Figure 5.21 and Figure 5.22, respectively. Experimental data from aging schedule B3 is considered in this section.

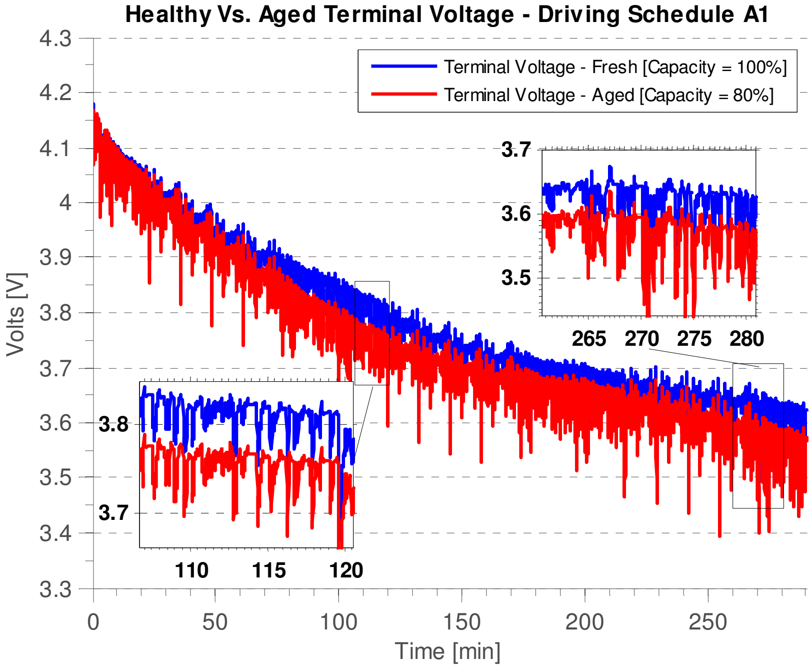

Figure 5.21. Terminal Voltage for fresh (Healthy) cell and aged cell at 80% capacity – Driving Schedule A1

Similarly, voltage and SOC data for both fresh and aged cell for driving schedule A2 are as shown in Figure 5.24 and Figure 5.23, respectively. As shown, it is important to update model parameters as battery ages since the model estimate of the SOC for a fresh battery is higher than the actual SOC of an aged battery, thus giving a false SOC estimate. For example, at the end of the driving cycle, model SOC is at approximately 19% while the SOC for fresh cell is at 32%; this is a relatively significant error.

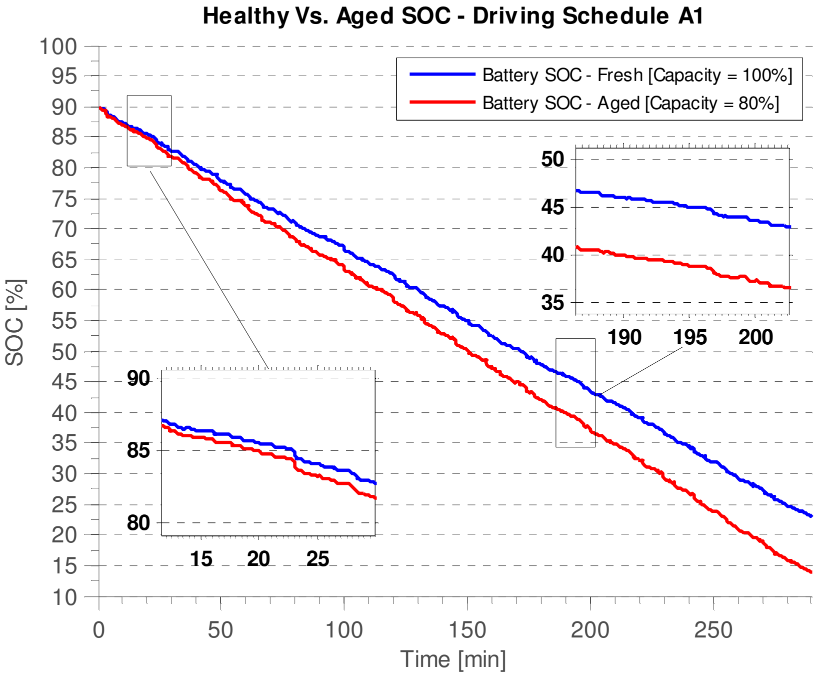

Figure 5.22. SOC for fresh (Healthy) cell and aged cell at 80% capacity – Driving Schedule A1

It is also important to highlight that other factors such as temperature and cell-balancing have not been accounted for in the scope of this paper. These factors will further contribute to modeling errors and worsen the terminal voltage and SOC estimate. Furthermore, this paper focuses mainly on cell level modeling and SOC estimation. In case of pack-level SOC estimation, the error will significantly increase.

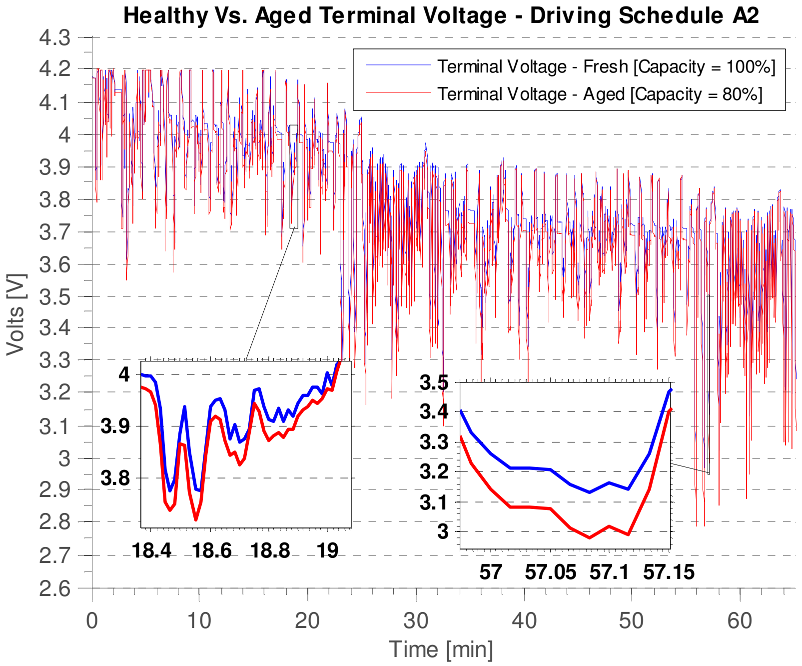

Figure 5.23. Terminal Voltage for fresh (Healthy) cell and aged cell at 80% capacity – Driving Schedule A2

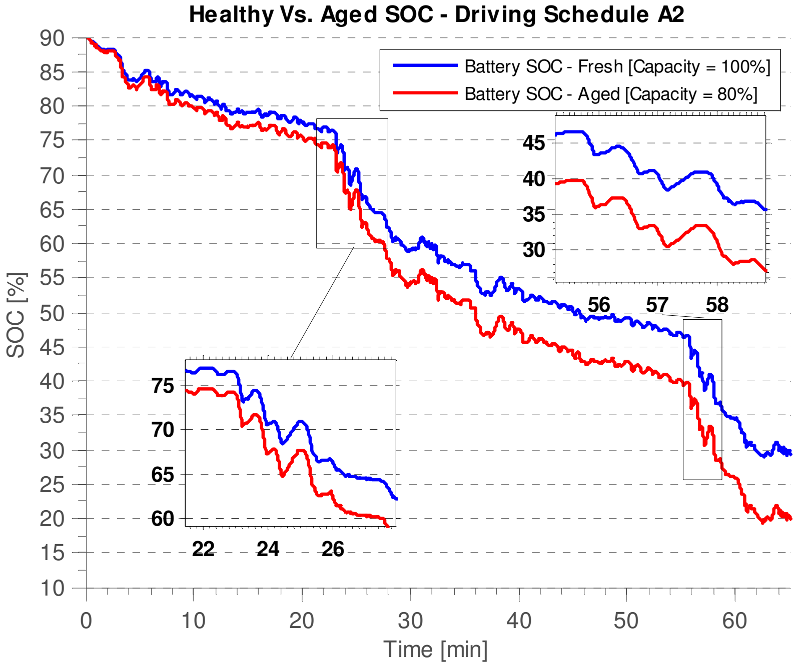

Figure 5.24. SOC for fresh (Healthy) cell and aged cell at 80% capacity – Driving Schedule A2

5.6 Online RLS Parameters Identification and Regressed-Voltage SOC Estimation

This section presents an estimation strategy to estimate the battery model parameters and SOC under a unified framework at various battery states of life. A linear regression model is constructed based on an OCV-R-RC (OCV: Open Circuit Voltage, R: Resistance, C: Capacitance) equivalent circuit-based model that correlates the behavior of a battery and the values of its circuit elements. For online parameter identification, a square-root version of the recursive least-squares (SR-RLS) algorithm with forgetting factor is deployed, [35]. The outputs of this algorithm are the battery electrical parameters and the OCV. Subsequently, the SOC is inferred from the estimated OCV using a SOC-OCV map.

5.6.1 Online Recursive Least Squares Estimation

The first step in the construction of an optimal battery state estimator is to develop a suitable model of the battery that can describe the salient features of both steady-state and transient responses. It has been found that the OCV-R-RC model provides a reasonable compromise between model accuracy and simplicity. For this reason, we develop a state estimator based on this model in the following sections.

Deriving a Linear Regression Model for Parameter Estimation

The governing equations of the circuit depicted in Figure 5.25 can be expressed as, [7, 8]:

$$V_{p,k} = aV_{p,k-1} + bI_{L,k-1} \tag{5.15}$$

$$V_{T,k} = V_{p,k} + cI_{L,k} + V_{oc} \tag{5.16}$$

Where the parameters $a = e^{-T_s/\tau}$, $b = R_p(1 - e^{-T_s/\tau})$ and $c = R_0$. Hence the transfer function from the load current (I_L) to the battery terminal voltage (V_T) in the Z-domain can be written as follows:

$$V_T(z) = \left(\frac{b}{z-a}\right) I_L(z) + cI_L(z) + V_{OC} \tag{5.17}$$

$$(z-a)\, V_T(z) = (b + c(z-a))\, I_L(z) + (z-a)\, V_{OC} \tag{5.18}$$

Because the open circuit voltage (V_{OC}) is treated as a constant, taking the inverse z-transform of (5.18) yields the following difference equation, [7, 8]:

$$V_{T,k} = (b - ac)\, I_{L,k-1} + c\, I_{L,k} + aV_{T,k-1} + (1-a)\, V_{OC} \tag{5.19}$$

The linear regression model can be compactly written as the inner product as follows, [7, 8]:

$$V_{T,k} = \theta^T \Phi_k \tag{5.20}$$

Where θ is the parameter vector and Φ_k is a regressor consisting of known signals, [7, 8]:

$$\theta = [(b-ac) \quad c \quad a \quad (1-a)V_{oc}]^T \tag{5.21}$$

$$\Phi_k = \left[\, I_{L,k-1} \quad I_{L,k} \quad V_{T,k-1} \quad 1\right]^T \tag{5.22}$$

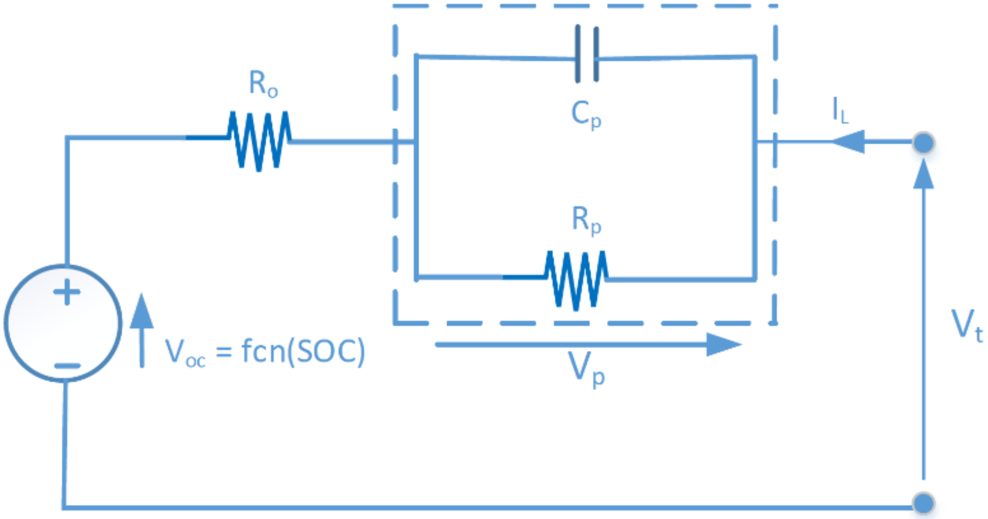

Figure 5.25. OCV-R-RC battery equivalent circuit model, [7, 8]

The most pragmatic solution to estimate θ from the ARX model is to apply the Recursive Least Squares (RLS) algorithm. A square-root version of the RLS method is used in this paper for its computational efficiency and stability, [35]. Since the square-root RLS algorithm guarantees a positive-definite and symmetric covariance matrix, it is highly numerically stable and achieves high estimation accuracy and robustness, [35]. In order to closely track slowly varying parameters, a forgetting factor is included in the RLS. The battery electrical parameters $R_0, R_p,\ C_p,$ and V_{OC} can be recursively estimated upon estimating θ as follows, [7, 8]:

$$\hat{R}_0 = \theta(2) \tag{5.23}$$

$$\hat{R}_p = \frac{\theta(1)+\theta(2)\theta(3)}{1-\theta(3)} \tag{5.24}$$

$$\hat{C}_p = \frac{T_s}{ln(\theta(3))}\frac{\theta(3)-1}{\theta(1)-\theta(2)\theta(3)} \tag{5.25}$$

$$\hat{V}_{OC} = \frac{\theta(4)}{1-\theta(3)} \tag{5.26}$$

5.6.2 Regressed-Voltage-based SOC Estimation

In the Regressed Voltage Method (RV Method), in which the open-circuit voltage (V_{OC}) estimated from the RLS algorithm is used to calculate the SOC according to a SOC-OCV map or a look-up table. Due to the fact that the SOC is coupled with a current integration technique and therefore it is a slowly time-varying signal, the noisy (spiky) SOC estimate obtained from the RV method, which we denote $S\hat{O}C_{nRV,k}$, is filtered by an exponentially-weighted moving average filter to get a clean and smooth SOC signal:

$$S\hat{O}C_{RV,k} = (1-\alpha)\, S\hat{O}C_{RV,k-1} + \alpha\, S\hat{O}C_{nRV,k} \tag{5.27}$$

where α is the filter gain and takes a small positive value, typically in the range of10^{-4} to 10^{-2}.

5.6.3 Experimental Results – Fresh Battery State

In order to test the SR-RLS and Regressed-voltage-based SOC estimation strategies [35], the two previously mentioned driving schedules; ***Schedule A1 and Schedule A2*** datasets have been used. Schedule A1 has been used for obtaining the regressed SOC from the estimated OCV and the second one is used for validation. Driving cycles scan the entire state of charge range from 90% to approximately 20%.

As shown in Figure 5.26, the strategy provides a good estimate of the battery SOC compared to the actual SOC obtained using Coulomb Counting technique from the Arbin Cycler. The battery SOC estimation error is as shown below in Figure 5.27. The maximum error is approximately 6%. The maximum error occurs at the flat region of the SOC-OCV around 45% to 65%.

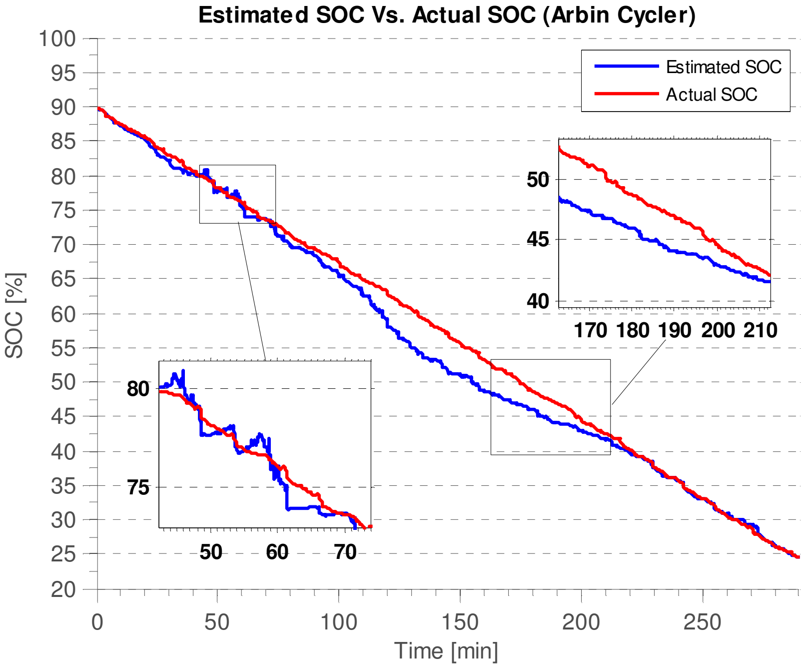

Figure 5.26. Estimated Vs. actual battery SOC for driving Schedule A1

This error is acceptable provided that the standalone RLS Regressed-Voltage method is applied. One of the main advantages of the Recursive Least Square (RLS) methodology and the regressed-Voltage based strategy is that no initial state of charge estimate is required. Moreover, no filter initialization or model parameter values is required.

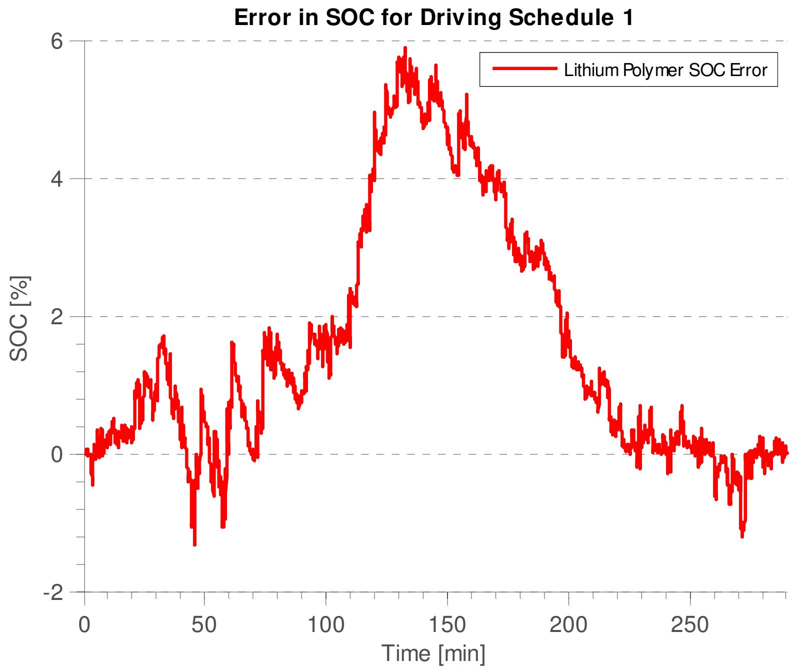

Figure 5.27. Estimated and actual SOC error obtained using Coulomb Counting (Arbin cycler) for Schedule A1

Estimated terminal voltage vs. actual (measured) voltage is as shown below in Figure 5.28. The error is relatively high during the first 2-3 minutes of the driving cycle since the parameters are not yet optimized. However, the error decreases drastically afterwards and the strategy provides a good estimate of the battery terminal voltage.

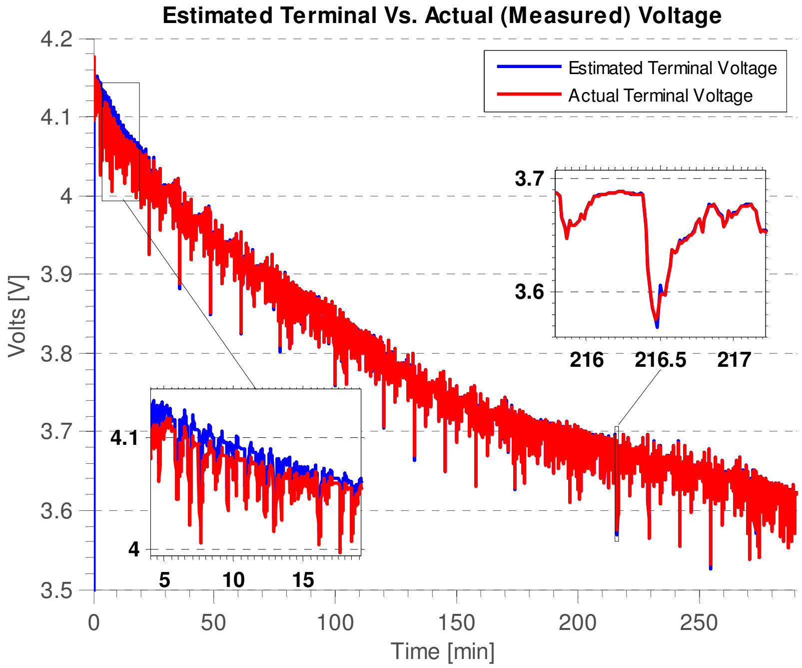

Figure 5.28. Estimated Vs. actual terminal voltage - Schedule A1

The estimated battery model RC branch parameters at fresh (healthy) battery state are as shown below in Figure 5.29. Model parameters change over the entire driving cycle at various battery states of charge. The RC branch resistance (R_1) changes between 0 to 0.1 Ω while the capacitance (C_1) changes between 1500 and 5000 F. The static resistance (R_1) and the estimated open circuit voltage values are as shown below in Figure 5.30. R_1 values remains constant over the entire SOC range while the OCV changes from approximately 4.14 to 3.6 V indicating cell discharge due to applied current.

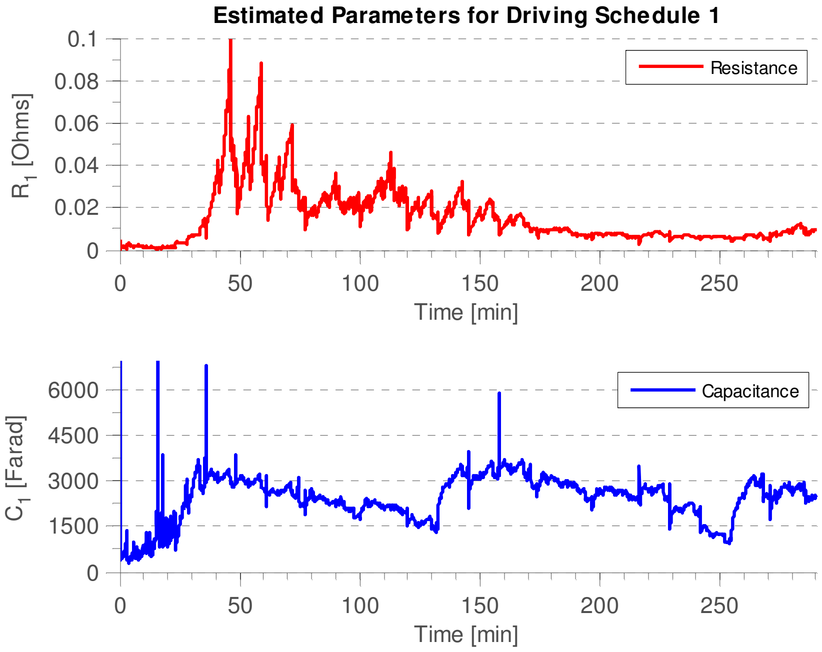

Figure 5.29. Estimated battery parameters for RC branch at fresh (healthy) state - Schedule A1

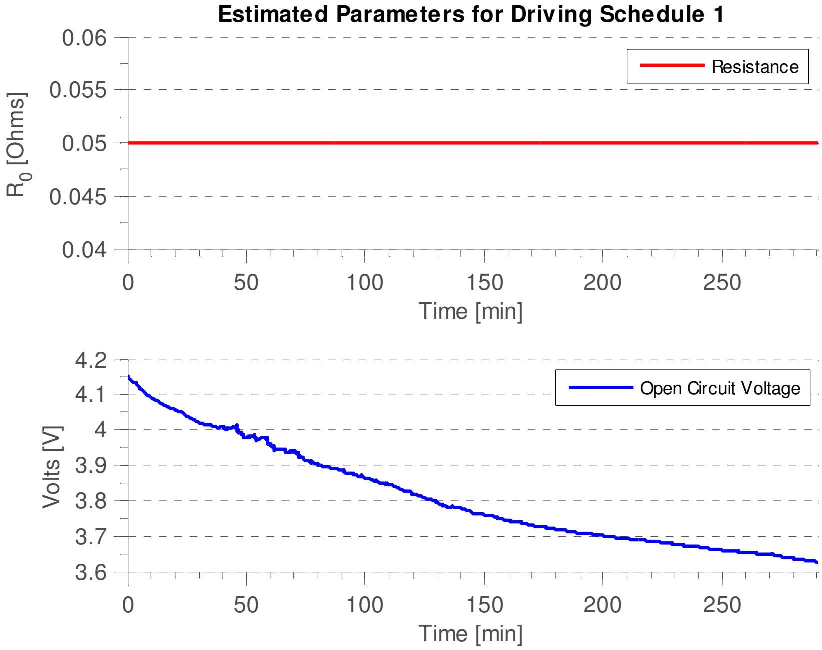

Figure 5.30. Estimated battery parameters: static resistance (R_0) and OCV at fresh (healthy) state - Schedule A1

The technique has been validated using driving **Schedule A2.** As shown in Figure 5.31, the strategy provides a good estimate of the battery SOC compared to the actual SOC obtained using Coulomb Counting technique from the Arbin Cycler. The estimation accuracy decreased in case of driving schedule A2 since this driving cycle entails a high C-rate current values. The maximum SOC error is approximately 10% at the same flat SOC-OCV region at 50% SOC. The accuracy is still acceptable provided that both model parameters and the battery SOC estimation is carried out online.

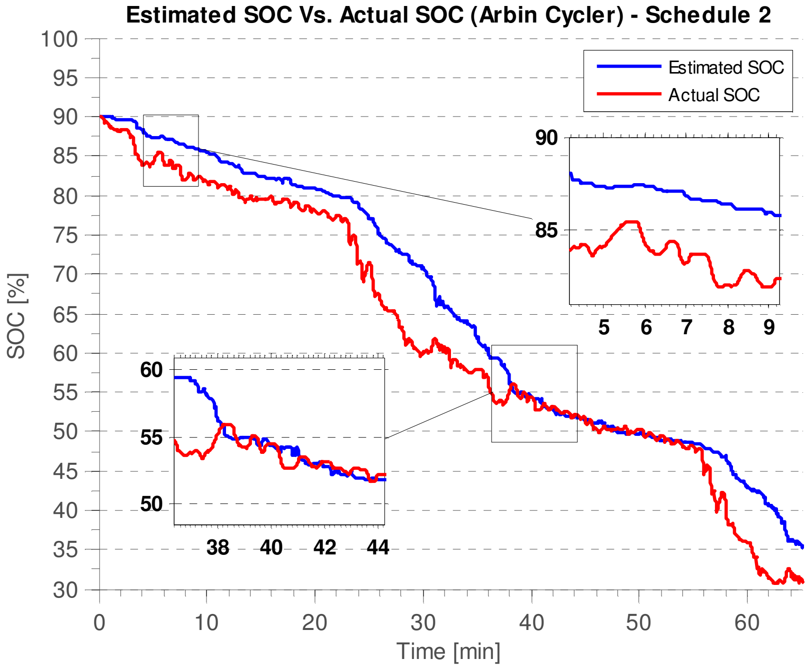

Figure 5.31. Estimated Vs. actual battery SOC for validation driving cycle - Schedule A2

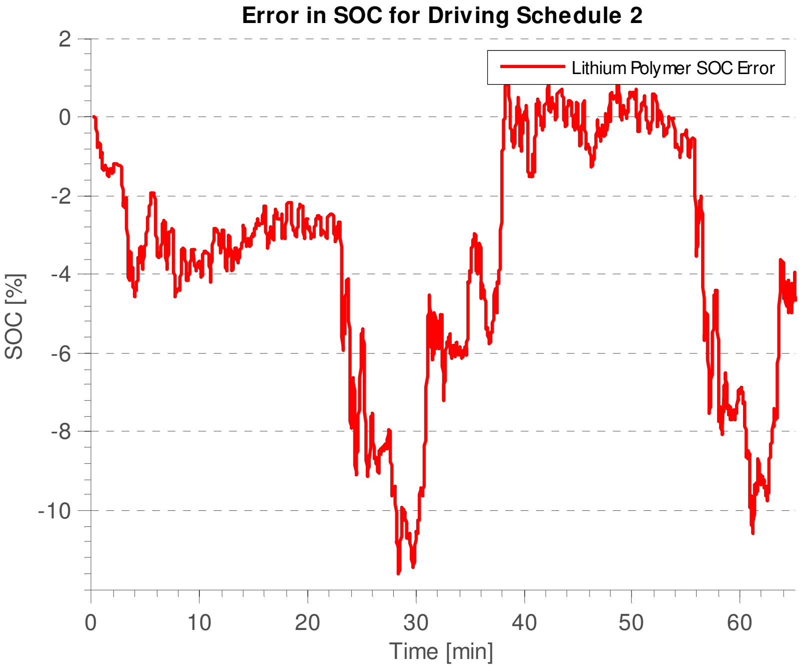

Figure 5.32. Error between estimated and actual SOC obtained from using Coulomb Counting (Arbin cycler) for Schedule A2

The estimated terminal voltage vs. actual (measured) voltage for driving Schedule A2 is as shown below in Figure 5.33. It is clear that the voltage dynamics is much faster compared to schedule A1 since schedule A2 current demand is much higher compared to schedule A1 over the entire SOC range. Similar to schedule A1, the error is relatively high during the first couple of minutes of the driving cycle since the parameters are not yet optimized. Afterwards, the strategy converges and the error considerably decreases. Results can be further enhanced using a combination of RLS-Regressed Voltage based strategy and the conventional coulomb counting.

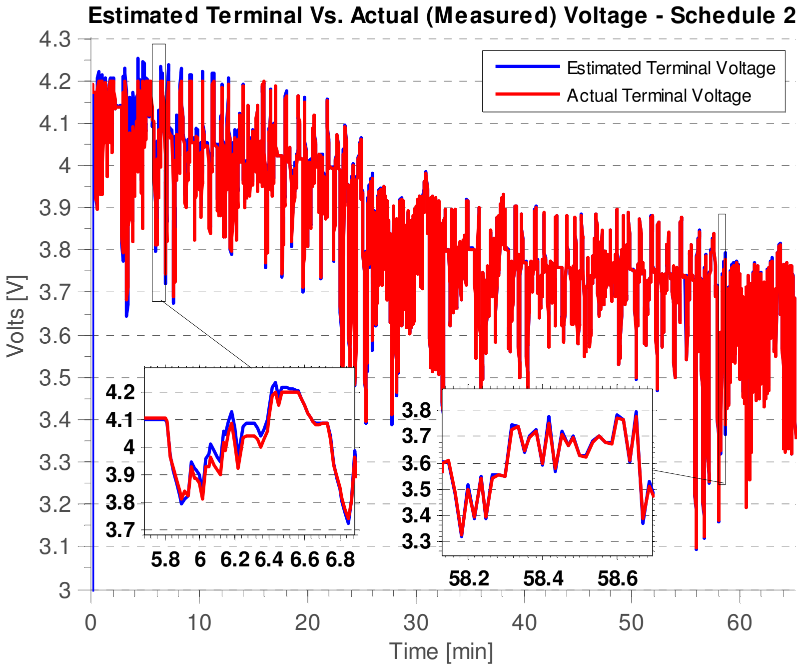

Figure 5.33. Estimated Vs. actual terminal voltage - Schedule A2

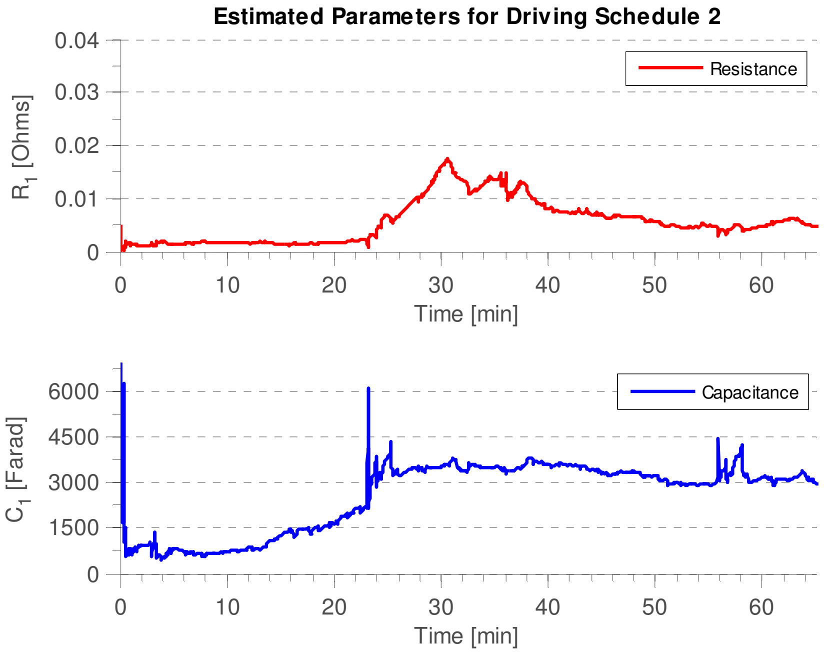

Figure 5.34. Estimated battery parameters for the RC branch at healthy state - Schedule A2

The estimated parameter values for driving Schedule A2 are as shown in Figure 5.34 and 5.35.

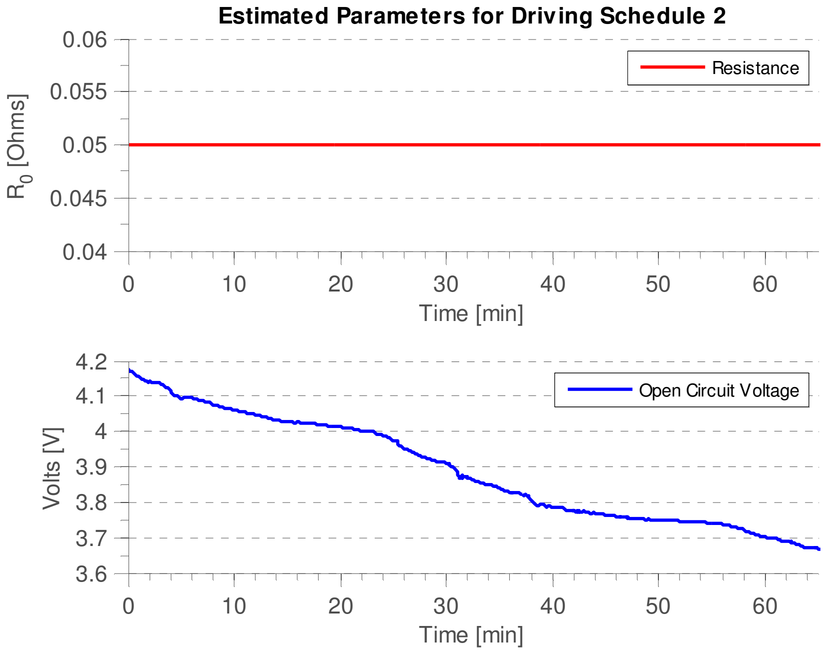

Figure 5.35. Estimated battery parameters: static resistance (R_0) and OCV at fresh (healthy) state - Schedule A2

5.6.4 Experimental Results – Aged Battery State (End-Of-Life)

As battery ages, model parameters change and if the same model parameters estimated at healthy state are used, significant errors are introduced in SOC estimation and terminal voltage prediction accuracy. Therefore, in order to test the proposed parameter estimation and regressed-voltage-based SOC estimation strategies, data from the aging study (Schedule B3) as previously described in section 5.3 is used. Experimental data from driving Schedule A1 and Schedule A2 are carried out at the battery end-of-life state. Battery capacity at the battery end-of-life is approximately 4.4 Ah. Battery SOC estimation and terminal voltage prediction for schedule 1 for aged cell are as shown below in Figure 5.36 and Figure 5.37, respectively.

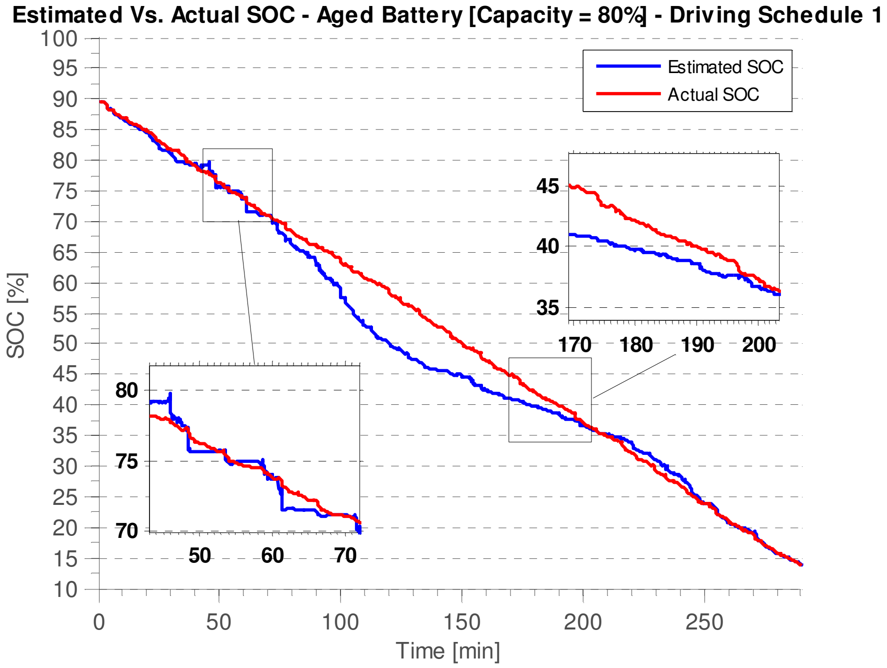

Figure 5.36. Estimated Vs. actual battery SOC for driving Schedule 1 for aged battery [Capacity = 80%]

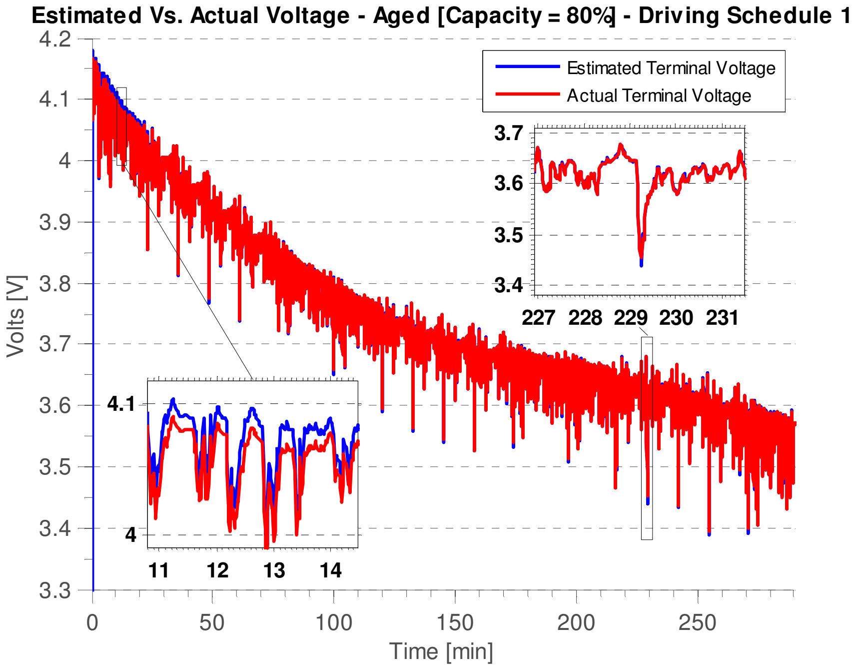

Figure 5.37. Estimated Vs. actual battery terminal voltage for driving Schedule 1 for aged battery [Capacity = 80%]

The strategy provides a good estimate even at aged battery state. The error has slightly increased as shown in Figure 5.38. The maximum error for driving schedule A1 at aged battery state is approximately 9% up from 6% at fresh state.

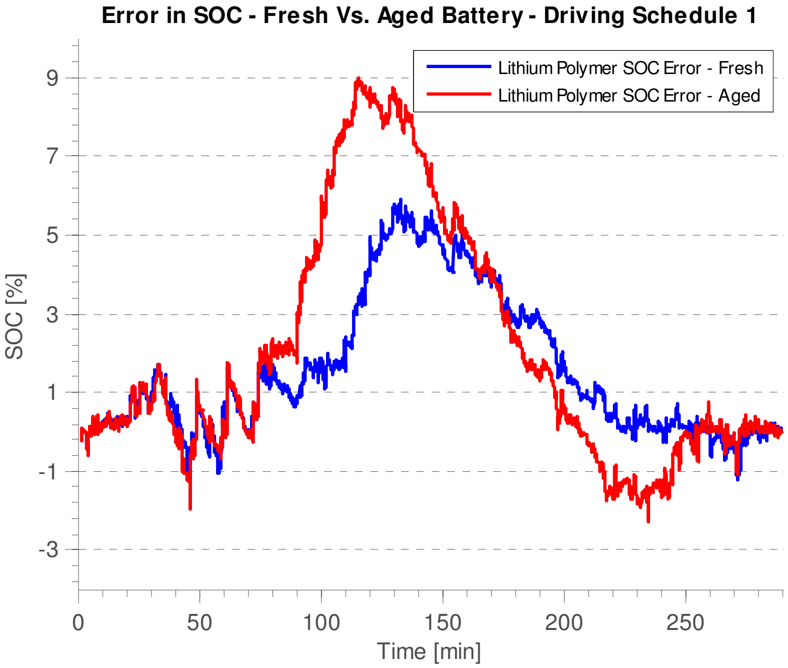

Figure 5.38. SOC error for fresh vs. aged cell - Driving Schedule A1

As shown in Figure 5.39, R_1 model parameter at aged battery state follows the same trend for the fresh one. However, slightly larger values are observed in the range from 100% to 50% SOC. This can be beneficial in estimating the battery SOH online by keeping track of the battery internal resistance estimate and compare it to nominal values for a fresh battery. The battery resistance R_0 remains unchanged, the algorithm take approximately 0.5 minute to converge to the actual value. The estimated OCV values are slightly less for an aged cell compared to the fresh one. Therefore, by applying the regressed-voltage-based method, the estimated SOC for aged cell is lower than the fresh state. In order to validate the proposed strategy, the same procedure has been repeated using schedule A2 which is characterized by high current C-rates as shown in Figure 5.41 and Figure 5.42.

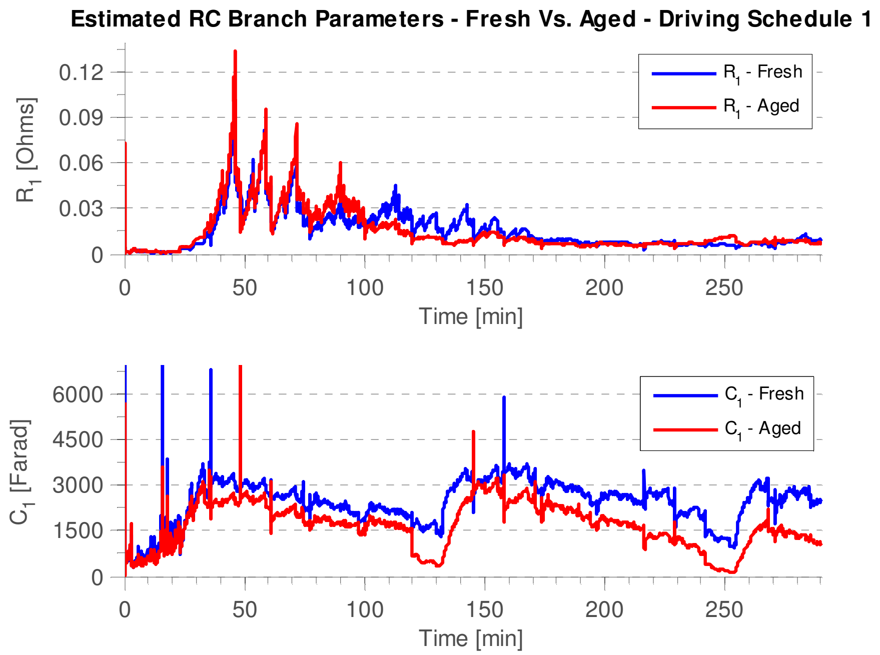

Figure 5.39. RC branch parameters for fresh vs. aged - Driving Schedule A1

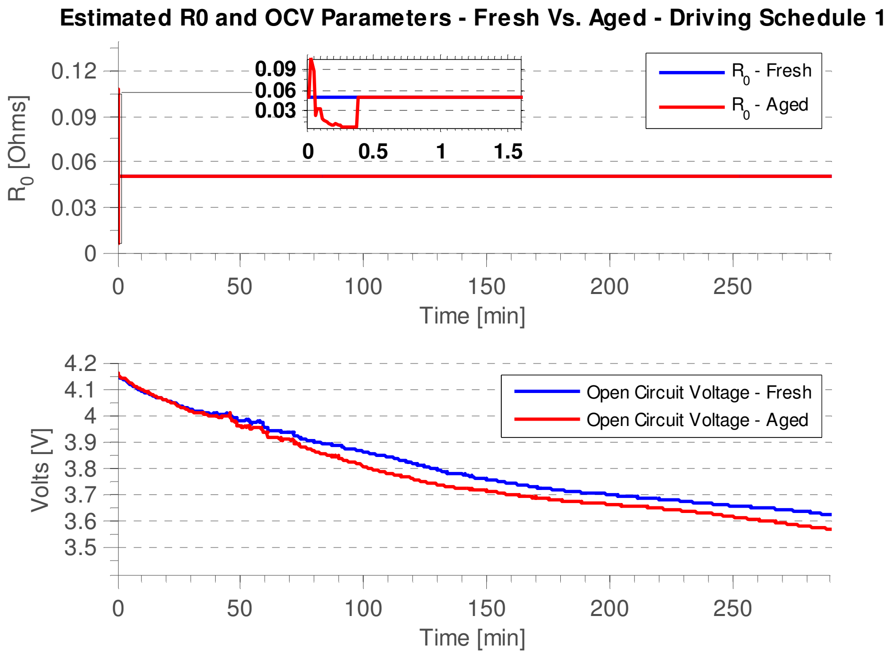

Figure 5.40. Static resistance and open circuit voltage estimate for fresh vs. aged cell - Driving Schedule A1

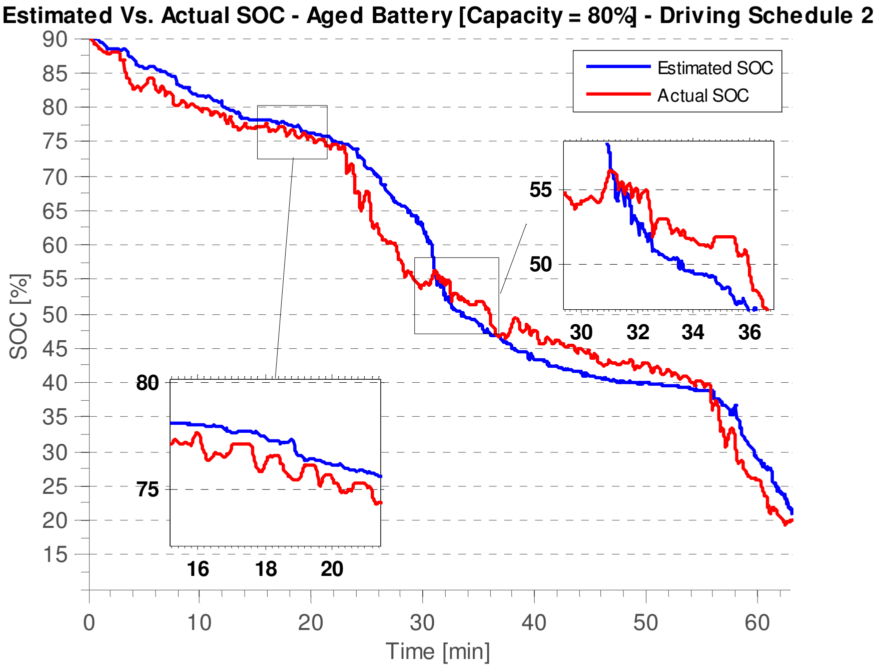

Figure 5.41. Estimated Vs. actual battery SOC for driving Schedule A2 for aged battery [Capacity = 80%]

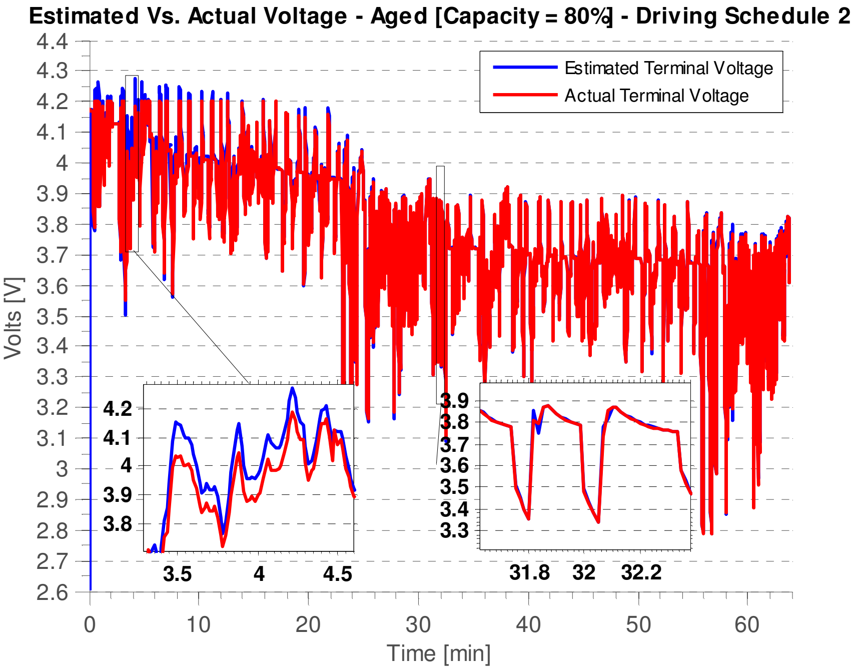

Figure 5.42. Estimated Vs. actual battery terminal voltage for driving Schedule A2 for aged battery [Capacity = 80%]

The strategy provides a good estimate even at the battery end-of-life state. The error has slightly increased as shown in Figure 5.43. The maximum absolute error for driving schedule A2 at aged battery state is approximately 11% up from 8% at fresh state.

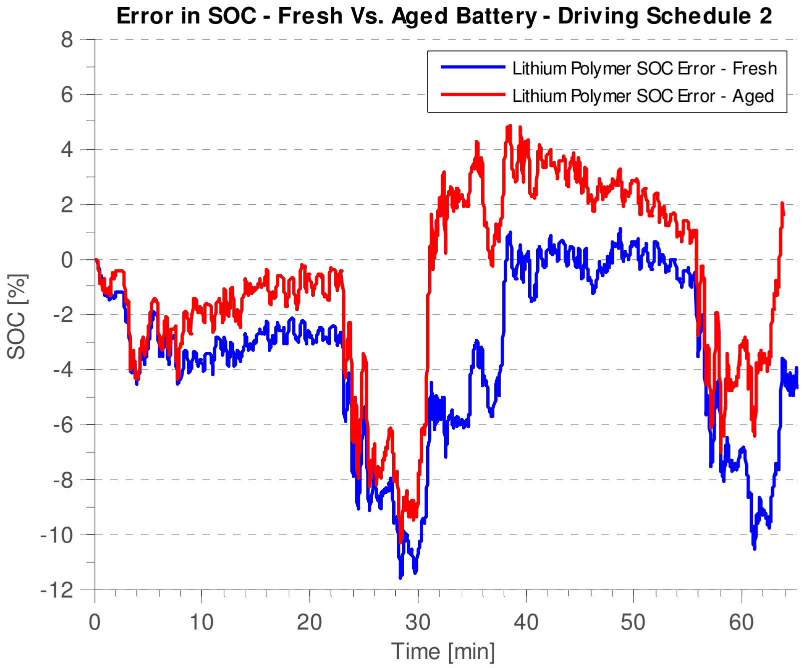

Figure 5.43. SOC error for fresh vs. aged cell - Driving Schedule A2

As shown in Figure 5.44, the estimated RC branch resistance at aged battery state is significantly higher than the one at fresh state at the region from 100% to approximately 50% SOC. This is consistent with the results obtained from Schedule A1. The capacitance maintains the same pattern with decreased values compared to the fresh battery state. Similar to driving schedule A1, the battery resistance R_0 remains unchanged. The estimated OCV values are slightly less for an aged cell compared to the fresh one. Therefore, by applying the regressed-voltage-based method, the estimated SOC for aged cell is lower than the fresh state.

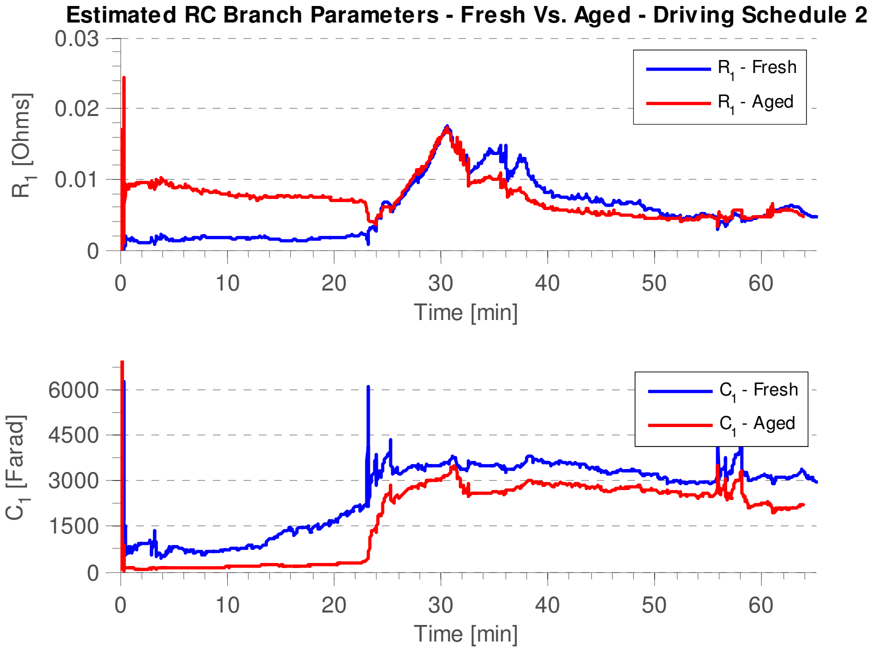

Figure 5.44. RC branch parameters for fresh vs. aged cell - Driving Schedule A2

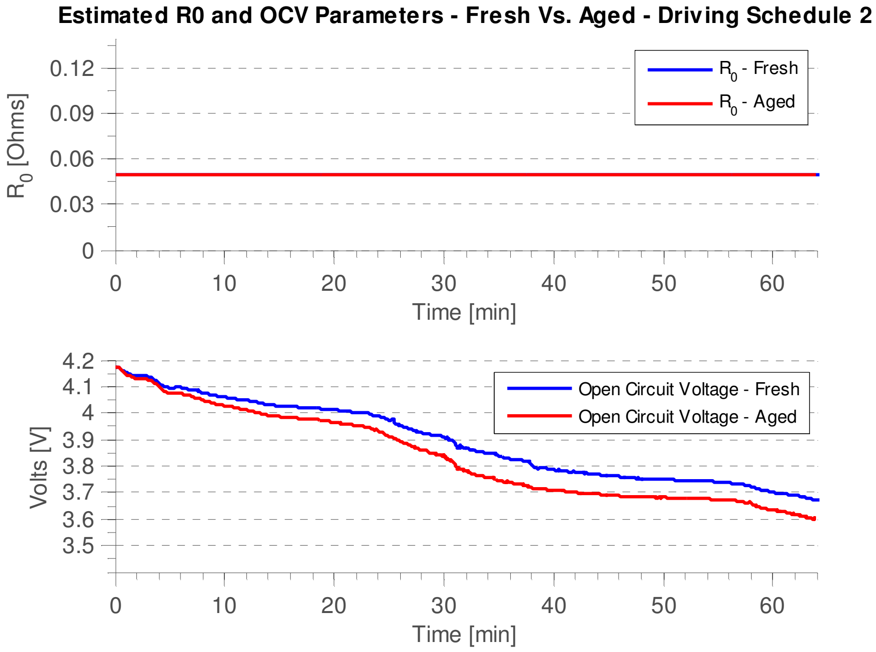

Figure 5.45. Static resistance and open circuit voltage estimate for fresh vs. aged cell - Driving Schedule A2

In the following section, a completely different approach has been implemented for parameters identification and battery SOC estimation. Offline parameters estimation has been applied and a relatively new estimation strategy has been implemented given that the model initial SOC is slightly far from the actual one.

5.7 Offline Parameters Identification and SVSF-based SOC Estimation

In this section, offline model parameters identification using Genetic Algorithm (GA) optimization strategy is presented. The GA has been used to obtain model parameters at various battery states of life. Based on the optimized battery model, an estimation strategy has been applied to the model to extract information regarding the battery SOC. The strategy is known as the Smooth Variable Structure Filter (SVSF). The filter works in a predictive-corrective form.

5.7.1 Offline Genetic Algorithm Optimization

Genetic algorithms are search techniques based on the evolutionary model. GA algorithm has been extensively applied in the literature since the algorithm does not require gradient calculation which is rather difficult to obtain in some complex optimization problems. The algorithm has been described in details in references, [36, 37]. A summary of the algorithm is illustrated below, [38]:

5.7.1.1 Creation of random initial population

An initial guess based on literature for parametric values and according to the authors' best knowledge has been adopted in this work. The initial range is set as illustrated in Table 5.5.

5.7.1.2 Generating a sequence of new populations as follows:

- *The fitness value of each population member is valuated and the raw fitness values are scaled to generate an operational range of values.*
- *Individuals are selected based on their fitness function, these individuals are called parents.*
- *Off springs are generated from the population by crossover or mutation.*
- *Low fitness individuals are replaced from current population by new off-springs to for the next generation.*

5.7.1.3 The steps are repeated until the stopping criteria is reached. This include a maximum number of iterations of 10.

Table 5.5. OCV-R-RC battery model optimizer bounds

Parameter name (symbol) (unit)	*Lower Bound*	*Upper Bound*
Static Resistance Charging ($\boldsymbol{R_0^+}$) ($\boldsymbol{\Omega}$)	0	0.09
Static Resistance Discharging ($\boldsymbol{R_0^-}$) ($\boldsymbol{\Omega}$)	0	0.09
RC Branch Resistance ($\boldsymbol{R_1}$) ($\boldsymbol{\Omega}$)	0	0.09
RC Branch Capacitance ($\boldsymbol{C_1}$) ($\boldsymbol{F}$)	150	10000

5.7.2 SVSF-based State of Charge Estimation

Similarly to the Kalman filter, the SVSF works in a predictor-corrector fashion, [39]. The filter is based on the sliding mode concept and has demonstrated robustness to modeling uncertainties and sensor noise, [39, 18]. The SVSF can be applied to both linear and non-linear systems. It works by using an SVSF gain that forces the states to converge to a neighborhood of the actual (or true) value, [39]. The gain forces the states to switch back and forth across the state trajectory within a region referred to as the existence subspace which is function of modeling uncertainties. The width of the existence space β is a function of the uncertain dynamics associated with the inaccuracy of the internal model of the filter as well as the measurement model, and varies with time, [39]. The SVSF can be applied to systems that are differentiable and observable, [39, 40]. The original form of the SVSF as presented in [39] did not include covariance derivations. An augmented form of the SVSF that includes the derivation of an error covariance matrix has been presented in [41]. Here, the latter is summarized.

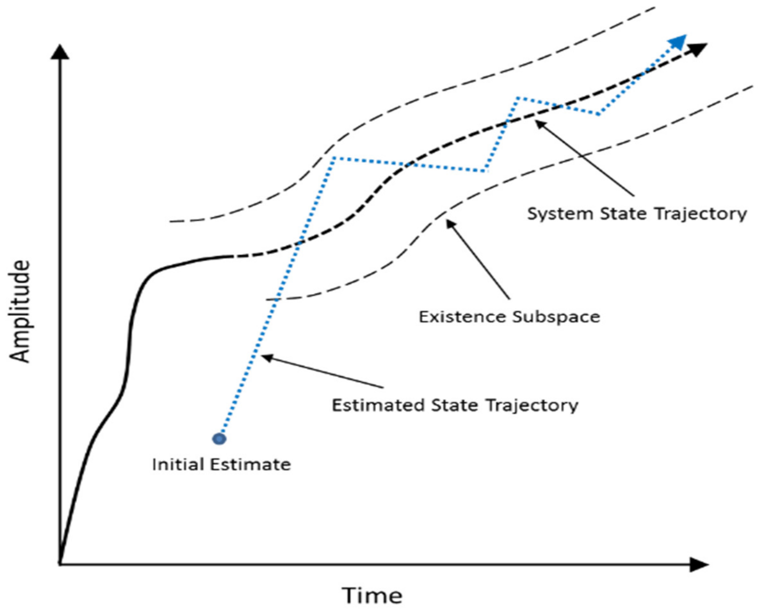

Figure 5.46. The SVSF estimation strategy starting from some initial value, the state estimate is forced by a switching gain to within a region referred to as the existence subspace, [39].

Consider a nonlinear system with a linear output (measurement) equation. The filter runs by generating a prediction of the state estimate (which represents the solid-electrolyte interface concentration) as follows:

$$\hat{x}_{k+1|k} = \hat{f}\left(\hat{x}_{k|k}, u_k\right) \tag{5.28}$$

The predicted estimates are then used to generate a predicted measurements $\hat{z}_{k+1|k}$ as follows, [39]:

$$\hat{z}_{k+1|k} = C_{k|linearized}\hat{x}_{k+1|k} \tag{5.29}$$

Where $C_{k|linearized}$ is the measurement matrix. Then the measurement error $e_{z,k+1|k}$ can be calculated as follows, [39]:

$$e_{z,k+1|k} = z_{k+1} - \hat{z}_{k+1|k} \tag{5.30}$$

The SVSF has predictor-corrector form. Its gain is a function of the a-priori and the a-posteriori measurement errors $e_{z_{k+1|k}}$ and $e_{z_{k|k}}$. It has a smoothing boundary layer widths ψ, a memory or convergence rate γ, as well as the linear measurement matrix $C_{k|linearized}$. For the derivation of the SVSF gain K_{k+1}, refer to [39, 41]. The SVSF gain is defined as follows, [39]:

$$K_{k+1} = {C_{k|linearized}}^{+} diag\left[\left(\left|e_{z_{k+1|k}}\right| + \gamma\left|e_{z_{k|k}}\right|\right) \circ sat\left(\frac{e_{z_{k+1|k}}}{\psi}\right)\right] diag\left(e_{z_{k+1|k}}\right)^{-1} \quad (5.31)$$

The updated states $\hat{x}_{k+1|k+1}$ are calculated as follows, [39]:

$$\hat{x}_{k+1|k+1} = \hat{x}_{k+1|k} + K_{k+1} e_{z_{k+1|k}} \quad (5.32)$$

The output estimates and the a posteriori measurement errors are then calculated respectively as follows, [39]:

$$\hat{z}_{k+1|k+1} = C_{k|linearized} \widehat{w}_{k+1|k+1} \quad (5.33)$$

$$e_{z_{k+1|k+1}} = z_{k+1} - \hat{z}_{k+1|k+1} \quad (5.34)$$

Equations 5.28 to 5.34 are iteratively repeated for every sampling time.

5.7.3 Experimental Results – Fresh Battery State

In this section, offline parameter identification using Genetic Algorithm optimization and SOC estimation using the SVSF are presented. Two states of life are considered; namely: fresh (healthy) battery state and aged (80% capacity). The GA algorithm has been applied to estimate battery parameters using current and voltage data from ***Schedule A1*** driving cycle. A static capacity discharge test has been conducted to obtain the SOC-OCV relationship utilized by the OCV-R-RC model.

The model is simulated once for every member of the population and the terminal voltage is further compared with the experimental terminal voltage. The GA optimization has been set to 5 runs and to 500 population size. The algorithm has been conducted on a mobile workstation with 3.0 GHz, quad Core i7-3940XM Extreme Edition processor. The parameter identification objective function used in this research is targeted at minimizing the error between the model output terminal voltage $\hat{V}(t)$ and the experimentally measured terminal voltage $V(t)$. The objective function is a cumulative sum of the squared voltage error as follows:

$$min \int_0^T \left(V(t) - \hat{V}(t)\right)^2 dt \tag{5.35}$$

Values of the optimized parameters for fresh battery state are as follows: $R_0^+ = 0.0094\ \Omega$, $R_0^- = 0.0096\ \Omega$, $R_1 = 0.0049\ \Omega$, and $C_1 = 3860.146$ F. The optimized terminal voltage vs. the actual (measured) voltage is as shown below in Figure 5.47. It is important to note that in this method, one set of parameters are used over the entire SOC range.

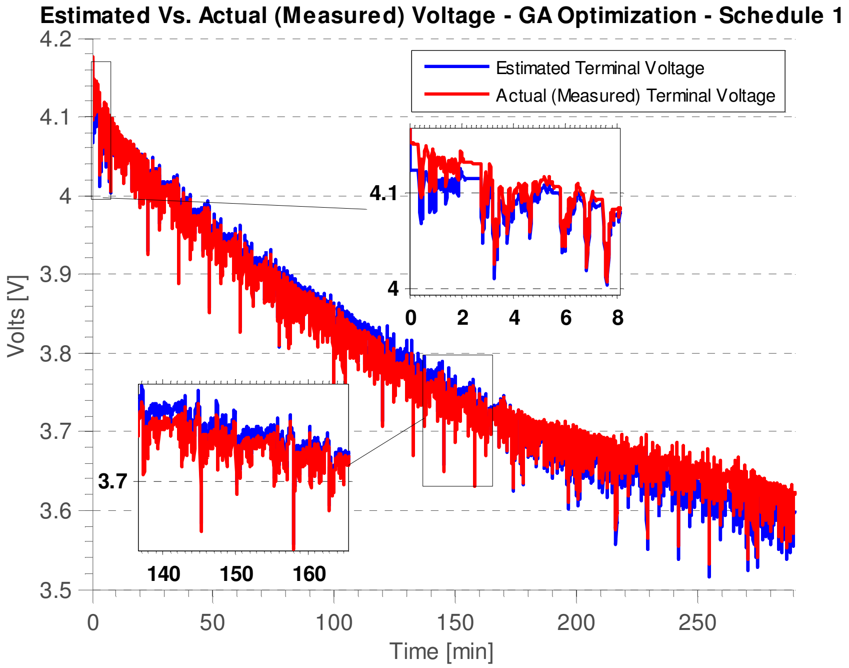

Figure 5.47. Estimated vs. actual (measured) voltage - GA optimization for driving Schedule A1

Based on the optimized model parameters, the SVSF has been applied to estimate the battery SOC. The SVSF parameters are tuned using GA optimization with population size of 20 and using 10 numbers of iterations. For the SVSF, four parameters required to be tuned, namely: the SVSF convergence or 'memory' is set to $\gamma = 0.8$, the boundary layer thickness $\psi = 4$, the initial a-priori estimate $e_{z,k+1|k} = 4.505$, and the damping element $\lambda = 0.1$. The initial model SOC is set to 80%. The battery SOC vs. Actual SOC is as shown below in Figure 5.48.

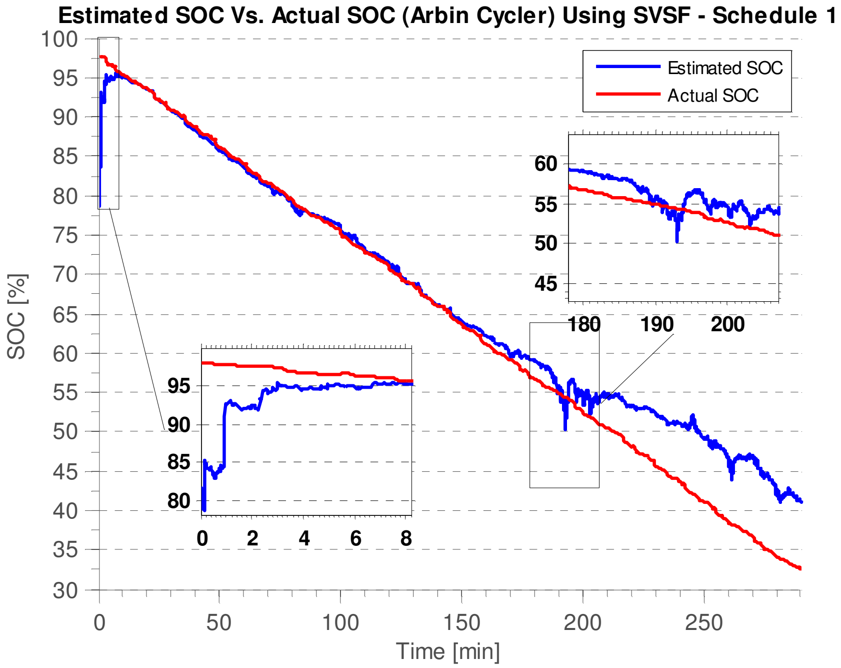

Figure 5.48. Estimated vs. actual SOC – SVSF estimation for driving Schedule A1

5.7.4 Experimental Results – Aged Battery State

Similar to the fresh battery state, current profile from the same driving cycle – Schedule 1 has been applied to the aged battery at 80% capacity. GA algorithm optimization has been applied to estimate the battery model parameters. In the GA optimization, population size of 1000 data sets have been used for 5 generations. Values of the optimized parameters for aged cell at the end-of-life are as follows: $R_0^+ = 0.016$, $R_0^- = 0.017$, $R_1 = 0.01$, $C_1 = 3212.71$

The optimized terminal voltage vs. actual (measured) voltage for aged cell is as shown below in Figure 5.49. Similar to fresh cell, only one set of parameters have been used over the entire range of SOC. The SVSF has been applied to estimate the battery SOC based on the optimized battery model parameters of the aged cell as shown in Figure

5.50. The initial battery SOC has been initialized to 50% and the actual SOC to approximately 98%. The SVSF provides fast convergence even though the error between the initial SOC and the actual SOC is quite significant. The largest error is noticed at the flat SOC-OCV region at approximately 35% to 55%. The estimated terminal voltage vs. measured voltage is as shown below in Figure 5.51.

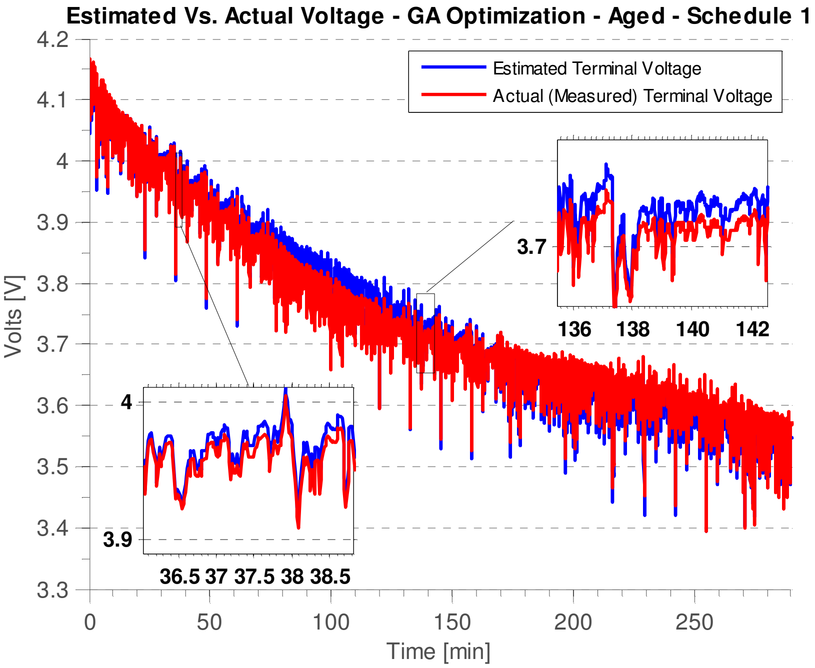

Figure 5.49. Estimated vs. actual (measured) voltage - GA optimization for driving Schedule A1 – Aged cell at 80% capacity

The SVSF provides a good SOC estimation accuracy if the estimator parameters are properly tuned. The initial SOC estimate affects the estimation accuracy and convergence. Therefore, keeping track of the SOC is beneficial to ensure filter convergence.

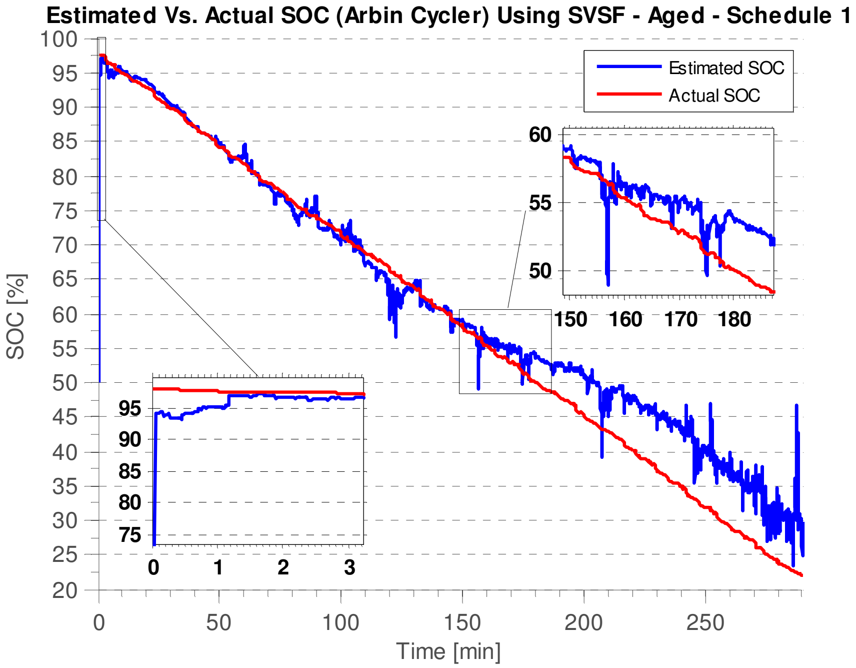

Figure 5.50. Estimated vs. measured SOC using SVSF for driving Schedule A1 – Aged cell at 80% capacity

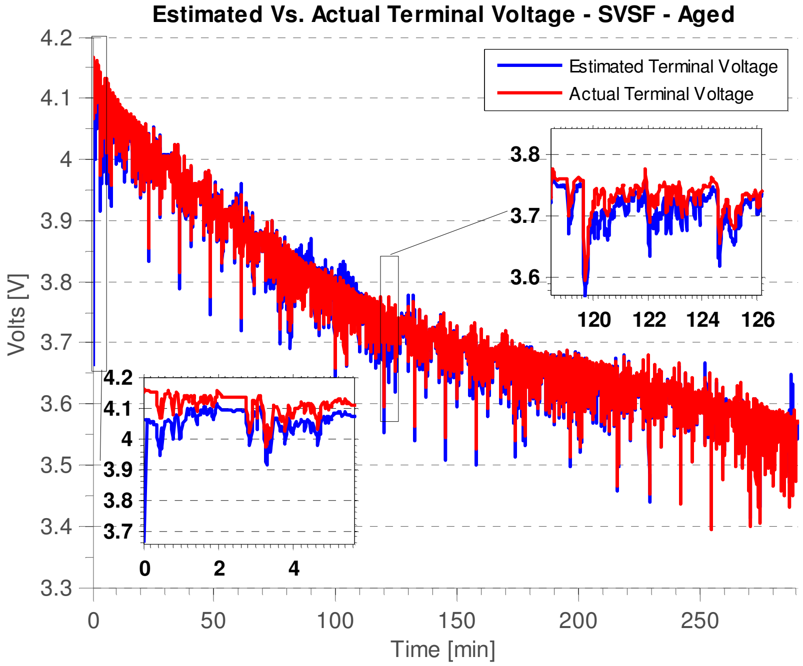

Figure 5.51. Estimated vs. actual (measured) voltage using SVSF for driving Schedule A1 – Aged cell at 80% capacity

5.8 Conclusion

In this paper, first-order equivalent circuit-based model parameters identification and state of charge estimation has been implemented in both online and offline settings. A recursive least square optimization strategy has been implemented for online parameters identification and a regressed-voltage based methodology has been implemented to map the estimated open circuit voltage to the battery state of charge. The technique provides robustness at various battery states of charge and states of life. The technique has been validated using two driving cycles at low and high C-rates. The technique accuracy is compromised at the flat region of the SOC-OCV curve but still provides an acceptable estimate.

Regarding offline-based parameters identification, a Genetic Algorithm optimization has been applied to identify battery model parameters for both fresh and aged battery cells. The technique identifies one set of parameters that can be utilized over the entire state of charge range at a specific temperature conditions. A relatively new state of charge estimation strategy known as the Smooth Variable Structure Filter (SVSF) has been applied to estimate the battery state of charge. The technique is robust to modeling uncertainties and sensor noise provided that filter parameters are properly tuned. Future research involves combining both strategies to improve the state of charge estimation accuracy and to estimate the battery state of health based on identified parameters.

References

[1] Y. Guezennec, W. Choi and T. Choi, "Optimized Dynamic Battery Model Suited for Power based Vehicle Energy Simulation," *International Journal of Automotive Technology,* vol. 13, no. 1, p. 133–141, 2012.

[2] S. E. Samadani, R. A. Fraser and M. Fowler, "A Review Study of Methods for Lithium-ion Battery Health Monitoring and Remaining Life Estimation in Hybrid Electric Vehicles," *SAE International ,* 2012.

[3] J. LeSage, "Long-term maintenance costs show benefit of electric vehicles over ICEs," Green Auto Blog, 2012.

[4] "www.mynissanleaf.com/wiki/," [Online].

[5] "Extended Kalman filtering for battery management systems of LiPB-based HEV battery packs Part 2. Modeling and identificatio," vol. 134, 2004.

[6] B. Pattipati, C. Sankavaram and K. R. Pattipati, "System Identification and Estimation Framework for Pivotal Automotive Battery Management System Characteristics," 2010.

[7] M. Verbrugge and E. Tate, "Adaptive state of charge algorithm for nickel metal hydride batteries including hysteresis phenomena," vol. 126, Febrary 16, 2004.

[8] X. Hu, S. Li and P. Huei, "A comparative study of equivalent circuit models for Li-ion batteries," vol. 198, 2012.

[9] Y.-H. Chiang, W.-Y. Sean and J.-C. Ke, "Online estimation of internal resistance and open-circuit voltage of lithium-ion batteries in electric vehicles," vol. 196, 2011.

[10] X. Hua, S. Lia and H. Penga, "A comparative study of equivalent circuit models for Li-ion batteries," vol. 198 , no. 359– 367, 2012.

[11] G. Plett, "Extended Kalman filtering for battery management systems of LiPB-based HEV battery packs," *Journal of Power Sources,* p. 252–261, 2004.

[12] R. L. H. II, "An Aging Model for Lithium-Ion Cells," Ph.D. Thesis, University of Akron, December, 2008.

[13] G. L. Plett, "Extended Kalman Filtering for Battery Management Systems of LiPB-Based HEV Battery Packs: Part 2. Modeling and Identification," *Journal of Power Sources,* vol. 134, no. 2, pp. 262-276, 2004.

[14] G. L. Plett, "Extended Kalman filtering for battery management systems of LiPB-based HEV battery packs: Part 3. State and parameter estimation," vol. 277–292, no. 134, 2004.

[15] M. Farag, R. Ahmed, A. Gadsden, J. JTjong and S. Habibi, "A Comparative Study of Li-Ion Battery Models and Nonlinear Estimation Techniques," Dearborn, Michigan, 2012.

[16] P. Kumar and P. Bauer, "Parameter Extraction of Battery Models Using Multiobjective Optimization Genetic Algorithms," 2010.

[17] H. Rahimi-Eichi, F. Baronti and M.-Y. Chow, "Modeling and Online Parameter Identification of Li-Polymer Battery Cells for SOC estimation," 2012 .

[18] S. R. Habibi and R. Burton, "The Variable Structure Filter," *Journal of Dynamic Systems, Measurement, and Control (ASME),* vol. 125, pp. 287-293, September 2003.

[19] S. R. Habibi and R. Burton, "Parameter Identification for a High Performance Hydrostatic Actuation System using the Variable Structure Filter Concept," *ASME Journal of Dynamic Systems, Measurement, and Control,* 2007.

[20] "www.MathWorks.com/Matlabcentral/fileexchange," [Online].

[21] "http://www.epa.gov/nvfel/testing/dynamometer.htm," U.S. EPA. [Online].

[22] R. E. Kruse and T. A. Huls, "Development of the Federal Urban Driving Schedule," May 14, 1973.

[23] "http://www.wired.com/autopia/2010/11/honda-finds-evs-a-perfect-fit," [Online].

[24] C. Hua, B. D. Younb and J. Chung, "A multiscale framework with extended Kalman filter for lithium-ion battery SOC and capacity estimation," 2012.

[25] "www.epa.gov/nvfel/testing/dynamometer.htm," EPA United States Environmental Protection Agency. [Online].

[26] U. D. o. Energy, "Plug-In Hybrid Electric Vehicle Value Proposition Study," U.S. Department of Energy, ORNL/TM-2010/46, July, 2010.

[27] G. Pistoia, Electric and Hybrid Vehicles, Rome, Italy: Elsevier, 2010.

[28] USABC EV battery Test Procedures Manual, Laboratory, U.S. DOE/Argonne National, 1996.

[29] U. DOE/INEEL, "PNGV Battery Test Manual," 2000.

[30] "Battery Test Manual for Plug-In Hybrid Electric Vehicles," U.S. Department of Energy, Idaho National Laboratory, Idaho Falls, Idaho 83415, March 2008.

[31] M. Conte, V. C. Fiorentino , I. D. Bloom, K. Morita, T. Ikeya and J. R. Belt, "Ageing Testing Procedures on Lithium Batteries in an International Collaboration Context," China, November, 2010.

[32] G. L. Plett, "Extended Kalman filtering for battery management systems of LiPB-based HEV battery packs: Part 3. State and parameter estimation," *Journal of Power Sources,* no. 134, p. 277–292, 2004.

[33] U. D. o. Energy, "Plug-In Hybrid Electric Vehicle Value Proposition Study," U.S. Department of Energy, ORNL/TM-2010/46, July, 2010.

[34] L. Serrao, Z. Chehab, Y. Guezenne and G. Rizzoni, "An Aging Model of Ni-MH Batteries for Hybrid Electric Vehicles," in *Vehicle Power and Propulsion, 2005 IEEE Conference*, 2005.

[35] M. Moonen and J. Vandewalle, "A Square Root Covariance Algorithm for Constrained Recursive Least Square Estimation," *Journal of VLSI Signal Processing systems For Signal, Image, and Video technology,* vol. 3, no. 3, pp. 163-172, 1991.

[36] J. Holland, "Adaptation in Natural and Artificial Systems," *University of Michigan Press, Ann Arbor,* 1975.

[37] D. Goldberg, "Genetic Algorithms in search, Optimization, and MAchine Learning," *Addison-Wesley, Reading, Massachusetts,* 1989.

[38] M. Inc, "www.mathworks.com/help/grads/how-the-genetic-algorithm-works.html," 2013. [Online].

[39] S. R. Habibi, "The Smooth Variable Structure Filter," *Proceedings of the IEEE,* vol. 95, no. 5, pp. 1026-1059, 2007.

[40] M. Al-Shabi, "The General Toeplitz/Observability SVSF," Hamilton, Ontario, 2011.

[41] S. A. Gadsden and S. R. Habibi, "A New Form of the Smooth Variable Structure Filter with a Covariance Derivation," in *IEEE Conference on Decision and Control*, Atlanta, Georgia, 2010.

Chapter 6: Aged Battery State of Charge Estimation based on Interacting Multiple Models

Ryan Ahmed[1], Andrew Gadsden[1], Mohammed El Sayed[1], Saeid Habibi[1]
Centre for Mechatronics and Hybrid Technologies (CHMT), Department of Mechanical Engineering, McMaster University, Hamilton, Canada

Jimi Tjong[2]
[2]Ford Motor Company of Canada, Powertrain Engineering Research and Development Center (PERDC), Windsor, Canada

Abstract

Lithium-Ion batteries are increasingly being used and are one of the most important components in hybrid electric vehicles (HEVs), plug-in HEVs (PHEVs), and battery electric vehicles (BEVs). Therefore, real-time and accurate monitoring of the State of Charge (SOC) and terminal voltage is essential for avoiding any failure or degradation in performance of the battery overtime due to over or under discharging. High-fidelity battery models in conjunction with robust estimation strategies are used to estimate the SOC and State of Health (SOH). However, as battery ages due to multiple charging and discharging cycles, model parameters such as internal resistance and capacity will significantly change and this can lead to inaccurate estimation of SOC or even numerical instability of monitoring strategies. This paper presents a SOC estimation strategy known as the interacting multiple models based on the Smooth variable structure filter (IMM-SVSF). The proposed methodology can adapt to various aging conditions and can provide an accurate approach that can be implemented in a real-time on-board Battery Management System (BMS).

Keywords: Battery Management Systems (BMS), Interacting Multiple Models (IMM), State of Charge (SOC), State of Health (SOH), Filtering, Estimation

Corresponding Author:

Ryan Ahmed, M.A.Sc, P.Eng., SCPM
Research and Development Engineer
Stanford Certified Project Manager

Direct: +1(519) 944 - 8587
Mobile: +1(226) 975 - 3248
Email: ryan.ahmed@mcmaster.ca

6.1 Introduction

Recently, Hybrid electric vehicles (HEVs), plug-in HEVs (PHEVs) and battery electric vehicles (BEVs) have received significant attention in both industrial and academic settings due to their sustainability, reliability, high efficiency, and their potential to ultimately reduce harmful gas emissions. Lithium-Ion-based battery chemistry provides numerous advantages compared to other battery chemistries such as high energy density, slow loss of charge when left unused, and no memory effect, [1]. Therefore, Lithium-Ion batteries are increasingly being considered as the most promising energy storage devices for the next generation HEVs, PHEVs, and BEVs, [1]. In order to ensure Lithium-Ion battery safety, a real-time tracking of the battery SOC is critical to ensure that the battery operates within the tolerable, safe range of operation and to circumvent over-charge or under-charge conditions, [2].

This paper presents a relatively new estimation strategy known as the Interacting Multiple Models based on the Smooth Variable Structure filter (IMM-SVSF) as applied to battery management systems, [3]. This paper presents a proof of concept to the applicability of adaptive techniques in battery SOC and SOH estimation. The IMM-SVSF technique is applied to extract the State of Charge (SOC) information based on an equivalent circuit-based battery aging model. The SVSF is a predictor-corrector estimator based on sliding mode concepts, and can be applied to both linear and nonlinear systems, [4]. This technique is capable of tracking the battery SOC and terminal voltage under aging conditions. As battery ages, parameters such as the internal resistance and capacity change overtime and thus the battery model has to adapt to these variations in order to provide accurate estimates associated with various charging/discharging cycles until the end-of-life (EOL). Computer simulations show the effectiveness of the proposed technique for its implementation in real-time BMS applications.

State and parameter estimation techniques such as the Kalman filter are essential for information processing in model-based condition monitoring systems. Estimation theory comprises real-time information extraction by tracking change in systems and physical parameters. The Extended Kalman Filter (EKF) is one of the most widely used techniques for state and parameter estimation. It can be used for battery SOC estimation and can provide high accuracy in real-time applications, [5, 6]. In the literature, various techniques have been implemented for SOC and SOH estimation. Saha et al. [7] proposed an estimation of battery SOC, SOH, and RUL using Bayesian framework, Relevance vector machines (RVMs), and particle filters. A combination of equivalent-circuit based models and statistical models of state-transitions and aging processes have been applied to experimental batteries, [7].

A dual estimation strategy has been applied for estimating battery model parameters and SOC using lumped parameters in [8, 9]. One filter is used to estimate battery model parameters and the second filter is used for SOC estimation. A SOH estimation of the battery can be conducted in 3 minutes as documented in [10]. In [10], Artificial Neural Networks have been trained on fuzzified data and the outputs are then defuzzified. One of the main advantages of neural networks is its ability to adapt and self-learn through experience. The more batteries are tested using this technique, the more accuracy is achieved later on, [10]. A real-time, impedance-based parameter identification method for

SOC and SOH estimation has been proposed in, [11]. The EKF can estimate the battery model parameters based on the Randles model, [11]. More RC blocks are used to model the Warburg impedance but this modification has led to over-parameterization thus causes EKF divergence problems. The technique has been verified using the UDDS Cycle, [11]. A SOH technique based on the Extended Kalman filter (EKF) has been presented in [12]. In this research, EKF has been used to estimate the bulk capacitance thus provides an indication of the battery SOH. Experimental results demonstrate the accuracy of the proposed technique compared to other techniques in estimating the SOC (with 2% accuracy) and SOH, [12].

Multiple model strategies can provide accurate estimates for both linear and non-linear systems. Using a finite number of models, these techniques can utilize information from all models to provide robustness and adaptability to model uncertainties, [13].

One of the most widely adopted adaptive estimation strategy is known as the 'multiple model' (MM), [14]. Numerous forms exist, namely: static MM [15], dynamic MM [13], generalized pseudo-Bayesian (GPB) [16, 17, 18, 19], and the interacting multiple model (IMM) [13, 20, 21]. The IMM strategy is generally preferred in challenging estimation problems, therefore, it has been widely implemented in the literature, [3]. Numerous fault detection and isolation problems have been tackled using the IMM in conjunction with the KF strategy. Most recently, the IMM was combined with the SVSF for fault detection and diagnosis, [3, 22]. In [23], the IMM-SVSF demonstrated improved estimation accuracy as well as more confident fault detection results.

The rest of the paper is organized as follows. Section 6.2 provides a description of the model implemented in this paper. Section 6.3 provides an overview of the IMM-SVSF technique. Section 6.4 provides the simulation results of the proposed methodology and Section 6.5 contains the conclusion.

6.2 Battery Model Selected

The model selected for the IMM-SVSF technique is known as the simple model and has been presented by Plett in [8]. Plett has developed a series of nonlinear battery models based on empirical observations. These models can accurately track cell voltage variations at various SOCs even at highly nonlinear regions (extreme cases when the battery is fully charged or depleted), [24]. The following section describes the model that is selected to characterize battery aging. The model is an evolution of the combined model as follows.

6.2.1 Combined Model

Various battery models have been presented in the literature. A number of simplified models have been formulated and are adopted in [8] and [25]. The following three are amongst the most popular combined models, [8]:

- Shepherd: $y_k = E_0 - Ri_k - K_i/z_k$
- Unnewehr universal model: $y_k = E_0 - Ri_k - K_i z_k$
- Nernst: $y_k = E_0 - Ri_k + K_2 \ln(z_k) + K_3 \ln(1 - z_k)$

In these models, y_k is the cell terminal voltage, R is the cell internal resistance (different values may be used for charge/discharge at different SOC levels), R_i is the polarization resistance, and $K_{\#}$ are constants chosen to make the model fit the data, [8]. A combined model based on the three aforementioned models is shown below, [8]:

$$z_{k+1} = z_k - \left(\frac{\eta_i \Delta t}{C}\right) i_k \tag{6.1}$$

$$y_k = K_0 - Ri_k - \frac{K_1}{z_k} - K_2 z_k + K_3 \ln(z_k) + K_4 \ln(1 - z_k) \tag{6.2}$$

6.2.2 Simple Model

As presented in [8], the output equation is divided into two parts; the first part is a function of the battery SOC and the second part depends on the input current.

$$f(z_k) = K_0 - \frac{K_1}{z_k} - K_2 z_k + K_3 \ln(z_k) + K_4 \ln(1 - z_k) \tag{6.3}$$

$$f(i_k) = Ri_k \tag{6.4}$$

As explained in [8], by combining all the model parameters that are functions of the SOC in one combined term yields:

$$z_{k+1} = z_k - \left(\frac{\eta_i \Delta t}{C}\right) i_k \tag{6.5}$$

$$y_k = OCV(z_k) - Ri_k \tag{6.6}$$

Where OCV represents the open circuit voltage which is function of the state of charge z_k. As battery ages, model parameters will significantly change. In order to simulate the battery aging phenomenon, the internal resistance is increased and capacity fade occurs until it reaches end-of-life (80% remaining capacity). Then the IMM-SVSF technique is used to estimate the SOC and terminal voltage using various battery models at different states of life.

6.3 SVSF-based Interacting Multiple Models

The Interacting Multiple Models based on the SVSF (IMM-SVSF) is an adaptive strategy for battery state of charge estimation. Instead of relying on a single battery model at one state of life during the entire lifetime of the battery, multiple models can interact collaboratively to achieve a more accurate and robust voltage prediction and state of charge estimate. This is beneficial in all electric and hybrid vehicles to ensure that the battery operates within the acceptable range of operation. The proposed model-based estimation strategy is applicable to all types and sizes of electrochemical battery cells. The proposed strategy is computationally efficient for simulation, design, and real-time management of battery-powered systems. This technique is able to adapt to changes in model parameters such as internal resistance and capacity fade as battery ages. If the same model is used for all battery states of health, the model will progressively lose its accuracy in determining terminal voltages and SOC estimation. Accordingly, adaptive techniques such as the IMM are best-suited for these applications.

In order to compare the effectiveness of the proposed strategy, the technique has been compared to the standalone filter based on one battery model at one state of life. Subsection 6.3.1 describes the Smooth Variable Structure Filter and section 6.3.2 describes the IMM-SVSF strategy.

6.3.1 Smooth Variable Structure Filter

Similarly to the Kalman filter, the SVSF works in a predictor-corrector fashion, [4]. The filter is based on the sliding mode concept and has demonstrated robustness to modeling uncertainties and sensor noise, [4, 26]. The SVSF can be applied to both linear and nonlinear systems. It works by using an SVSF gain that forces the states to converge to a neighborhood the actual or true value, [4]. The gain forces the states to switch back and forth across the state trajectory within a region referred to as the existence subspace which is function of modeling uncertainties. The width of the existence space β is a function of the uncertain dynamics associated with the inaccuracy of the internal model of the filter as well as the measurement model, and varies with time, [4]. The SVSF can be applied to systems that are differentiable and observable [4, 27]. The original form of the SVSF as presented in [4] did not include covariance derivations. An augmented form of the SVSF that includes the derivation of an error covariance matrix has been presented in [28]. Here, the latter is summarized.

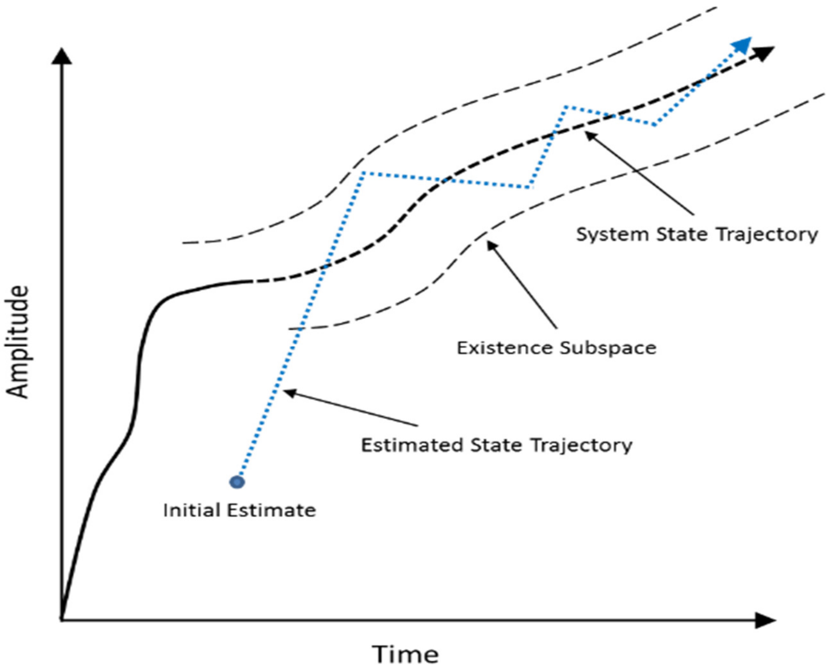

Figure 6.1. The SVSF estimation strategy starting from some initial value, the state estimate is forced by a switching gain to within a region referred to as the existence subspace, [4].

Consider a nonlinear system with a linear output (measurement) equation. The filter runs by generating a prediction of the state estimate (which represents the solid-electrolyte interface concentration) as follows, [4]:

$$\hat{x}_{k+1|k} = \hat{f}(\hat{x}_{k|k}, u_k) \tag{6.7}$$

The predicted estimates are then used to generate a predicted measurements $\hat{z}_{k+1|k}$ as follows, [4]:

$$\hat{z}_{k+1|k} = C_{k|linearized}\hat{x}_{k+1|k} \tag{6.8}$$

Where $C_{k|linearized}$ is the measurement matrix, then the measurement error $e_{z,k+1|k}$ can be calculated as follows, [4]:

$$e_{z,k+1|k} = z_{k+1} - \hat{z}_{k+1|k} \tag{6.9}$$

The SVSF has predictor-corrector form. Its gain is a function of the a-priori and the a-posteriori measurement errors $e_{z_{k+1|k}}$ and $e_{z_{k|k}}$. It has a smoothing boundary layer widths ψ, a memory or convergence rate γ, as well as the linear measurement matrix $C_{k|linearized}$. For the derivation of the SVSF gain K_{k+1}, refer to [4, 28]. The SVSF gain is defined as follows, [4]:

$$K_{k+1} = {C_{k|linearized}}^{+} diag\left[\left(\left|e_{z_{k+1|k}}\right| + \gamma\left|e_{z_{k|k}}\right|\right) \circ sat\left(\frac{e_{z_{k+1|k}}}{\psi}\right)\right] diag\left(e_{z_{k+1|k}}\right)^{-1} \tag{6.10}$$

The updated states $\hat{x}_{k+1|k+1}$ are calculated as follows, [4]:

$$\hat{x}_{k+1|k+1} = \hat{x}_{k+1|k} + K_{k+1} e_{z_{k+1|k}} \tag{6.11}$$

The output estimates and the a posteriori measurement errors are then calculated respectively as follows, [4]:

$$\hat{z}_{k+1|k+1} = C_{k|linearized} \widehat{w}_{k+1|k+1} \tag{6.12}$$

$$e_{z_{k+1|k+1}} = z_{k+1} - \hat{z}_{k+1|k+1} \tag{6.13}$$

Equations 6.7 to 6.13 are iteratively repeated for every sample time.

6.3.2 The IMM-SVSF Technique

The interacting multiple model (IMM) strategy relies on a finite number of models and state estimators that run in a parallel fashion, [3]. Each filter provides a state estimate, a covariance, and a likelihood calculation (which is a function of the measurement error and innovation covariance). These outputs are utilized to calculate mode probabilities. Mode probability indicates how close the filter model operates in comparison to the actual (true) system model, [3].

The IMM has been shown to work significantly better than single model methods, since it is able to make use of more information, [13]. Therefore, the IMM strategy has been used for multiple applications in radar and target tracking, where there more than one model that describes the target trajectory, [13]. The IMM-SVSF methodology has been reported in [3] and is briefly described here for completeness and readability.

The IMM is implemented as per [13]. The strategy involves SVSF estimation as applied on a finite number of models. As an example, Figure 6.2 shows two models. The

IMM-SVSF estimator consists of five main steps: (1) calculation of the mixing probabilities, (2) mixing stage, (3) mode-matched filtering via the SVSF, (4) mode probability update, and (5) state estimate and covariance combination.

First, the strategy calculates the mixing probabilities $\mu_{i|j,k|k}$ (i.e., the probability of the system currently in mode i, and switching to mode j in the next step). The mixing probabilities are calculated as follows, [13]:

$$\mu_{i|j,k|k} = \frac{1}{\bar{c}_j} p_{ij} \mu_{i,k} \tag{6.14}$$

$$\bar{c}_j = \sum_{i=1}^{r} p_{ij}\, \mu_{i,k} \tag{6.15}$$

Where p_{ij} is defined as the mode transition probability, and is a design parameter. $\mu_{i,k}$ values can range from 0 to 1, it denotes the probability of the mode i being truthful, and differs from the mixing probabilities $\mu_{i|j,k|k}$, [13].

The calculated mixing probabilities $\mu_{i|j,k|k}$ are further used during the mixing stage. In addition to the mixing probabilities, the previous mode-matched states $\hat{x}_{i,k|k}$ and covariance's $P_{i,k|k}$ are also used to calculate the mixed initial states and covariances for the filter matched to M_j (which is model j consisting of associated A_j and B_j matrices). The mixed initial conditions are calculated as follows, [13]:

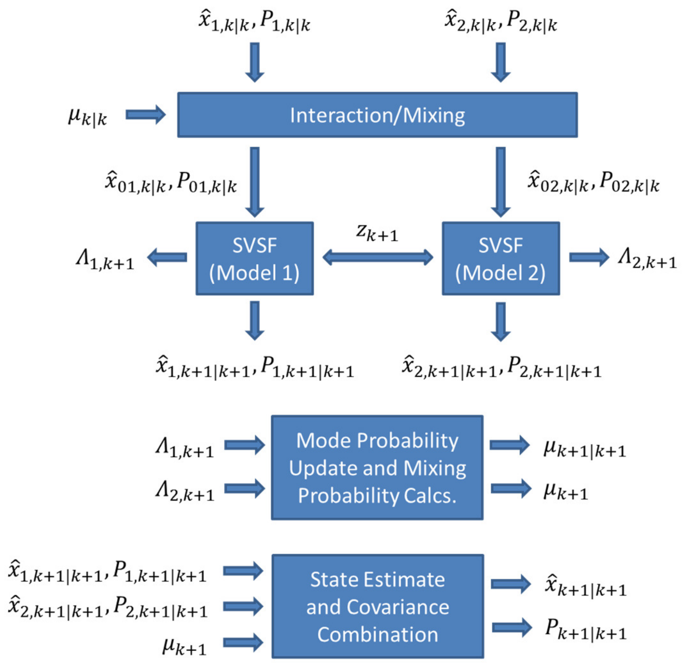

Figure 6.2. IMM-SVSF Strategy (Adapted from [13] and [3])

$$\hat{x}_{0j,k|k} = \sum_{i=1}^{r} \hat{x}_{i,k|k}\mu_{i|j,k|k} \tag{6.16}$$

$$P_{0j,k|k} = \sum_{i=1}^{r} \mu_{i|j,k|k}\left\{P_{i,k|k} + \left(\hat{x}_{i,k|k} - \hat{x}_{0j,k|k}\right)\left(\hat{x}_{i,k|k} - \hat{x}_{0j,k|k}\right)^T\right\} \tag{6.17}$$

The SVSF is applied to perform mode-match filtering by utilizing equations (6.16) and (6.17). In addition, the SVSF utilizes the measurement z_{k+1} and the system input u_k to calculate an updated state estimates (6.23) and covariance matrix (6.24). The modified prediction stage (for linear systems) is as follows. The state estimates $\hat{x}_{0j,k|k}$ (6.16) and corresponding covariance $P_{0j,k|k}$ (6.17) for each model j are used to predict the state estimate $\hat{x}_{j,k+1|k}$ (6.18) and calculate the a priori state error covariance matrix $P_{j,k+1|k}$ (6.19), [4].

$$\hat{x}_{j,k+1|k} = A_j\hat{x}_{0j,k|k} + B_j u_k \tag{6.18}$$

$$P_{j,k+1|k} = A_j P_{k|k}^{0j} A_j^T + Q_k \tag{6.19}$$

From (6.18) and (6.19), the mode-matched innovation covariance $S_{j,k+1|k}$ (6.20) and mode-matched a-priori measurement error $e_{j,z,k+1|k}$ (6.21) are calculated as follows, [3]:

$$S_{j,k+1|k} = C_j P_{j,k+1|k} C_j^T + R_{k+1} \tag{6.20}$$

$$e_{j,z,k+1|k} = z_{k+1} - C_j \hat{x}_{j,k+1|k} \tag{6.21}$$

The mode-matched SVSF gain $K_{j,k+1}$ is calculated (6.22) and then utilized to update the state estimates $\hat{x}_{j,k+1|k+1}$ (6.23), [3].

$$\begin{aligned} K_{j,k+1} = C_j^+ diag\Big[&\Big(\left| e_{j,z,k+1|k} \right|_{Abs} + \gamma_j \left| e_{j,z,k|k} \right|_{Abs} \Big) \\ &\circ sat\big(\bar{\psi}_j^{-1} e_{j,z,k+1|k} \big) \Big] diag\big(e_{j,z,k+1|k} \big)^{-1} \end{aligned} \tag{6.22}$$

$$\hat{x}_{j,k+1|k+1} = \hat{x}_{j,k+1|k} + K_{j,k+1} e_{j,z,k+1|k} \tag{6.23}$$

The state error covariance matrix $P_{j,k+1|k+1}$ is then calculated (6.24) and the a-posteriori measurement error $e_{j,z,k+1|k+1}$ can be calculated (6.25), [3].

$$P_{j,k+1|k+1} = \big(I - K_{j,k+1} C_j \big) P_{j,k+1|k} \big(I - K_{j,k+1} C_j \big)^T + K_{j,k+1} R_{k+1} K_{j,k+1}^T \tag{6.24}$$

$$e_{j,z,k+1|k+1} = z_{k+1} - C_j \hat{x}_{j,k+1|k+1} \tag{6.25}$$

Based on the mode-matched innovation matrix $S_{j,k+1|k}$ (6.20) and the mode-matched a-priori measurement error $e_{j,z,k+1|k}$ (6.21), mode-matched likelihood function $\Lambda_{j,k+1}$ based on the SVSF estimation strategy is formulated as follows, [13]:

$$\Lambda_{j,k+1} = \mathcal{N}\big(z_{k+1}; \hat{z}_{j,k+1|k}, S_{j,k+1} \big) \tag{6.26}$$

Equation (6.26) may be solved as follows, [13, 29]:

$$\Lambda_{j,k+1} = \frac{1}{\sqrt{\left|2\pi S_{j,k+1}\right|_{Abs}}} exp\left(\frac{-\frac{1}{2} e_{j,z,k+1|k}^{T} e_{j,z,k+1|k}}{S_{j,k+1}}\right) \quad (6.27)$$

By applying the mode-matched likelihood functions $\Lambda_{j,k+1}$, the mode probability $\mu_{j,k}$ can be updated by, [13]:

$$\mu_{j,k} = \frac{1}{c} \Lambda_{j,k+1} \sum_{i=1}^{r} p_{ij}\, \mu_{i,k} \quad (6.28)$$

Where the normalizing constant is defined as, [13]:

$$c = \sum_{j=1}^{r} \Lambda_{j,k+1} \sum_{i=1}^{r} p_{ij}\, \mu_{i,k} \quad (6.29)$$

Finally, the overall IMM-SVSF state estimates $\hat{x}_{k+1|k+1}$ (6.30) and corresponding covariance $P_{k+1|k+1}$ (6.31) are calculated, [3].

$$\hat{x}_{k+1|k+1} = \sum_{j=1}^{r} \mu_{j,k+1} \hat{x}_{j,k+1|k+1} \quad (6.30)$$

$$P_{k+1|k+1} = \sum_{j=1}^{r} \mu_{j,k+1} \Big\{ P_{j,k+1|k+1} + \left(\hat{x}_{j,k+1|k+1} - \hat{x}_{k+1|k+1}\right)\left(\hat{x}_{j,k+1|k+1} - \hat{x}_{k+1|k+1}\right)^{T} \Big\} \quad (6.31)$$

The IMM-SVSF strategy can be iteratively repeated and may be summarized by equations (6.14) through (6.31), where there are $i, j = 1, \dots, r$ models, [13].

6.4 Simulation Results

In this paper, three different models with various parameters have been used for simulation. The charging, discharging resistances, and the battery capacity for a fresh battery (Life

Fraction (LF) = 0) are as follows: 0.05 Ω, 0.1 Ω, 3.2 Ah. The battery parameters at its End-of-life (EOL) (20% capacity fade) (LF = 1), assuming linear resistance variations are as follows: 0.07 Ω, 0.14 Ω, 2.56 Ah.

In order to generate the current profile from the velocity profile of a driving cycle, an electric vehicle battery model has been modified from an existing hybrid vehicle model, [30]. The model has been simulated using SimScape in Matlab environment. A model of a mid-size sedan has been used with an approximate driving range of 200 kilometers per full charge. The simulation model, as shown in Figure 6.3, consists of a DC electric motor, vehicle dynamic model, lithium-Ion battery pack, DC-DC convertor, and vehicle speed controller.

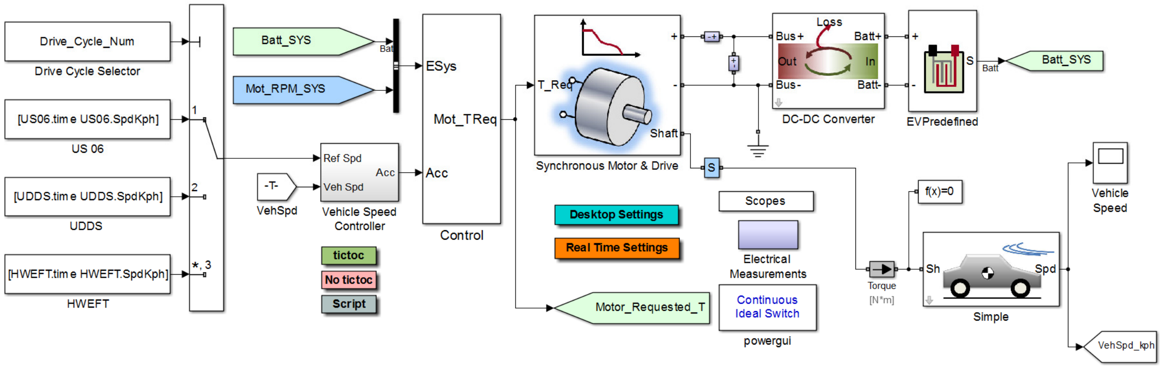

Figure 6.3. All-Electric Mid-size Sedan Simulation Model in SimScape (Adopted from [30])

A benchmark driving schedule known as the Urban Dynamometer Driving Schedule (UDDS) has been used in the simulation, [31]. The UDDS driving cycle represents a city driving condition, the UDDS cycle (commonly known as “LA4” or “the city test” or Federal Test Procedure “FTP-72”) was originally used for light duty fossil-fueled vehicle testing, [31].

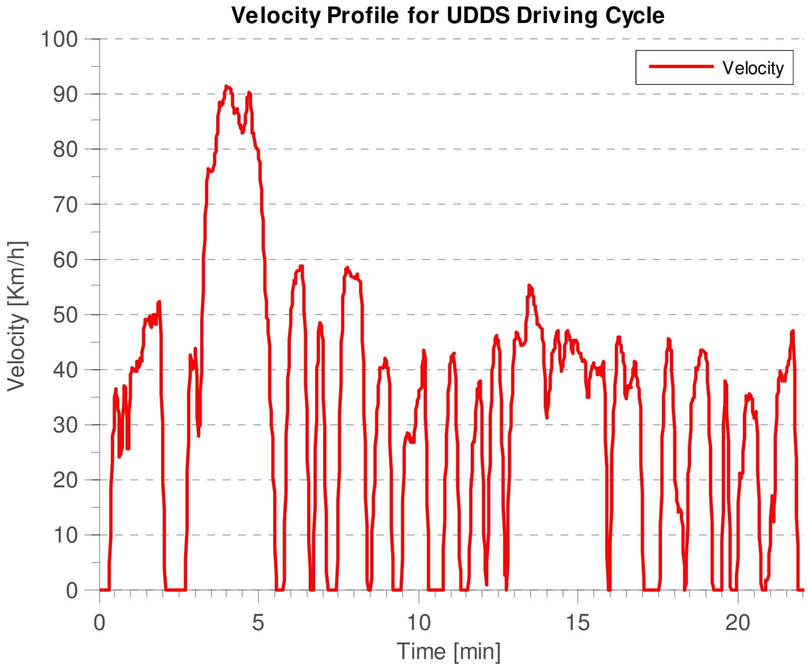

Figure 6.4. UDDS Velocity Profile

It has been developed to imitate average speed, idle time, and number of stops that the average driver performs in real-world conditions, [32]. Even though the driving behavior of an average driver may likely vary, this driving cycle has been extensively utilized to verify and validate algorithms. The UDDS cycle is characterized by approximately 1369 seconds, 7.45 kms, and an average speed of 19.59 mph. The cell used in this study has a nominal capacity of 3.2 Ah. The vehicle velocity profile for the UDDS cycle is shown in Figure 6.4. The corresponding profile for battery current, state of charge, and terminal voltage are as shown in Figure 6.5.

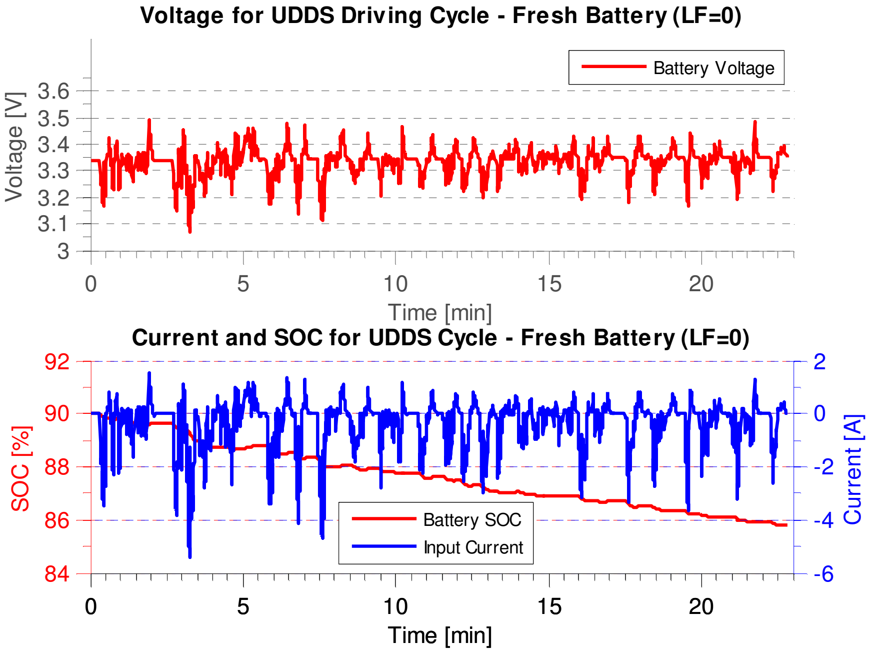

Figure 6.5. Battery Voltage (Upper Figure), SOC and Current (Bottom Figure) for one UDDS Cycle

In this paper, negative current values indicate battery discharging and positive values for charging. The UDDS driving cycle depletes the battery from 90% SOC to approximately 85% with regenerative braking. For each model, the terminal voltage as a function of time was captured, as well as the state of charge as shown in Figure 6.6 and Figure 6.7, respectively.

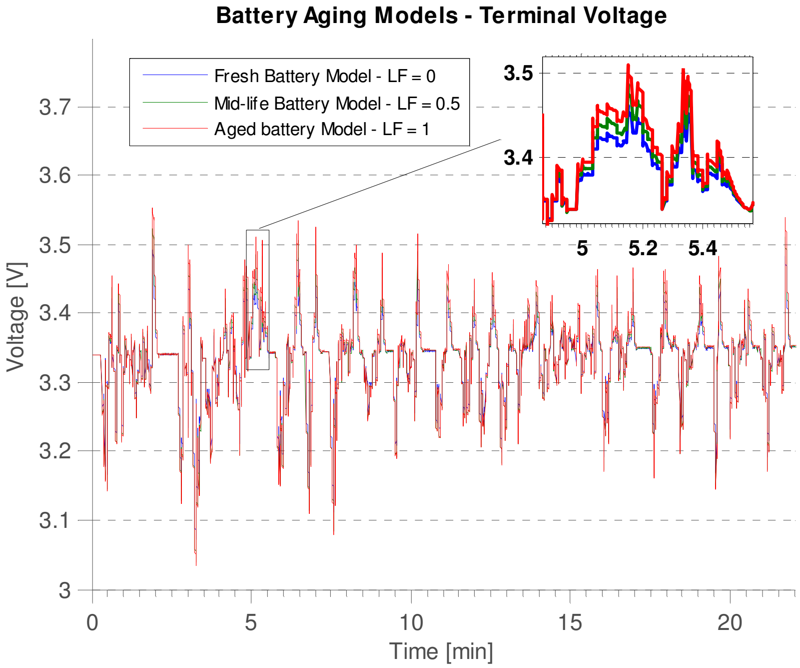

Figure 6.6. Terminal Voltage for Battery Aging Models at 3 Distinct States of Life; Fresh, Mid-life, and Aged State

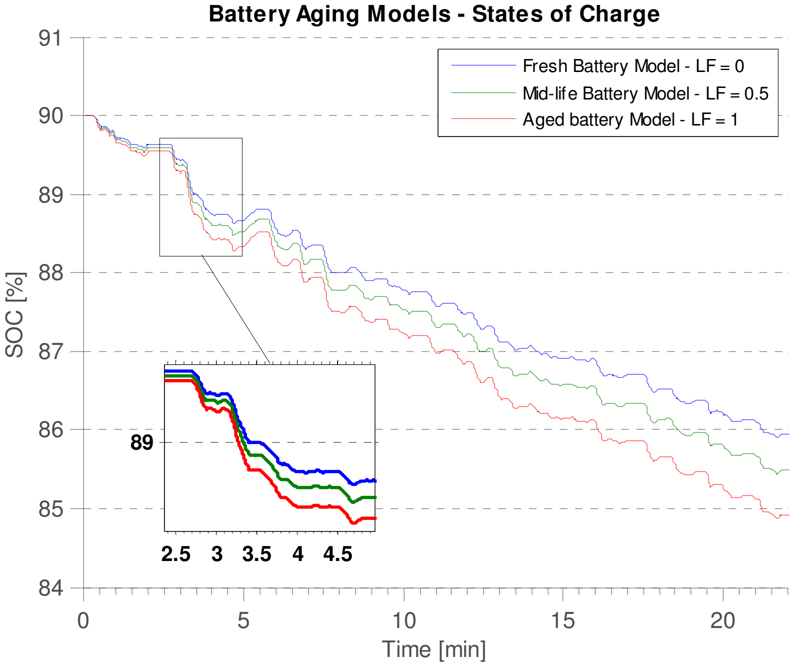

Figure 6.7. Battery State of Charge for Various Aging Battery Models at Three Distinct States of Life; Fresh, Mid-life, and Aged State

Figure 6.7 shows the battery state of charge at various states of life starting from a fresh (healthy) state till the end of life specified at 80% remaining capacity for a UDDS cycle. In order to demonstrate the effectiveness of the disclosed strategy to battery state of charge estimation, the standalone SVSF is compared to the IMM-SVSF. The model initial state of charge is initialized at 85% while the actual battery initial state of charge is at 90%. The SVSF convergence well when the model is accurate. However, as battery ages, model parameters such as internal resistance and capacity significantly change, therefore if the same parameters are used, the estimator will suffer from divergence problems and provide misleading state of charge estimate. Therefore, an adaptive method such as the IMM-SVSF will circumvent this problem by incorporating different battery models obtained across the life time of the battery. In order to demonstrate the ability of the proposed technique to extract battery cell SOC information, the technique has been compared to the standalone SVSF and data for a battery with 0.5 life fraction (mid-life) has been used for testing. The IMM-SVSF considers more battery models to provide a more accurate SOC estimate.

The SVSF parameters are tuned using Genetic Algorithm (GA) optimization with population size of 100 and using 10 numbers of iterations. For the standalone SVSF, four parameters required to be tuned, namely: the SVSF convergence or 'memory' is set to $\gamma = 0.13$, the boundary layer thickness $\psi = 352.39$, the initial a-priori estimate $e_{z,k+1|k} = 7.28$, and the damping element $\lambda = 0.15$. Regarding the IMM-SVSF, the 12 optimized parameters are as follows: the initial noise covariance matrix $R = 79320.9$, the initial system error covariance matrix for model 1 (fresh) $Q = 207765.82$, the initial system error covariance matrix for model 2 (aged) $Q = 226602.34$, the initial value of the state error covariance matrix is set to $P = 236.07$, the mode transition probabilities $p_{11}, p_{12}, p_{21}, p_{22}$ are 0.13, 0.929, 0.898, 0.9767, the SVSF convergence or 'memory' for model 1 is set to $\gamma = 0.763$, the boundary layer thickness $\psi = 3.929$, the SVSF convergence or 'memory' for model 2 is set to $\gamma = 0.5$, and the boundary layer thickness $\psi = 5.27$.

As shown in Figure 6.8, voltage data from a battery at mid-life state is used for testing the standalone SVSF and the IMM-SVSF. The IMM-SVSF technique provides good estimation accuracy and stability compared to the standalone SVSF. The SVSF, when used with the fresh battery or with an aged battery, will chatter due to model uncertainties. Conversely, the IMM-SVSF technique adapts to these variations as it takes into account the combined results of all the models across the battery lifetime thus provides a smoother and more accurate estimate.

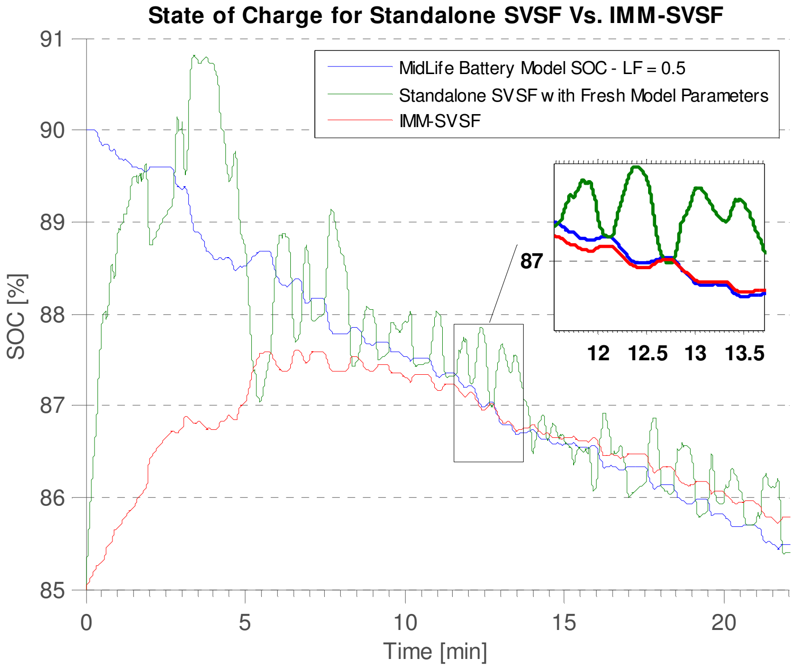

Figure 6.8. Battery Estimated State of Charge for Standalone SVSF Vs. IMM-SVSF Tested at Mid-life Battery State of Life

6.5 Conclusion

In this paper, a proof of concept to the applicability of adaptive techniques such as interacting multiple models for the estimation of the SOC and terminal voltages based on aged battery models. This is beneficial in BEVs and HEVs to ensure that the battery operates within the acceptable range of operation. The proposed model/estimation strategy is applicable to other types and sizes of electrochemical battery cells. The proposed strategy is computationally effective for simulation, design, and real-time management of battery-powered systems. This technique is able to adapt to changes in model parameters such as internal resistance and capacity fade as battery ages. Simulation results show the effectiveness of the proposed technique. One of the limitations of the proposed strategy is the extensive effort required to tune filter parameters. In addition, the initial SOC estimate has to be close enough to the actual SOC in order to guarantee convergence. Future research will include changing the battery model structure as battery ages which in turn would improve accuracy and stability.

References

[1] J. Zhang, L. Liao and J. Lee, "Prognostics and Health Monitoring of Li-ion Battery for Hybrid Electric Vehicle," Detroit, Michigan, United States, SAE 2010 World Congress & Exhibition, 13 April 2010.

[2] A. Jossen, V. Spath, H. Doring and a. J. Garche, "Battery management systems (BMS) for increasing battery life time," *Proceesdings of the 21st INTELEC Conference,* 1999.

[3] S. A. Gadsden, "Smooth Variable Structure Filtering: Theory and Applications," Hamilton, Ontario, 2011.

[4] S. R. Habibi, "The Smooth Variable Structure Filter," *Proceedings of the IEEE,* vol. 95, no. 5, pp. 1026-1059, 2007.

[5] G. Plett, "Extended Kalman filtering for battery management systems of LiPB-based HEV battery packs: : Part 3. State and Parameter Estimation," *Journal of Power Sources,* vol. 134, p. 277–292, 2004.

[6] W. Kexin and C. Qiaoyan, "Battery SOC Estimation based on Multi-model Adaptive Kalman Filter," in *Advanced Materials Research Vols. 403-408* , 2012.

[7] M. I. Bhaskar Saha, K. Goebel, S. Poll and J. Christophersen, "Prognostics Methods for Battery Health Monitoring Using a Bayesian Framework," vol. 58, no. 2, Feb, 2009.

[8] G. L. Plett, "Extended Kalman Filtering for Battery Management Systems of LiPB-Based HEV Battery Packs: Part 2. Modeling and Identification," *Journal of Power Sources,* vol. 134, no. 2, pp. 262-276, 2004.

[9] M. Farag, R. Ahmed, A. Gadsden, S. Habibi and J. Tjong, "A Comparative Study of Li-Ion Battery Models and Nonlinear Estimation Techniques," Dearborn, Michigan, 2012.

[10] I. Buchmann, "Artificial Intelligence Reads Battery State-of-Health in Three Minutes," Cadex Elextronics Inc., 22000 Fraserwood Way, Richmond B.C. Canada V6W 156, 2001.

[11] D. V. Do, . C. Forgez, K. El Kadri Benkara and G. Friedrich, "Impedance Observer for a Li-Ion Battery Using Kalman Filter," vol. 58, no. 8, 2009.

[12] B. S. Bhangu, P. Bentley, D. A. Stone and C. M. Bingham, "Nonlinear Observers for Predicting State-of-Charge and State-of-Health of Lead-Acid Batteries for Hybrid-Electric Vehicles," vol. 54, no. 3, May, 2005.

[13] Y. Bar-Shalom, X. Rong Li and T. Kirubarajan, Estimation with Applications to Tracking and Navigation, New York: John Wiley and Sons, Inc., 2001.

[14] X. R. Li, Advances in Aerospace Systems Dynamics and Control Systems (Volume 76), C. T. Leondes, Ed., New York: Academic Press, 1996.

[15] D. T. Magill, "Optimal Adaptive Estimation of Sampled Stochastic Processes," *IEEE Transactions on Automatic Control,* Vols. AC-10, pp. 434-439, 1965.

[16] G. A. Ackerson and K. S. Fu, "On State Estimation in Switching Environments," *IEEE Transactions on Automatic Control,* Vols. AC-15, no. 1, pp. 10-17, January 1970.

[17] A. G. Jaffer and S. C. Gupta, "Recursive Bayesian Estimation with Uncertain Observation," *IEEE Transactions on Information Theory,* Vols. IT-17, pp. 614-616, September 1971.

[18] A. G. Jaffer and S. C. Gupta, "Optimal Sequential Estimation of Discrete Processes with Markov Interrupted Observations," *IEEE Transactions on Automatic Control,* Vols. AC-16, pp. 417-475, October 1971.

[19] C. B. Chang and M. Athans, "State Estimation for Discrete Systems with Switching Parameters," *IEEE Transactions on Aerospace and Electronic Systems,* Vols. AES-14, no. 5, pp. 418-425, May 1978.

[20] H. A. P. Blom, "An Efficient Filter for Abruptly Changing Systems," in *23rd IEEE Conference on Decision and Control*, Las Vegas, Nevada, December, 1984.

[21] H. A. P. Blom and Y. Bar-Shalom, "The Interacting Multiple Model Algorithm for Systems with Markovian Switching Coefficients," *IEEE Transactions on Automatic Control,* Vols. AC-33, no. 8, pp. 780-783, August 1988.

[22] S. A. Gadsden, S. R. Habibi and T. Kirubarajan, "A Novel Interacting Multiple Model Method for Target Tracking," in *13th International Conference on Information Fusion*, Edinburgh, UK, 2010.

[23] S. A. Gadsden, Y. Song and S. R. Habibi, "A Novel Model-Based Estimator for the Purposes of Fault Detection and Diagnosis," no. Under Review, 2013.

[24] S. Haykin, Kalman Filtering and Neural Networks, New York: John Wiley and Sons, Inc., 2001.

[25] K. Sakurai, K. I. Muramoto and T. Yamazaki, "Estimation of the Recharge Capacity of Sealed Lead-Acid Batteries by Neural Network," in *IEEE ITEC*, San Francisco, CA, 1998.

[26] S. R. Habibi and R. Burton, "The Variable Structure Filter," *Journal of Dynamic Systems, Measurement, and Control (ASME),* vol. 125, pp. 287-293, September 2003.

[27] M. Al-Shabi, "The General Toeplitz/Observability SVSF," Hamilton, Ontario, 2011.

[28] S. A. Gadsden and S. R. Habibi, "A New Form of the Smooth Variable Structure Filter with a Covariance Derivation," in *IEEE Conference on Decision and Control*, Atlanta, Georgia, 2010.

[29] M. S. Grewal and A. P. Andrews, Kalman Filtering: Theory and Practice Using MATLAB, 3 ed., New York: John Wiley and Sons, Inc., 2008.

[30] "www.MathWorks.com/Matlabcentral/fileexchange," [Online].

[31] "http://www.epa.gov/nvfel/testing/dynamometer.htm," U.S. EPA. [Online].

[32] R. E. Kruse and T. A. Huls, "Development of the Federal Urban Driving Schedule," May 14, 1973.

Chapter 7: Summary, Conclusions, and Recommendations for Future Research

This short chapter provides a summary of the research conducted and illustrated through the entire thesis. The chapter also includes recommendations for future research.

7.1 Research Summary

The research presented in this thesis concentrated on advancing the development and implementation of electrochemical and equivalent-circuit-based battery models. Most battery models did not account for aging and degradation over the entire vehicle lifetime. In addition, electrochemical battery model studies are mainly based on simulation studies and therefore the full-set of the reduced-order electrochemical model parameters have not been identified using a real-world driving cycle while calculating the state of charge.

Hence, Chapter 3 of this thesis introduces a new electrochemical model-based state of charge parameterization strategy based on the number of spherical shells (model states) and on the final value theorem. The final value theorem is applied in order to calculate the initial values of lithium concentrations at various shells of the electrode. Then, this value is used for setting up a constraint for the optimizer in order to achieve an accurate state of charge estimation. The state of charge parameterization model has been developed to adjust the spherical volume-based state of charge calculation. The technique has been used to estimate the full-set of the reduced-order electrochemical model parameters for 3.3V, 2.3Ah Lithium Iron Phosphate (LiFePO4) batteries at various states of life.

In order to fit the electrochemical battery model parameters, electric current input from an Urban Dynamometer Driving Schedule (UDDS) has been used. Battery models have been validated using a variety of aggressive driving cycles such as the light duty drive cycle for high speed and high load (US06) and the highway fuel economy test (HWFET). In order to generate the current profile from driving cycles, an electric vehicle model (based on SimScape) has been utilized. The electrochemical model with identified parameters fits voltage experimental data very well with a RMSE of approximately 0.2 mV over a UDDS cycle. Moreover, spherical average concentration can be effectively used for state of charge calculation provided that the initial State of charge is provided. The reduced-order model results in heavy loss of information from the full-order model. However, it still maintains a strong connection to the internal battery potential and diffusion dynamics which are beneficial for state of health estimation.

The second major contribution of this thesis is presented in Chapter 4. In this Chapter, development of a battery aging and degradation model has been conducted. The thesis extends on existing electrochemical battery models to accommodate for aging and degradation that happens overtime. An aging battery model is developed by changing the effective electrode volume to model capacity degradation. A non-invasive genetic algorithm has been applied to estimate model parameters for aged batteries. Main parameters that contribute to battery aging are: the OCV-SOC relationship, the solid-electrolyte interface resistance (c_{se_p}), the solid diffusion coefficient (D_s), the electrode effective volume (τ), and the minimum and maximum stoichiometry values ($\theta_{p_{0\%}}$) and ($\theta_{p_{100\%}}$). The battery loss of capacity due to aging is attributed to the increase in the battery solid electrolyte interface resistance, the decrease in diffusion coefficient, and the decrease in the battery electrode effective volume, those changes reflect the electrode tendency to resist further lithium diffusion as battery degrades. Extensive accelerated aging and reference performance tests have been conducted on lithium-iron phosphate cells. Reference tests have been conducted at two distinct states of life, namely: 100% and 80% capacity.

Furthermore, a critical state of charge estimation strategy has been implemented using the SVSF methodology. The SVSF can be used to estimate the critical surface charge and the battery overall state of charge at steady state conditions.

In Chapter 5, based on equivalent circuit-based battery models, a technique for parameters identification in both online and offline settings at various battery states of life has been conducted. In the online technique, a recursive least square method has been applied to estimate battery model parameters and to estimate the open circuit voltage (OCV). Based on the estimated battery OCV, a regressed-voltage method has been applied to map the OCV to the battery state of charge thus provides an estimate of the battery state of charge at various states of life.

In the offline technique, a Genetic Algorithm (GA) optimization strategy has been applied to estimate the battery model parameters at various states of life. Based on the optimized model parameters, a battery state of charge estimation strategy has been designed to estimate the state of charge based on the identified battery model parameters. A strategy based on the SVSF has been presented for battery state of charge estimation. The proposed strategy has been selected since it demonstrated robustness to modeling uncertainties and sensor noise in previous publications. The strategy has been applied to estimate the battery state of charge at various states of life from fresh state (100% capacity) to 80% retained capacity.

An adaptive state of charge estimation strategy that can accommodate for battery aging has been presented in Chapter 6. The chapter presents a relatively new estimation strategy known as the Interacting Multiple Models based on the Smooth Variable Structure filter (IMM-SVSF) as applied to battery management systems. A proof of concept to the applicability of adaptive techniques in battery state of charge estimation is presented. The IMM-SVSF technique is applied to extract state of charge information based on an equivalent circuit-based battery aging model.

Therefore, instead of relying on one battery model at single state of life, the IMM-SVSF strategy can incorporate different battery models obtained across the life time of the battery. In order to demonstrate the ability of the proposed technique to extract battery cell state of charge information, the technique has been compared to the standalone SVSF and data for a battery with 0.5 life fraction (mid-life) has been used for testing. The IMM-SVSF technique provides good estimation accuracy and stability compared to the standalone SVSF. The SVSF, when used with the fresh battery or with an aged battery, will exhibit chattering in the state of charge estimate due to model uncertainties. Conversely, the IMM-SVSF technique adapts to these variations as it takes into account the combined results of all the models across the battery lifetime thus provides a smoother and more accurate estimate.

7.2 Recommendation for future work

This thesis includes a number of improvements to battery electrochemical and equivalent circuit-based models and state of charge estimation strategies. Since vehicle electrification is a relatively new research area, a significant amount of research areas are still unexplored. The first recommendation for the work presented in this thesis is to expand the developed models and strategies from the cell-level to the module and pack-level. This will introduce a new challenge for the strategies since they must account for cell-to-cell balancing and thermal effects. Future studies should involve looking at this extension.

Regarding the accelerated-life aging test, instead of relying on battery data from an accelerated-life aging test using cyclers in controlled environment (i.e.: thermal chambers), data logged from on road electric vehicles in real-world operation (acquisition of load cycles using data logger with GPS capability connected to the CAN bus of the vehicle) can be used to assess the degradation models and state of charge estimation strategies especially at the end-of-life state. However, this test will require a very long period of time until the odometer of on road electric vehicles reaches 150,000 miles. In addition, besides the driving cycles, considering loading cycles such as air conditioning and heating loads would enhance the accuracy and prediction of aging models.

Another substantial recommendation for future work involves coupling the reduced-order electrochemical model with a battery thermal model. This will enhance the battery model accuracy and in turn will improve the state of charge estimation trustworthiness at various operating temperature conditions. This is beneficial since electric vehicle driving range reduces significantly at lower temperatures conditions.

Battery electrochemical models accuracy can be significantly enhanced by allowing models to account for recovery and rate-capacity effects. Therefore, a hybrid model can be developed by combining electrochemical battery models with battery hydrodynamic models. Future research can look into the development of the combined model and into the application of the state of charge estimation strategies based on the developed hybrid model. Finally, a sensitivity analysis on reduced-order electrochemical model parameters should also be conducted.

Although the field of vehicles electrification and in particular; battery modeling, and state of charge estimation is a relatively new field, the developed strategies demonstrated a number of improvements compared to existing methodologies. The contributions of this thesis should provide a strong starting point for future improvements to battery modeling, State of charge, and State of health estimation.

APPENDIX: Electric Vehicle Model

This section summarizes the electric vehicle sub-models used to generate the current profile from the velocity profile.

A. Vehicle speed Controller

A Proportional Integral (PI) controller is used to generate the accelerator command. This is conducted by comparing the vehicle actual speed with the reference (desired) speed which varies based on the driving cycle selected. The block output is fed to the motor controller (next block)

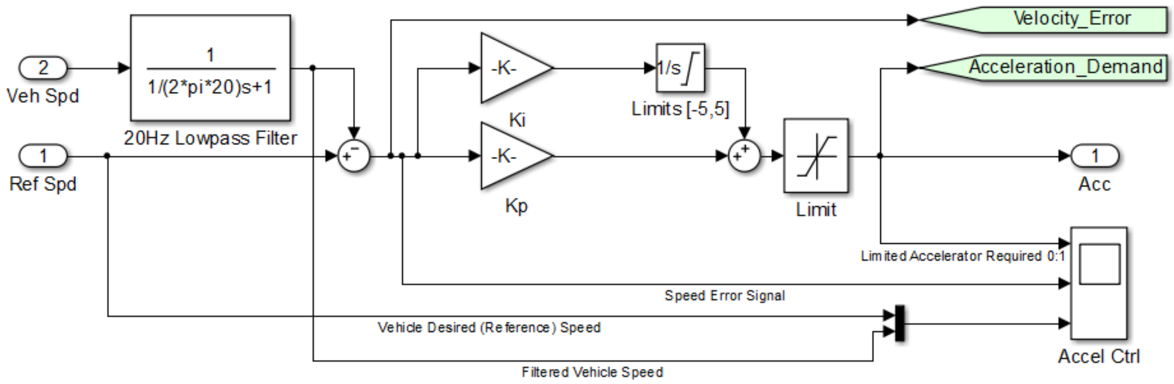

B. Motor Controller

The accelerator commanded output is linearly converted to motor speed command which is sent to the motor controller block as shown in the figure below:

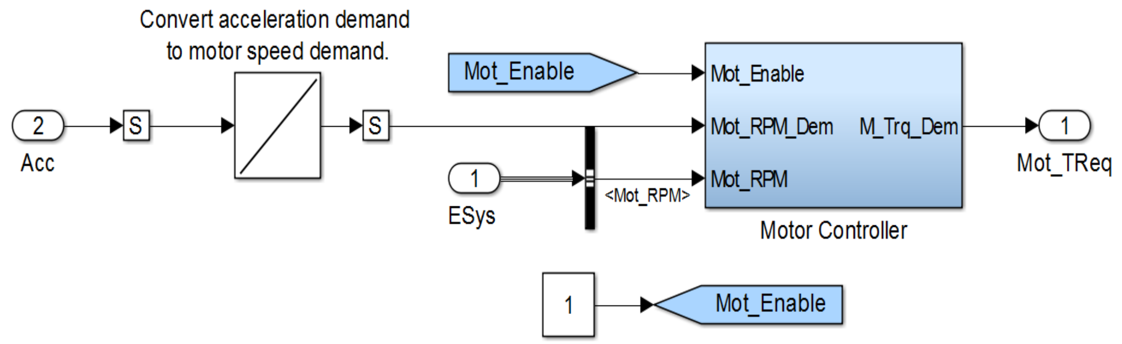

Convert acceleration demand to motor speed demand.

The motor controller block contains a PI controller that controls the motor speed by comparing the reference (desired) speed to the actual motor speed (after a low pass filter). The motor RPM Control signal is sent to enable torque demand block which in turn is sent to the electric motor driver.

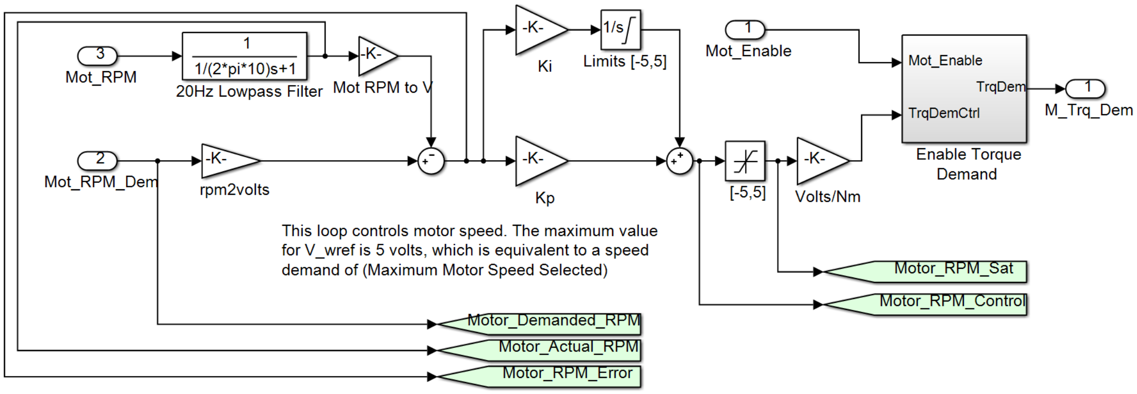

This loop controls motor speed. The maximum value for V_wref is 5 volts, which is equivalent to a speed demand of (Maximum Motor Speed Selected)